D I S S E R T A T I O N

# Measurement and interpretation of disc cutting forces in mechanized tunneling

A contribution to the understanding of rock failure mechanisms
and the advancement of TBM performance prediction

eingereicht an der Montanuniversität Leoben
Lehrstuhl für Subsurface Engineering

von

Dipl.-Ing. **Martin ENTACHER**

Matr.Nr.: 0525435
Vorgartenstraße 221/5.24
1020 Wien
Österreich

Erstbegutachtung:

Univ.-Prof. Dipl.-Ing. Dr.mont. **Robert GALLER**
Lehrstuhl für Subsurface Engineering
Montanuniversität Leoben

Zweitbegutachtung:

Univ.-Prof. Dr. habil. **Kurosch THURO**
Lehrstuhl für Ingenieurgeologie
Technische Universität München

Leoben, im August 2013

# Abstract

Hard rock tunnel boring machines (TBM) are equipped with disc cutters as their main excavation tools. Each cutter is nominally loaded with about 250 kN. The knowledge of cutting forces is restricted to the measurement of global thrust from which individual forces are estimated. However, it is known that actual cutting forces vary greatly with peaks that are a multiple of the nominal load. Their knowledge would open a wide range of possibilities to improve TBM tunnelling. They include gaining a deeper understanding of rock breakage, improving TBM performance prediction models, establishing new ways of geological documentation of the tunnel face as well as improving cutter and cutterhead design with respect to peak forces and load collectives.

Consequently, the development of a new cutter force measurement method is presented. In contrast to previous approaches, sensors are placed in the cutter saddle as opposed to the cutter itself. Thereby, they are independent from frequently occurring disc cutter changes and thus suitable for a lasting in situ use. After extensive simulations and laboratory tests, the method was implemented on a TBM at Koralm tunnel. Results are presented with respect to the geology of the tunnel face. It is shown that anisotropic features and fractured areas can be identified.

A foundation for the interpretation of cutting forces was built by means of full and small scale laboratory rock cutting tests. The analyses range from macroscopic spatial observation of crack propagation and microscopic investigations in the direct vicinity of the cutter tip to correlations of sound emissions, cutting forces and failure events. Such in-depth analyses were made possible by the development of a new small scale cutting test rig that allows for high-precision investigations in a controlled laboratory environment. The interpretation of results highlights common misperceptions in previous studies regarding the meaning of peak forces and subsequent force drops as well as crack propagation.

Measurement and interpretation of cutting forces is inherently linked to TBM performance prediction. While full scale cutting tests are considered to be the best laboratory experiment in this regard, they require large samples which are hardly available before a tunnel is built. Furthermore, it was proven that common prediction models based on classical strength parameters such as uniaxial compressive strength are not capable of predicting cutting forces in certain rock types. Thus, it was shown that the newly developed small scale cutting test delivers superior input parameters for a new TBM performance prediction model.

With the developed in situ measurement method and laboratory experiments at hand, tools for major improvements of TBM tunnelling were provided. A profound understanding of tool-rock interaction might even in future enable fully automated TBM control with cutting forces as the main input parameter.

# Kurzfassung

Das wichtigste Abbauwerkzeug von Tunnelbohrmaschinen (TBM) sind Schneiddisken, die auf eine Last von etwa 250 kN ausgelegt sind. Die Belastung im Betrieb kann in der Regel nur über die Gesamtvorschubkraft abgeschätzt werden. Die tatsächliche Belastung der Diske variiert jedoch stark, wobei Spitzenkräfte auftreten, die um ein Vielfaches größer sind als die nominelle Last. Eine Onlineerfassung der individuellen Diskenkräfte würde eine Vielzahl von Möglichkeiten eröffnen, um TBM-Vortriebe entscheidend weiterzuentwickeln. Dazu gehört ein tieferes Verständnis des Lösemechanismus, die Weiterentwicklung von TBM Leistungsprognosemodellen, die Verbesserung der geologischen Dokumentation der Ortsbrust sowie eine verbesserte Auslegung von Disken und Bohrkopf durch die Kenntnis von Spitzenkräften und Lastkollektiven.

Um eine Onlineerfassung der tatsächlichen Diskenkräfte zu ermöglichen, wurde eine Messmethodik entwickelt, die einen dauerhaften Einsatz auf einer TBM ermöglichen soll. Im Gegensatz zu vorherigen Versuchen sind die dafür notwendigen Sensoren im Auflager der Diske montiert und somit unabhängig vom regelmäßig stattfindenden Diskenwechsel. Nach der Bestätigung der Machbarkeit durch umfangreiche Simulationen und Laborversuche, wurde die neu entwickelte Messmethode auf der ersten TBM des Koralmtunnels implementiert. Die Ergebnisse zeigen, dass durch die Kraftmessung geologische Merkmale wie Anisotropie oder stark zerlegte Zonen zuverlässig erkannt werden können.

Das grundlegende Verständnis für die Interpretation von Schneidkräften wurde mithilfe von Gesteinsschneidversuchen im Labor erarbeitet. Die Untersuchungen reichen dabei von makroskopischer Rissbildanalyse, über mikroskopische Beurteilung der Versagensmechanismen unter der Diske, bis hin zur Korrelation von Schalldruck, Schneidkräften und Bruchereignissen. Solche tiefgreifenden Analysen wurden durch die Entwicklung eines Modellschneidversuchs ermöglicht, der präzises Arbeiten unter kontrollierten Laborbedingungen ermöglicht. Die Interpretation der Ergebnisse zeigt, dass die Bedeutung von Spitzenkräften und des darauffolgenden Kraftabfalls sowie die Rissausbreitung in der Vergangenheit noch nicht ausreichend verstanden wurden.

Die Messung und Interpretation von Schneidkräften ist untrennbar mit dem Gebiet der TBM Leistungsprognose verbunden. Vollmaßstäbliche Schneidversuche werden im Allgemeinen als das zuverlässigste Mittel zur Leistungsprognose angesehen, allerdings bedarf es dafür großer Probekörper, die schwer oder mitunter gar nicht zu bekommen sind. Darüber hinaus wird gezeigt, dass gängige Prognosemodelle, welche auf Eingangsparametern wie der einaxialen Druckfestigkeit basieren, nicht imstande sind, Schneidkräfte für bestimmte Gesteinsarten ausreichend genau abzuschätzen. Es wird gezeigt, dass der Modellschneidversuch als Standardversuch für ein neues Penetrationsprognosemodell wesentlich besser geeignet ist.

Mit der neu entwickelten Kraftmessmethodik, dem Modellschneidversuch und dazugehörigen Analysemethoden werden Werkzeuge bereitgestellt, die Möglichkeiten für

wesentliche Weiterentwicklungen bei TBM-Vortrieben eröffnen. Ein grundlegendes Verständnis der Interaktion zwischen Gebirge und Diske könnte sogar die Grundlage für eine zukünftige vollautomatisierte Steuerung einer TBM auf Basis von gemessenen Diskenkräften schaffen.

# Contents

# Abbreviations

| | |
|---|---|
| **AE** | Acoustic emission |
| **AG** | Augengneiss |
| **BG** | Brixen granite |
| **BTS** / $\sigma_{BTS}$ | Brazilian tensile strength |
| **CMS** | Calcareous mica schist |
| **CSM** | Colorado School of Mines |
| **DEM** | Distinct element method |
| **DRI** | Drilling rate index |
| **FEM** | Finite element method |
| **FPI** | Field penetration index |
| **GG** | Granite gneiss |
| **HS** | Herdecke sandstone |
| **IS** | Imberg sandstone |
| **ISRM** | International society of rock mechanics |
| **KAT** | Koralmtunnel |
| **LCM** | Linear cutting machine |
| **NATM** | New austrian tunnelling method |
| **NG** | Neuhauser granite |
| $F_N$ | Normal force |
| **NTNU** | Norwegian University of Science and Technology |
| **PLCM** | Portable linear cutting machine |
| $\nu$ | Poisson's ratio |
| $F_R$ | Rolling force |
| **RQD** | Rock quality designation |

| | |
|---|---|
| **RS** | Red sandstone |
| **SEM** | Scanning electron microscope |
| **sd** | Standard deviation |
| $F_S$ | Side force |
| **TBM** | Tunnel boring machine |
| **TEN** | Trans-european networks |
| **UCS** / $\sigma_{UCS}$ | Uniaxial compressive strength |
| **E** | Young's modulus |

# List of figures

# List of tables

# 1. Introductory Remarks

## 1.1. Motivation

The use of tunnel boring machines (TBM) is one of main construction methods in today's tunnelling industry. In contrast to conventional methods such as the New Austrian Tunnelling Method (NATM), mechanized tunnelling tends be much faster and less labour-intensive but traditionally also less flexible regarding its capability to cope with heterogenous ground conditions. In soft ground - typically found in urban areas - modern TBMs are able to excavate at shallow depths underneath sensitive infrastructure even in poor ground conditions. In hard rock conditions - such as in most alpine base tunnels - the main challenges are posed by fault zones which can include squeezing ground conditions, severe water ingress as well as highly fractured or blocky rock mass. Such obstacles can pose the risk of machine jamming, failure of segmental lining elements, highly inefficient rock excavation or significant cutterhead and tool damage. Conditions like that are found in all three major upcoming Austrian infrastructure tunnels, i.e. Brenner base tunnel, Koralm tunnel and Semmering base tunnel. The choice of the right machine type that allows for successful construction in all geological areas of a specific tunnel is a demanding engineering task. Nevertheless, modern TBMs are capable of crossing difficult geological areas by installing various types of rock support close to the tunnel face and the possibility to drill ahead of the tunnel face for purposes of forecasting or ground improvement by means of injections. This increase in flexibility has opened wider and wider areas of application for mechanized tunnelling. A thorough review of hard rock and soft rock mechanized tunnelling can be found in Maidl et al. (2008) and Maidl et al. (2012) respectively.

In hard rock - which is the focus of this thesis - three main types of TBMs are used: Open gripper, single shield and double shield TBMs. As an example, the main functions of an open gripper TBM are explained. Fig. 1.1 shows a Herrenknecht TBM with a cutterhead diameter (a) of approximately 9 m which is equipped with about 60 excavation tools (b), i.e. 17" single disc cutters. Buckets (c) in the gauge area of the cutterhead are used to pick up excavated material and feed a conveyor belt which is placed right behind the cutterhead. To support the machine during the boring process, it is clamped to the surrounding rock mass with grippers (d) and thrust into the rock with propel cylinders (e). After a full stroke, rear support legs (f) are extended to support the machine weight while the gripper plates are retracted and replaced to allow for a new stroke. The area right behind the cutterhead is protected by a roof support (g). Behind this shield, support

measures such as rock bolts, steel arches or wire mesh can be installed in the so-called L1 area (h).

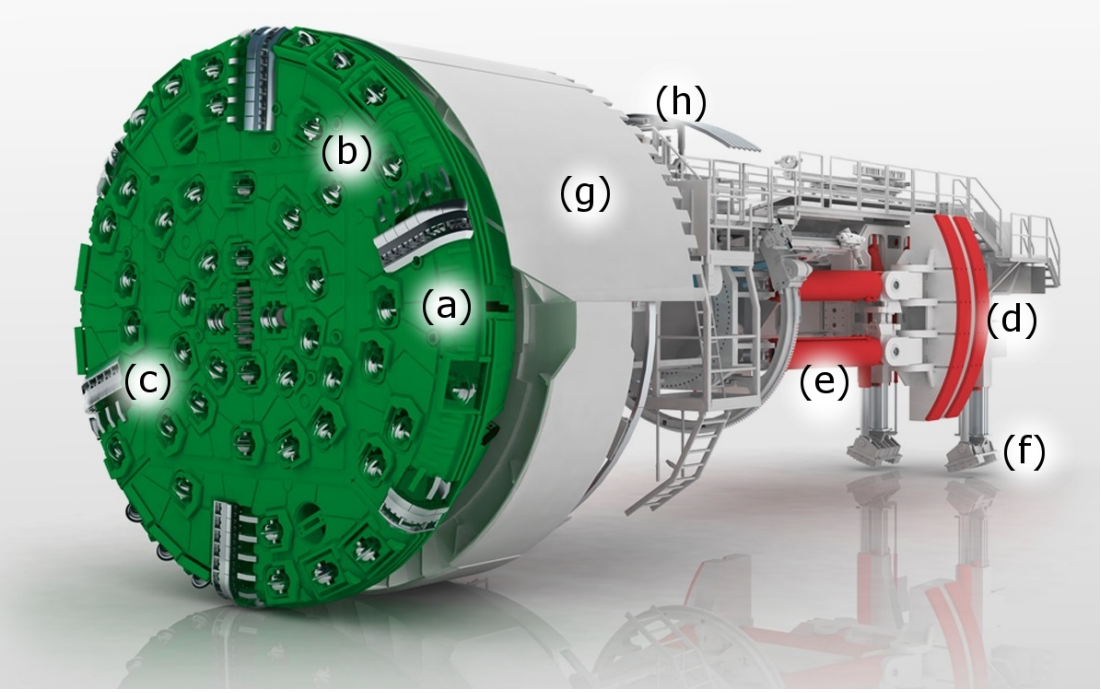


**Fig. 1.1.:** Open gripper TBM (©Herrenknecht)

The nominal load of a typical 17" inch disc cutter is about 250 kN. During operation, this load is determined by subtracting friction forces from global thrust and then dividing it by the number of excavation tools. The true loading of a cutter is however strongly oscillating with force peaks that are a multiple of the nominal load and unequally distributed depending on its position (see section B.4). Hence, an estimation derived from global thrust contains only very limited information about the complex processes of rock excavation. It is therefore highly desirable to obtain real-time information about cutter loading. Besides the knowledge that was gained from extensive rock cutting tests in a laboratory environment, there have been several attempts - some of them being very successful - to measure cutting forces in situ. None of the previous approaches however proved to be practical in the sense of lasting use during TBM operation.

The knowledge of cutting forces is inherently linked to the prediction of net penetration rates, commonly referred to as TBM performance prediction modelling. The goal of such models is to determine a penetration rate, i.e. TBM advance rate per cutterhead revolution (mm/rev), as a function of cutter load for different ground conditions and other factors such as cutter size, spacing, etc. Penetration rate is the basic parameter that is needed to determine construction time, a key parameter for large infrastructure projects. Two of the most widespread TBM performance prediction models were developed at the Colorado School of Mines (CSM, Rostami and Ozdemir 1993, Rostami

1997) and at the Norwegian University of Science and Technology (NTNU, Bruland 1998). They are in worldwide use and have proved to be a valuable aid for many different projects. In spite of their great success, both models have downsides that leave room for major improvements. It is therefore necessary to establish a more fundamental understanding of rock failure mechanisms, and to subsequently introduce basic model parameters that are more closely related to the actual cutting process.

## 1.2. Objective

The objective of this thesis is to develop and implement a cutter force measurement method for TBM disc cutters. Subsequently, the measured forces and the results of laboratory rock cutting tests shall be analysed to improve the understanding of rock failure mechanisms and to create a foundation for the advancement of TBM performance prediction modelling. The steps taken to achieve this objective were:

- Analysis of a disc cutter and its corresponding casing to identify suitable options for sensor placement.
- Design of different sensor setups and confirmation of feasibility for a cutter force measurement method in a laboratory environment.
- Implementation and calibration of this method on a TBM and subsequent confirmation of feasibility for in situ applications.
- Assessment of established TBM performance prediction models with a focus on basic geotechnical input parameters.
- Development of a small scale cutting test rig which is compared to state-of-the-art geotechnical parameters regarding their suitability for TBM performance prediction.
- Investigation of rock failure mechanisms by means of full and small scale rock cutting tests, macro- and microscopic failure analysis and evaluation of cutting forces.

## 1.3. Remote cutter monitoring

Monitoring the geological situation at the tunnel face is an important task in tunnelling. In conventional tunnelling, it can be done visually - sometimes even after every round - because the face is usually easily accessible. In mechanized tunnelling however, the face is typically inspected once a day which is approximately every 20 m. These inspections are also limited in the sense that they are only possible through small manholes and bucket openings. In addition, the use of a geological compass is inexpedient due to the

heavy steel environment of a cutterhead. As a result, the overall quality of geological monitoring is of lesser quality in TBM tunnelling.

Besides the need for geological / geotechnical information, it is highly desirable to monitor the status of excavation tools automatically. This includes checking for proper operation (e.g. rotating / non-rotating), monitoring of excessive loading or vibration which could lead to tool or cutterhead damage, as well as the monitoring of wear status, to be able systemically to plan cutter changes. A successful monitoring of these parameters would result in a tremendously improved TBM operation by reducing inspection downtimes and by early-recognition of improper operation that can result in severe damage such as cutter wipeouts, a chain reaction failure of a large number of cutters.

Today, developments in the field of remote cutter monitoring are conducted by all major TBM manufacturers. This includes efforts to monitor rotational speed and / or rotational status of a cutter, temperature, tool wear, cutting forces and vibration. A review of the activites of Robbins was presented by Shanahan and Box (2011) at the World Tunnel Congress. The activities of Herrenknecht, Robbins and Japanese manufacturers are also documented by a number of patents (Starloy Corporation 2003, Burger et al. 2006, Lindbergh et al. 2012, Edelmann and Himmelsbach 2013). To the best knowledge of the author, all of these efforts are still suffering from teething trouble, mostly related to robustness, durability and data transmission. In other words, none of the current systems is fully functional over longer time periods. However, there is a marked trend that remote cutter monitoring will be further pursued. A clear indication is that owners are starting to demand the use of such methods in their tender documents, e.g. in the third construction lot of Koralm tunnel (KAT 3).

Fig. 1.2 shows a cut-view of a 17" single disc cutter, the most common excavation tool used on hard rock TBMs. The main parts of the cutter are an axis on which two tapered roller bearings are placed. On top of the bearings is the cutter main body and a replaceable cutter ring which is made of high-alloy heat-treated steel which is optimized with respect to an optimal balance between resistance against abrasion and toughness. O-seals guarantee proper lubrication of the bearings. The overall weight of such cutters is between 130 and 200 kg, depending on the specific layout.

Previous generations of cutterheads used front loading systems to attach the cutting tools (Fig. 1.3a). These systems are very convenient because they allow for large gaps between cutter tip and steel structure which reduces cutterhead wear and consumes less energy for inefficient grinding. Today, they are used in TBMs with very small diameters and some other mechanical excavators such as raise boring reaming heads. On large TBMs, their use is unacceptable because miners have to climb in between the tunnel face and the cutterhead structure for changing cutters, which is very dangerous. In addition, changing cutters is faster in modern cutterheads where the excavation tools are fixated with back-loading systems (Fig. 1.3b).

**Fig. 1.2.:** Cut-view of a single disc cutter (©Herrenknecht)

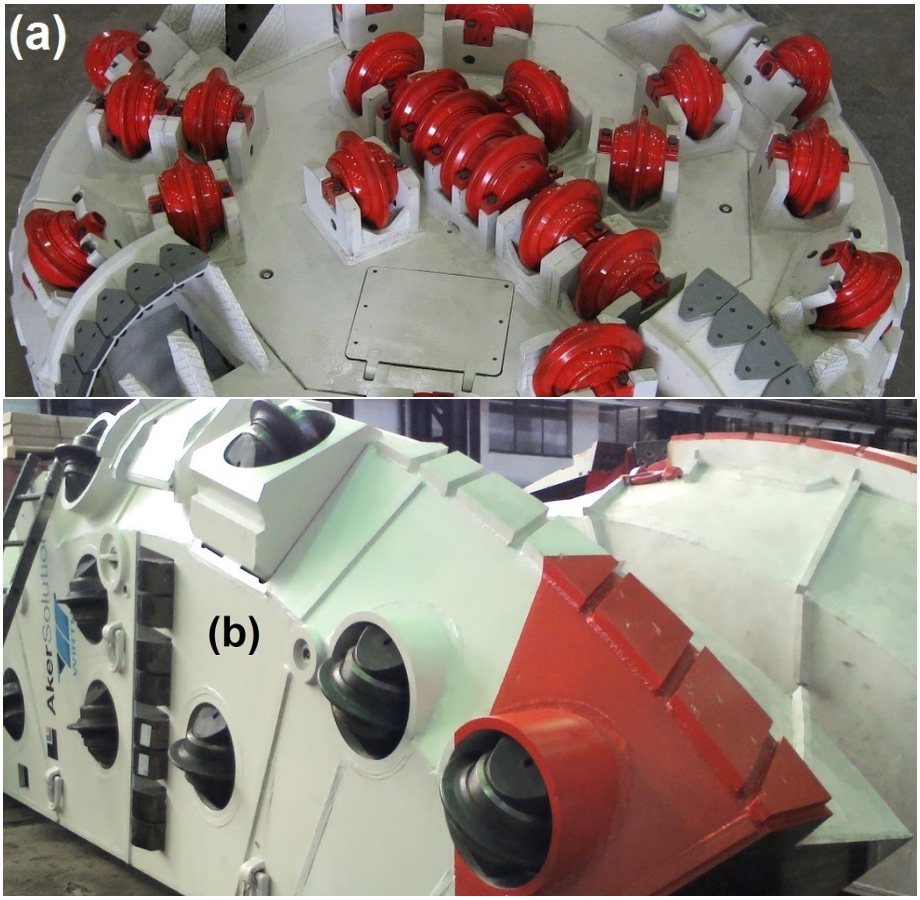


**Fig. 1.3.:** Cutterhead with front-loading system (a, ©Palmieri), segment of a cutterhead with back-loading system (b)

Today, there are two different basic back-loading systems which are used on most TBMs. The first is one is the Wedge-Lock system, preferably used by Herrenknecht and Robbins, the second is the conical saddle or bayonet system, preferably used by Aker Wirth. Fig. 1.4 shows these systems in an isometrical and cross-sectional view.

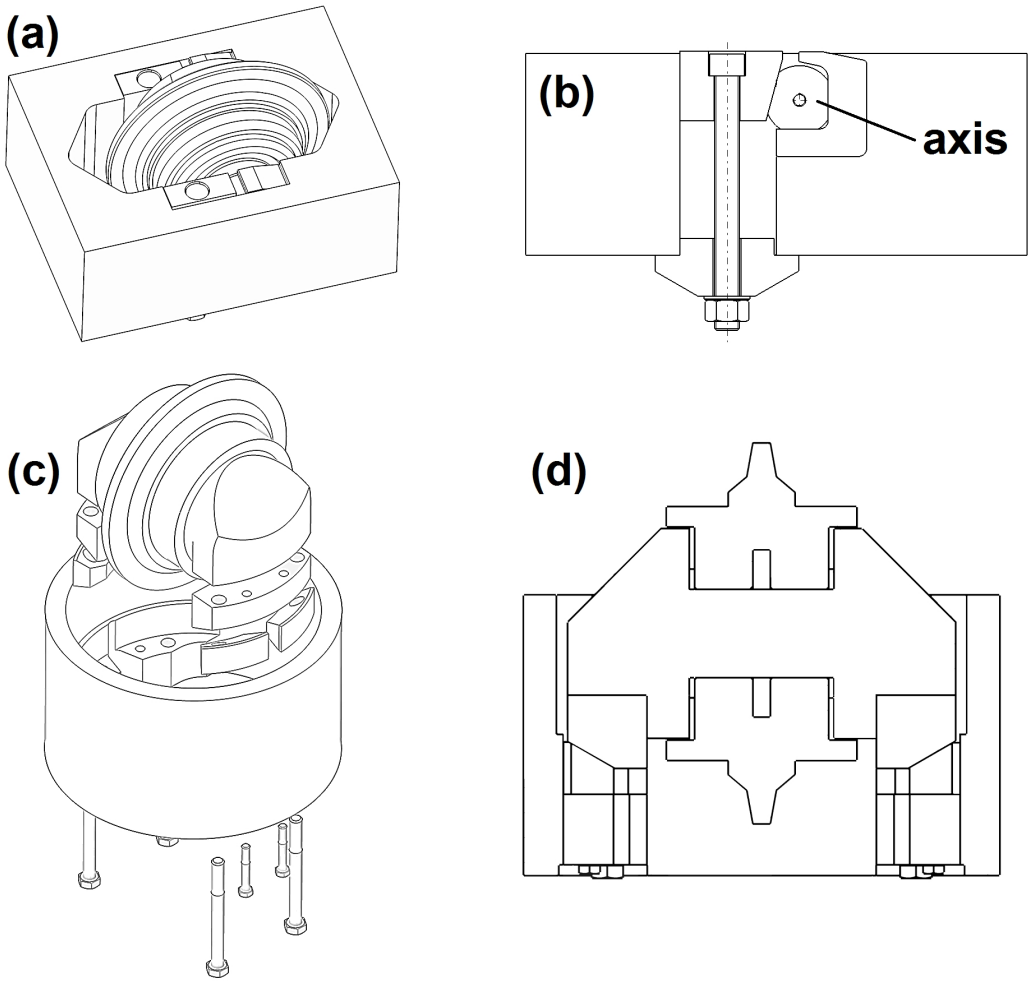


**Fig. 1.4.:** Cutter mounted with a Wedge-Lock system (a), cross-sectional view of Wedge-Lock system (b), explosion drawing of conical saddle / bayonet system (c) and cross-sectional view of mounted cutter (d)

A cutter change for Wedge-Lock systems is done by removing the Wedge and pulling the cutter backwards. For conical saddle systems, the four bolts have to be removed after which the cutter is twisted by 90° and then pulled backwards. This is done with special tools offered by the manufacturers. The frequency of cutter changes varies greatly depending mostly on the abrasiveness of the rock mass. In very abrasive rock, cutters are sometimes changed every day. Thus, placing sensors and cables in a cutter or in its vicinity has to be done with great care, otherwise it will result in a severe disturbance of the construction process.

The environmental conditions during TBM operation are extremely harsh. Abrasive rock chips destroy unprotected parts, water and fine particles penetrate even the smallest openings and heavy vibrations pose high demands regarding durability. The combination of these conditions and frequent tool changes are very challenging when it comes to installing measurement equipment.

A number of researchers have attempted to measure cutting forces. Gobetz (1973) equipped a cutter of a Robbins cutterhead with strain gauges and successfully measured forces on an excavation length of about four meters. Hopkins and Foden (1979) successfully equipped the cutter of a raise borer reaming head in South Africa. Remarkably, they used a wireless data transfer module. Fenn et al. (1981) were equally successful by equipping the cutter of a Robbins reaming head. In 1984, Samuel and Seow managed to equip two cutters of a TBM and record 20 minutes of data. The next successful attempt was conducted by Zhang et al. (2001, 2003a,b) who instrumented button cutters on a TBM at Äspö hard rock laboratory in Sweden. All these projects offered valuable insights in the characteristics of cutting forces which were unknown at the time. The first attempt to industrialize cutter force measurement and use it for longer time periods was done within the Tunconstruct research project and was called “Mobydic” (Beer 2009). It is designed to monitor not only cutting forces, but also cutter rotation and temperature. To the knowledge of the author, the system proved to be successful in certain projects. However, together with all other mentioned designs, it has a serious disadvantage. The sensors, i.e. strain gauges, are attached to the cutter axis which requires specially designed cutters and results in an unacceptable disturbance during cutter change because of the need for an electrical connection between a spare part (cutter) and the cutterhead / cutter casing.

The cutter force measurement method that is presented in this thesis was thus developed under the constraint that changing cutters must remain unaffected and independent of the measurement equipment. Otherwise, there is no chance for a lasting implementation. Consequently, it was decided to place all sensors outside the cutter. A simulation of a disc cutter and its corresponding casing revealed that the cutter saddle is a potentially suitable spot for sensor placement. However, it is clear that influences affecting the measurement signal increase, as the distance from the point of interest, the cutter ring tip, increases. Fig. 1.5a shows the axis which behaves like a beam in bending. It is a very convenient spot for instrumentation and was used in all previous attempts. In Fig. 1.5b, the saddle is highlighted which turns out to be an appropriate spot for sensor placement too. Detailed descriptions of the development and implementation of a new cutter force measurement method are presented in section A and section B, respectively.

Knowledge of cutting forces can contribute to a variety of fields. First of all, it can be expected that the distribution of cutting forces on the tunnel face is closely related to its geotechnical properties. It will be possible to detect many different features that are of great importance for TBM operations. An illustrative example is the recognition of the orientation of schistosity and degree of anisotropy in metamorphic rock types. It was shown that the relative angle between cutting direction and anisotropic feature

significantly influences forces required to cut rock (Entacher and Lassnig 2012b). As a disc cutter rotates around the tunnel and passes through every angle relative to the foliation, a pattern is created that should be clearly visible in the processed data. A schematic sketch with generic data of such a situation is shown in Fig. 1.6. It is assumed that forces of three tools at different radii are recorded.

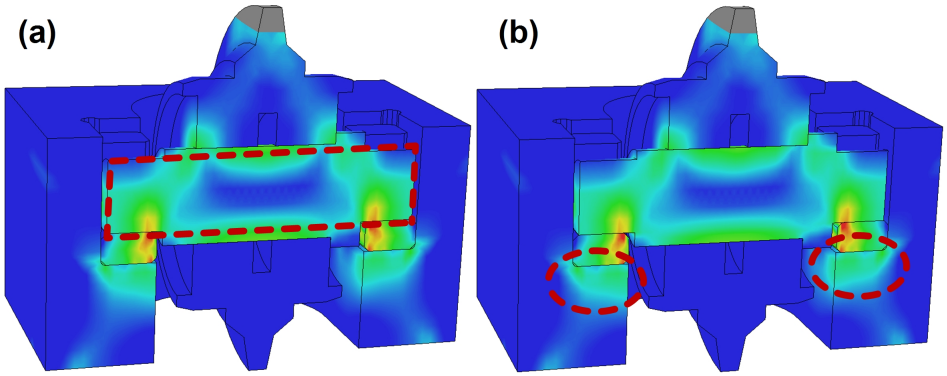


**Fig. 1.5.:** Qualitative stress distribution (von Mises stress) with highlighted spots for convenient sensor placement, cutter axis (a) and cutter saddle (b)

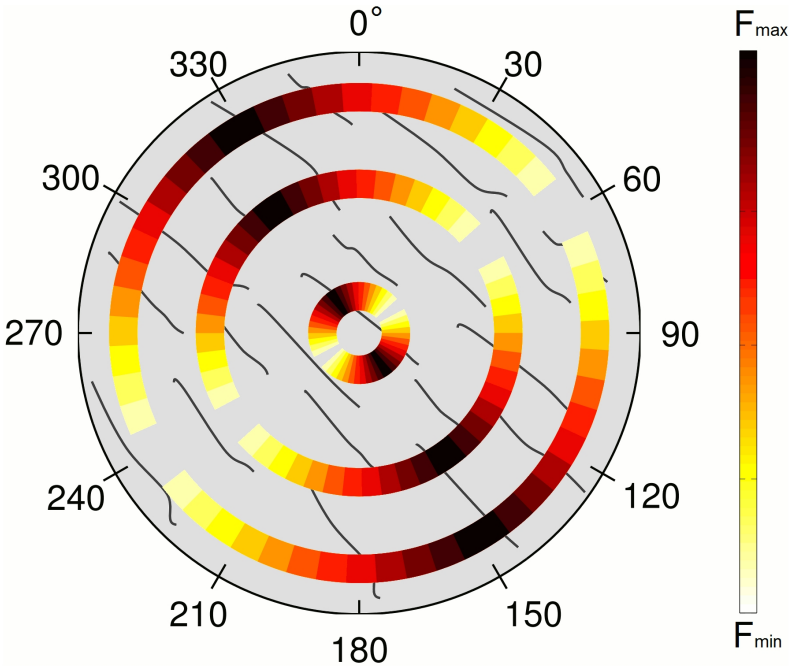


**Fig. 1.6.:** Generic sketch of cutting force distribution of three cutters in anisotropic rock. The forces are expected to be much higher when the cutting kerf is perpendicular to the foliation

Another important geological feature that could be detected, is the existence of different lithologies with different cuttability, e.g. stiff hard rock and soft rock layers. Such a

situation is illustrated in Fig. 1.7. Similarly, many more features could be detected such as rock type changes, changes in the distance of planes of weakness, blocky rock masses and approaching fault zones. To summarize, cutter force measurement offers a significant improvement to densify and enhance geological documentation and interpretation in mechanized tunnelling.

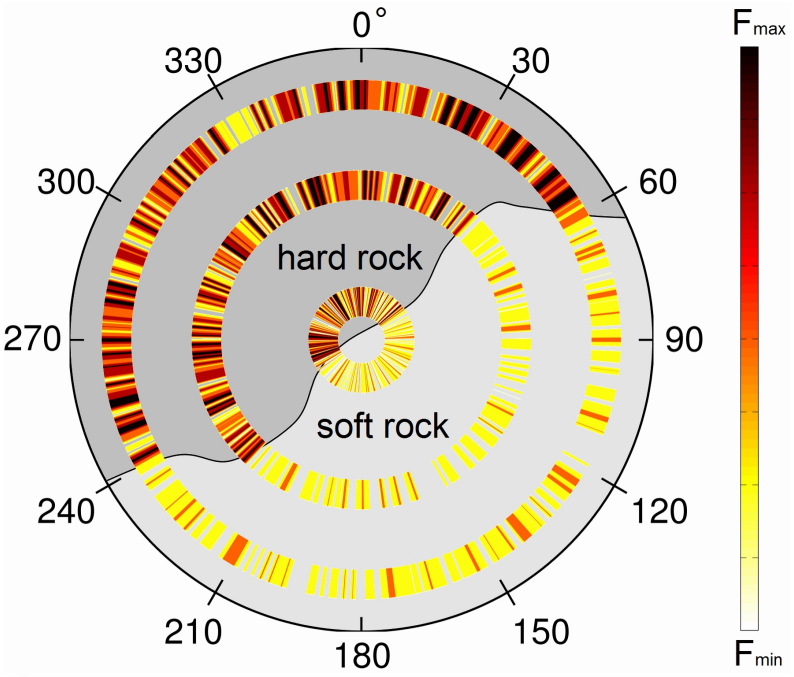


**Fig. 1.7.:** Generic sketch of cutting force distribution of three cutters. The tunnel face consists of a hard rock and a soft rock layer

Cutting forces are obviously not only related to geological features. They are also related to basic design parameters such as cutter size and spacing and operational effects such as wear or uneven pressure distribution during turns. Hence, they will also give a deeper insight in cutting efficiency. For example, a certain fraction of the excavated material piles up in the tunnel invert due to gravity. This results in unnecessary energy consumption due to extensive material crushing. Measuring this effect could lead to more effective bucket designs and allocations. It was mentioned that the gap between cutter tip and cutterhead structure is significantly different in front-loading and back-loading tool mounting systems. The impact of the size of this gap regarding cutting and crushing efficiency is expected to be significant, but it has not yet been investigated.

From a mechanical engineering point of view, cutter force measurement will lead to more effective cutterhead design because it provides a foundation for many aspects of optimization. For example, it could lead to stiffness adaptions in specific areas or to adaptions in spacing, such as larger spacings in the face and smaller spacings in the gauge area to ensure even load distribution. The life of cutters will potentially be

increased as their design can be set on a more fundamental basis as soon as peak forces and load collectives are known.

Finally, online monitoring of cutting forces leads to a tremendous knowledge increase during actual TBM operation. As mentioned, a typical tunnel face is rarely homogeneous. Instead, there are sections that require much more energy to be excavated, and sections with fractured material, favourable foliation angles or soft layers whose excavation requires much less energy. Deriving an operational thrust limit from global thrust is thus clearly inadmissible because it gives an averaged value that has little to do with potentially excessive loading in small areas of the tunnel face.

## 1.4. TBM performance prediction

The main goal of TBM performance prediction models is to determine a net penetration rate (mm advance rate per cutterhead revolution) which in combination with time for regripping, lining erection (and other rock support measures), cutter and cutter maintenance, conveyor belt extensions and other downtimes results in the total boring time of a tunnel. This is a key parameter that is carefully looked at in every design stage of a TBM hard rock tunnel and many researchers have tried to develop accurate prediction models for it. A paper that reviews many of the commonly used models was published by Farrokh et al. (2012).

There are a number of different basic approaches that were used to develop such models. While theoretical models are insignificant, the semi-empirical / semi-theoretical CSM model (Rostami and Ozdemir 1993, Rostami 1997) is among the most important ones. It is based on a large series of full scale cutting tests conducted in various massive rock types and requires the knowledge of uniaxial compressive strength (UCS) and Brazilian tensile strength (BTS) as basic geotechnical input parameters. The apparent downside of this model is the absence of any possibility to consider discontinuities and schistosity. Supplementary work to overcome this downside was done for example by Yagiz (2002) and Ramezanzadeh (2005).

The NTNU model, developed since the 1970's and comprehensively published by Bruland (1998) is the second of the most famous performance prediction models. It represents a large group of models that were derived by comparing TBM operational data with corresponding geological and geotechnical documentations. In the case of the NTNU model, data from penetration tests were used which helped to obtain data from a more controlled situation. The goal of such tests is to record TBM data under very controlled conditions with changing parameters such as torque and thrust. A recent proposal on how to conduct such tests was published by Frenzel et al. (2012). The NTNU model utilizes geotechnical input parameters that are derived from specially developed experiments. The brittleness value S20 is determined in a test where an impact hammer crushes a rock sample and the Sievers' J-Value is derived from a miniature drilling test.

These values are combined to obtain the drilling rate index (DRI). These tests are only carried out in Norway which is a significant downside of the model. A recent paper of Zare and Bruland (2013) reviews indices such as the DRI and its applications. Another limitation is the underlying data basis which comprises a large number of Norwegian hard rock tunnels. In non-Scandinavian conditions, the model tends to greatly overestimate the influence of discontinuities such as joints.

Besides these models that are in worldwide use, the model of the Austrian engineer Karlheinz Gehring (1995) contributed considerably to the advancement of TBM performance prediction models. His paper contains many basic thoughts regarding rock failure processes that are still a valuable source. Unfortunately, the model development is - compared to other models - based on a very small data base. Besides that, the basic architecture of the model is much liked by the industry. There is a basic relation between thrust force and penetration that is purely based on UCS. All other parameters, e.g. cutter spacing, cutter size, rock toughness, distance between planes of weakness and primary stress conditions are included with factors in subsequent steps. Hence, a basic penetration can be calculated very easily, but with more information available, more accurate results are obtained. For the sake of its simplicity, a model architecture similar to Gehring's model was chosen as the basis for developments in the ABROCK research group. ABROCK is a network of Universities and industry partners that seek to develop a new performance and wear prediction model for hard rock TBMs. The Chair of Subsurface Engineering, Montanuniversität Leoben, is an active partner in this project and has both learned from and contributed to the periodical ABROCK meetings.

In recent times, researchers were often able to utilize large databases, sometimes comprising more than 100 km of hard rock tunnels. A variety of models was developed based on such large datasets with little or no pre-assumptions, just by means of single or multivariate regression or soft computational methods such as artificial neural networks, fuzzy logic or particle swarm optimization (e.g. Zhao et al. 2007, Yagiz and Karahan 2011). These models are generally speaking bias-free due to the lack of pre-assumptions. At the same time, this is a significant disadvantage because many different situations are mixed up without thorough engineering judgement. It turns out that such models are often able to cover a large variety of rock types, i.e. the ones that are represented in the database, but they are mostly limited to a rather general prediction in early project phases. Furthermore, some of the models are black box models from which no explicit equations can be derived (e.g. neural network models). Needless to say, this is a serious limitation for practical applications. An interesting model developed with multivariate regression analysis was published by Hassanpour et al. (2008). On the one hand, it offers a rule of thumb equation to predict the field penetration index (FPI) as a function of rock quality designation (RQD) and UCS. On the other hand, it contains a comprehensive, illustrated table ranging from laminated/sheared to massive rock mass with UCS from 25 to 200 MPa that allows for a quick estimation of FPI in early project phases.

The controlling factors that influence excavability were comprehensively summarized

by Thuro and Plinninger (2003). Regarding net penetration rate, they can be divided into three major categories:

- Intact rock properties,
- rock mass parameters,
- machine parameters.

Intact rock properties mostly include UCS and/or BTS or DRI in the case of the NTNU model. In this model, porosity is also included. However, it shows a strong correlation with UCS which suggests that it can be disregarded without an unacceptable loss of accuracy. A superior alternative to intact rock properties can be obtained by conducting direct measurements of cuttability, i.e. full scale cutting tests. This is however costly and adequate sample material is often not available.

Rock mass parameters significantly influence penetration rate. A favourable alpha angle, the smallest relative angle between tunnel axis and plane of weakness, can increase penetration by a factor of up to two. A plane of weakness could be a joint or foliation. The studies of Thuro (2002) revealed that in metamorphic rocks, the degree of anisotropy is paramount regarding the impact of this increase. Yet, there are no publications that quantify this influence. Besides the spatial orientation of a weakness plane and the degree of anisotropy in metamorphic rocks, the distance between planes of weakness, i.e. rock joints, is one of the main influencing factors. A high frequency of joints can increase penetration by a factor of up to two or even more as suggested by the NTNU model. The strong emphasis of this factor in a model derived from Norwegian hard rock indicates that this factor is not independent of rock strength, i.e. the impact of joints is more significant in hard rock than in soft rock conditions. Another important factor is the primary stress state which can be significant in base tunnels with high overburden. High overburden leads to sudden stress release as the cutter penetrates into the rock. This can be potentially favourable or very troublesome. A discussion of this topic is found in section C.4.

Machine parameters include cutter type, size, shape, kerf spacing, global thrust and torque. It is well-known that other parameters such as cutterhead diameter influence penetration, i.e. the larger the machine, the smaller penetration becomes. This phenomen could be explained by size-related stiffness reduction of the boring system, changed rock mechanical conditions due to the large cross-sectional area and perhaps unfavourable rock dynamical effects as a result of increased loading rates due to increased angular speed in the gauge area.

Generally speaking, TBM performance prediction models are valid as long as the boring process is not superimposed by adverse operational conditions such as very blocky rock masses or instabilities of the tunnel face. Such situations were described in detail by Delisio et al. (2013).

## 1.5. Outline of the thesis

The main part of this thesis consists of four publications that were published, accepted for publication or submitted to international journals. The main focus is on the measurement of cutting forces, their interpretation with respect to rock failure and the subsequent implications for the development of TBM performance prediction models. Within the scope of the doctoral research, two inventions were protected with a patent and a utility patent (Entacher and Galler 2013a, b).

**Publication A** describes the development of a cutter force measurement method for TBM disc cutters. It reviews previous related work in the field of remote cutter monitoring and explains the need for a new cutter force measurement approach, i.e. a method that works independently of cutter change. In order to find an optimum sensor layout, FEM simulation results are presented from which setups for laboratory tests are derived. By means of extensive laboratory testing, the feasibility of the measurement method is successfully confirmed. It is protected by a utility patent.

The subsequent implementation on a hard rock TBM is described in **Publication B**. Three disc cutter saddles of the first Koralm tunnel TBM were equipped with sensors. To account for the changed structural stiffness of a cutterhead compared to the laboratory setup, an in situ calibration was carried out in the starting cavern of the TBM. Many different loading cases were simulated to ensure an accurate calibration procedure. At the same time, the in situ measurement chain was tested. It includes a programmable controller, devices for wireless radio communication and a database in which all data is stored. Results of in situ cutting forces are presented and analysed with special regard to a comparison with geological features of the tunnel face.

While the first papers deal with in situ cutting forces, the third is dedicated to building a foundation of understanding, and interpreting cutting forces by means of laboratory experiments. **Publication C** covers a wide range of laboratory testing ranging from full scale to small scale cutting tests, macroscopic analysis of crack propagation and microscopic investigation of rock failure in the direct proximity of the cutter tip. Rock failure mechanisms are compared with corresponding cutting forces to establish a new understanding of the damage induced by force peaks followed by sudden stress release.

**Publication D** closes the loop between new measurement methods, a deeper understanding of rock failure and the practical application within TBM performance prediction. While the most accurate method to predict the net penetration rate of hard rock TBMs are full scale cutting tests, they are impractical or even impossible for many projects due to the required large sample size. At the same time, the results presented in the paper reveal that common prediction models based on uniaxial compressive and Brazilian tensile strength are not capable of predicting the cuttability of certain rock types. Thus, a new laboratory test, namely a small scale cutting test is developed. It is proposed as the geotechnical standard test for a new TBM performance prediction model. The developed test rig is protected by a patent.

# A. Cutter force measurement on tunnel boring machines - System design

This paper is authored by Martin Entacher, Gerhard Winter, Thomas Bumberger, Klaus Decker, Istvan Godor and Robert Galler and was published in *Tunnelling and Underground Space Technology* 31 (2012), pages 97-106

Loading of a TBM disc cutter is usually derived by dividing the total thrust by the number of cutters which gives an approximate average loading of 250 kN for a typical 17" cutter. However, laboratory cutting tests infer that the loading of a cutter oscillates strongly and can reach peaks that are a multiple of the average forces. Knowledge of the true forces acting on a disc cutter is of great importance to gain further insight in areas such as cutter wear, brittle fracture of cutter rings, fatigue and the mechanism of rock breakage in different geological formations.

Consequently, the development of a measurement method to determine the three-dimensional loading situation of a disc cutter in real-time was conducted. An investigation of the deformation state of a typical disc cutter and its casing was performed by means of the finite element method. Subsequently, a measurement method that is not affected by cutter change was developed by finding suitable spots for sensor placement in the cutter saddle. Laboratory tests proved the feasibility of the developed measurement method that is now ready for implementation on a TBM.

## A.1. Introduction

### A.1.1. Motivation

Remote cutter monitoring is of increasing importance in mechanized tunneling. It allows gaining information about the excavation process at the place where cutters and tunnel face are interacting, a region that cannot be observed by other means. Recently, TBM manufacturers started to develop and implement technologies that allow for continuous observation of temperature, rotational speed and vibration of a cutter (Shanahan 2011). This article presents a measurement method for monitoring cutting forces.

The normal force acting on a cutter is, at present, calculated by dividing the total thrust minus friction forces by the number of cutters. It is known from laboratory cutting tests (Entacher et al. 2012a) and in situ measurements (Hopkins and Foden 1979, Samuel and Seow 1984, Zhang et al. 2003b) that peaks of cutting forces can be a multiple of the mean force, so this approach is a serious simplification. The knowledge of the true forces acting on a disc cutter is of great interest for several reasons. Presuming that cutting forces correlate with geotechnical parameters like strength and stiffness, continuous observation of cutting forces would allow for mapping geological conditions at the tunnel face. Fukui and Okubo (2006) presented an easy and feasible approach to correlate the total TBM thrust with the compressive strength of rock mass. Such methods could be extended widely with the knowledge of individual cutting forces. A first scientific outline of this topic is given in Entacher et al. (2012a).

It is very likely that the characteristics of cutting forces include valuable information about rock breakage mechanisms. There are serious efforts to simulate the process of rock cutting (Su and Akcin 2011, Rojek et al. 2011, Wang et al. 2011) but until now it is not possible to model the complex excavation process satisfactorily, especially not for disc cutting. Hence, a lot of experimental and field data is needed to gain further understanding of the underlying mechanisms.

Laboratory cutting tests are successfully used to investigate rock breakage and to predict penetration rates (Gertsch et al. 2007). Obviously such tests cannot fully simulate real excavation conditions but cutter monitoring could help to understand the differences between laboratory setups and real site conditions and define what areas can be sufficiently investigated with cutting tests and what lies beyond their scope.

According to Rostami (2008), the distribution of cutters over the cutterhead is of great importance in cutterhead design in order to reach a sufficiently distributed loading situation. Monitoring of cutter forces could help optimize this process by gaining information about the influence of cutterhead stiffness, different rotational speeds and dynamic loading situations.

Regarding TBM operation, force monitoring will indicate the cutter state, e.g. a significant increase of rolling force could be a sign for a blocked cutter. Gajewski and Jonak (2011) recently presented a suitable method to identify worn picks by monitoring cutting forces and torque. Knowledge of cutting forces will indicate the percentage of thrust force that actually reaches the tunnel face and allow for an observation of uneven force distribution during a turning maneuver.

Some previous approaches to measure cutter forces were of great success, but to the knowledge of the authors, none of them is used on TBM sites on a frequent basis. One of the main reasons for this is that in all previous works sensors are placed at the cutter shaft with cables connected to the casing. This results in great disturbance of the construction process during cutter change and is therefore not suitable for continuous use.

### A.1.2. Related work

The first successful measurement of cutting forces on a TBM was performed by Gobetz (1973). It was possible to acquire measurement data on an excavation length of 12 ft. It was discovered that cutting forces oscillate strongly and that peak forces are much higher than assumed at that time.

Hopkins and Foden (1979) successfully equipped a cutter of a raise boring reaming head with strain gauges to measure its loading. They used a telemetry system to transfer the measured data which made data transfer a lot easier but the instrumentation was still not reliable enough.

Samuel and Seow (1984) again instrumented two cutters of a TBM and found techniques that allowed for more thorough investigations than before. In all, about 20 minutes of excavation were recorded. They concluded that, in spite of the dynamic characteristic of cutting forces, no significant spectral energy was recorded above 10 Hz in the frequency domain.

Zhang et al. (2001, 2003a, 2003b) measured forces acting on button cutters and offered various interpretations regarding rock breakage (i.e. crack length observations) and TBM operation. They dealt very thoroughly with the calibration of the implemented sensors and included aspects of temperature in their work.

All of the previously described work was conducted as successful research projects but did not have the potential to be implemented in TBM tunneling on a regular basis. The first system with that goal was developed within the framework of Tunconstruct (Beer 2009). The “Mobydic”-system aims to monitor disc cutter health in shield tunneling by measuring cutter forces, temperature and rotation. Even though the system is successfully implemented on some tunnel boring machines, it suffers from a serious disadvantage that it has in common with all projects mentioned. The instrumentation is located inside the cutter and thus affects the construction process, i.e. cutter change, in a way that is not accepted by construction companies in the long term. The reason for the choice of this location is a clear deformation state of the cutter shaft and the chance to measure the deformation of the structure as near to the tunnel face as possible. However, this paper presents a very feasible way to accurately measure cutting forces in the cutter saddle.

## A.2. Finite element simulation model

### A.2.1. Cutter design

History of cutter design and recent improvements are described by Sänger (2006) and Roby et al. (2008). Due to health and safety requirements and the need for efficient

cutter changes, front loading systems have lost importance in TBM traffic tunneling. The most used back-loading systems are wedge-lock and conical saddle systems. A detailed investigation by means of numerical simulation of the wedge-lock system can be found in Bumberger et al. (2011). This section describes the numerical simulation of a conical saddle system with the software Abaqus CAE 6.10.

The goal of the finite element simulation model was to calculate realistic deformations of the disc cutter and its casing to determine feasible locations for sensor placement. Hence, all structurally relevant parts were modeled in adequate detail whereas parts such as sealings were neglected. As the focus lies on the investigation of the cutter saddle, cutter ring, hub and bearing were modeled as one part (Fig. A.1a). It interacts with the cutter shaft with a "hard contact" boundary condition. This means that interacting parts cannot penetrate each other in the normal direction, whereas their relative movement in the lateral direction is controlled by Coulomb friction with an associated friction coefficient (0.1 in all cases). The conical bottom side of the shaft (Fig. A.1b) was placed on top of four conical inserts (Fig. A.1c) that interact with the casing (Fig. A.1d) on their back- and bottomside. All interaction zones were again defined as "hard contact". All parts are held together with one M16 (Fig. A.1e) and one M24 bolt (Fig. A.1f) on each of the four supports.

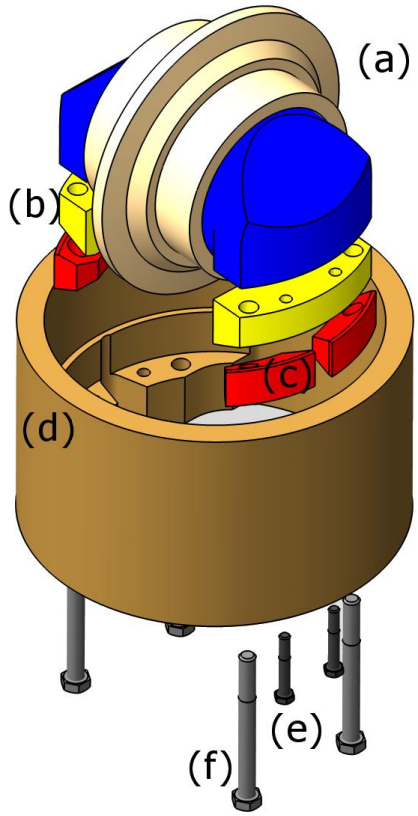


**Fig. A.1.:** Explosion drawing of a conical saddle system

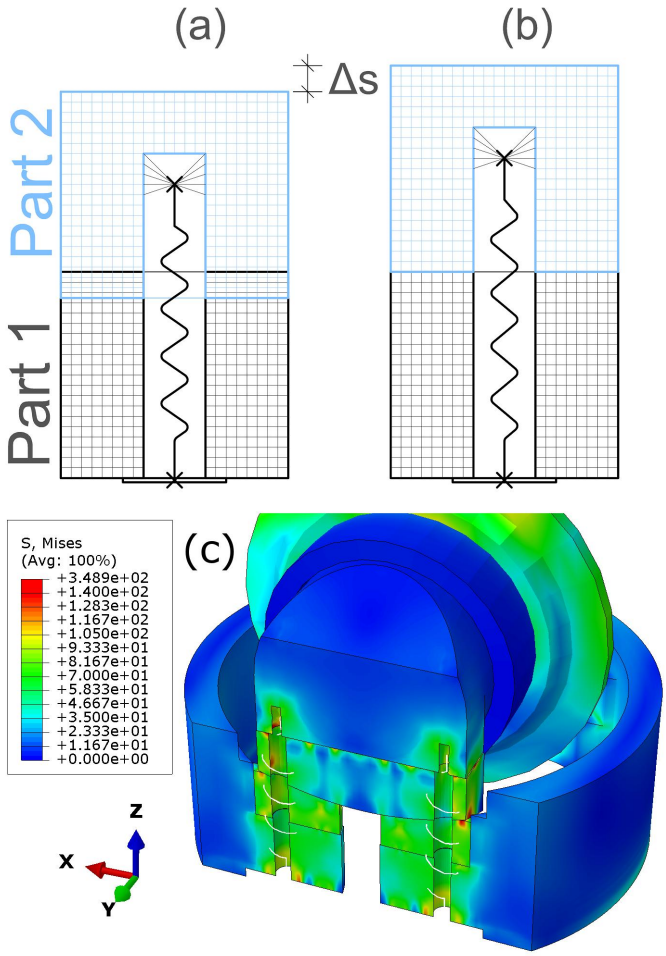


**Fig. A.2.:** Pre-stressed bolts, (a) spring without tension, (b) tensioned spring, (c) simulation result (stress according to von Mises yield criterion)

The material law was chosen to be linear elastic with a Young's modulus of 210 GPa. The bearings in a hard rock cutter are pre-stressed very firmly which results in an approximately linear stress-strain relationship. Hence, the mistake that results from simplified modeling of the bearings is very small.

Normal and side forces were applied to a rigid section on top of the cutter in accordance with Fig. A.10 that approximately represents the indentation area of a cutter. With that technique, extreme peaks due to the application of point loads can be avoided. Rolling forces were applied in such way that the resultant goes through the center of the cutter because the rotation of the cutter was not blocked in the model. Due to the geometry of the structure this load application still produces a moment that is similar to the application of rolling forces on top of the cutter ring, but smaller.

All parts were meshed "structurally" with 8-noded hexahedron elements with reduced integration. In order to avoid the use of tetrahedron elements, extensive partitioning of

all parts was required.

Many techniques that are used to model pre-stressing of bolts are not capable of calculating the changes of pre-stress due to external loads. As this parameter was one of the major desired outputs, great care was taken to model the bolts accurately. It was achieved by using spring elements that were connected with two reference points in the area of the screw head and the thread. The reference points were connected to all nodes within the screw head area and all nodes that would interact with the thread, respectively. At the beginning of the simulation, the parts that were pressed together with bolts intersected one another (Fig. A.2a). Subsequently, the upper part was pulled apart until contact was found (Fig. A.2b). After the application of external loads, the change of pre-stress $\Delta F$ was then found by calculating the difference in displacement of the reference points in vertical direction $\Delta u_3$ multiplied by the bolt's stiffness k, i.e. $\Delta F = \Delta u_3 \, k$. A representation of the springs in the simulation can be seen in Fig. A.2c.

### A.2.2. Results

It shows that the conical saddle system ensures a very good load distribution. Fig. A.3 shows the mises stress in the cutter, the inserts and the casing. It can be seen that the inserts are the most stressed parts. However, they are nitrified and can be changed if they happen to wear out, hence the casing is well-protected from severe damage.

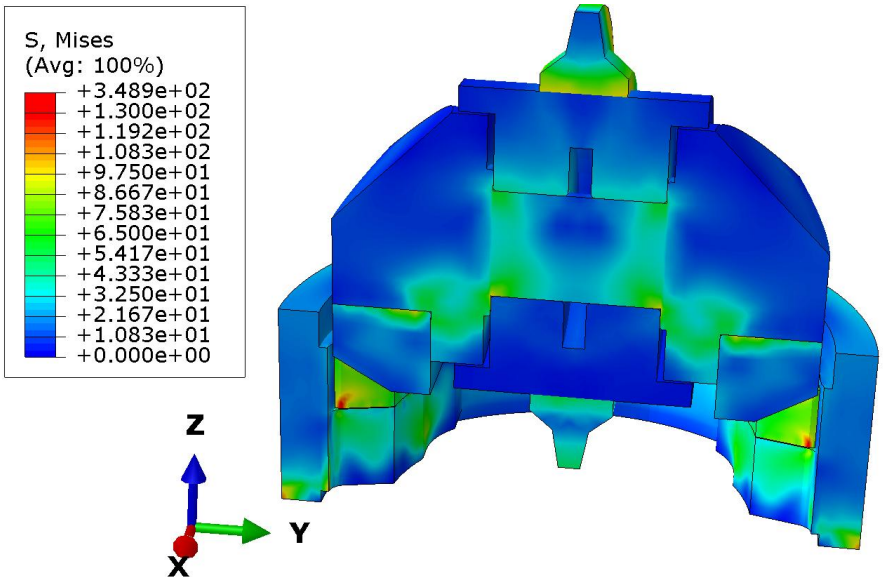


**Fig. A.3.:** Cut view of the simulation model (stress according to von Mises yield criterion)

Fig. A.4 shows the $\sigma_{33}$-distribution on the bottom side of the casing after the application of normal and side forces. On close examination, slight differences in the stress distribution under the M16 screw heads can be observed. The same differences would

be observed for the M24 bolts, if the scale was adapted. It indicates that utilization of the bolts as measurement instruments could be a promising approach.

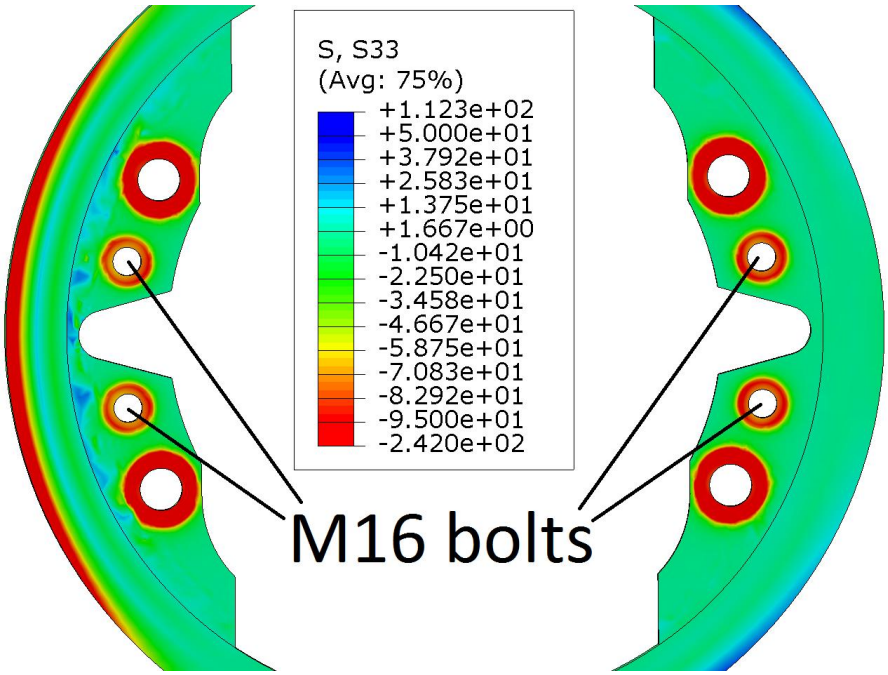


**Fig. A.4.:** $\sigma_{33}$ under the screwheads at the bottomside of the casing

## A.3. Measurement method

### A.3.1. Measurement bolts and washers

The goal was to develop a robust measurement method to measure cutting forces in real-time that withstands the rugged environmental conditions in TBM tunneling and reduces the disturbance caused by the construction process to a minimum. Based on the observed deformations of the finite element simulation model, different locations for sensor placement were evaluated theoretically. Consequently, the most suitable design was chosen and a setup for laboratory testing was defined considering realistic loading conditions. All sensors were placed in the cutter saddle in such way that cutter changes would not be affected.

Fig. A.5 shows the distribution of displacements after load application (a) and one step before that, after pre-stressing of the bolts (b). It can be seen that the deformation indicates an inclined flow of forces. In the conceptual stage, different strain gauge locations were evaluated theoretically. It was found that application of strain gauges on one of the inner edges of the casing would not bring very significant results. Designs

where strain gauges are placed in openings inside the saddle were considered to be feasible, but they were too complicated in terms of manufacturing.

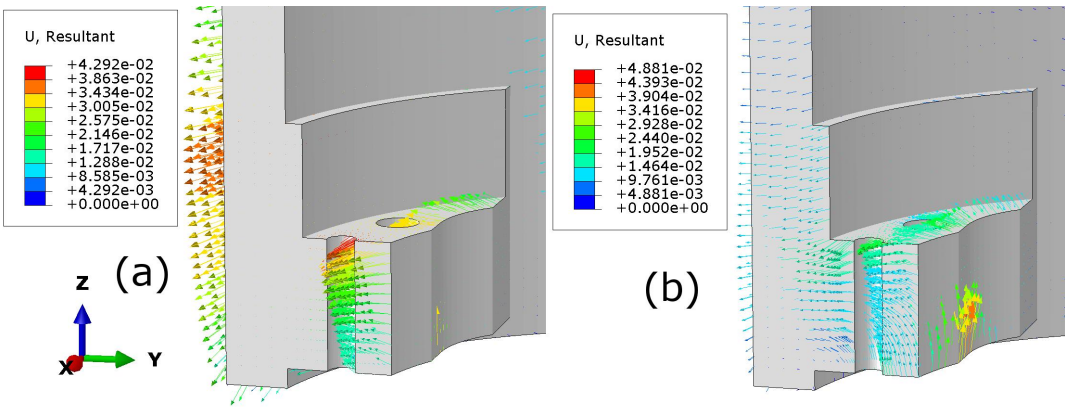


**Fig. A.5.:** Distribution of displacements in the cutter saddle, (a) after load application (b) after pre-stressing of the bolts in mm

As shown in the previous section, the simulation indicated that the reaction of the bolts would display a change in side force correctly (see Fig. A.4). Hence, it was decided to concentrate on the measurement of bolt forces. Whereas the M24 bolts are changed on a very regular basis, e.g. daily, the M16 bolts that keep the inserts in position, are changed very rarely (e.g. every two months). Consequently, equipping these bolts with sensors appeared to be very convenient.

It was chosen to use two different types of sensors: First, measurement washers were placed beneath the screw head (Fig. A.6a). They have an integrated strain gauge full bridge that is calibrated in such a way that it measures the bolt force. Second, measurement bolts with a strain gauge full bridge inside the bolt shaft were used (Fig. A.6b). The strain is again calibrated to correlate with the bolt force.


**Fig. A.6.:** Measurementh washers (a), installation of measurement bolts (b)

The back calculation of forces by measuring the vertical shortening or elongation of the bolts is explained in Fig. A.7. It shows that forces can be identified clearly by

looking at the translation and the rotation of the illustrated plane. From a mathematical point of view, three measurement points would be needed to calculate three force components. The fourth point allows for an error quantification.

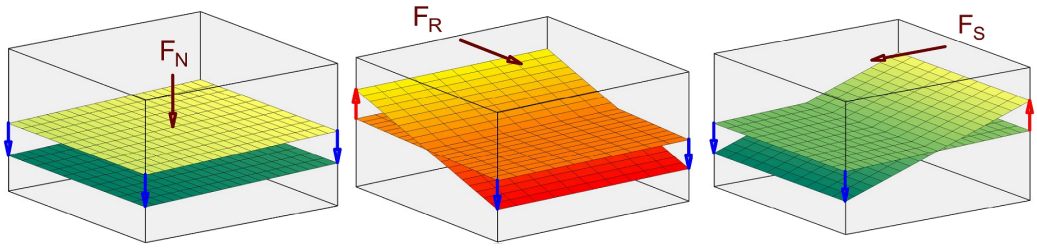


**Fig. A.7.:** Schematic sketch of the back-calculation of forces from bolt forces

### A.3.2. Strain gauges and prescale films

Additional strain gauges were applied to the casing and the inserts to obtain more information about the structure during laboratory testing. Furthermore, prescale films were used to measure the occurring surface pressure between casing and inserts (see Fig. A.8). When loaded, a chemical reaction causes a discoloration of the film that correlates with the applied surface pressure. In order to obtain good results, great care must be taken during the calibration of the films regarding humidity, temperature and loading time.

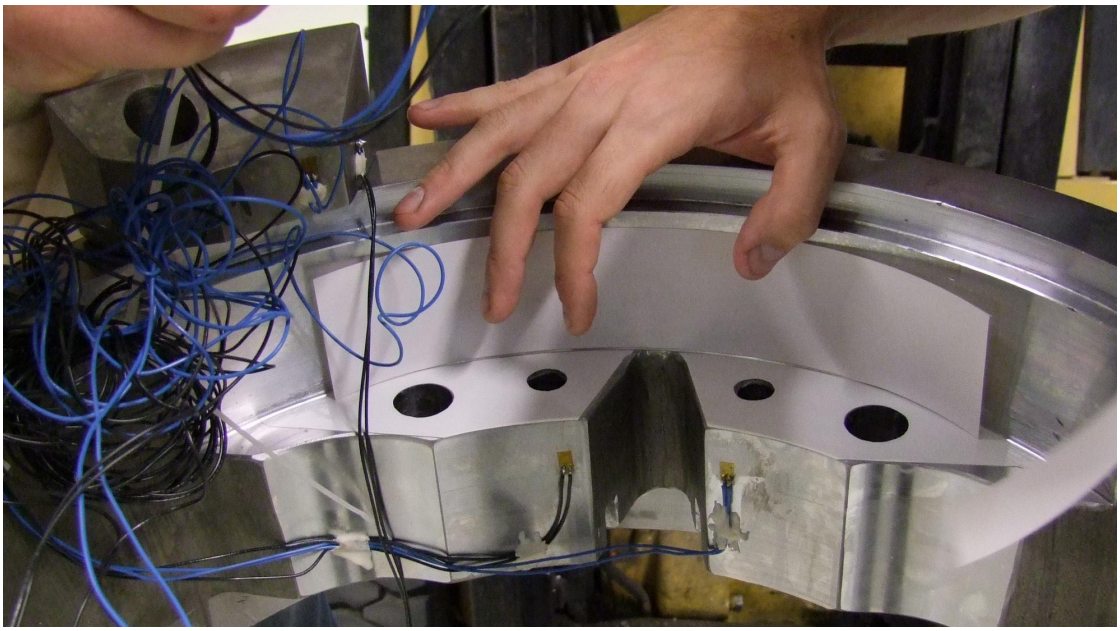

**Fig. A.8.:** Application of single strain gauges and prescale films

## A.4. Laboratory testing

### A.4.1. Experiment setup

Fig. A.9 shows the experiment setup. All tests were performed at the chair of Subsurface Engineering, Montanuniversitaet Leoben, Austria using a MTS 815 servo-hydraulic press with digital feedback control. In order to be able to apply loads in three different directions, the rotation of the cutter was blocked and the ring was replaced with a spherical cap (a). The load application element was designed to be able to move freely in the horizontal direction (b). It ensures sufficient distribution and centric transfer of loads for all loading cases. Above that device, a 1000 kN load cell was installed (c). The cutter casing was identical to a real one except from being a little smaller in height for practical reasons. It was placed in a clamping device (d) where it was fixed with four bolts.

The assembly was done in the following order: (1) Connection of casing and inserts with measurement bolts and washers (200 Nm tightening torque), (2) fixture of the cutter with four M24 bolts (800 Nm tightening torque) to the casing, (3) attachment of the casing to the clamping device, (4) connection of all sensors to the amplifiers, installation of load cell and load application element.

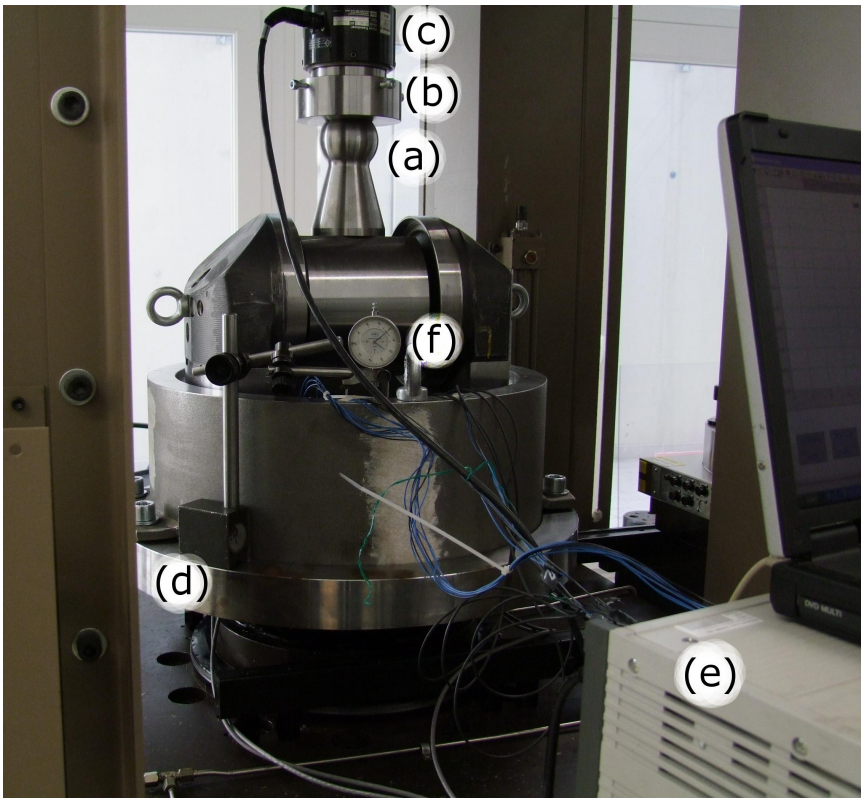


**Fig. A.9.:** Experiment setup

The measurement bolts (four strain gauge full bridges) were connected to a HBM Spider (digital signal amplifier). All other sensors, namely measurement washers (four strain gauge full bridges), additional strain gauges (8 single strain gauges) and two temperature gauges were connected to an amplifier of the type HBM MGCplus (e). Additionally, an analogue dial gauge (f) was used during testing to observe relative movements of the structure. Applied load and deformation were obtained by connecting the MTS hydraulic controller to the MGCplus. Both amplifiers were then connected to a Laptop where the software Catman AP was used during testing. The post processing was done with MATLAB.

## A.4.2. Loading cases

The loading of a disc cutter consists of three major components: normal force ($F_N$), rolling force ($F_R$) and side force ($F_S$). Their definition and the positions of sensors can be seen in Fig. A.10. Previous studies (Gobetz 1973, Zhang 2003a) have shown that the occurring twisting moment is negligible. Consequently, it was not measured.

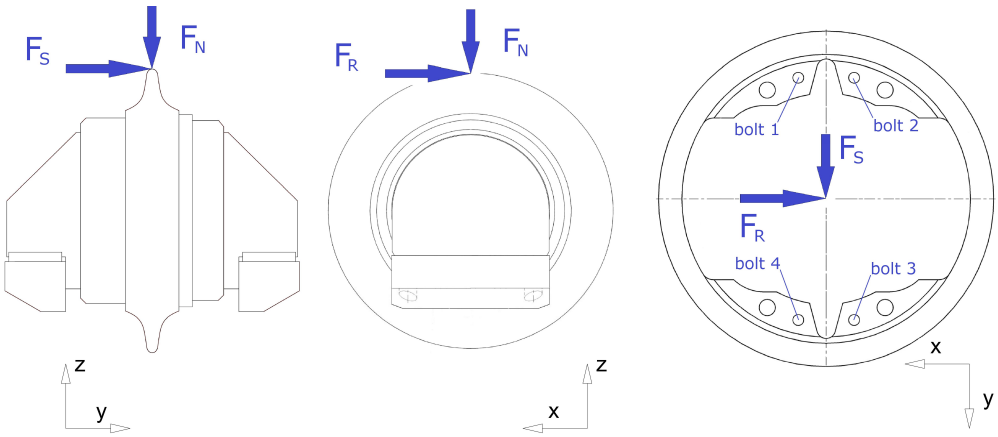


**Fig. A.10.:** Definition of cutting forces and measurement positions

Fig. A.11 shows the forces that were measured during linear cutting tests on Imberg Sandstone with a 10" disc cutter in the time domain (a) and a spectral analysis of the same data that was obtained using a discrete fourier transform algorithm (b).

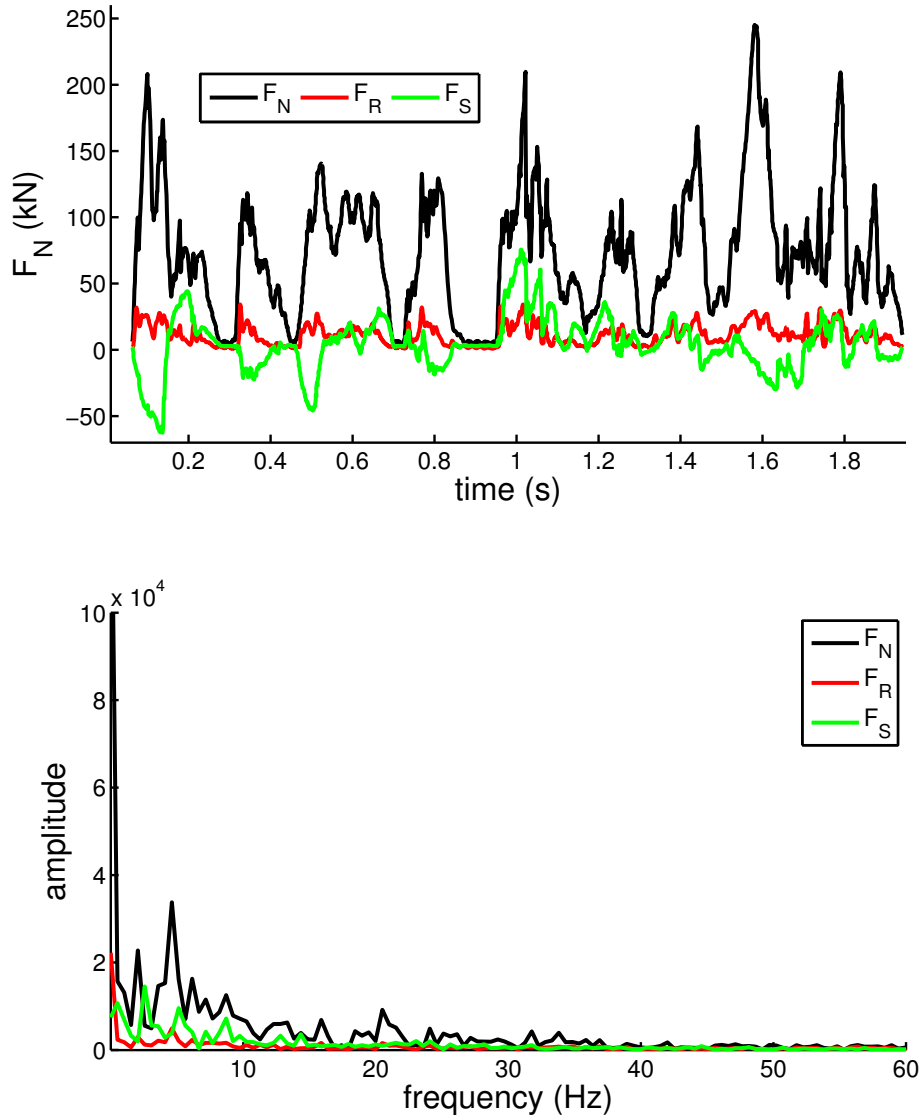


**Fig. A.11.:** Cutting forces recorded during a linear cutting test, (a) time-domain, (b) frequency-domain

The cutting test in Fig. A.11 was performed with a cutting velocity of approximately 1.5 m/s. It shows that the majority of the spectral energy lies below 10 Hz which is in accordance with Samuel and Seow (1984). However, cutting frequencies are obviously dependent on the cutting speed which can be around 3.0 m/s in the gauge area of the cutterhead on common TBMs. Hence, frequencies of up to 20 Hz should be accounted for using disc cutters. That is significantly lower than the cutting frequencies that occur when using point attack picks which can be in the range of a few hundred Hz (Rojek et al. 2011).

As a disc cutter is a very stiff structure, relevant resonance frequencies are well above 20 Hz. Hence, true dynamic effects are not relevant for the calibration process. For

laboratory testing, the load was applied with 10 Hz regularly and twice with up to 20 Hz. The mean normal force of a cutter is about 250 kN. As can be seen in Fig. A.11, peaks are a multiple of that value. Therefore, tests were performed with normal forces of up to 990 kN.

Two different clamping devices, a flat one and one with an inclination of 11°, were used (Fig. A.12 and Fig. A.13). The flat one was used to obtain a loading situation of pure normal force (0°). The inclined one was used to simulate three different loading cases depending on the relative position of the cutter casing within the clamping device. This resulted in one loading case with a combination of normal and rolling force (11°R), one with a combination of normal and side force (11°S) and one with a combination of all three force components (11°RS). An overview of loading cases 0°, 11°R, 11°S and 11°RS is given in table A.1.

**Fig. A.12.:** 0° test setup with flat clamping device

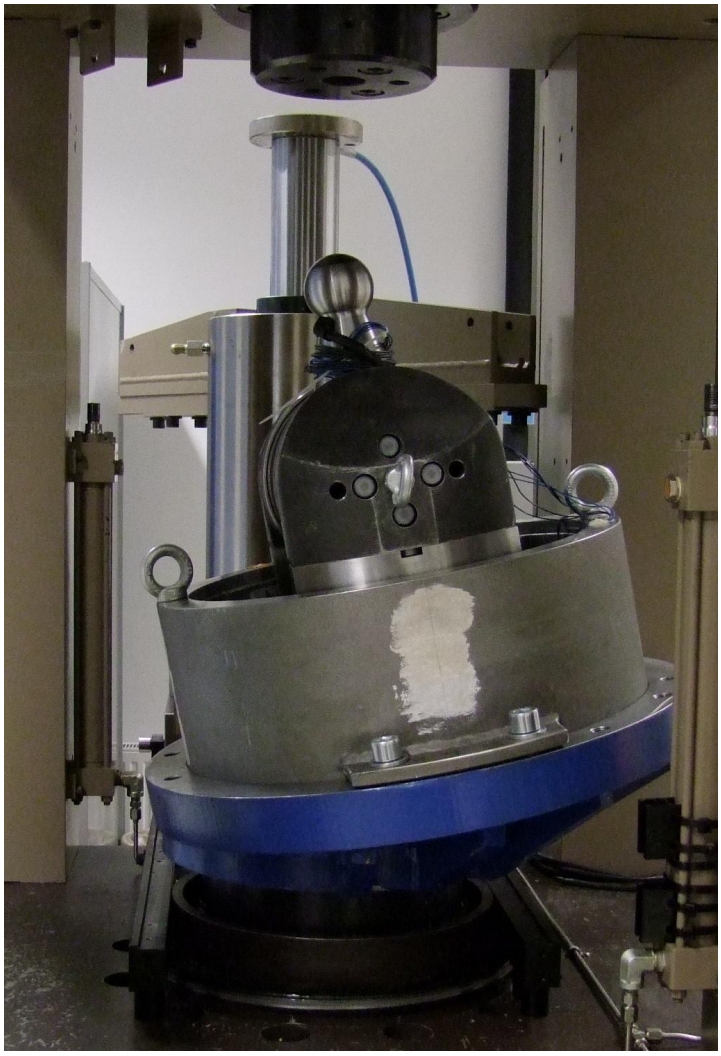

**Fig. A.13.:** 11° test setup with inclined clamping device

| Loading Case | $F_N$ | $F_R$ | $F_S$ |
|---|---|---|---|
| 0°: | $F_{MTS}$ | 0 | 0 |
| 11°R: | $F_{MTS}$ x cos(11) | $F_{MTS}$ x sin(11) | 0 |
| 11°S: | $F_{MTS}$ x cos(11) | 0 | $F_{MTS}$ x sin(11) |
| 11°RS: | $F_{MTS}$ x cos(11) | $F_{MTS}$ x sin(11) x cos(45) | $F_{MTS}$ x sin(11) x sin(45) |
| | | | |
| 0°: | 100.00 % | 0.00 % | 0.00 % |
| 11°R: | 98.16 % | 19.08 % | 0.00 % |
| 11°S: | 98.16 % | 0.00 % | 19.08 % |
| 11°RS: | 98.16 % | 13.49 % | 13.49 % |

**Table A.1.:** Loading cases for the laboratory tests

| 0° (990 kN) | bolt 1 | bolt 2 | bolt 3 | bolt 4 |
|---|---|---|---|---|
| reduction of bolt force | 1.45 kN | 1.23 kN | 1.21 kN | 1.37 kN |
| signal quality | very good | very good | very good | very good |

| 11°R (350 kN) | bolt 1 | bolt 2 | bolt 3 | bolt 4 |
|---|---|---|---|---|
| reduction of bolt force | 0.13 kN | 0.37 kN | 0.38 kN | 0.20 kN |
| signal quality | good | very good | very good | good |

### A.4.3. Results

Fig. A.14 shows a comparison of applied load and reduction of pre-stress in the measurement washers and bolts for loading case 0°. All sensors sufficiently follow the load path but the results of the measurement bolts are far better. It is known that measurement washers are very sensitive to eccentric loading. As can be observed in Fig. A.5, the flow of forces is not vertical in the cutter saddle, which might worsen the signal of the washers. Hence, they were not considered further.

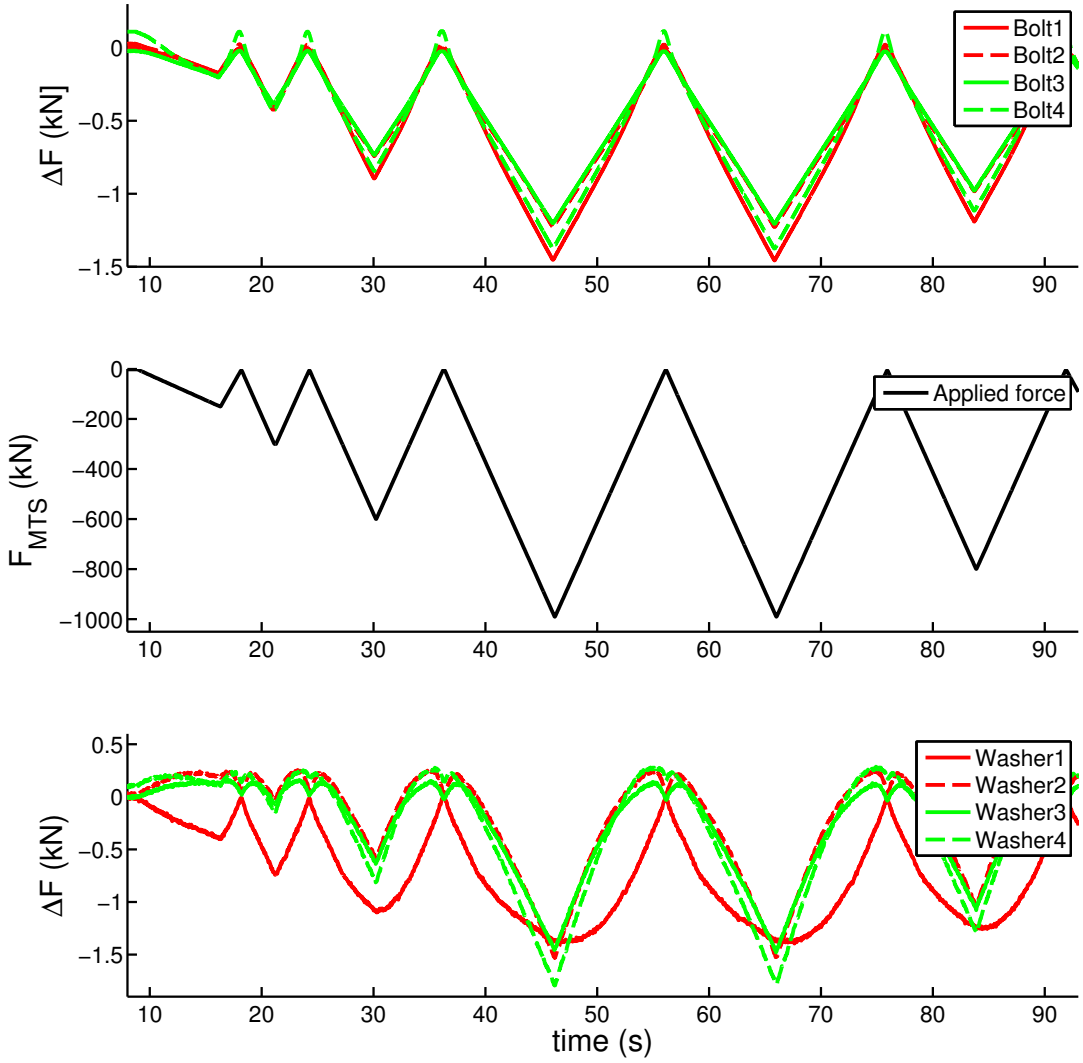


**Fig. A.14.:** Results for loading case 0°

Fig. A.15 shows a result of loading case 11°R, a combination of $F_N$ and $F_R$. Bolts 1 and 4 should have the same values but in the direction of $F_R$ there is a very short distance between the measurement bolts (compare Fig. A.6b). Hence, the results were usually not as clear as for other loading cases. However, the tendency is still very good.

Fig. A.16 shows a result of loading case 11°S, a combination of $F_N$ and $F_S$. As expected, positions 1 and 2 show a significantly larger loss of pre-stress than bolts 3 and 4. The distorted characteristic of the latter will be discussed in section A.5.3.

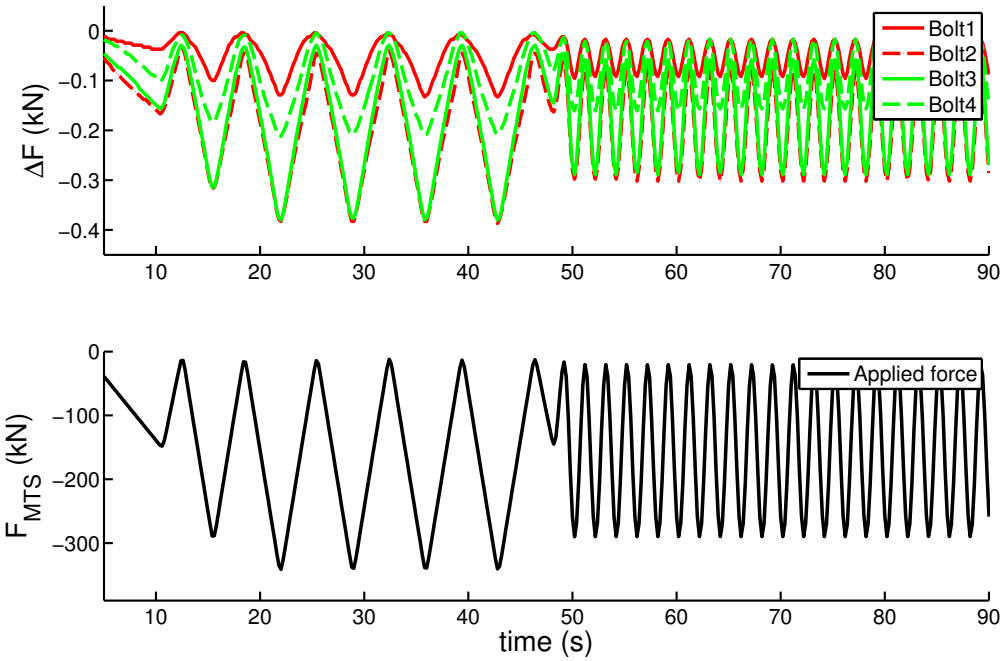


**Fig. A.15.:** Results for loading case 11°R

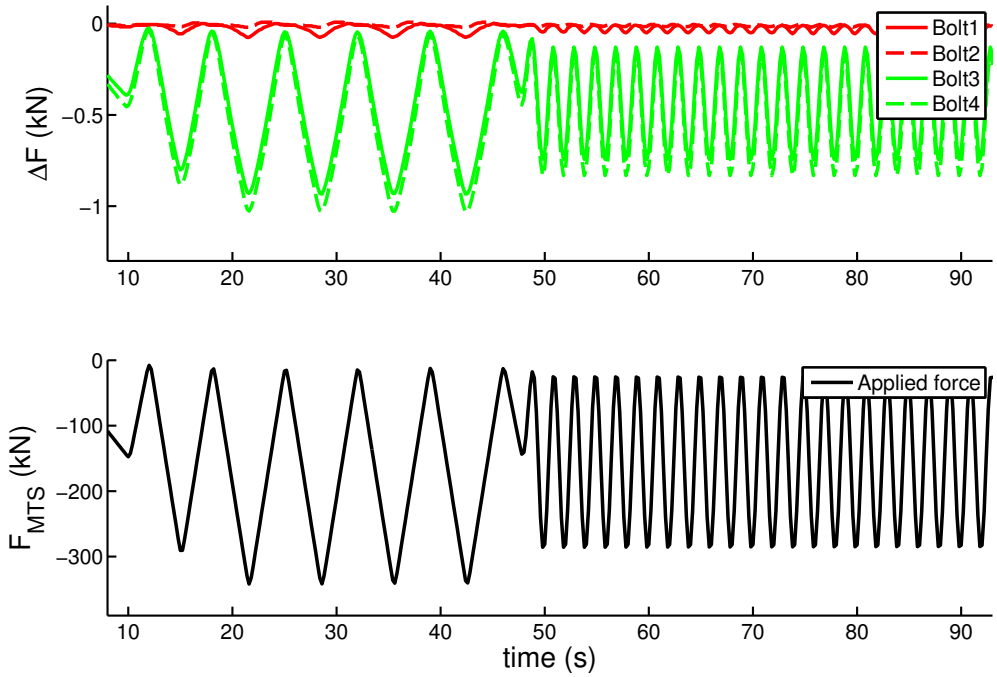


**Fig. A.16.:** Results for loading case 11°S

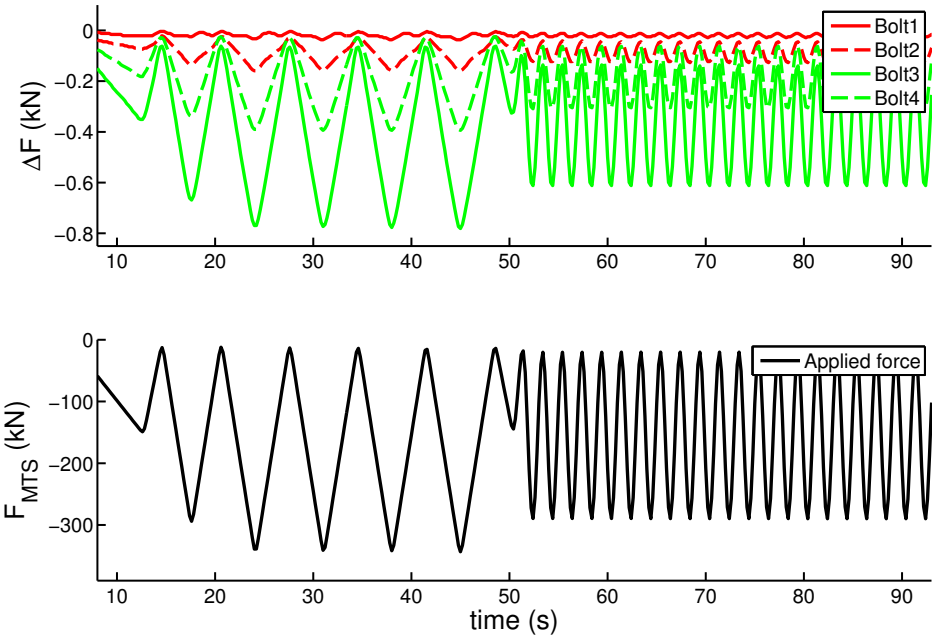


**Fig. A.17.:** Results for loading case 11°RS

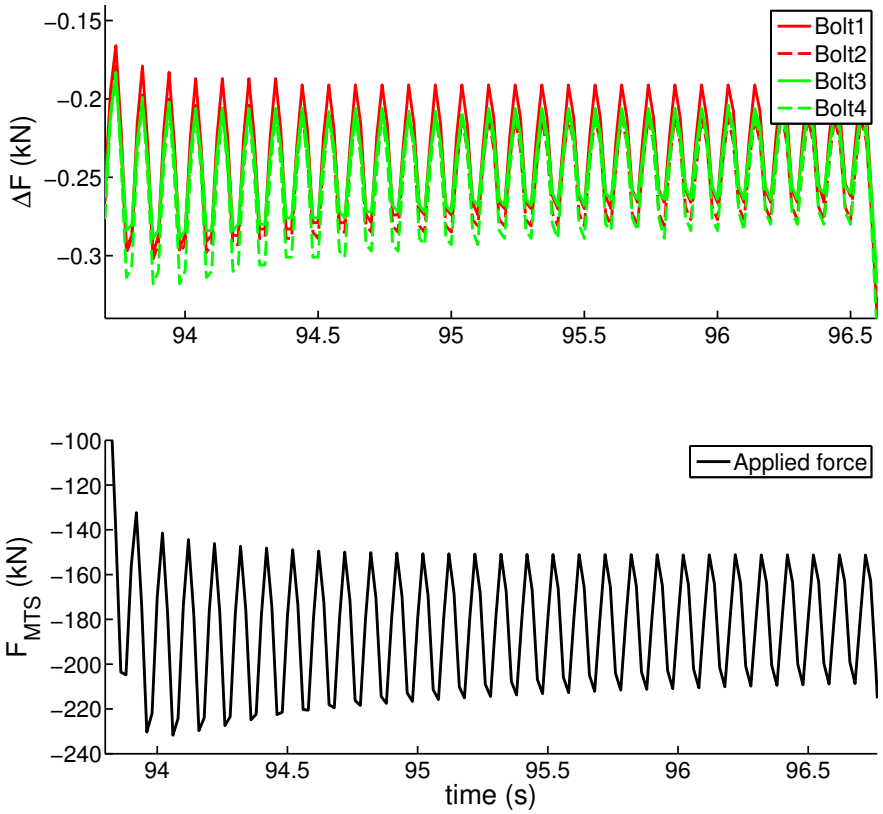


**Fig. A.18.:** Close-up result for loading with 10 Hz

Fig. A.17 shows a result of loading case 11°RS, a combination of $F_N$, $F_R$ and $F_S$. It shows a perfectly inclined plane as would be expected by combining the separate pictures in Fig. A.7. Again, the signal of bolt 1 is rather distorted.

Some tests were performed with frequencies of up to 20 Hz. It showed that the quality of the results did not decrease. However, most tests were performed with frequencies up tp 10 Hz in order to prevent damaging the hydraulic press (Fig. A.18). Table A.2 gives a short summary of the presented results.

| **0° (990 kN)** | **bolt 1** | **bolt 2** | **bolt 3** | **bolt 4** |
|---|---|---|---|---|
| reduction of bolt force | 1.45 kN | 1.23 kN | 1.21 kN | 1.37 kN |
| signal quality | very good | very good | very good | very good |
| **11°R (350 kN)** | **bolt 1** | **bolt 2** | **bolt 3** | **bolt 4** |
| reduction of bolt force | 0.13 kN | 0.37 kN | 0.38 kN | 0.20 kN |
| signal quality | good | very good | very good | good |
| **11°S (350 kN)** | **bolt 1** | **bolt 2** | **bolt 3** | **bolt 4** |
| reduction of bolt force | 0.07 kN | 0.03 kN | 0.94 kN | 1.03 kN |
| signal quality | distorted | distorted | very good | very good |
| **11°RS (350 kN)** | **bolt 1** | **bolt 2** | **bolt 3** | **bolt 4** |
| reduction of bolt force | 0.03 kN | 0.16 kN | 0.39 kN | 0.77 kN |
| signal quality | distorted | very good | very good | very good |

**Table A.2.:** Summary of the results obtained with measurement bolts

The prescale films were used in loading case 0° with a loading of 400 kN (Fig. A.19). Compared to the pre-stress of the bolts which is about 240 + 70 = 310 kN in each of the supports of the casing, an additional loading of 100 kN (400 kN / 4 supports = 100 kN / support) is not much. Even though the reduction of pre-stress in the bolts is about the same at all supports, the surface pressures vary significantly. That is because a certain moment applied with a torque wrench always results in different pre-stress. Hence, all supports are loaded differently. This effect can be reduced with the use of screw paste.

The films range from 50 to 130 MPa. Both, the results of the film and the numerical simulation show a similar stress gradient from the inside to the outside, hence the general behavior was captured satisfactorily. However, the average stress level seemed to be higher during laboratory testing. That could be due to high M24 bolt forces. As said before, tightening with a specific torque will always result in different force levels.

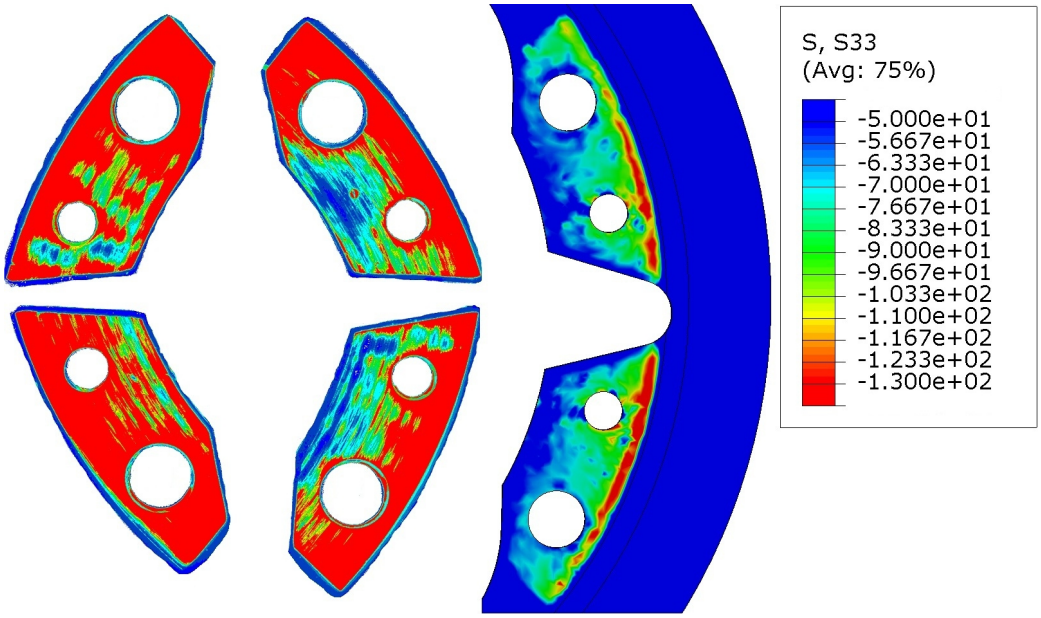


**Fig. A.19.:** Results of the prescale films (left) compared with $\sigma_{33}$ of the simulation (right)

## A.5. Discussion

### A.5.1. Comparison with related work

The introduction gives an overview of previous work in the field of remote cutter monitoring, focusing on the measurement of cutter forces. In all previous attempts, the cutter shaft was instrumented with strain gauges which in the opinion of the authors is one of the main handicaps that prevents frequent use on TBMs. This article presents a feasible way of measuring cutting forces at the cutter saddle which is not affected by cutter changes.

### A.5.2. Non-linearities and assembly tolerances

Gobetz (1973) and researchers after him observed the phenomenon of elastic hysteresis that describes a slight non-linearity in the force - deformation relationship of the cutter. As said before, the sensors that led to this observation were placed at the cutter shaft which is very close to the location of load application. Every construction element shows signs of non-linearities due to settling, friction and contact, especially when assembled from several separate parts. Therefore, a measurement very close to the tunnel face, i.e. the point of load application, will give clearer results than a measurement that is taken further away, where more and more parts interact and small structural non-linearities accumulate. However, by looking at an evaluation of this effect in Fig.

A.20 and more importantly the results in section 4.3, the present study comes to the conclusion that this effect is again negligible.

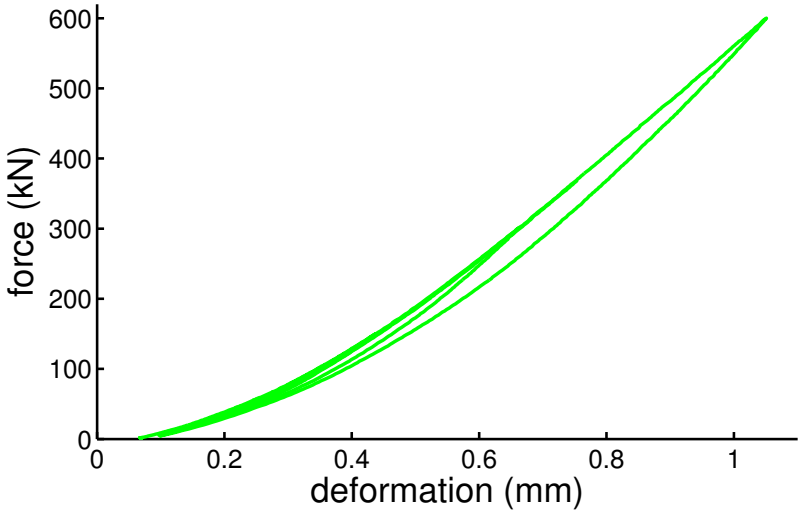


**Fig. A.20.:** Force-deformation relationship of the structure during laboratory testing

The assembly of cutter, inserts and casing always allows certain tolerances that are needed to account for manufacturing tolerances and for practical cutter installation and change. Fig. A.21 shows the results of the prescale films from the back side of the inverts for vertical loading. Even though the films only capture stresses in the range from 50 to 130 MPa, the uneven stress distribution due to asymmetric assembly can be seen very well.

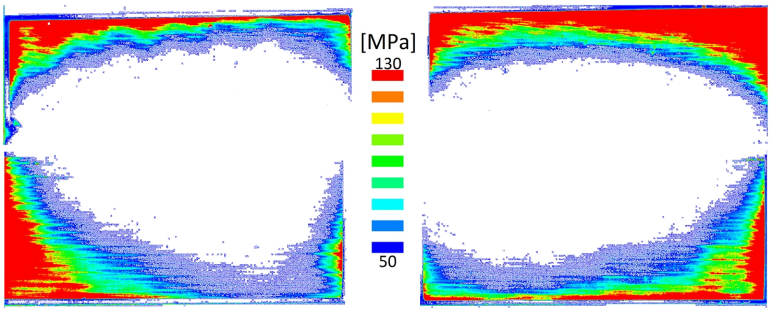


**Fig. A.21.:** Results of the prescale films from the backside of the inserts

A certain tightening torque applied multiple times will result in different bolt forces. Hence, each of the four supports will experience different surface pressures and also different structural stiffnesses which could influence the flow of forces. It was tried to capture this effect in the numerical simulation and it was found to be negligible, but it could be a further small source of non-linearity.

### A.5.3. Quality of the results

In section A.4.3, sensor outputs during loading were presented. It was seen that in loading case 11°S and 11°RS the bolts that were loaded less due to the inclination of the cutter sent signals that had a rather distorted characteristic compared with the direct and precise reaction of other bolts.

Fig. A.22 sketches the occurring forces during cutter assembly. The conical saddle has an inclination of about 30°. As the coefficient of friction is very low (about 0.1 or 0.15), the shearing force parallel to the surface of the insert is greater than the restoring force and causes a sliding down of the cutter until the bolt shaft is in contact with the drill hole.

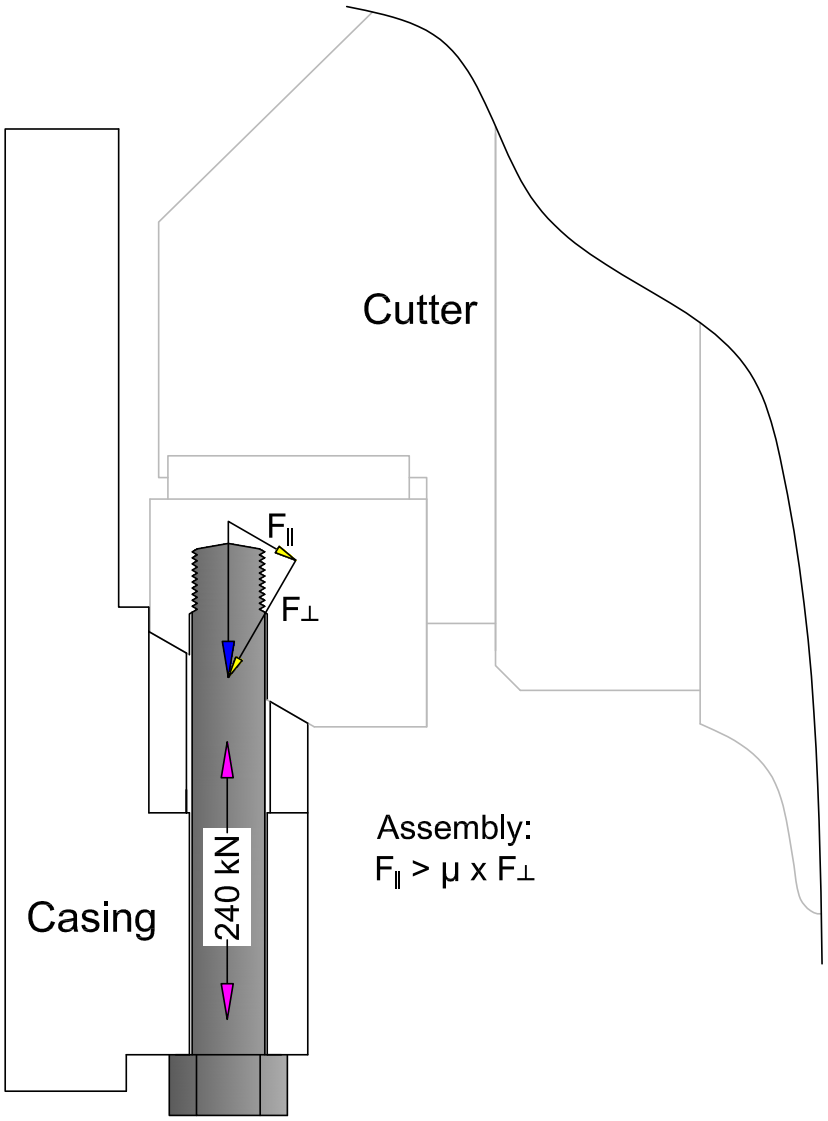


**Fig. A.22.:** Activation of shear resistance in the bolt

The system reaches equilibrium and is capable of taking considerable side forces even without the shearing resistance of the bolts, as soon as one of the opposite screws is tightened. As shown before, at least one bolt is in contact with the bore hole after assembly. Furthermore, the structure is not rigid, hence deformations will take place until an equilibrium in the lateral direction is reached. Therefore, the distorted characteristic of the sensor signals in certain loading cases could be explained by a disturbance of the force flow resulting from a tight contact between bolt and bore hole. Fig. A.23 sketches the applied load in loading case 11°S where the distorted signals were observed.

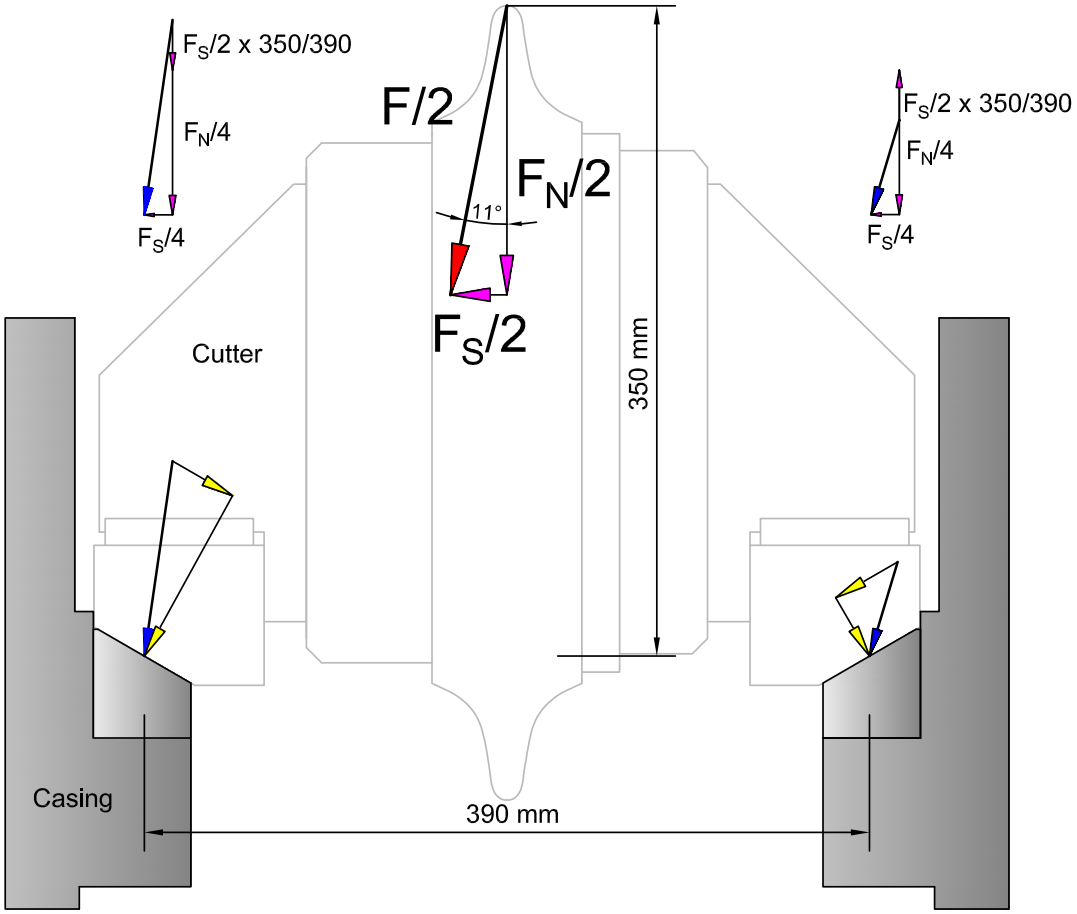


**Fig. A.23.:** Applied load in the laboratory (loading case 11°S)

It was observed that the quality of the sensor signals increases over loading time. This can be explained by leveling of surface roughness and assembly imperfections that were mentioned before. As a result of this settling, screws sometimes became loose. Sänger (2006) criticizes the danger of loosened screws as one of the main disadvantages of the conical saddle system. However, this danger can be avoided by retightening the bolts after a certain loading time, e.g. after one TBM stroke. It was found that the quality of the results and thus the flow of forces in general increases significantly when bolts

are retightened. Consequently, the authors strongly recommend retightening of bolts in order to increase the durability of a disc cutter.

### A.5.4. Limits of laboratory testing and further steps

The deformation behavior of a cutter shaft can be reproduced in a laboratory rather easily. An investigation of the cutter saddle, however, is more difficult because its stiffness is to a certain extent dependent on the overall cutterhead stiffness and varies in each position. Fig. A.24 shows a strongly enlarged view of the deformations of a cutter casing depending on its boundary conditions; (a) represents the situation on a cutterhead, (b) represents the laboratory setup. It can be seen that the deformation characteristic is slightly different.

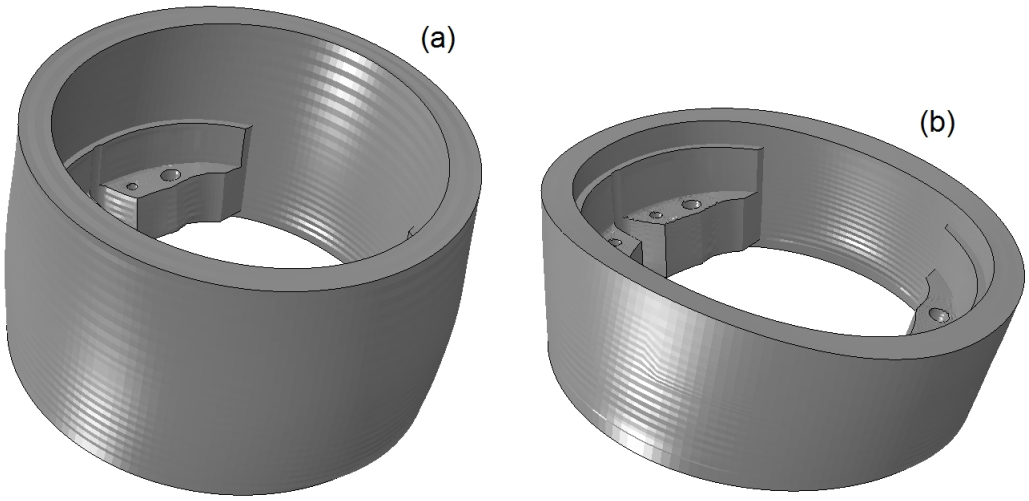


**Fig. A.24.:** Enlarged deformation of the casing with different boundary conditions, (a) in situ, (b) laboratory setup

Thus, the laboratory tests were used to confirm the feasibility of the developed measurement method, but not for a complete calibration.

In order to account for the stiffness of the casing in different cutter positions and to ensure sufficient accuracy, in situ tests will be performed to calibrate the sensor signals for each individual position. These tests should take place during the pre-assembly of a TBM and will be carried out using a specially designed clamping device that allows to load a cutter that is readily installed on the cutterhead. It will then be possible to derive a general equation for every desired position to obtain cutting forces from sensor signals.

## A.6. Conclusions

A measurement method for the monitoring of cutting forces on a TBM disc cutter has been developed in the laboratory. In contrast to previous systems, its main innovation lies in the placement of the sensors within the cutter saddle. Thus, it provides an opportunity for continuous use on a TBM without disturbing the construction process. The acquired data could allow for geological mapping of the tunnel face, e.g. detection of mixed face conditions and will help to detect undesirable peak forces and damaged cutters. Hence, the system can help to improve TBM operation.

Furthermore, it should help finding answers to fundamental questions regarding rock breakage, cutter and cutterhead design. The conclusions of this paper are the following:

- The general feasibility of the developed measurement method was proven.
- A complete calibration of the sensors will be performed in an in situ test where individual differences in the stiffness of the cutter casing will be considered.
- To collect, pre-process and transmit sensor signals to the operator's control computer in real-time, a suitable telemetric data transfer system is under development in cooperation with Geodata ZT GmbH (Austria). It will enable analysis and visualisation of the collected data within a modern tunnel information system.
- Remote cutter monitoring is on the rise. Measurement of forces requires a relatively large number of channels and sampling rate compared to measuring rotation or temperature. However, the insights that such measurements can offer are in the opinion of the authors manifold and paramount for the development of TBM tunneling.

## Acknowledgements

The authors gratefully acknowledge the financial support of this work by the Austrian Research Promotion Agency (FFG) within the Eurostars program (Eurostars project E!5514 EMSAT – Enhanced Monitoring and Simulation Assisted Tunneling). Furthermore, they are indebted to Aker Wirth GmbH for their extensive help and the cooperation provided.

# B. Cutter force measurement on tunnel boring machines - Implementation at Koralm tunnel

This paper is authored by Martin Entacher, Gerhard Winter and Robert Galler and was accepted for publication in *Tunnelling and Underground Space Technology*.

Loading of a disc cutter on tunnel boring machines (TBM) is usually estimated on the basis of global machine thrust. In order to be able to measure cutting forces of an individual disc cutter, a new measurement method was developed and published in a previous paper (Entacher et al. 2012c). This study presents the implementation process of the measurement method at the first TBM of the Austrian Koralm tunnel. Results show that peak forces are a multiple of average forces and that the distribution of forces across the tunnel face can be very irregular. The occurring forces are in very good agreement with geological features of the tunnel face such as highly fractured zones and orientation of schistosity.

## B.1. Introduction

The present paper is a continuation of the article "Cutter force measurement on tunnel boring machines - System design" published by Entacher et al. (2012c) in which a newly developed measurement method was described. The presented method is suitable for measuring forces acting on disc cutters – the main excavation tool of hard rock tunnel boring machines (TBM) – in real time. Previous attempts to measure cutting forces were carried out by Gobetz (1973), Hopkins and Foden (1979), Samuel and Seow (1984) and Zhang et al. (2003). These studies give valuable insight into the behavior of a disc cutter during rock cutting. However, in all studies the measurement equipment was designed in such way that it affects TBM operation, i.e. cutter change. Hence, recordings were conducted in a very limited time period and used for scientific purposes only. Within the Mobydic project which was part of Tunconstruct (Beer 2009), an instrumented cutter was designed that aimed to monitor disc cutters by measuring cutting forces, tem-

perature and rotation. It is reported that these cutters were used in various tunneling projects. However, as in all other previous attempts, the sensors for force measurement are located inside the cutter which results in a disturbance of the construction process when cutters are changed because data links have to be disconnected and reconnected in the dirty environment of a TBM cutterhead.

The development of the new measurement method was governed by the constraint that cutter change must remain unaffected. This should allow for a potential long-term use on a TBM. Besides scientific insight, cutter force measurement could then prove to be a valuable tool for tunneling sites by e.g. detecting cutter overloading and correlating cutting forces with geological features in real-time. Consequently, the main difference between the newly developed method and previous ones is that all sensors are placed in the cutter saddle instead of the cutter itself. Fig. B.1 schematically shows how the measurement method works. The outer larger bolts (cutter disc bolts) are used for cutter change. The smaller inner bolts (saddle bolts, marked red in Fig. B.1a) hold the inserts in place. They are equipped with strain gauges whose signal is calibrated to be proportional to the bolts' pre-stress. As soon as a load is applied to the cutter, pre-stress decreases due to the deformation of the structure. Hence, normal, rolling and side force can be calculated from the saddle bolts' signals. It should be noted that the measurement bolts remain fixed during cutter change. They are only loosened when inserts are changed which rarely happens.

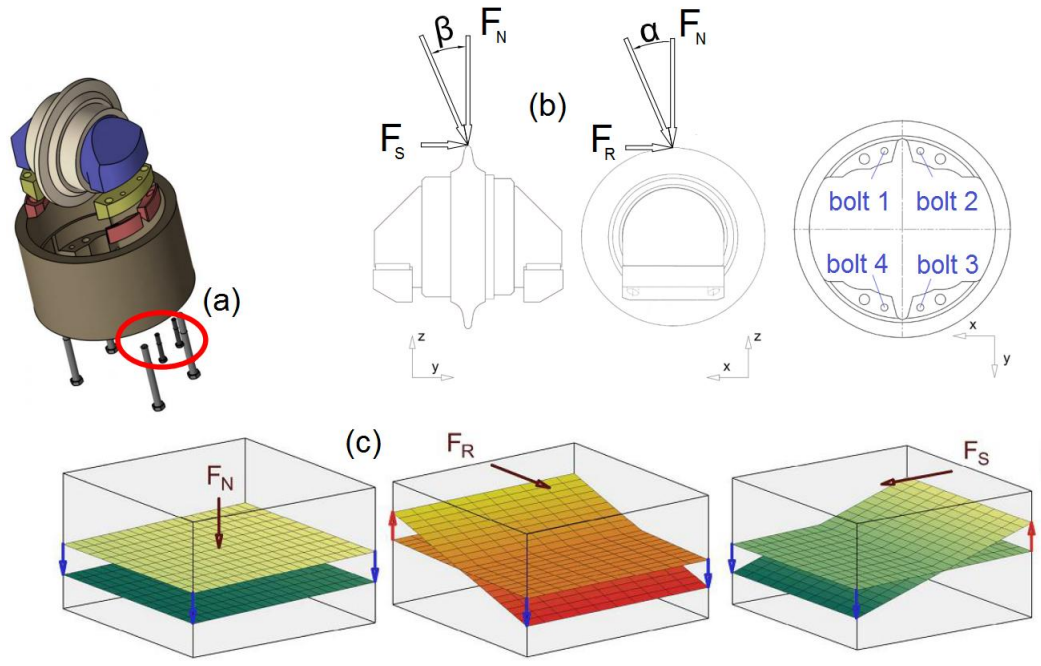


**Fig. B.1.:** Cutter force measurement method, measurement bolts (a), definition of normal ($F_N$), rolling ($F_R$), side ($F_S$) force, α and β (b), schematic sketch of bolt deformation during loading (c)

In January 2013, the first TBM of the Koralm tunnel main construction lot (KAT 2) became operational. Three cutters of this TBM were equipped with sensors to measure cutting forces. The present study describes the implementation of the measurement equipment ranging from calibration tests, arrangement of protection devices, design of data communication and storage to TBM operation and presentation of results. The works were carried out in close cooperation with Geodata GmbH, Net-Automation GmbH, Aker Wirth GmbH and the construction consortium KAT 2 (Strabag AG and Jäger Bau GmbH).

## B.2. Implementation at Koralm tunnel

### B.2.1. Project description

The 32.9 km Koralm tunnel is the most important part of a new high-speed railway connection between Austrian cities Graz and Klagenfurt. This link is also a key element of the Baltic-Adriatic Axis which runs from Helsinki and Gdansk to Warsaw and Northern Italy. It was suggested by the European Commission in 2011 as a top-priority axis for the re-evaluation of the TEN (trans-European) networks.

The tunnel which is designed for a travel speed of up to 250 km/h consists of two single-track tubes, with cross-cuts every 500 m and one emergency stop. The tunnel is divided into three main contracts. The first one, KAT 1, was built conventionally with the New Austrian Tunneling Method (NATM), KAT 2 and KAT 3 will be built with TBM. The maximum overburden is 1200 m and altogether 80% of the tunnel will be supported with segmental lining.

The central part of the tunnel goes through the Koralpe mountain massif which consists mainly of gneisses and mica schists with subsidiary marbles, amphibolites and eclogites. A more detailed description of the project can be found in Harer and Koinig (2010).

Aker Wirth GmbH provided two telescopic shield TBMs for the construction of main contract KAT 2. They have a diameter of 9.93 m, about 80 17" single disc cutters with an average cutter spacing of 65 mm. Including the back-up, each TBM has a length of approximately 160 m and a total weight of about 1,800 t.

### B.2.2. Installation of measurement equipment

Three cutters were equipped with force measurement sensors. They are aligned along one line (see Fig. B.2) with one close to the center (at a radius of r = 0.7 m), one in the face area (r = 2.65 m) and one close to the gauge area (r = 4.2 m). By covering these positions it is possible to obtain an adequate representation of the tunnel face which

enables the recognition of geological features by observing cutting forces in different areas of the tunnel face. In order to be able to do so, the rotational angle of the cutterhead has to be known at all times. In addition, cutterhead stiffness decreases with increasing radius and cutting speed increases. Hence, valuable information regarding cutterhead structure and rock breakage, i.e. rock cutting efficiency was expected.

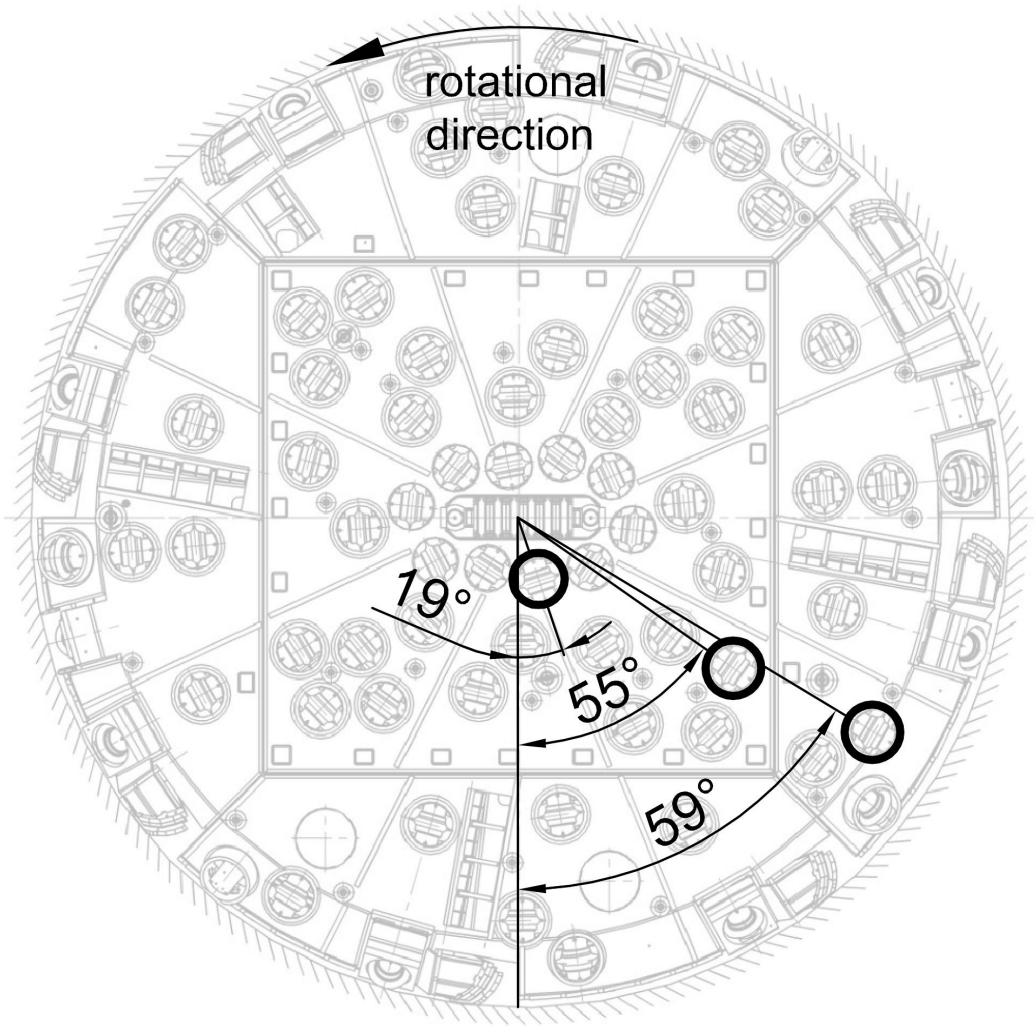


**Fig. B.2.:** Cutterhead with three sensor-equipped disc cutters (cutterhead picture ©Aker Wirth)

Fig. B.3 shows a sensor-equipped cutter. During installation, the measurement bolts are first tightened with a moment of 200 Nm in order to hold the inserts (Fig. B.3a) in place. Second, cables Fig. B.3b) are plugged onto the bolts which are then routed into the cutterhead structure for protection. After that, a steel cap (Fig. B.3c) is installed to protect bolt and cable. It is important to seal the bottom side of the cap with silicone in order to avoid water ingression which could possibly reduce durability. The 12 cables (4 for each cutter) are gathered to one bundle and covered by a protective hose. They are routed to a programmable controller where all data is recorded with a sampling rate of

100 Hz, processed and sent to a second programmable controller at the non-rotating part of the TBM using wireless radio communication. All data is then stored in a database from where it can be processed or exported. It can be accessed from the control cabin of the TBM operator and from the building-site office on the surface.

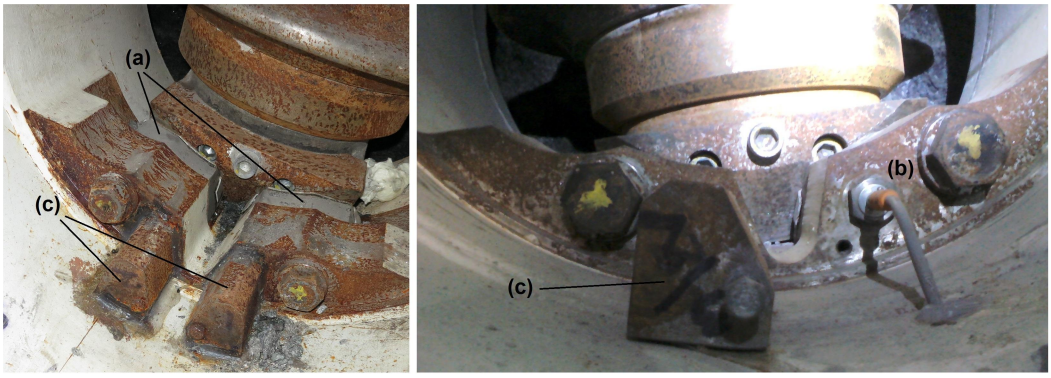


**Fig. B.3.:** Inserts between saddle and cutter (a), measurement bolt with cable (b), protective steel cap (c)

Because of the chosen cutter positions, cable lengths between sensor and programmable controller vary between 1.5 and 5 m. In order to find out whether this affects measurement results, cable lengths between 1 and 10 m were tested and compared in the laboratory. It was found that the influence is negligible.

## B.3. Calibration procedure

### B.3.1. In situ calibration

The first paper confirmed the feasibility of the developed measurement method in the laboratory. However, for the implementation on a TBM further steps have to be taken.

First, an in situ calibtration test has to be performed because the cutter saddle is embedded in the cutterhead structure resulting in a different structural stiffness than in the performed laboratory tests. Hence, the behavior of the measurement bolts is expected to slightly change. As stated in section B.1 previous researchers placed all sensors for cutter force measurement inside the cutter structure. Thus, the structural stiffness does not really change when going from laboratory to a full scale cutterhead. Consequently, none of them ever performed an in situ calibration test. The improved design with sensors in the cutter saddle however requires this additional effort. Second, the laboratory tests were carried out using measurement bolts and measurement washers at the same time. As the use of measurement washers was disregarded for TBM operation, the installation situation is slightly different with normal washers. Third, the number of different

loading cases that were simulated with the laboratory experiment setup was limited. In order to find a set of mathematical equations to be able to convert sensor signals reliably into cutter loading, a higher number of loading cases was desired.

A new clamping device that enables loading of a disc cutter mounted on a TBM was designed (see Fig. B.4). While the laboratory setup allowed for a loading of up to 1,000 kN, it was decided to dimension the in situ clamping device for a maximum loading of 250 kN which is the nominal load for common 17" cutters. The load is applied through a hydraulic cylinder (Fig. B.4a) that is operated with a hand pump. On top of the cylinder is an aluminum adapter on which a load cell (Fig. B.4b) is attached to accurately measure the applied force. A load application element (Fig. B.4c) that can move freely perpendicular to the loading direction ensures that no undesired loads are transferred to the disc cutter. The disc cutter is replaced with a calibration cutter with a hemispherical cap that was already used in the laboratory calibration procedure. As mentioned, the clamping device should enable various loading cases from different directions. Hence, it was decided that the attachment to the cutterhead should consist of four arms with adjustable lengths (Fig. B.4d). Dependent on the length of the four arms which are adjusted by hand with turnbuckles, different ratios of normal, rolling and side forces are applied. The dimensions of the base plate (Fig. B.4e) were found using a simple FEM analysis.

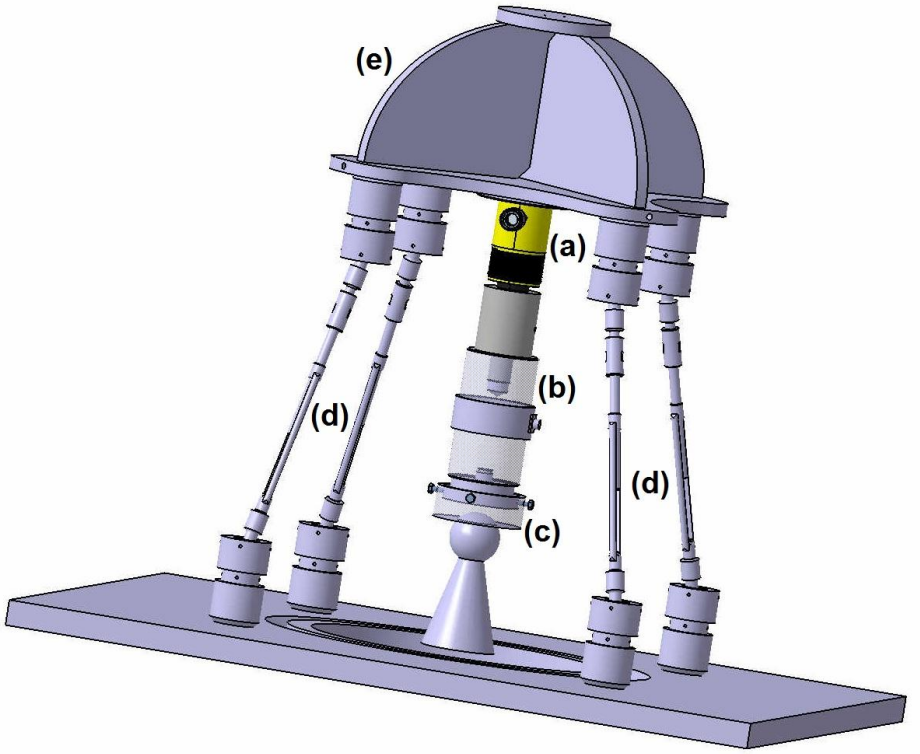


**Fig. B.4.:** Clamping device for in situ calibration, hydraulic cylinder (a), load cell (b), load application element (c), adjustable arms (d), base plate (e)

The platform on top of the plate is used to attach a two-dimensional inclination sensor (Fig B.5a) that automatically records two of the three desired angles that are needed to determine the exact loading direction. The third angle is determined by hand using a tape measurer and trigonometric functions because rotation around the vertical axis cannot be easily measured automatically.

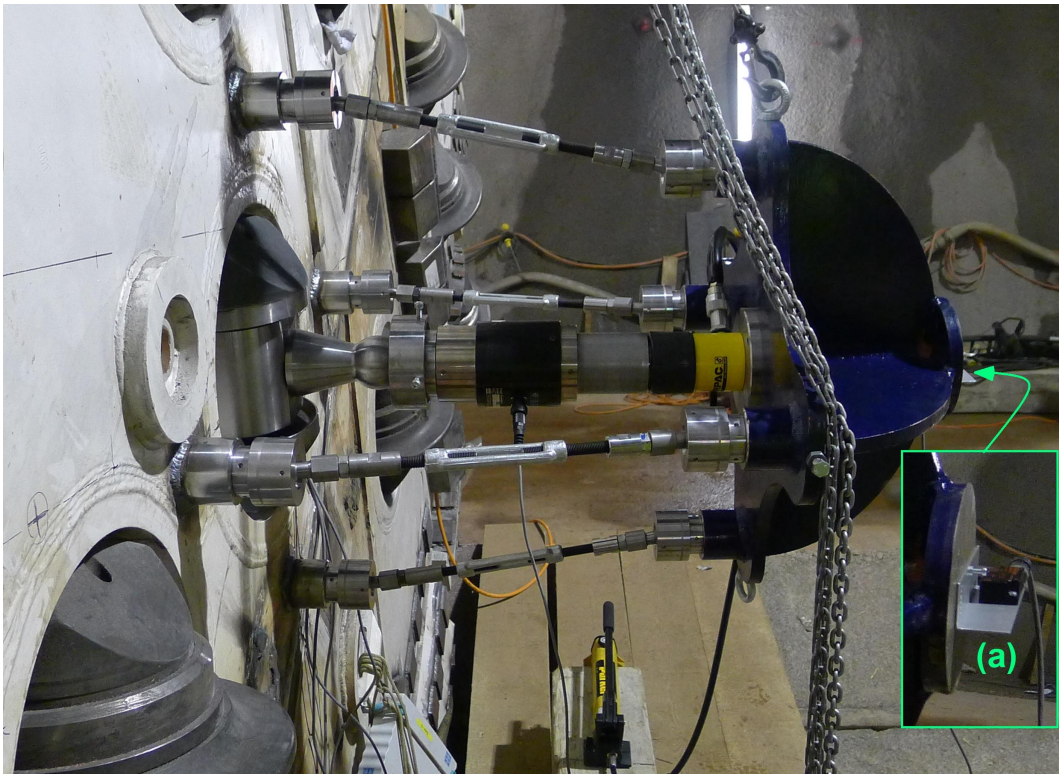


**Fig. B.5.:** Clamping device for in situ calibration with inclination sensor (a)

The signals of the four measurement bolts were amplified with a HBM Spider8 digital signal amplifier and recorded on a laptop. The inclination sensor (two channels) and the load cell were linked to a HBM Quantum-X digital signal amplifier and recorded on a second laptop. This measurement chain is very similar to the laboratory configuration. In addition, the measurement chain for the in situ operation was tested. In this configuration, the measurement bolts were linked to a programmable controller from where the data was transmitted via radio communication to a second programmable controller and then to the control cabin of the TBM operator. The results of the two measurement chains were compared and found to be the same.

The first step of the calibration procedure is to exchange the disc cutter with an adapted cutter with a spherical load application area and blocked rotation. Subsequently the in situ clamping device is attached to the cutterhead and its position adjusted. After that, load is applied using the hydraulic hand pump. As shown in Fig B.2 cutting forces are measured on three positions. The calibration procedure as it is described in this section was, however, performed only on the cutter in the face area of the cutterhead.

Thus, it is assumed that the difference in structural stiffness between laboratory and cutterhead is notable, but sufficiently small in the proximity of the three cutter saddles which is reasonable considering cutterhead design.

The results show that the decrease of pre-stress in the measurement bolts is about 25 to 30% higher for a given load during in situ tests compared with the laboratory setup. Also, the magnitude of the sum of all four bolt forces depends on the loading direction. This dependency proved to be slightly less significant during in situ testing than in the laboratory setup. These findings are considered in the derivation of a mathematical relationship between sensor signals and forces which is presented in section B.3.3.

In the laboratory setup, the cutter saddle is in a horizontal position. The cutter is placed on the inserts, the position adjusted and then fastened. In contrast to that assembly situation, the cutter saddle is in a vertical position during a real cutter change. Thus, when a new cutter is mounted, gravity drags it down and makes it difficult to fix the cutter in a centered position. Hence, the cutter is fastened slightly eccentrically resulting in an uneven loading and uneven signal of the measurement bolts. It is possible to avoid this eccentricity by carefully tightening the lower cutter disc bolts first until the cutter is lifted up a little bit. Special care was taken to ensure that the three measurement cutters were mounted in such a way.

It was reported in the first paper (Entacher et al. 2012c) that the quality of sensor signals increases over loading time and that cutter disc bolts have to be retightened after the structure has been heavily loaded for a certain time. This is due to the evening out of contact imperfections (i.e. settling) of the different parts of the structure (cutter saddle, inserts and cutter). Unfortunately, this increase of signal quality could only be achieved to a very limited extent during in situ testing. As mentioned, the clamping device was designed for a load of up to 250 kN for practical handling reasons. It turned out that this is probably not sufficient to trigger these settling effects.

In summary, the vertical mounting situation and the mentioned contact imperfections between different parts led to an uneven reduction of pre-stress of the four measurement bolts even for centric loading. This problem could be solved by carefully positioning the cutter in the right place before fixating it, however, this cannot be guaranteed at all times during TBM operation.

### B.3.2. Aluminum sheets

In order to overcome this drawback a solution to reduce the effects of contact imperfections was sought. The position of the cutter is never clearly defined. For handling reasons, it can be moved a little bit in all directions before cutter disc bolts are tightened. Consequently, heavy loading will always change the position of a cutter. In order to ensure a positioning which is close to optimum from the beginning on, the idea was to put a layer of soft material between cutter and inserts. Due to deformation of this

layer during fixation of the bolts imperfections should be reduced. It was decided to use aluminum sheets of different thicknesses and test them in the laboratory. Aluminum has a Young's modulus of about 70 GPa which is sufficiently small compared with approximately 210 GPa of steel. Several configurations were tested with a variation of the following parameters:

- poor / proper positioning of the cutter before assembly,
- signal quality after assembly / after retightening of cutter disc bolts,
- no aluminum sheets / sheets with 1 or 2 mm thickness.

All following figures show the pre-stress decrease of four measurement bolts for pure normal force loading as shown in Fig B.6. In a poor assembly situation, i.e. the cutter is not positioned precisely in the center, the load distribution can be very uneven which is illustrated in Fig B.7.

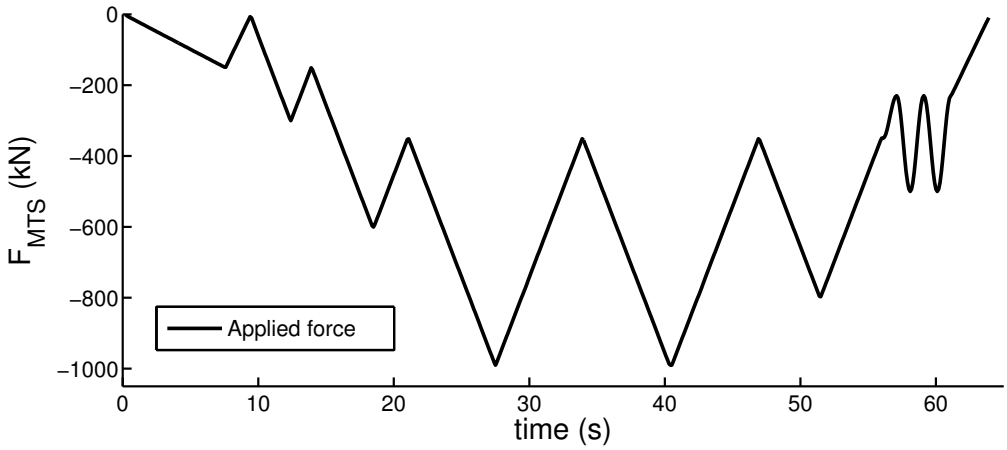


**Fig. B.6.:** Normal force applied by hydraulic press in laboratory

After several load cycles, the bolts holding the cutter were retightened. Fig B.8 and Fig B.9 show the result of the first loading cycle after retightening and after five loading cycles, respectively. After that, no more changes were observed. When comparing the results before and after retightening, it is obvious that settling effects took place. However, in some cases – as in the one presented – the load is still unevenly distributed among the four supports. The sum of all bolt pre-stress reductions usually remains constant even when load distribution is not perfectly even. Obtaining an evenly distributed deformation requires a very careful assembly which cannot always be guaranteed during TBM operation.

Fig. B.11 shows the signals of the measurement bolts with 2 mm aluminum sheets glued on top of the nitrited inserts (Fig. B.10). Right after assembly the force distribution is very uneven but after five loading cycles the signal quality improves dramatically which indicates that imperfections are evened out (Fig. B.12). Subsequently, Fig. B.13

shows the final result with the aluminum sheets, i.e. after retightening of the cutter disc bolts and several loading cycles.

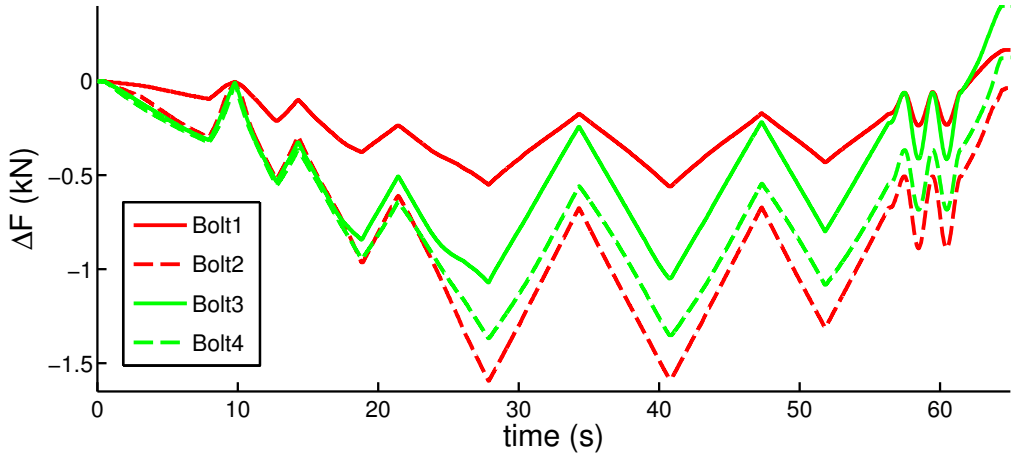


**Fig. B.7.:** Reduction of bolt pre-stress after assembly

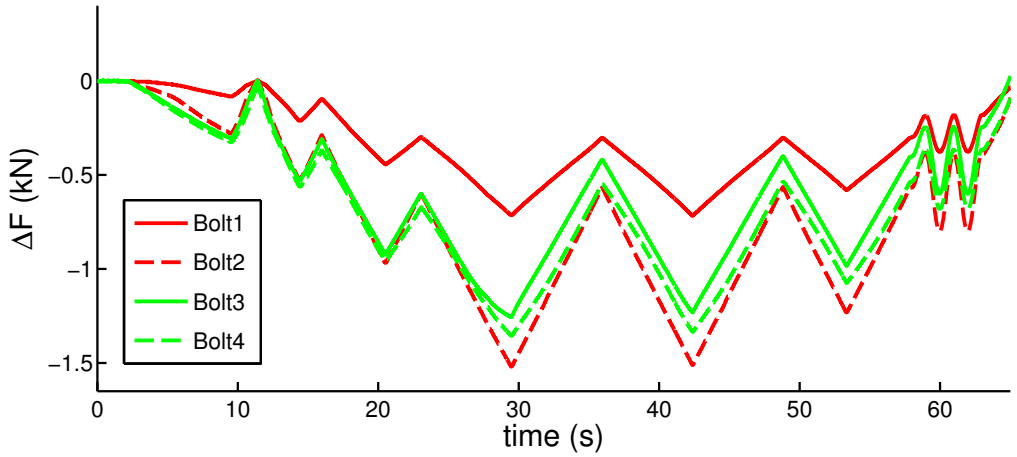


**Fig. B.8.:** Reduction of bolt pre-stress right after retightening

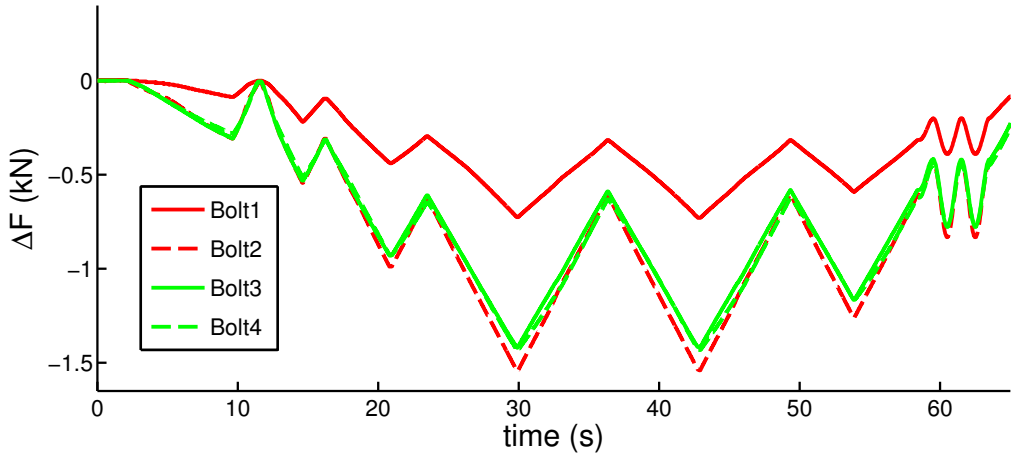


**Fig. B.9.:** Reduction of bolt pre-stress after retightening and multiple loading cycles

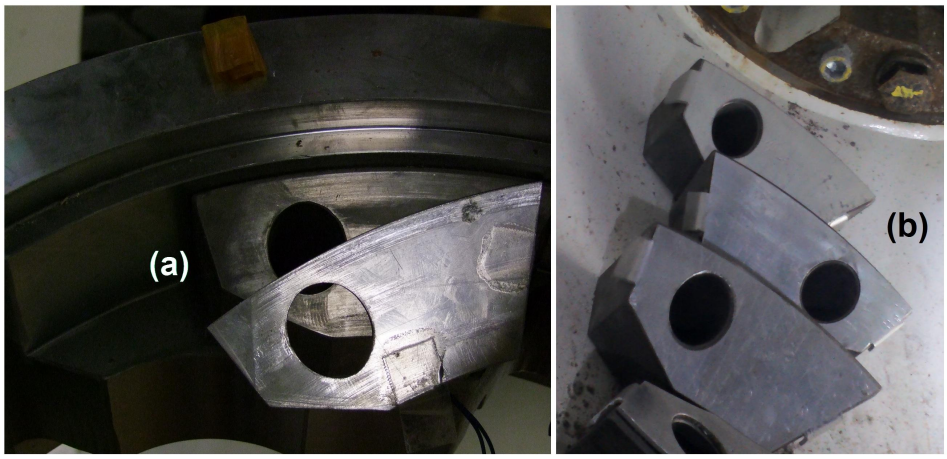


**Fig. B.10.:** Aluminum sheets with a thickness of 2 mm, laboratory (a) and in situ (b)

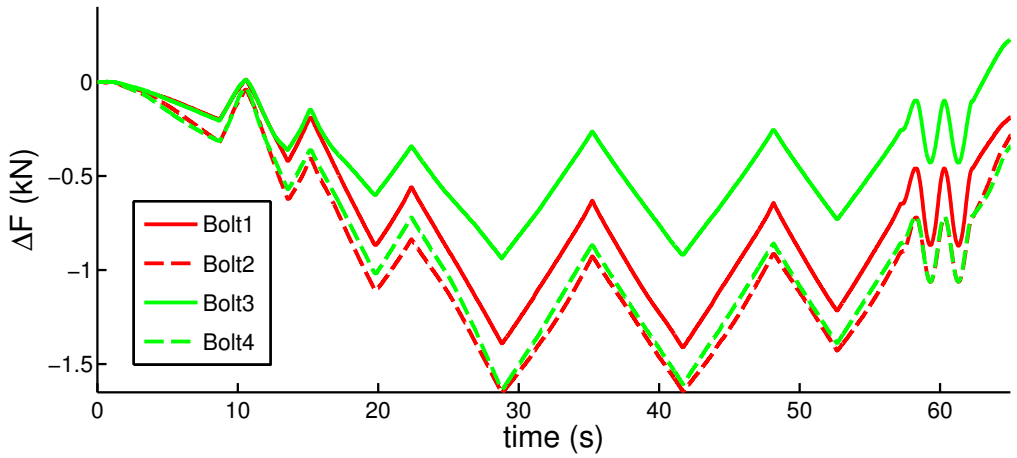


**Fig. B.11.:** Reduction of bolt pre-stress with aluminum sheets (first loading after assembly)

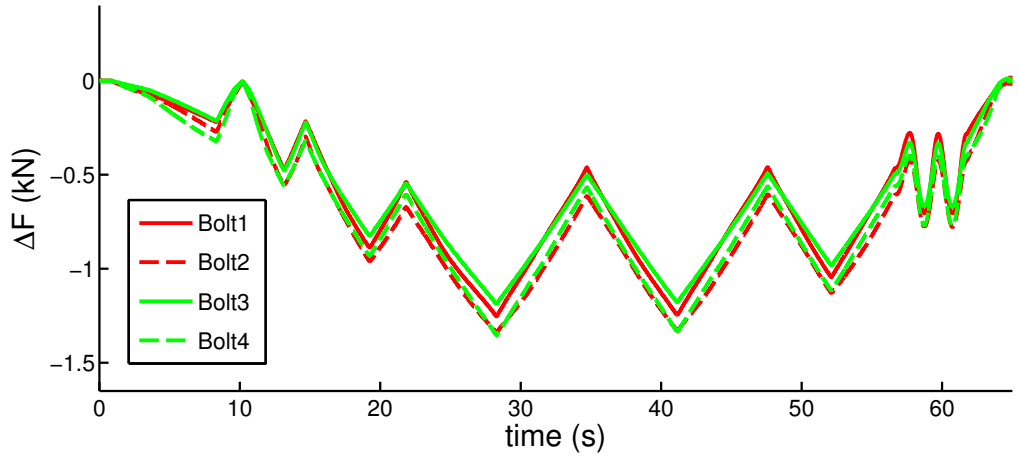


**Fig. B.12.:** Reduction of bolt pre-stress with aluminum sheets after multiple loading cycles

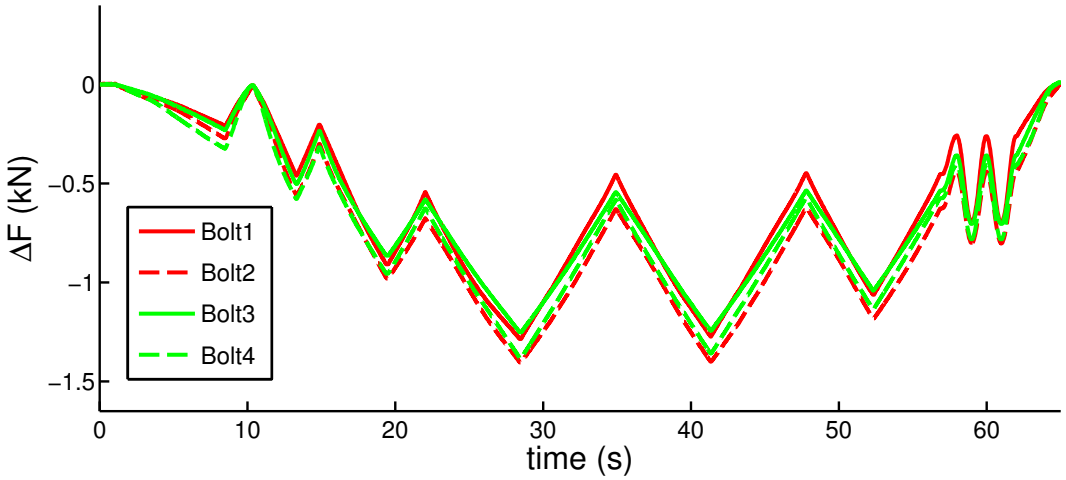


**Fig. B.13.:** Reduction of bolt pre-stress with aluminum sheets after retightening and multiple loading cycles

The figures clearly indicate that 2 mm aluminum sheets on top of the inserts significantly improve the quality of the results. For their in situ use, there were concerns regarding the additional deformation caused by the soft sheets, because due to heavy loading, loosening of cutter disc bolts is always a concern in TBM tunnelling. Hence, it had to be estimated whether the aluminum sheets promote this loosening process or not. For extreme loading, a contact pressure underneath the cutter of 300 MPa is assumed. Assuming uniaxial compression of the aluminum sheets (which is conservative because the stress state is clearly triaxial due to the small thickness of the sheet), Hooke's law for uniaxial loading is applied: $\varepsilon = \sigma/E = -300\,MPa\ /\ 70{,}000\,MPa = -0.0043$. The change in thickness then becomes $\Delta l_{alu} = -0.004286\,x\,2mm = -0.0086mm$. The M24 cutter disc bolts have a cross section of approximately 450 $mm^2$ and are pre-stressed with about 200 kN. Hence, they are exposed to a tensile stress of about 450 MPa,

a strain of $\varepsilon = -450\ MPa\ /\ 210{,}000\ MPa = -0.0021$ and an elongation of $\Delta l_{steel} = 0.0021\ x\ 230\ mm = 0.4928\ mm$ after assembly. The elastic deformation of the aluminum sheets is smaller by two orders of magnitude compared to the elastic elongation of the cutter disc bolts even with conservative assumptions. Consequently, elastic deformations of the structure are clearly not responsible for the loosening of cutter disc bolts with or without aluminum sheets. Instead, it can be concluded that it is a problem caused by contact imperfections during assembly. Besides elastic deformations, it has to be tested whether aluminum sheets survive the harsh conditions regarding heavy loading and abrasion. It was decided that aluminum sheets with sufficient strength should be tested during operation.

The measurement bolts remain unaffected by this change. Besides achieving a more evenly distributed loading of the supports, the magnitude of the measured signal does not change. In addition, the angle dependence of the signal also remains unaffected. Thus, the mathematical relationship between cutting forces and sensor signals does not change, and the results of the in situ test are still valid.

### B.3.3. Calculation of cutting forces

The basic idea of the measurement method is to measure the change of pre-stress of four bolts that hold the inserts (Fig. B.3a) in place. These bolts are tightened with a torque wrench with approximately 200 Nm which results in a tensile force of about 60 to 80 kN. These values have to be initialised in order to serve as reference for zero loading. When the cutter is loaded, pre-stress of the bolts will decrease. Subtracting the actual measurement bolt values during loading from the initialised values gives the reduction of pre-stress, i.e. $\Delta B_i$ that serve as input parameters for the calculation. Zhang et al. (2003) described the calibration process to calculate cutting forces from strain gauges placed on a disc cutter axis in great detail. As it was mentioned in the prequel of this paper (Entacher et al. 2012c) the cutter axis is a very suitable spot for measurement because of its clear deformation state. Hence, Zhang et al. used a system of linear equations for their calibration process. While this is very reasonable, it is more difficult in the present situation. B.14 shows the decrease of pre-stress of the four measurement bolts for a combined normal, rolling and side force loading. It is interpolated with a non-linear surface and plotted into a drawing of the cutter saddle. It shows that a system of linear equations will not be able to cover the occurring non-linearities appropriately. Also, superposition as it is schematically indicated in Fig. B.1c is not possible. Hence, a different approach is chosen.

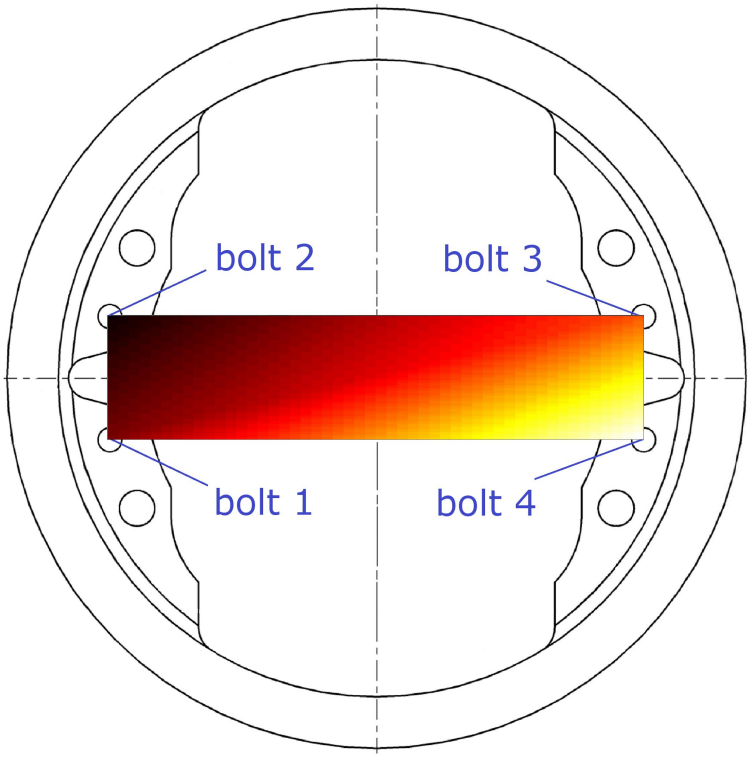


**Fig. B.14.:** Reduction of pre-stress for combined normal, rolling and side force loading visualized as a contour plot to highlight non-linearities

First, angles $\alpha$ and $\beta$ (see Fig B.1b) are calculated to obtain the direction of loading and therefore the ratio between normal, rolling and side force. It was shown in the first paper that the three bolts with the largest decrease of pre-stress have a significantly better signal quality than the bolt with a small reduction of pre-stress. Consequently, the three bolts with the highest loss of pre-stress are used to create a linear plane from which preliminary angles $\alpha_1$ and $\beta_1$ are calculated. In the next step, the non-linearity is accounted for by using the following polynomials to determine $\alpha$ and $\beta$ as functions of $\alpha_1$ and $\beta_1$:

$$\alpha = p_{00} + p_{10}\alpha_1 + p_{01}\beta_1 + p_{20}\alpha_1^2 + p_{11}\alpha_1\beta 1 + p_{02}\beta_1^2 + p_{30}\alpha_1^2 + p_{21}\alpha_1^2\beta_1 + p_{12}\alpha_1\beta_1^2 \tag{B.1}$$

$$\beta = u_{00} + p_{10}\alpha_1 + u_{01}\beta_1 + u_{20}\alpha_1^2 + u_{11}\alpha_1\beta 1 + u_{02}\beta_1^2 + u_{30}\alpha_1^2 + u_{21}\alpha_1^2\beta_1 + u_{12}\alpha_1\beta_1^2 \tag{B.2}$$

The unknown constants $p_{ij}$ and $u_{ij}$ $(i = 0,1,2,3; j = 0,1,2)$ are determined using the results of the in situ and laboratory calibration tests. The results are shown in Fig B.15 and B.16.

The ratio between the different force components is now known. Next, the magnitude of the load has to be determined. For this purpose, the decrease of pre-stress of all bolts

is added up ($\sum \Delta B_{i=1...4}$) and multiplied with factor $T$. To account for non-linearities $T$ is determined with another polynomial surface function with $\alpha$ and $\beta$ as input parameters. The angular dependence of $T$ is illustrated in Fig. B.17. It shows that the magnitude of the signal is dependent on $\alpha$.

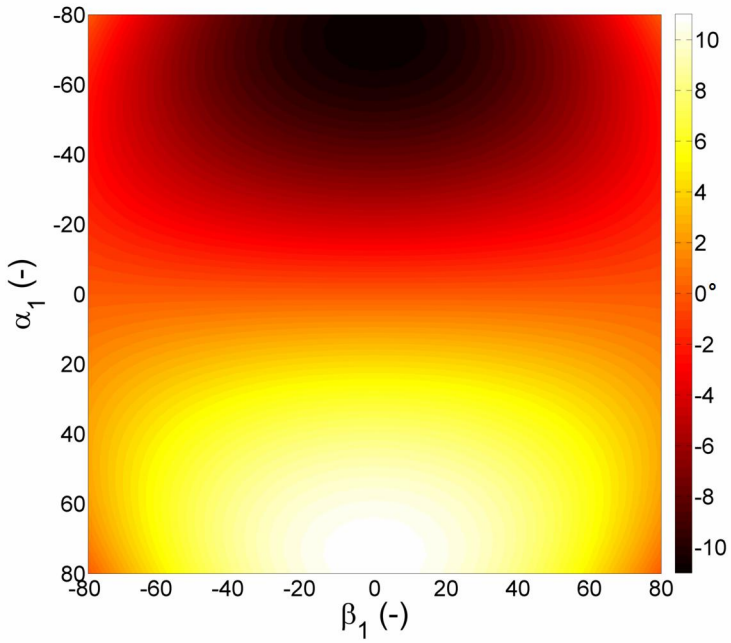


**Fig. B.15.:** Loading angle $\alpha$ (°) as a function of auxiliary values $\alpha_1$ and $\beta_1$

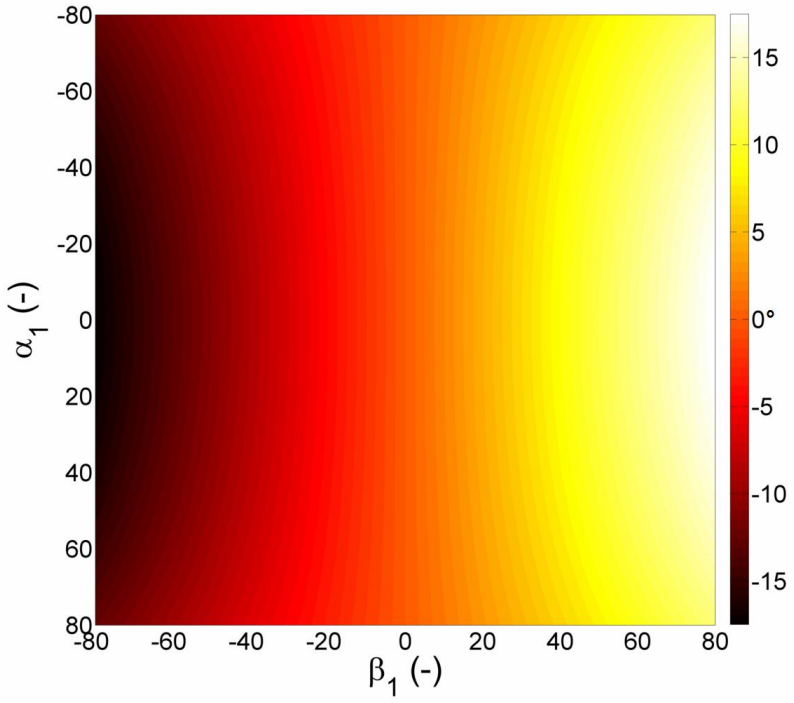

**Fig. B.16.:** Loading angle β (°) as a function of auxiliary values $\alpha_1$ and $\beta_1$

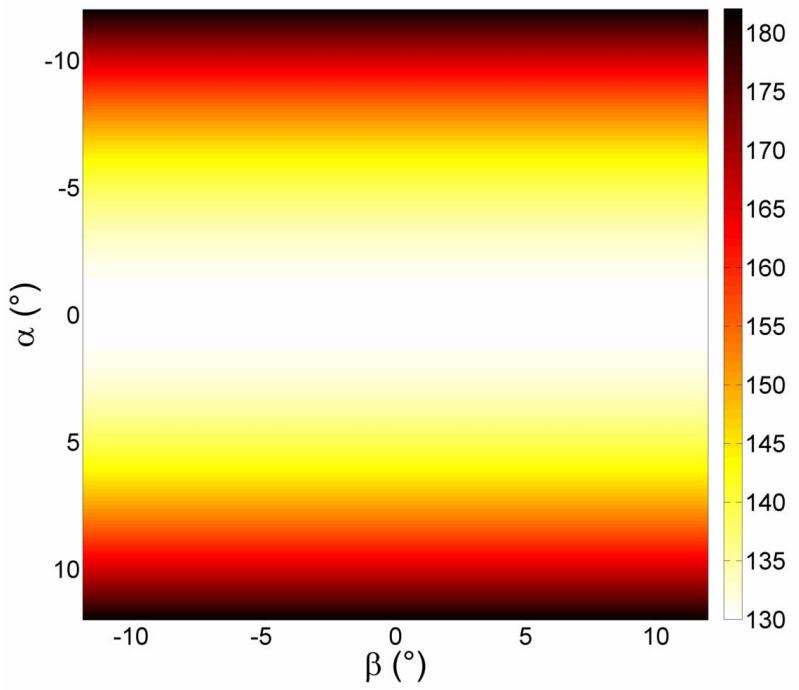


**Fig. B.17.:** Correction factor $T$ as a function of loading angles α and β

Finally, the resulting force $F_{tot}$, normal force $F_N$, rolling force $F_R$ and side force $F_S$ are obtained with the following equations:

$$F_{tot} = T \sum \Delta B_{i=1\ldots4} \tag{B.3}$$

$$F_N = F_{tot} \cos\alpha \cos\beta \tag{B.4}$$

$$F_R = F_{tot} \sin\alpha \cos\beta \tag{B.5}$$

$$F_S = F_{tot} \cos\alpha \sin\beta \tag{B.6}$$

The presented calculation uses four bolt signals to obtain three forces. In case one bolt fails, the calculation can still be carried out, but with slightly less accuracy. In this case, the missing bolt signal is extrapolated from the three remaining signals. If in reality the missing bolt experiences the highest loss of pre-stress, forces are slightly underestimated. If it experiences the lowest loss of pre-stress, forces are slightly overestimated.

Fig. B.18 shows a block diagram of the calibration process. A load is applied to the cutter, sensor signals are amplified, recorded and visualized. After that, they are compared with the applied load in order to find a mathematical relationship between input and output. The calibration has to be done very carefully because after it is finished, i.e.

all parameters such as $p_{ij}$ and $u_{ij}$ are determined, the quality of the calculated results cannot be improved during operation. This is illustrated in Fig. B.19. In contrast to a defined load, the cutters are now exposed to random excitation. The laboratory setup is replaced by a robust installation that withstands the harsh environmental conditions. Signals are not only amplified, but transmitted wirelessly with the help of a programmed controller.

From the experience of calibration, the accuracy of normal ($F_N$) and side ($F_S$) force is within a range of $\pm$ 10%. Rolling force however was found to be less accurate due to the small distance between measurement bolts in the rolling direction. The calibration procedure was carried out for one cutter position only. It is expected that it is valid for the other two positions also, but it might be a source for slight inaccuracies.

In order to obtain high-quality results, it is of great importance to fixate the cutter in a centric position and to retighten all cutter disc bolts after a TBM stroke. In addition, the use of aluminum sheets as described in section B.3.2 is strongly recommended.

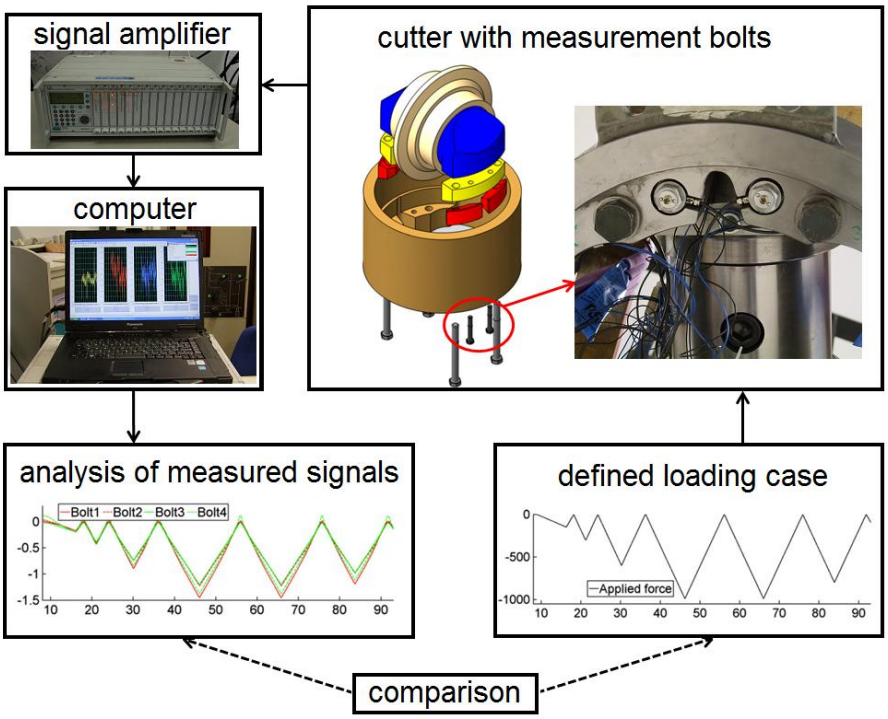


**Fig. B.18.:** Block diagram illustrating the calibration process

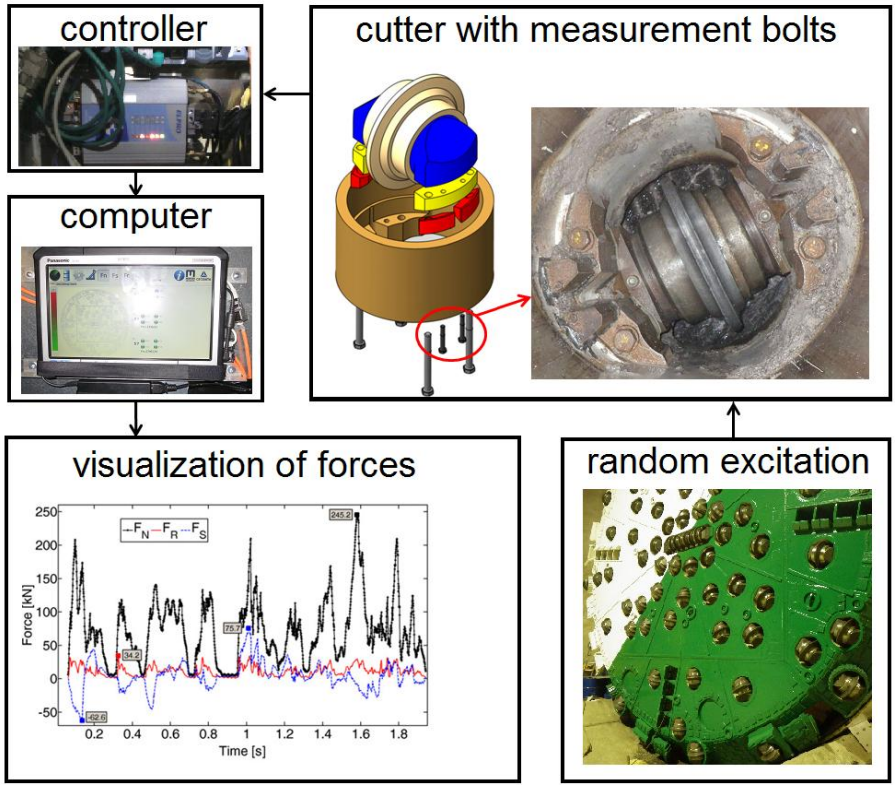


**Fig. B.19.:** Block diagram illustrating the measurement chain during TBM operation

## B.4. Results

The results in this section were obtained at the end of January 2013. At this time the TBM had excavated its first 100 m. At this station there is mainly moderately fractured, massive, unweathered schistose Gneiss with subsidiary silicatic marble and mica-schist. There are areas with highly fractured material along slickensided surfaces and dripping water with a total inflow of about 0.3 l/sec. The highly anisotropic schistose Gneiss has a uniaxial compressive strength of about 50 - 100 MPa when loaded perpendicularly to its schistosity. The tunnel face is predominantly stable with small breakaways in the area of slickensided surfaces, the overburden is 270 m. Fig. B.20 shows a geological mapping of the tunnel face. The numbers are dip direction (°) and dip (°) respectively. The tunnel axis has a direction of 258°. All presented geological information is based on Ulrich Ritter's documentation (2013).

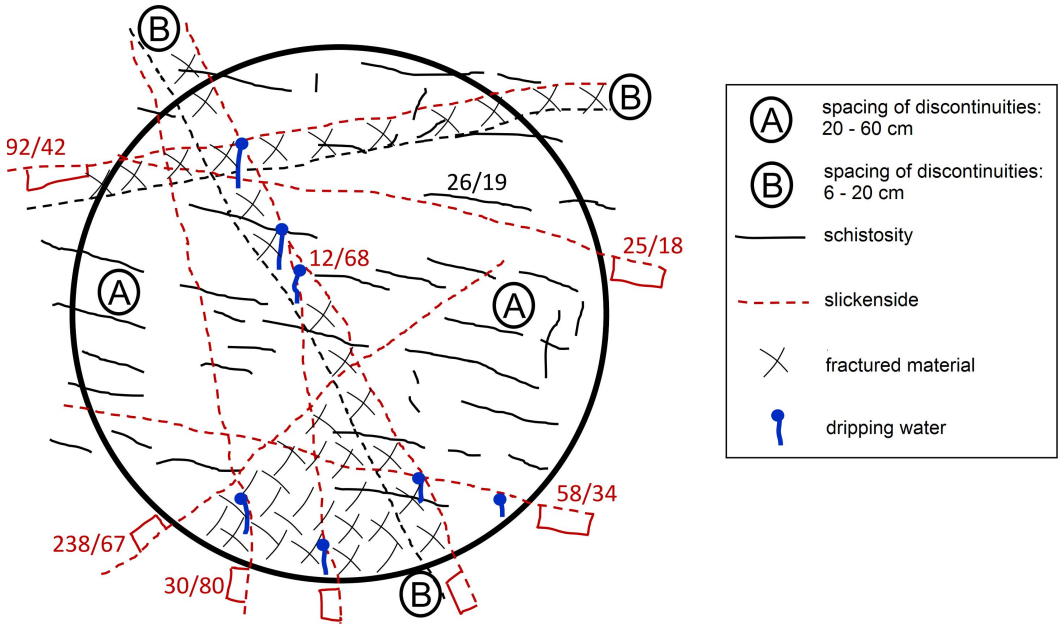


**Fig. B.20.:** Geological mapping of the tunnel face (based on Ritter, 2013)

Fig. B.21 shows the normal forces $F_N$ acting on the three sensor equipped cutters for a duration of 80 seconds. Fig. B.22 shows the corresponding side forces $F_S$. Rolling forces $F_R$ are not very reliable (see section B.3.3) and are thus not presented.

In addition to the measurement bolts signals, the angular position of the cutterhead is recorded. With that information it is possible to localise the occurring forces on the tunnel face and compare them with the geological mapping. Fig. B.23 shows the cutterhead rotational angle plotted against time. It can be seen that one revolution took about 26 seconds, i.e. the cutterhead was rotated with 2.3 rev/min. For further processing, the angle is approximated with a step function so that each value becomes an integer between 0° and 360°.

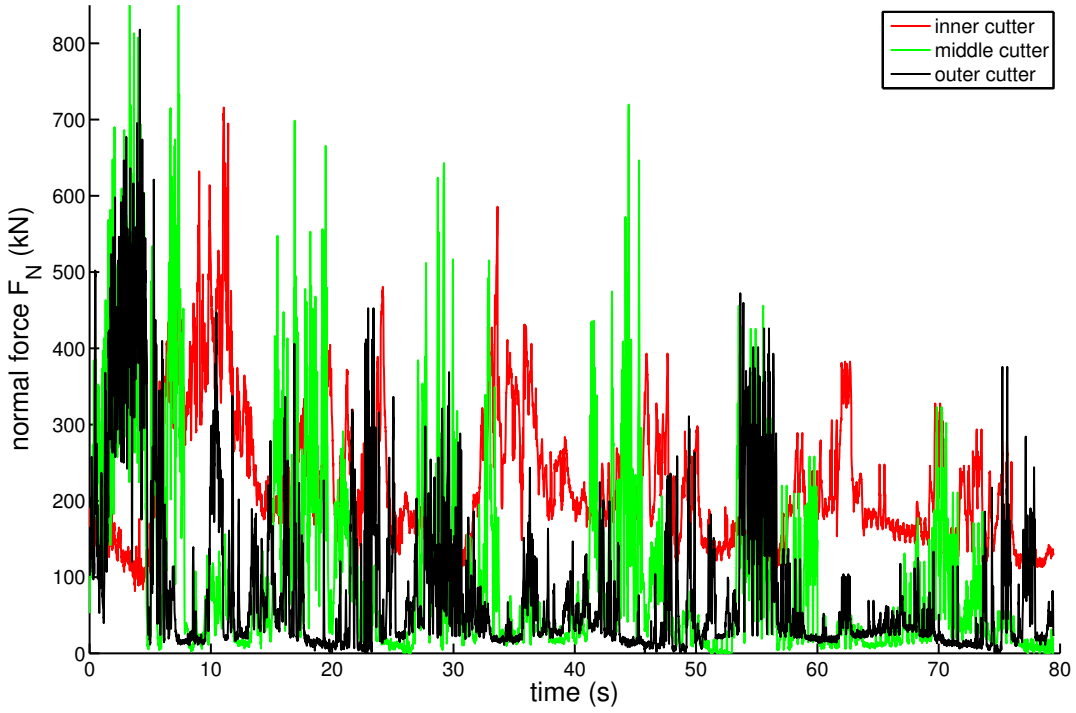


**Fig. B.21.:** Normal force $F_N$ plotted against time

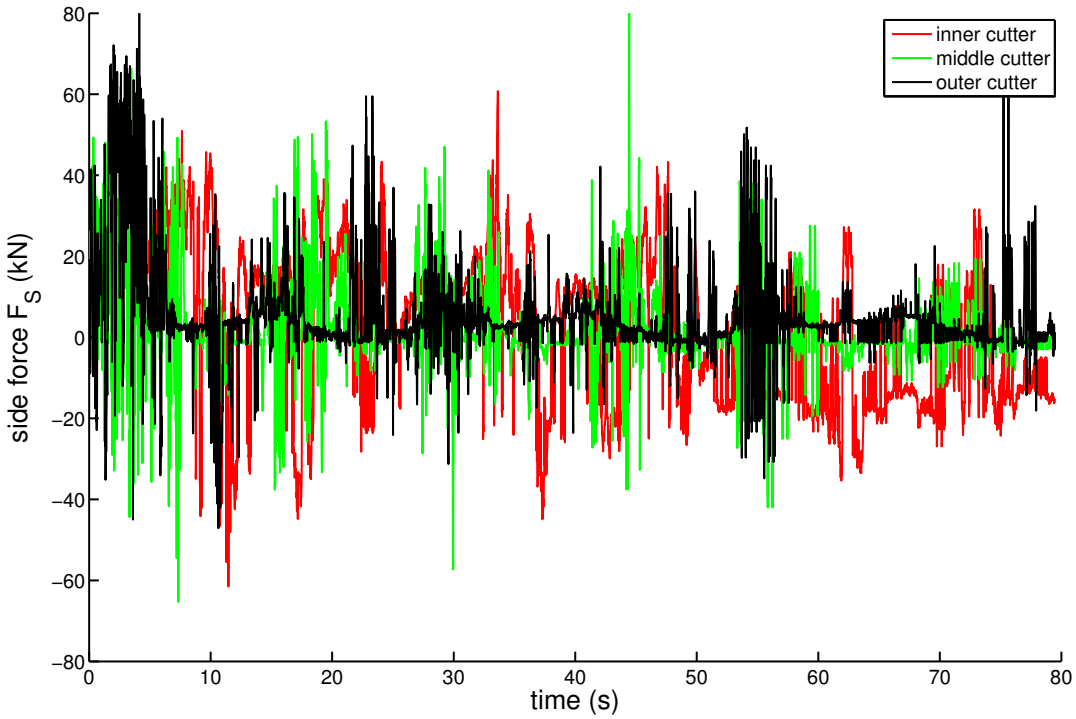


**Fig. B.22.:** Side force $F_S$ plotted against time

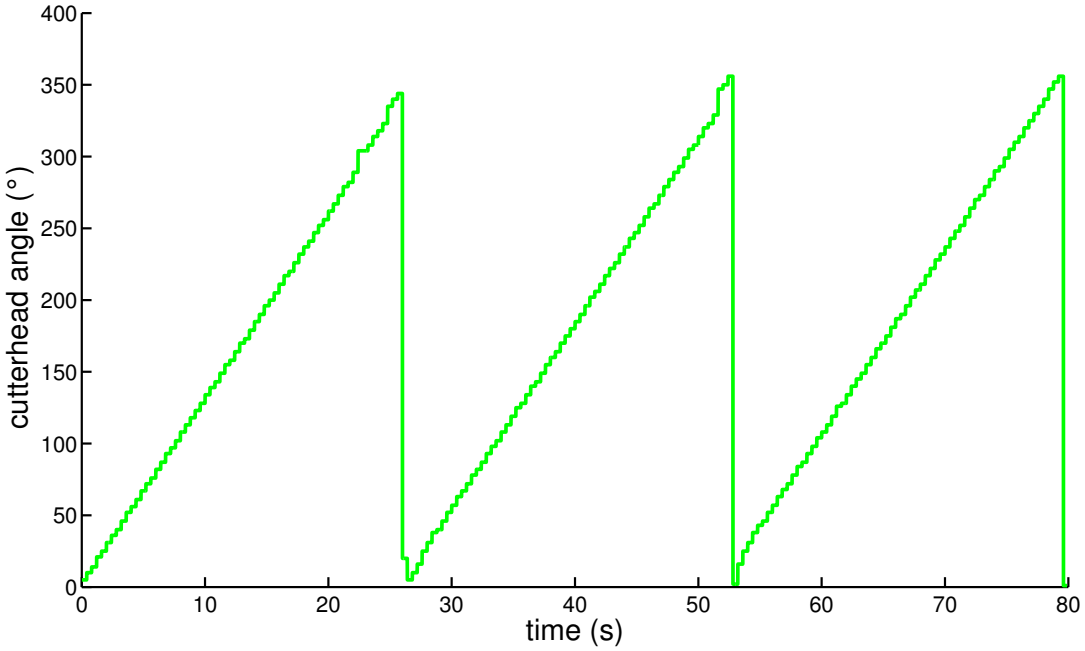


**Fig. B.23.:** Signal of cutterhead angle sensor

All force values with the same angle are then averaged and visualized in a contour plot with 360 coloured segments. The contour plots in Fig. B.24a to c show the normal forces that occurred during three consecutive cutterhead revolutions. The underlying data is the same as in Fig. B.21. In order to get a better representation of the occurring forces Fig. B.24a to c were averaged and plotted separately with a comparison of the geological mapping (Fig. B.24d).

The TBM had a total thrust of about 8 MN, cutterhead torque of about 1.3 MNm at a rotational speed of about 2.3 rev/min and a penetration of 3.5 mm/rev. The peak and average force was 720 and 210 kN respectively for the inner cutter, 900 and 110 kN for the middle cutter and 820 and 85 kN for the outer cutter.

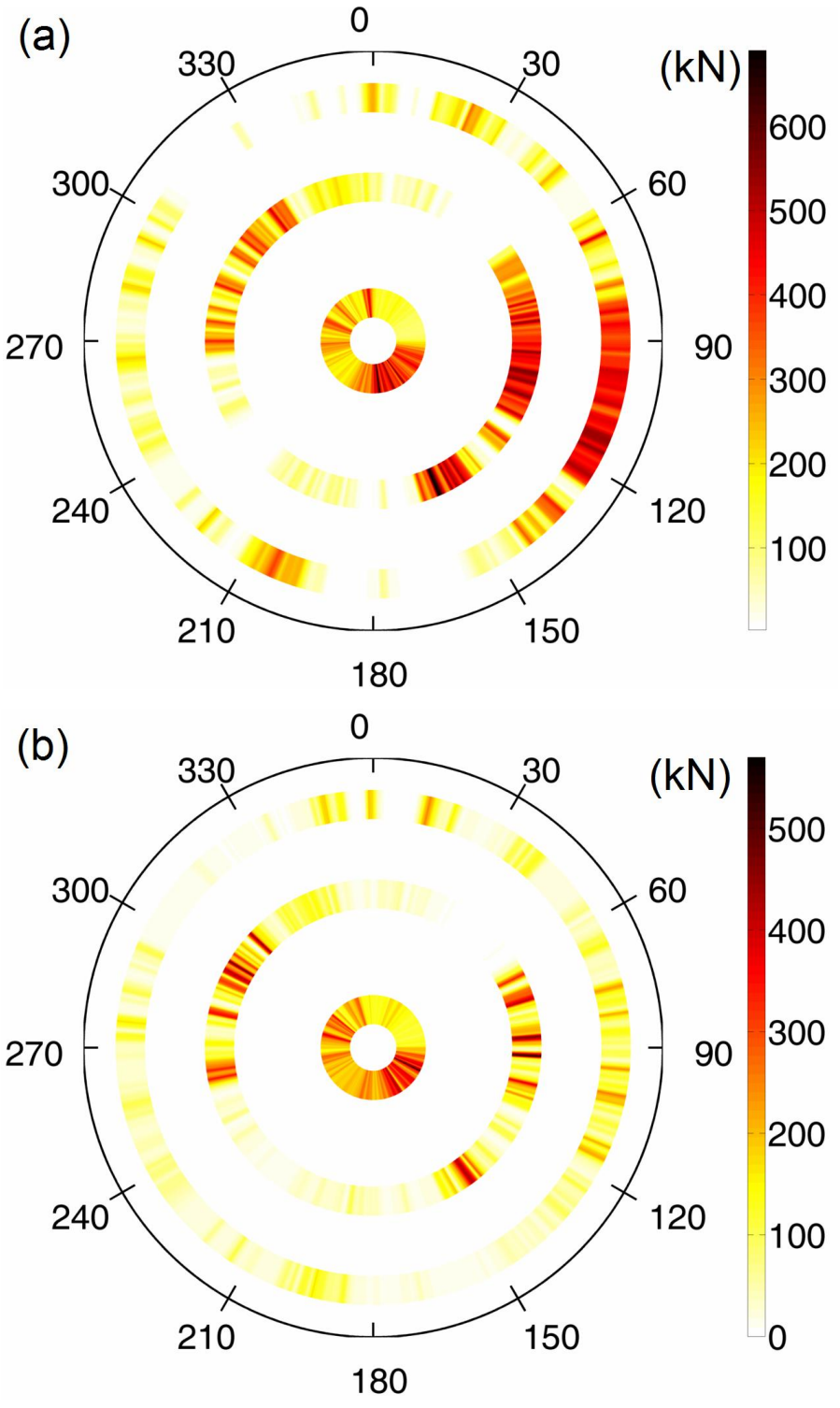
(a)
0
30
60
90
120
150
180
210
240
270
300
330
(kN)
600
500
400
300
200
100
(b)
0
30
60
90
120
150
180
210
240
270
300
330
(kN)
500
400
300
200
100
0

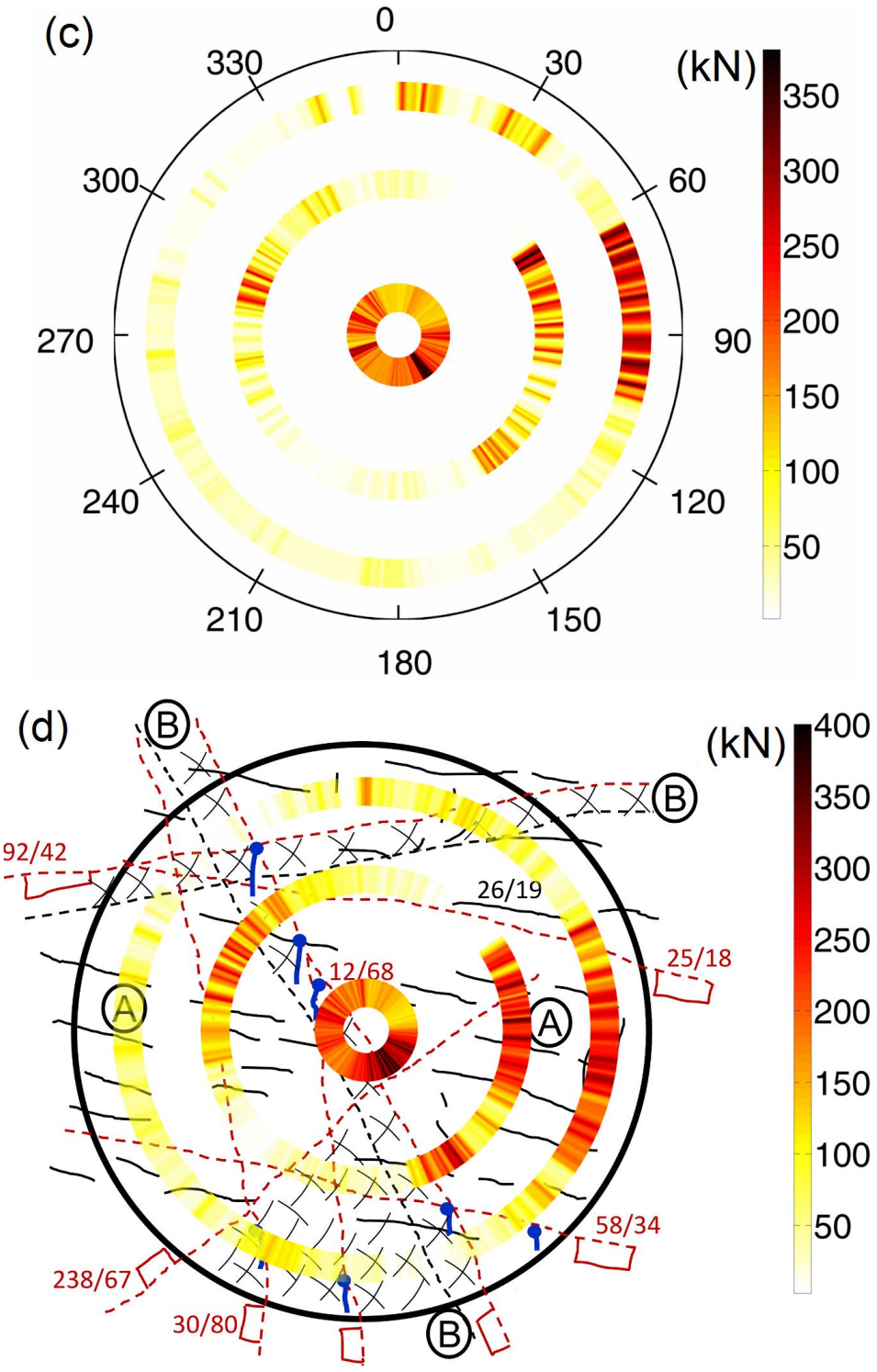


**Fig. B.24.:** Normal forces $F_N$ during three consecutive cutterhead revolutions (a) to (c) and the averaged forces of these figures compared with the corresponding geological mapping (d)

## B.5. Discussion

### B.5.1. Interpretation of cutting forces

Fig. B.24 shows a very uneven force distribution across the tunnel face. The most characteristic feature is that forces are generally higher in the lower right and the upper left area of the tunnel face. This is in very good accordance with the orientation of schistosity (black lines). Entacher and Lassnig (2012) published results from linear rock cutting tests carried out at the Colorado School of Mines with anisotropic metamorphic rocks that were cut in different directions relative to their schistosity. The results showed that it takes much less force to cut rock when the cutting direction is parallel to the schistosity compared to the schistosity being perpendicular to the cutting kerf. The schistose Gneiss that was cut at Koralm tunnel is highly anisotropic, thus, the results clearly confirm the laboratory tests. This observation has a very practical implication for TBM operation. When a TBM is operated with a thrust that is calculated by a nominal load of 250 kN multiplied with the number of cutters in anisotropic rock mass, it means that some cutters will have a load much less and some much greater than this nominal value. The more anisotropic the rock mass gets, the more pronounced this difference will be.

Average forces are much higher on the right side of the tunnel face. During steering of a TBM, there is constant need compensate the direction of excavation according to the information provided by the guidance system. Consequently, cylinder pressure is sometimes higher on the left or right cylinder group. In the area of interest, the pressure of the right cylinder group was 39 bar compared to the left cylinder group with 22 bar. The lower cylinder group had a pressure of about 70 bar compared to the upper cylinder group with 32 bar. The lower cylinder group usually has a much higher pressure than the upper one in order to overcome gravity that pulls down the cutterhead.

Fig. B.24a, b and c show a similar force distribution on a large scale. However, there are very distinct localized effects in each of the pictures. Consequently, looking at a single revolution would not be feasible. Several are needed to get a representative average to cancel out singular events. This is again in accordance with experience that was gained from linear cutting tests. It was observed that subsequent cuts are dependent on each other, i.e. a very high force level will cause a lower force level during the next cut in the same kerf. Large forces causing an overbreak might even cause zero forces in a subsequent cut. Thus, general statements that go beyond the analysis of a singular event should not be based on a single cut or a single revolution.

The peak normal forces for the three cutters listed in section B.4 (720, 900 and 820 kN) approximately lie in the same order of magnitude. 900 kN is about 3.5 times higher than a nominal cutter load of 250 kN. A factor in this range was expected from the experience of laboratory cutting tests. However, in the area of interest the average load was much less than 250 kN. For the outer cutter the maximum force of 820 kN is almost

10 times higher than its average loading of 85 kN which is truly remarkable and was not observed in this clarity during laboratory cutting tests. Fig. B.24d shows large areas with very small forces. These are on the one hand areas with highly fractured material such as on the very bottom and in the top left corner, and on the other hand smaller areas where the cutting kerf seems to be parallel to the direction of schistosity. These areas significantly pull down average forces. Whereas peak forces seem to be in the same range for all three cutters, average forces differ significantly. A larger cutting kerf radius also means that the chance of covering zones with distinctly different material behaviour (such as zones with highly fractured material) increases. This might cause the cutter not engaging with the tunnel face, such as in the top left area of Fig. B.24a. Besides that, cutterhead stiffness might play a very important role. Distortion of the cutterhead will be much higher in the gauge area than in the center, causing unbalanced cutting behaviour. In addition, cutters on the inside are constrained by the small cutting kerf radius. Hence, they will produce more fines, cut less efficiently and need more energy to achieve the same penetration.

### B.5.2. Outlook

Today's state of the art cutterhead is typically not equipped with electronic components. In contrast to conventional tunneling, the tunnel face cannot be observed during excavation which makes it very hard to monitor the excavation process. Thus, monitoring can only be done by observing global machine data such as thrust, torque, advance speed or muck volume. However, such global parameters will rarely allow to detect damaged cutters, muck buckets or other parts of the cutterhead at an appropriate time, i.e. before serious damage has occured. Hence, a true monitoring concept would mean a significant improvement for TBM operation and could potentially save large amounts of money. This statement is emphasized by the research activities of major TBM manufacturers. They are working on ways to equip their cutterheads with sensors that measure parameters such as cutter rotation, temperature, vibration, wear or cutting forces as presented in this study. Hence, there is a clear trend that monitoring with sensors will play an increasing role in the future of TBM operation and geotechnical monitoring.

The main obstacle that has to be overcome is the harsh environment at a TBM cutterhead. First, all sensors, cables, controllers, etc. have to be protected from mechanical impact and water inflow. Second, the cutterhead is exposed to excessive vibration which can reduce durability of electronic parts dramatically. Third, it must be possible to carry out maintenance works under dirty and wet conditions. In addition, the rotation of the cutterhead requires radio communication because data has to be transferred from a rotating to a stationary part. Besides the problems caused by vibration and mechanical impact, radio communication devices are very difficult to implement because of the heavy steel environment which significantly affects the connection quality. To summarize, the step from laboratory scale to in situ application is large and requires careful planning. Ideally, cable trunks and other required modifications should be considered

from the beginning on during cutterhead design.

## B.6. Conclusions

The present study is a sequel to a previously published paper (Entacher et al. 2012c) in which the development of a new cutter force measurement method for disc cutters was presented. Subsequent to this development, it was implemented on three disc cutters of the first Koralm tunnel TBM in Austria. The steps of the implementation process were described and first results presented. The conclusions of this paper are:

- The measurement method was implemented successfully. Compared to previous approaches, the disturbance of TBM operation has decreased significantly because no sensors are placed inside the cutter.
- The step from laboratory to in situ application is difficult and requires careful planning because of the harsh environmental conditions at a TBM cutterhead. Durability of electronic parts is very hard to achieve.
- Average forces decrease significantly from the center to the gauge area of the cutterhead because of geological features and possibly cutterhead stiffness. Peak forces are in the same order of magnitude at all positions and a multiple of average forces.
- The occurring forces can be correlated with geological features such as areas with highly fractured material and orientation of schistosity. Hence, cutter force measurement could prove a valuable tool for geological monitoring.

## Acknowledgements

We gratefully acknowledge the financial support of this work by the Austrian Research Promotion Agency (FFG) within the Eurostars program (Eurostars project E!5514 EMSAT – Enhanced Monitoring and Simulation Assisted Tunneling). We are indebted to Geodata GmbH, Net-Automation GmbH, Aker Wirth GmbH and the construction consortium KAT 2 (Strabag AG and Jäger Bau GmbH) who implemented the measurement method with us. On behalf of all technicians and miners of Koralm tunnel, we want to thank Karlheinz Peter for his extensive help. We would like to thank Ulrich Ritter who provided us with geological data. The help of Rene Pfingstl, Stefan Barwart, Oliver Wanek and Florian Nurschinger during the calibration procedure is greatly appreciated.

# C. Rock failure and crack propagation beneath disc cutters

This paper is authored by Martin Entacher, Erik Schuller and Robert Galler and was submitted to *Rock Mechanics and Rock Engineering*.

Analysis of rock failure mechanisms beneath disc cutters are presented. Full scale cutting tests are conducted to assess the global energy input in comparison with rock chips and excavated volume. Small scale cutting tests are subsequently used for macro- and microscopic analyses of rupture modes and crack propagation. A high spatial resolution allows to obtain pictures of crack networks in different rock types. It is shown that all specimens develop lateral cracks in sufficiently confined areas whereas median cracks typically develop in boundary regions. Regarding cutting forces, a hypothesis is proposed that associates sudden force drops accompanied by loud bangs with transgranular failure of minerals in the proximity of the cutter tip.

## C.1. Introduction

### C.1.1. Motivation and scope

Disc cutters are the main excavation tools of hard rock tunnel boring machines (TBM). A deep understanding of rock failure mechanisms during disc cutting is thus paramount for successful and economic TBM operations. Many researchers have analysed disc cutting analytically, experimentally and by means of numerical simulation. However, due to the complexity of the involved mechanisms and experiments, very few results are available that allow for a comprehensive understanding. The present study focuses on the analysis of cutting forces and corresponding rock failure mechanisms. This includes full and small scale rock cutting tests and subsequent macro- and microscopic assessment of rupture modes with a special focus on crack propagation. Due to the manageable specimen size used for the small scale cutting tests, it was possible to obtain crack network pictures with a high spatial resolution that give a complete picture of the macroscopic crack network. Hence, new insights in the understanding of rock failure beneath disc cutters are offered.

### C.1.2. Related work

Detailed investigations of rock specimens that were exposed to disc cutting are rare. One of the few analysis of rock cutting failure was done by Zhang et al. (2003) who analysed rock cores taken from a tunnel face that was cut with button cutters at Äspö Hard Rock Laboratory in Sweden. Crack analysis showed deep median cracks as well as distinct lateral cracks. Another example is the analysis of Howarth and Bridge (1988b) who investigated crack patterns at the bottom of the percussion and diamond drill holes. They discovered highly localized damage with pronounced lateral cracks.

Even though the number of such investigations is small, the failure mechanisms of rock cutting have very often been investigated by means of indentation testing. This analogy is feasible when it comes to disc cutting because rotation of a disc cutter does not allow for the propagation of high tensile stress into the rock in front of the cutter. The neglected rolling force usually is approximately 10% of the normal force. Hence, the mechanics of disc cutting and indentation testing lead to similar highly triaxial stress states. In contrast to disc cutting, the mechanics of cutting with picks is different. Due to the fixed position and rake angle of the pick, the rock is exposed to high tensile stress which leads to more efficient chipping towards the free surface. The kinematics of this process were described by Nishimatsu (1972). In spite of higher efficiency, picks wear much faster due to heat exposure and less wear volume.

Much of the fundamental understanding of failure processes in rock indentation fracture was adopted from the knowledge that was gained from materials such as glass. In contrast to rock, glass is a homogenous, isotropic, elastic brittle medium that can be analysed more precisely than geomaterials. In addition, the failure mechanisms can be observed more easily during testing due to transparency. Swain and Lawn (1976) compared indentation fracture of brittle media such as glass with rock. Failure mechanisms in rock are substantially more complex due to its large variety of microstructural features and flaws. In spite of the mentioned differences, some universal rules regarding fracture patterns in relation to certain stress states and indenter shapes can be adopted for the understanding of rock failure. Very precise calculations of indentation fracture in brittle solids were, for example, done by Marshall et al. (1982) and Chen et al. (2005). Their analysis are combined analytical-numerical approaches based on fracture mechanics principles. A very comprehensive review of indentation fracture in brittle solids was written by Lawn and Wilshaw (1975). Another important review paper with a focus on rock excavation was published by Mishnaevsky (1995). While performance prediction models of rock cutting processes rely to great extent on strength parameters (e.g. uniaxial compressive strength (UCS) and Brazilian tensile strength (BTS)), the above references clearly indicate that yield strength is negligible when it comes to crack propagation. Instead, the cracking process is governed by typical fracture mechanical parameters such as fracture toughness or surface energy.

It is generally accepted, yet not sufficiently quantified, that brittleness has significant influence on rock cutting efficiency (e.g. Gong and Zhao 2007). Definitions of rock

brittleness (Hucka and Das 1974) are mostly based on parameters derived from UCS- and BTS-testing (e.g. ratio UCS/BTS, elongation at failure or post-failure behaviour). Kahraman and Altindag (2004) correlated such parameters with mode I fracture toughness and found partially good agreement. Besides fracture toughness which can be determined according to ISRM's suggested methods (Ouchterlony 1988), Swain and Atkinson (1978) proposed the determination of surface energy by means of an indentation test. In summary, indentation tests are not only suitable to model rock excavation with disc cutters, they are also a convenient tool to determine surface energy which is closely related to fracture toughness.

Wagner and Schuemann (1970) published results from stamp indentation tests with rock specimens embedded in a steel ring. Their theoretical calculation as well as their crack analysis showed that the first cracks are tensile ring cracks in the lateral direction, commonly known as Hertzian cone cracks. Subsequent chipping is attributed to a volume expansion in the crushed zone under the indenter. Besides this explanation of failure mechanisms, they observed a size effect, i.e. contact failure stress increases significantly as the stamp gets smaller and smaller. Cook et al. (1984) carried out similar stamp indentation tests with acoustic emission (AE) measurement and different confinement levels. They were able to correlate the expansion of the crushed zone with AE events. In addition, they observed a transition from split tensile failure at no confinement to a lateral cracking system (Hertzian cone cracks) at higher confinement levels which is accompanied by a slight increase of indentation strength.

Gnirk and Cheatham (1965) published results of consecutive rock indentation tests with different spacing and confinement. They described the changing failure mode at higher confinement levels with a transition from brittle to ductile material behaviour at a confining stress of 7 to 17 MPa (depending on the lithology). Similar results were obtained by Kaitkay and Lei (2004). Both studies reveal a significant indentation force increase at higher confinement levels. Brittle-ductile transition in triaxial rock testing is described very profoundly by Hori and Nemat-Nasser (1986). However, the results of Gnirk and Cheatham, Kaitkay and Lei might be misleading when it comes to rock excavation because in their studies confining stress was applied hydrostatically, i.e. also on the cutting surface. This is not representative of the conditions at a tunnel face. With a reference to this experimental setup, Chen and Labuz (2006) compare their own experiments with the paper of Gnirk and Cheatham. The stress state is however different because they use slender plates which result in plane stress conditions compared to a hydrostatic confinement in the studies of Gnirk and Cheatham. Consequently, Chen and Labuz observed no significant indentation pressure increase at higher confinement levels. The paper of Chen and Labuz shows that a large median crack is dominant at low confinement levels, whereas the direction of cracks goes upwards into a lateral direction at higher confinement levels even for a sharp indenter.

Pang and Goldsmith (1990) loaded different rock samples embedded in a steel casing with a sharp indenter statically and dynamically. The resulting crack patterns are a mixture of a few to many radial cracks in lateral and sometimes vertical direction. Even

for this very sharp tip, no clear preference towards a distinct median crack was observed. Gertsch (2000) carried out numerous indentation tests with a spherical indenter on small rock cores and large rock blocks. His results showed clearly that major cracks occurred in a vertical direction for the rock cores, whereas there were typically no vertical cracks in the rock blocks. Instead, chips were formed as a result of horizontal cracks.

Several studies used advanced measurement techniques to detect rock indentation failure mechanisms in real time. Lindqvist et al. (1984) precisely observed the failure mechanisms of indentation tests with a scanning electron microscope (SEM) in real-time. Larson et al. (1987) described the failure mechanism of fine grained dolomite plates and Zhang et al. (2012) used digital image correlation to obtain a continuous displacement field of their samples. Due to the opacity of rock, such techniques only work when the indenter is very close to a free surface which inevitably results in changed stress conditions such as plane stress states and consequently changed crack patterns. This trade-off which was observed in the above mentioned papers and others (e.g. Howarth and Bridge 1988a) has, in the view of the authors, given rise to a slight misunderstanding of rock indentation fracture with an overemphasis of median crack development. A dominant role of the median crack is for example depicted in numerous well-known sketches of the cutting process of the Colorado School of Mines (e.g. Rostami and Ozdemir 1993). These sketches have been replicated many times.

Besides experimental work, various researchers have attempted to study the rock failure process due to disc cutting or indentation by means of numerical simulation. Cho et al. (2013) used a Finite Element Method (FEM)-code with a strain-rate dependent constitutive law to simulate the excavation process of two adjacent cutters in 3D. Saksala (2013) recently published the results of a FEM-simulation that investigates the dynamic process of percussive drilling in 3D. His results are in good agreement with the experimental work of Howarth and Bridge (1988b). One of the most profound 2D FEM-analysis was carried out by Liu et al. (2002). Their $R-T^{2d}$ code is able to account for heterogeneous material which is derived from thin sections with a mesoscopic mechanical model. Huang et al. (1998) carried out elastoplastic FEM-simulations of sharp indentation tests at different confinement levels. They clearly showed that the point of crack initiation, i.e. development of a median crack or lateral crack is highly dependent on the confinement situation. Chiaia (2001) and Carpinteri and Invernizzi (2005) used lattice models to simulate rock indentation. Besides FEM-analysis, a number of papers (e.g. Moon and Oh 2011, Huang and Detournay 2012) use the Distinct Element Method (DEM) to simulate rock fracture.

Some of the papers mentioned attempted to compare failure processes with corresponding forces or energy input. It was shown that typical force - displacement curves of indentation and cutting tests have a sawtooth shape with a number of significant force drops. Force peaks or force drops were often associated with the formation of rock chips or cracks. Gertsch (2000) correlated rock chip size with the characteristic length of the sawtooth curve. The significance of such observations will be discussed extensively in the present paper.

## C.2. Description of methods and material properties

### C.2.1. Full scale cutting tests

From January to April 2012 a series of linear rock cutting tests were conducted at the Earth Mechanics Institute of the Colorado School of Mines under the supervision of Christian Frenzel and Brian Asbury. A detailed description of the test rig can be found in Gertsch et al. (2007). The tests presented in this study were carried out with a 17" constant cross section disc cutter with a tip width of 15.8 mm, penetration depths ranging from 1.27 to 6.35 mm (1/20" to 1/4") and a cutting speed of about 1 m/s. The samples of Brixen Granite blocks with a length of 20 cm, a height of 20 cm and a width of 40 cm were assembled one after another and embedded in concrete to ensure adequate confinement conditions. Each pass consisted of a series of five consecutive cuts with a spacing of 80 mm. The three central cutting kerfs were taken as measurement cuts whereas the exterior ones were excluded from further analysis (see Fig. C.1). Cutting forces were measured with a triaxial transducer from which normal ($F_N$), rolling ($F_R$) and side force ($F_S$) were derived. Prior to each change of penetration depth, conditioning passes were carried out to ensure steady state cutting conditions. After each pass, rock debris was removed from the block with a broom and a vacuum cleaner to ensure cutting conditions similar to a vertical tunnel face where debris falls down due to gravity.

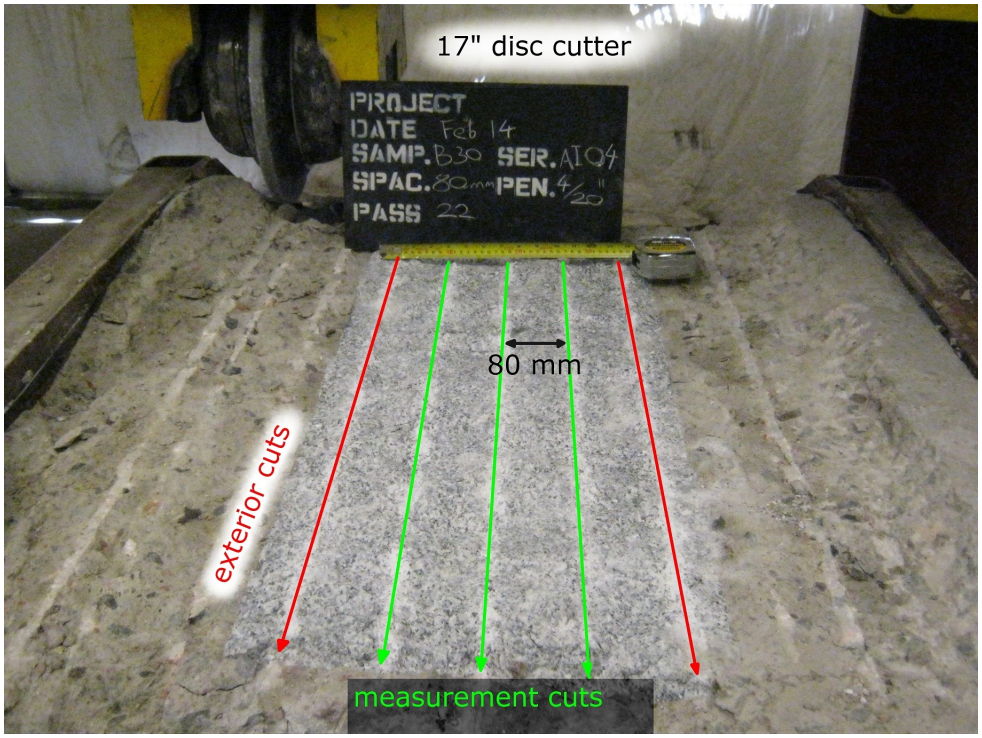


**Fig. C.1.:** Rock blocks for linear cutting tests embedded in concrete

### C.2.2. Small scale cutting tests

A new small scale cutting test rig was developed at the Chair of Subsurface Engineering, Montanuniversität Leoben. A detailed description of this test rig and an assessment of its suitability for TBM performance prediction can be found in Entacher et al. (2013c). The development was carried out in order to conduct accurate and cheap scaled cutting tests with commonly available sample sizes, i.e. rock cores with a diameter of 10 cm. The test rig (Fig. C.2) is designed as an attachment for hydraulic presses which are commonly available in rock mechanics laboratories. The excavation tool is a rotating disc cutter (Fig. C.2a) that is a 1:8 model of the cutter used in full scale cutting tests. The rock samples are 10 cm diameter half cylinders (Fig. C.2b) that are cemented into a steel specimen holder (Fig. C.2c) with a thin layer of epoxy resin (Sikadur-31 AUT R, Fig. C.2d) to ensure excellent confinement. The specimen holder can be attached to the test rig such that the cutting kerf (Fig. C.2e) is in the middle of the sample. By using the elongated holes it is also possible to conduct consecutive cuts with spacing in between. The penetration depth is between 0.5 and 7.5 mm and can be adjusted with spacers (Fig. C.2f) that lie between specimen holder and test rig. The rolling force is measured with a uniaxial transducer (Fig. C.2g) that is part of the hydraulic press. A load application element (Fig. C.2h) that can move freely in the horizontal direction ensures that only vertical forces ($F_R$) are measured by the load cell. Furthermore, a microphone (Fig. C.2i) is placed inside the test rig to record the audio signal of each cut. In order to remove the specimens from their holders, it was heated up to 200° C for about 3 hours which results in deterioration of the mechanical properties of the resin.

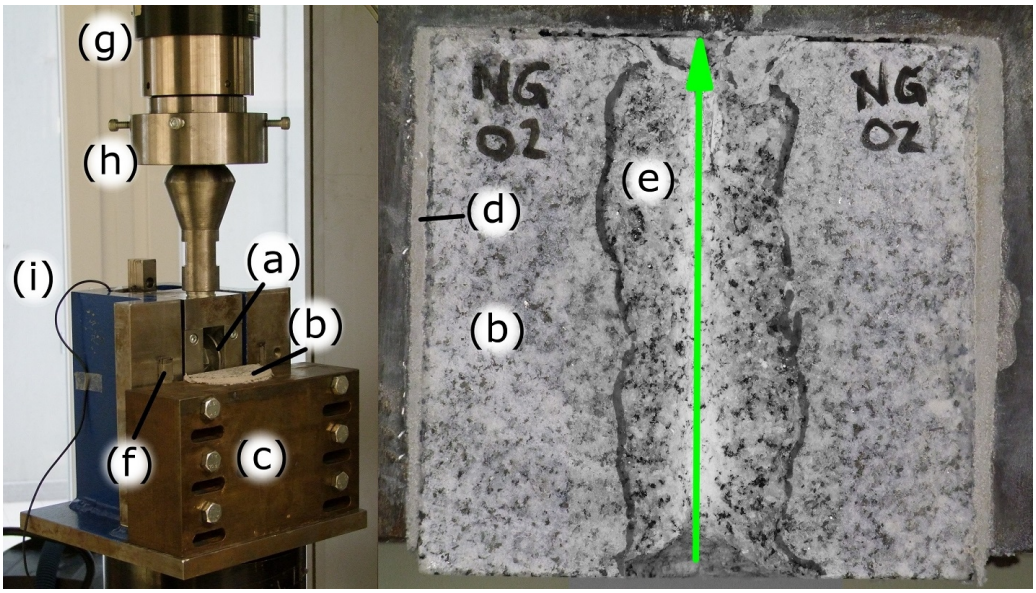


**Fig. C.2.:** Small scale cutting test rig: (a) Cutter, (b) specimen, (c) specimen holder, (d) epoxy resin cementation, (e) cutting kerf, (f) spacers for penetration depth adjustment, (g) force transducer, (h) load application element, (i) microphone cable

### C.2.3. Analysis of failure mechanisms

The specimens of the small scale cutting test were further analysed using two different methods. In method 1, a liquid two component epoxy resin with a fluorescent additive was poured onto the specimen. Subsequently, they were placed in a vacuum chamber. After the resin had hardened, the specimens were cut into plates of approximately 5-7 mm thickness to be able to investigate the crack network. The macroscopic damage was documented for each individual plate and thin sections were produced from selected plates to allow for microscopic damage analyses. This process is shown in Fig. C.3.

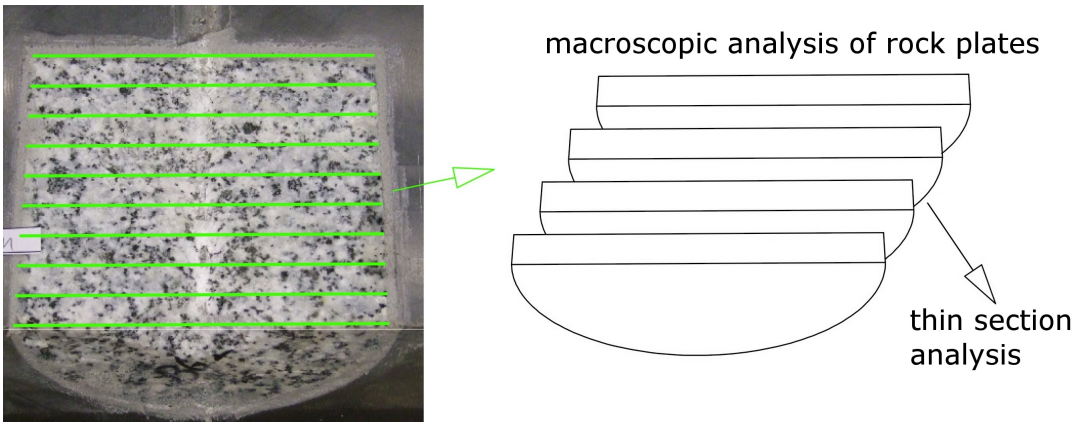


**Fig. C.3.:** Flow diagram of macroscopic and microscopic crack analysis

With the experience from method 1, it was decided to aim for a higher resolution of cross-sectional crack pattern analysis in subsequent samples. The specimens analysed with method 1 had a few cracks that were not filled with resin. As the plates were examined individually, this was not a problem. For further analysis however, it was decided to improve the resin impregnation process. Hence, in method 2, the specimens were placed into an exsiccator in which a partial vacuum was created. Subsequently, fluorescent resin was poured onto the samples through an injector valve. Thereby, it was ensured that all interconnected cracks were filled with fluorescent resin. After this preparation, the specimen were clamped into a grinding machine and the samples were ground down layer by layer. After 1 mm of rock was removed, photographs were taken in a dark room with UV-light. For each specimen, about 80 pictures of the crack network were taken to obtain a high spatial resolution of the crack network.

In order to check whether all cracks were filled with resin, dye penetrant tests were carried out with all specimens during the grinding process. In these tests, a dye is sprayed on the rock surface which penetrates into every opening. Subsequently, a developer is used to reveal for unfilled cracks. The tests did not reveal any additional cracks which proves that the obtained pictures represent the true crack network.

### C.2.4. Material properties

The full scale cutting tests were conducted with Brixen Granite (BG), a light-coloured, coarse grained granite from the southern alps. The first analysis method (Fig. C.3) that consisted of macroscopic analysis of sawn plates and subsequent thin section analysis was carried out for BG and Imberg Sandstone (IS), a light-coloured, fine grained sedimentary rock from the Ruhr region. The second analysis method, i.e. grinding down samples layer by layer to obtain a fine spatial resolution of crack patterns was done for three additional lithologies, Neuhauser Granite (NG), Calcareous Mica Schist (CMS) and Augengneiss (AG). NG is a very homogenous, compact, fine- to mid-grained granite from the Bohemian massif. CMS and AG are both metamorphic rocks from the Austrian Tauern window. CMS has rather low strength parameters with a very distinct anisotropy, whereas AG is a compact and homogenous high strength rock. For the anisotropic CMS and AG, uniaxial compressive strength (UCS) and Brazilian tensile strength (BTS) tests were carried out so that the loading direction was perpendicular to the foliation. Scaled cutting tests with AG and CMS specimens were conducted so that the cutting kerf was perpendicular to the foliation. Strength parameters including standard deviations and mineralogical composition are summarized in Table C.1, the latter is taken from Rauch (2012). The Young's modulus E was taken as the secant modulus of an unloading cycle.

| Lithology (abbreviation) | Loading direction relative to foliation | density (g/cm³) | $\sigma_C$ (sd) (MPa) | $\sigma_{BTS}$ (sd) (MPa) | E (sd) (GPa) | Mineral composition (Rauch, 2012) |
|---|---|---|---|---|---|---|
| Augengneiss (AG) | perpendicular | 2.6 | 206 (21) | 19 (0.5) | 35 (4) | feldspar, quartz, biotite |
| Calcareous mica schist (CMS) | perpendicular | 2.7 | 83 (5) | 9.9 (0.5) | 38 (14) | carbonate, quartz, muscovite |
| Brixen granite (BG) | isotropic | 2.7 | 160 (16) | 13.2 (1.1) | 43 (8) | feldspar, quartz, biotite, chlorite |
| Neuhauser granite (NG) | isotropic | 2.7 | 152 (4) | 11.8 (0.5) | 63 (4) | feldspar, quartz, biotite, muscovite |
| Imberg sandstone (IS) | isotropic | 2.6 | 141 (11) | 11.9 (0.6) | 33 (3) | quartz, carbonate, feldspar, muscovite |

**Table C.1.:** Material properties of the investigated lithologies including standard deviations (sd)

## C.3. Results

### C.3.1. Full scale cutting tests

The results that were obtained from full scale cutting tests are the three forces $F_N$ (normal), $F_R$ (rolling) and $F_S$ (side), as well as photographs of the cutting surface after each pass. A pass consists of five consecutive cuts, one in each kerf. The exterior cuts are

discarded due to boundary effects and the three central measurement cuts are used for further analyses. This sequence illustrated in Fig. C.5a. After one pass is completed, the cutter is retracted to the first kerf, indentation depth is increased and again five consecutive cuts, one in each kerf, are carried out. In order to get a full picture of each pass including interrelations of adjacent cutting kerfs, each pass was assembled to a contour plot as shown in Fig. C.4a and compared to the associated picture of the cutting surface. The left side of the picture shows force path diagrams of individual cuts. They were assembled with respect to the spacing between each cutting kerf and displayed as a contour plot which represents a view from above.

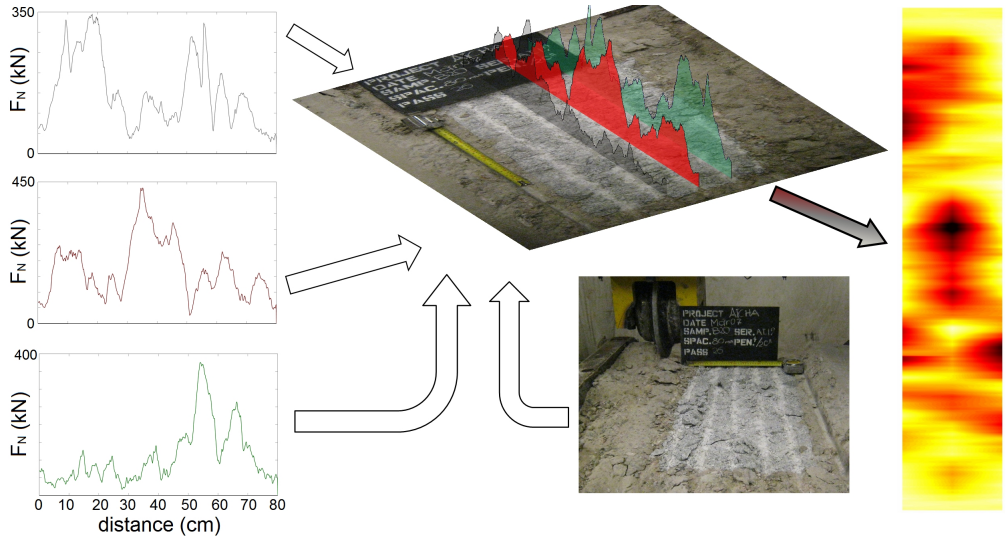


**Fig. C.4.:** All individual cuts of one pass were assembled and then displayed as a contour plot (top view)

With this contour plot representation, five consecutive passes of steady state cutting (i.e. cutting after proper conditioning passes) with constant parameters (spacing 80 mm, indentation depth 3.8 mm) will be looked at in detail. Consequently, the total indentation depth is 5 x 3.8 = 19 mm. This is like a model of 5 consecutive cutterhead revolutions of a TBM. Fig. C.5a to e show the results (the colour of the plot represents $F_N$ in kN).

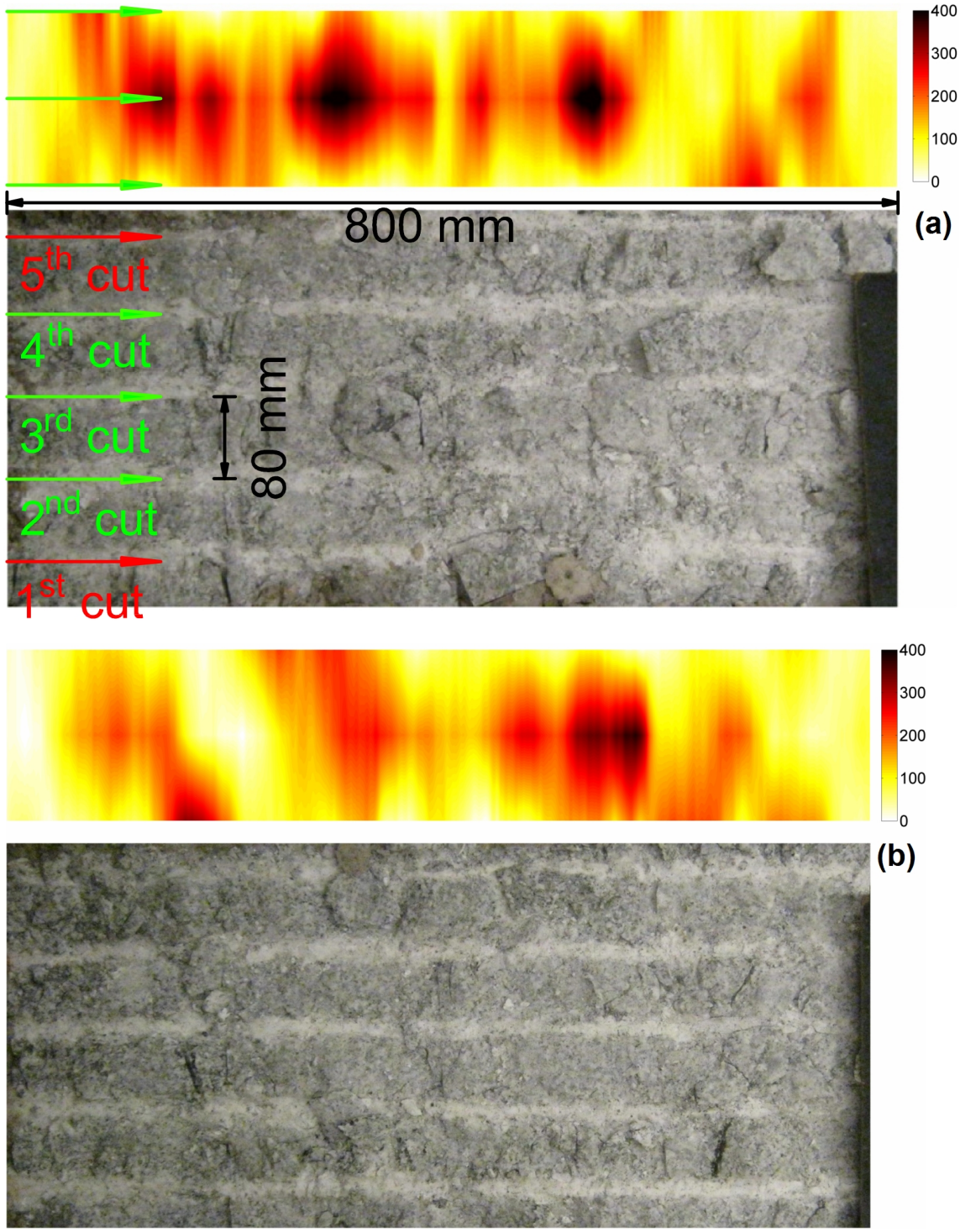
400
300
200
100
0
800 mm
(a)
5th cut
4th cut
3rd cut
2nd cut
1st cut
80 mm
400
300
200
100
0
(b)

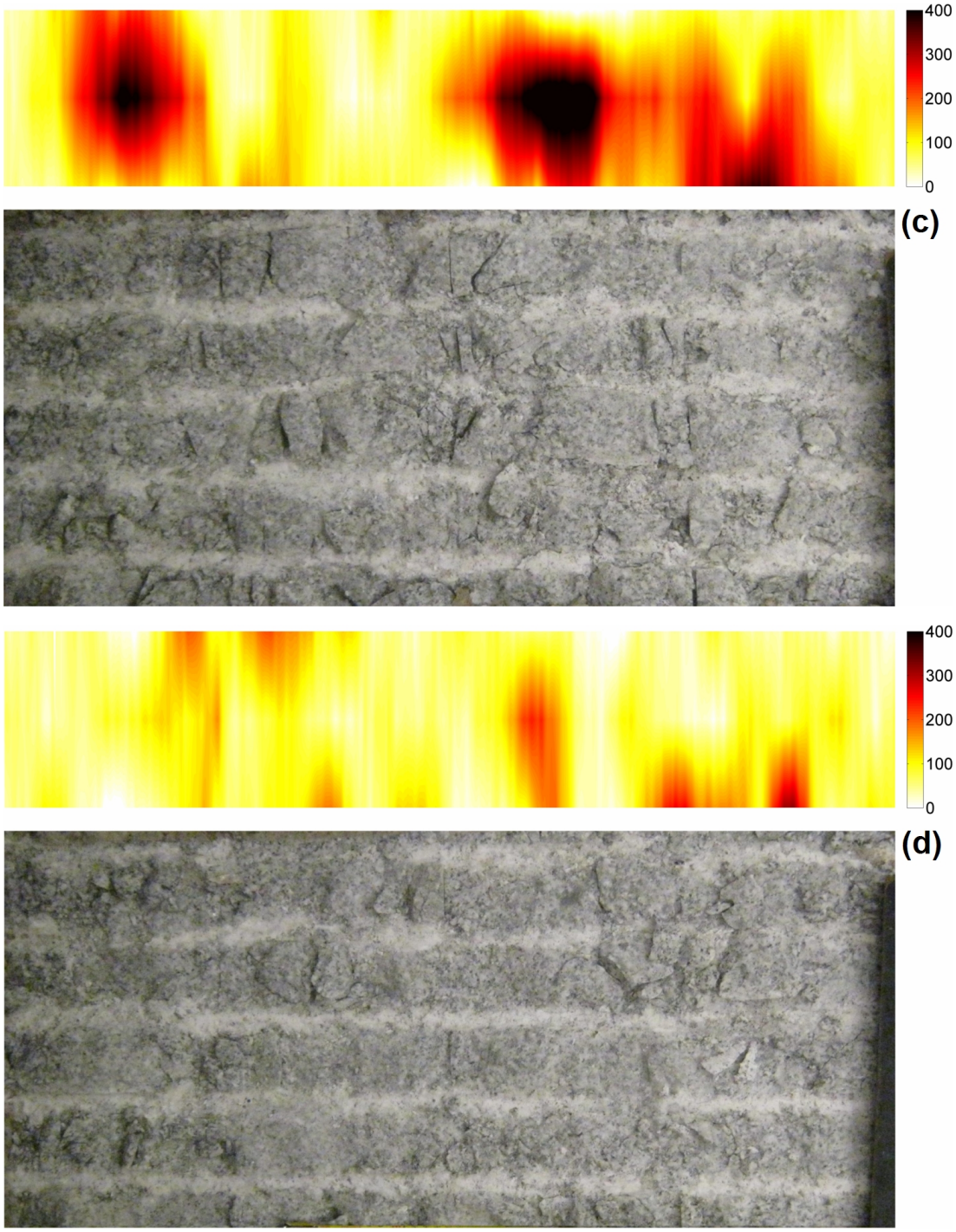
400
300
200
100
0
(c)
400
300
200
100
0
(d)

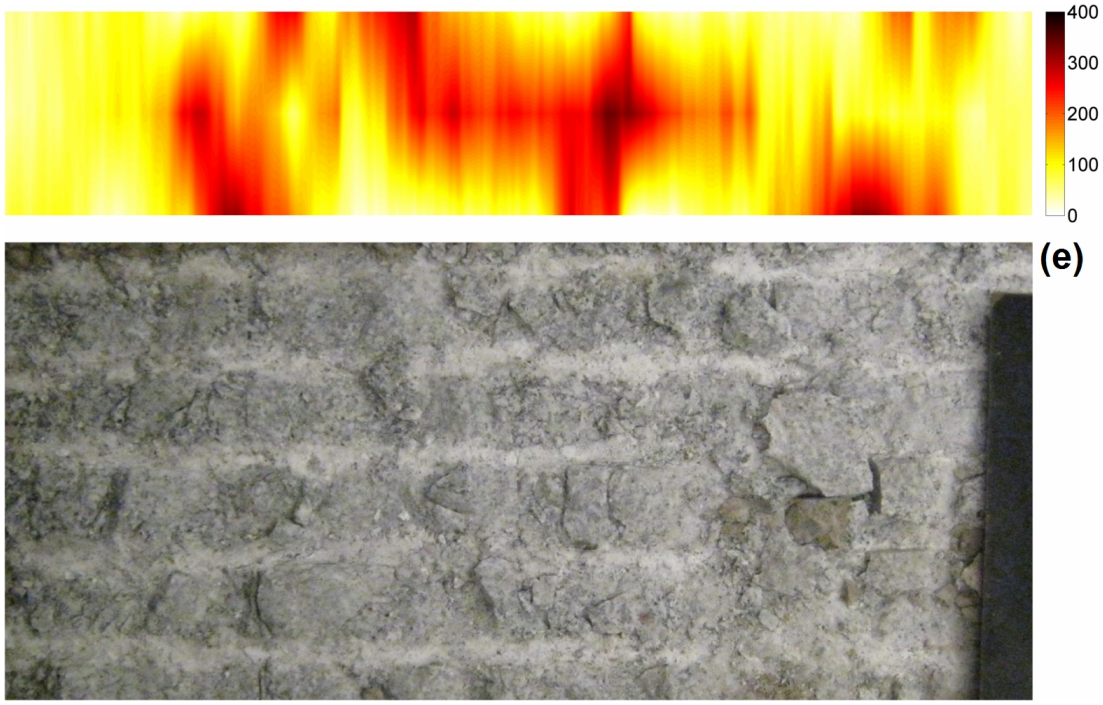


**Fig. C.5.:** Contour plot of normal force FN (kN) compared with associated cutting surface for five consecutive passes. After each pass (cutting sequence from $1^{st}$ to $5^{th}$ cut) the indentation was increased by 3.8 mm.

The forces strongly fluctuate between areas with 0 kN (cutter not engaged) and peaks of about 500 kN (Fig. C.5c) which is a multiple of the mean force. Subsequent passes interact, i.e. high or low forces in a certain spot often result in the opposite at the same spot in a subsequent pass. Because of this, a single cut should not be used for a quantification of cuttability.

Fig. 5a to e each show one individual pass consisting of three measurement cuts. Fig. C.6 shows 24 consecutive passes with a total indentation depth of 76.2 mm stacked up to a single plot. Thus, it represents the total forces acting on the specimen in all 24 consecutive passes in one contour plot. With the assumption that the specimen is sufficiently homogenous, it could be expected that forces are evenly distributed because at every spot in a cutting kerf the same rock volume was excavated. Even though the force distribution is more uniform than for individual passes, forces are still distributed unevenly. The result suggests that major fractions of the forces cannot be associated with the chipping process or efficient excavation. The fact that only parts of the energy input results in efficient crack propagation which leads to chipping will be discussed in section C.4.2. Another interesting observation is the existence of boundary effects which can be seen in the yellow areas at the left and right end of Fig. C.6.

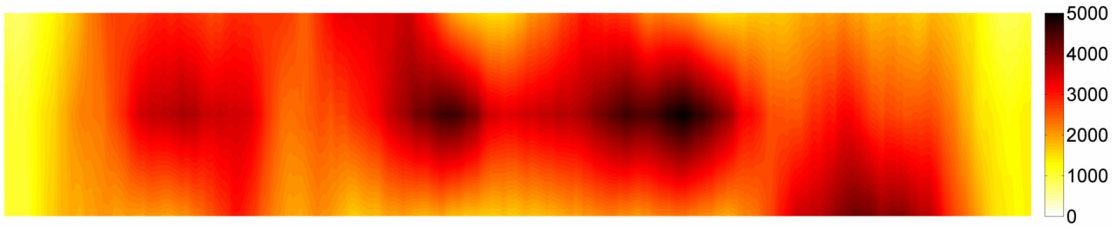


**Fig. C.6.:** Contour plot of normal force $F_N$ (kN) of 24 consecutive passes stacked up to a single plot

## C.3.2. Small scale cutting tests

### Cutting forces

All scaled cutting tests were carried out with a cutting speed of 1 mm/s. The investigated specimens had one central cutting kerf which was cut five times in a row with an indentation depth of 1.5 mm per cut. Hence, the total indentation depth was 1.5 x 5 = 7.5 mm. Furthermore, one BG and one IS specimen were cut only once instead of five times. Thus, it was possible to assess the effect of single pass cutting.

Fig. C.7 shows force path diagrams of the $1^{st}$ cut (undamaged rock), the last cut on the same specimen ($5^{th}$ cut) and the sum (stack) of all five cuts for AG, BG, IS and CMS. BG is not shown because the graphs look similar to NG. In addition to a green line, the first two graphs of each specimen are also plotted with red dots. Due to the constant cutting speed, the time between each of the red points is constant, i.e. about 0.005 s. Consequently, a large distance between red points, i.e. visibility of the green line indicates failure events with a duration of less than 0.005 s. AG (Fig. C.7a) shows very brittle behaviour, not only during the first cut, but also during the last one with an already well developed crushed zone. The NG samples such as the one displayed in Fig. C.7b behave in a slightly less, but still very brittle manner. The first cut on an undamaged surface on IS samples (Fig. C.7c) is - similarly to brittle rock types - typically accompanied by a number of sudden force drops with a significant noise signature. The consecutive cuts, however, rarely show sudden force drops. CMS (Fig. C.7d) is by far the most ductile rock type of all. Even during the first cut, sudden stress release is rare.

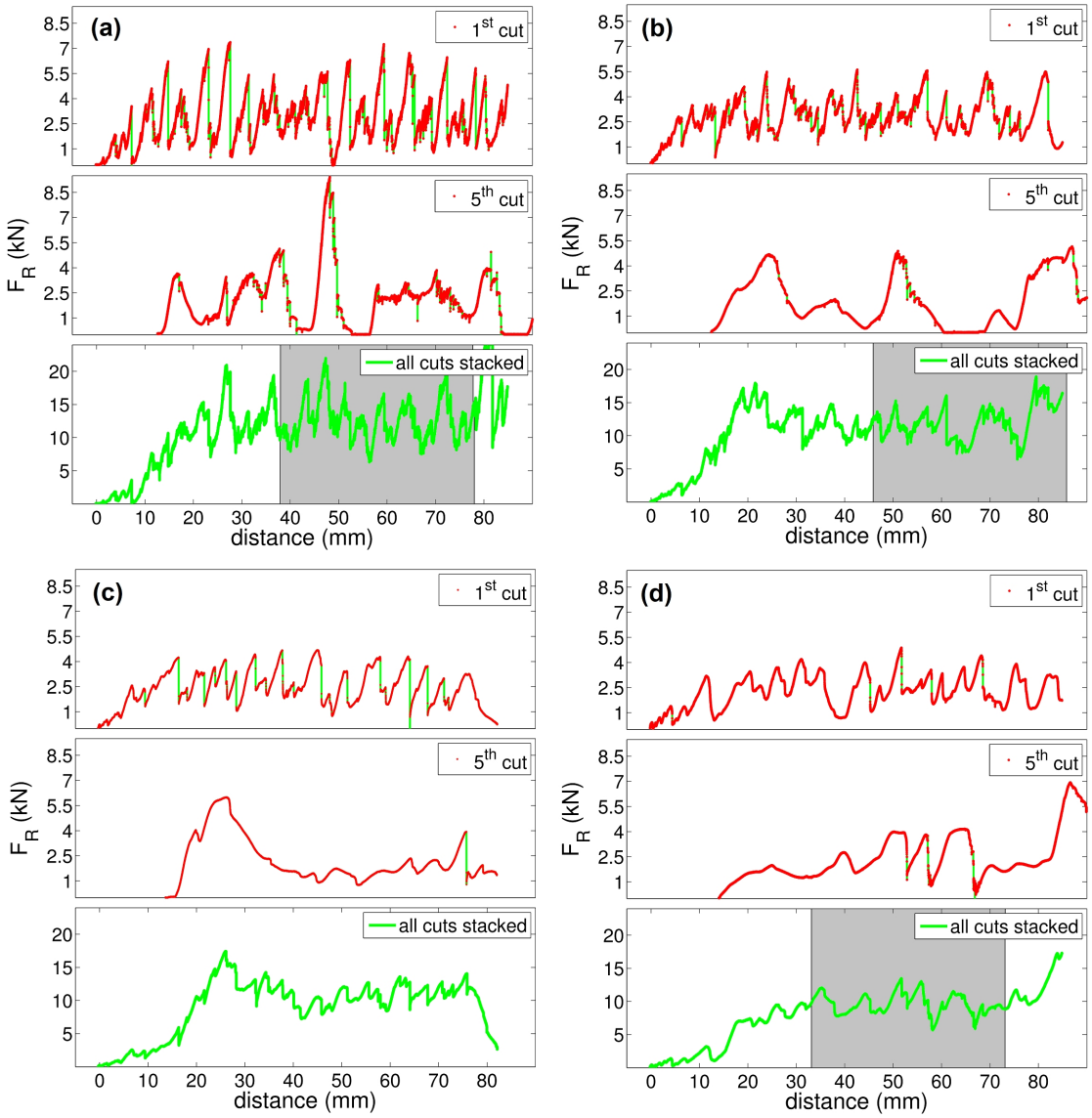


**Fig. C.7.:** Force path diagram from small scale cutting tests. The graphs show the first and last ($5^{th}$) cut on each specimens and the sum of of forces where all cuts are added up (stacked), (a) AG (b) NG (c) IS and (d) CMS

### Crack analysis

The AG, NG and CMS specimens that were analysed in Fig. C.7 were subject to a detailed crack analysis. Fig. C.8 to Fig. C.10 show the processed results of every second slice (every 2 mm) that were documented within the grey areas indicated in Fig. C.7.

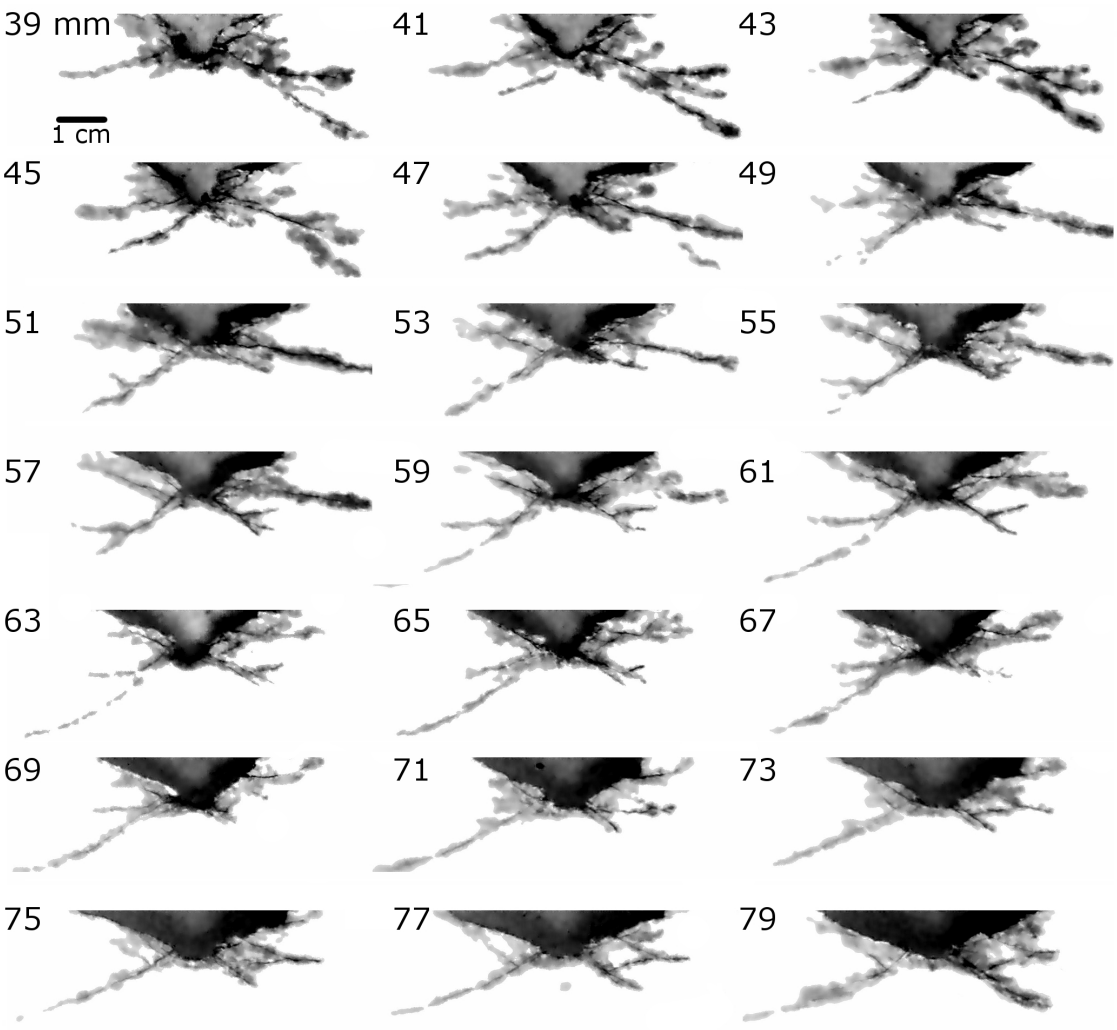


**Fig. C.8.:** Cross-sections of cracks every 2 mm of an AG sample

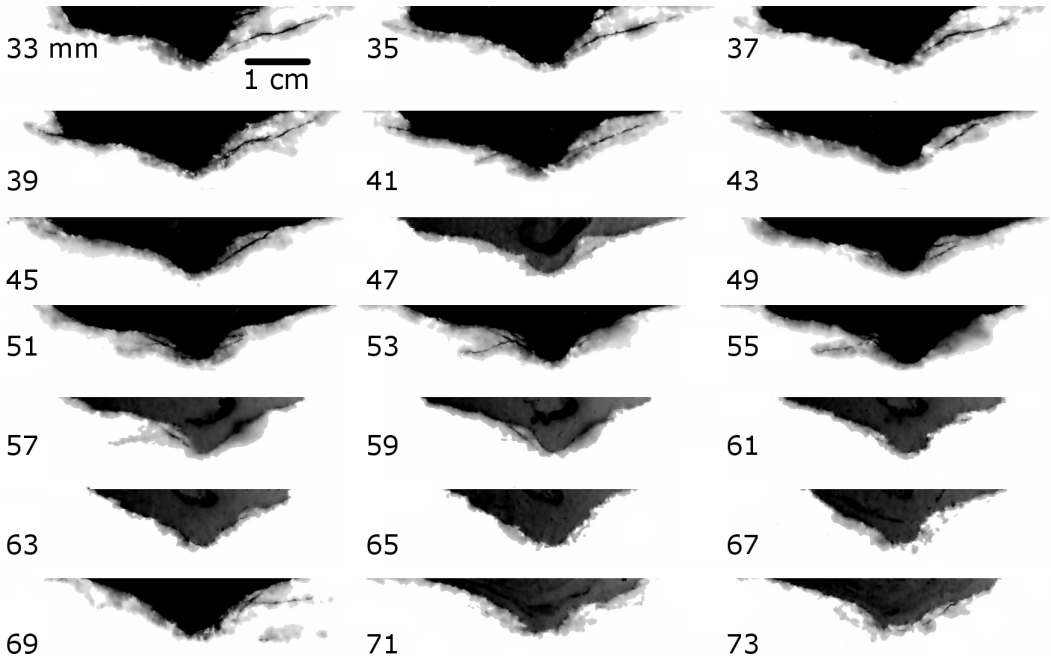


**Fig. C.9.:** Cross-sections of cracks every 2 mm of an NG sample

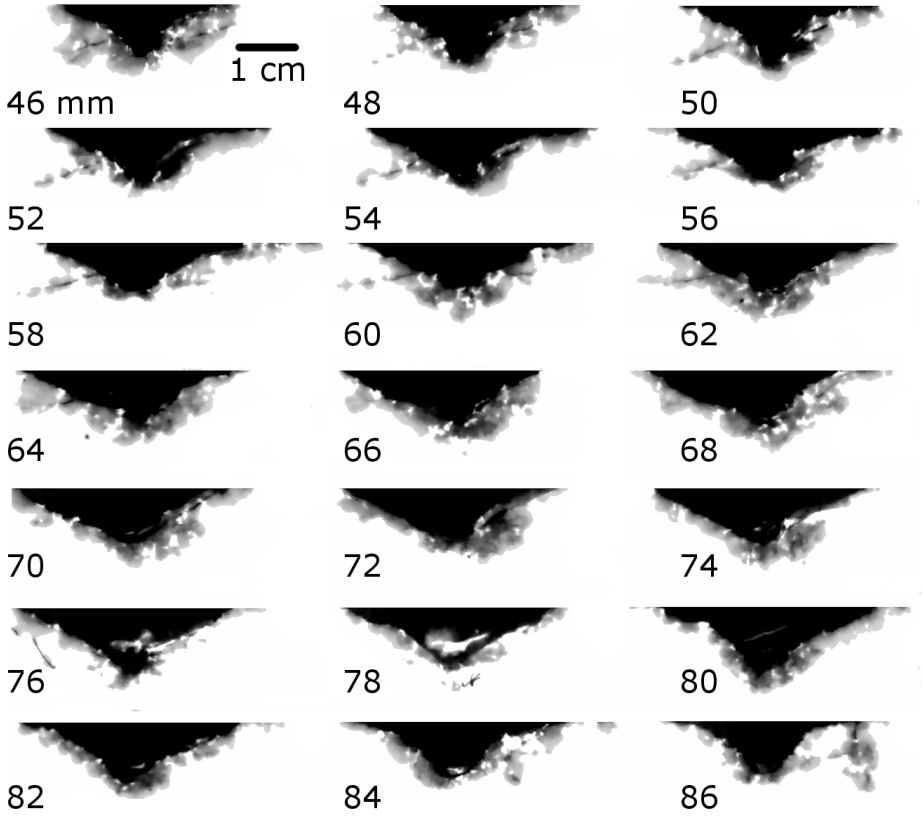


**Fig. C.10.:** Cross-sections of cracks every 2 mm of a CMS sample

The crack patterns differ significantly from each other. AG shows a distinct crack network with deep lateral cracks on one or both sides as well as a dense network of slightly shorter cracks. Fig. C.11 shows a 3d visualization of all slices in Fig. C.8.

**Fig. C.11.:** Visualization of the crack network in an AG specimen

The analysis of NG and CMS revealed that there are almost no cracks at all. This means that cracks reached the surface within the 5 cuts that the samples were subjected to. The first images in Fig. C.10 show a crack that scarcely missed the surface. Median cracks were only found in boundary areas with free surfaces, but not in the central areas with sufficient confinement.

In contrast to AG, NG and CMS specimens which were analyzed with method 2 (see section C.2.3), BG and IS specimens were subject to crack analysis with a coarser spatial resolution and subsequent thin section analysis (method 1). Most of the investigated cracks in BG specimens showed a well developed crack network with almost horizontal cracks, whereas IS samples mostly had long lateral cracks. Within central areas of the specimens, neither BG nor IS had median cracks whereas IS had prominently developed median cracks with a length of several centimetres in the boundary areas. Fig. C.12 exemplarily shows one photograph of the macroscopic crack network for BG and IS.

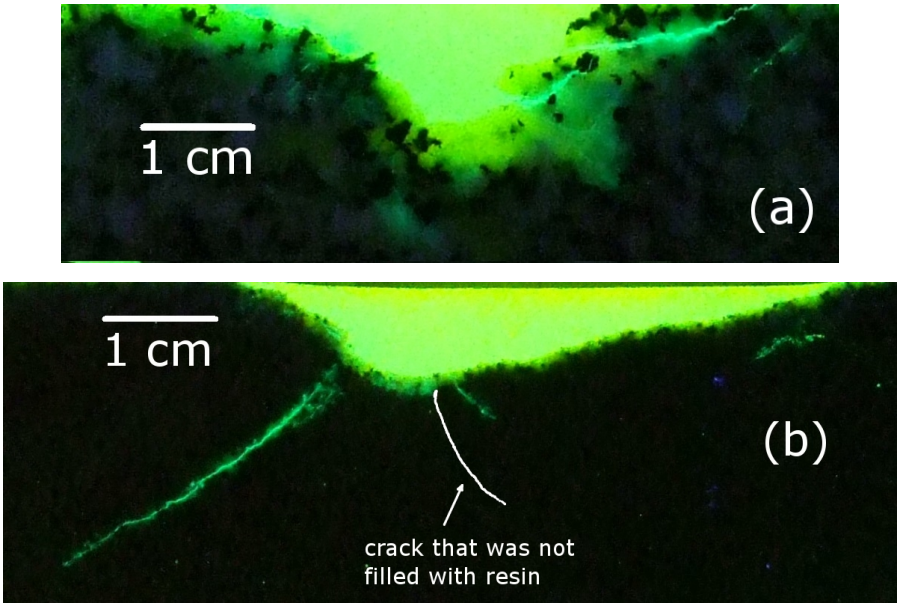


**Fig. C.12.:** Photographs of typical crack patterns in the central areas of (a) BG (b) IS specimens. The unfilled crack was observed in a specimen impregnated with method 1. Method 2 specimens (impregnation under partial vacuum) did not show any unfilled cracks.

Fig. C.13 shows a thin section of the area beneath the cutting kerf of a BG sample that was cut once (single pass cutting). The primary (not visible) and secondary crushed zone are well developed even after a single cut. The sample had almost no macroscopically visible cracks.

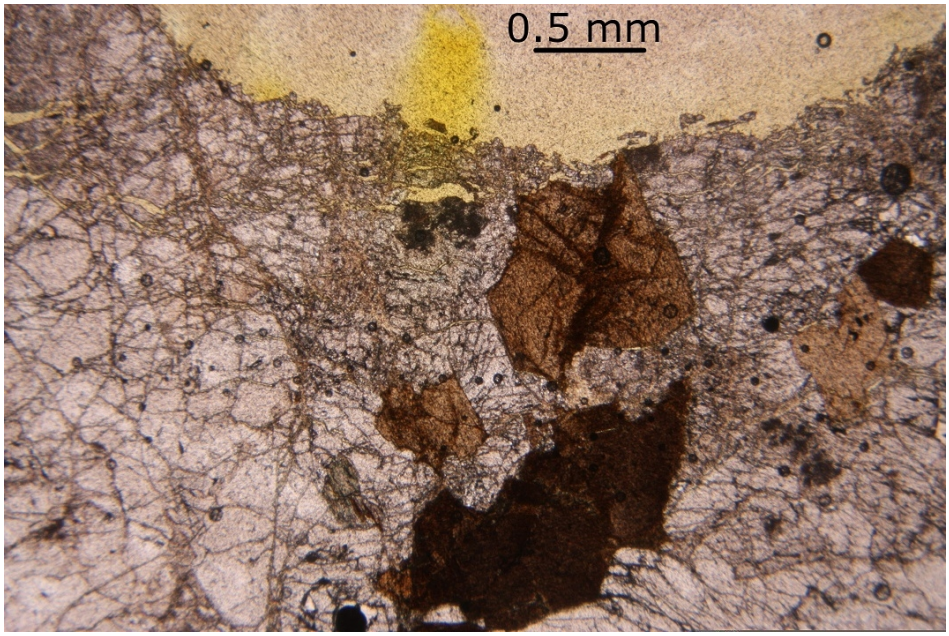


**Fig. C.13.:** Thin section of BG beneath the cutting kerf after one cut (single pass cutting)

## C.4. Discussion

### C.4.1. Effect of confinement

Fig. C.14 shows typical crack patterns from scaled rock cutting tests in the boundary areas of different specimens. Many, but not all of the investigated samples had prominent median cracks in the boundary areas and all samples had a crack network that was generally much more pronounced. In the central areas however, none of the specimens of all rock types had median cracks (see Fig. C.8 to Fig. C.10). Three of the five rock types (CMS, NG, BG) even had no significant cracks that were sub-horizontal. The other two (AG, IS) typically had cracks with an inclination of about 45°.

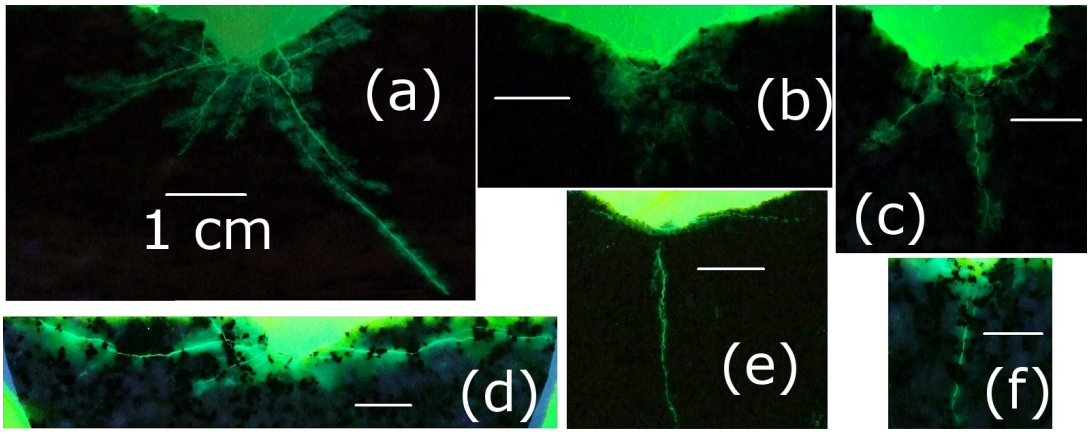


**Fig. C.14.:** Typical crack patterns in the vicinity of a free edge (boundary area): (a) AG (b) CMS (c) NG (d) BG (e) IS (f) BG

An investigation of analytical stress fields in an elastic half-space (Boussinesq and Hertzian stress fields) led Lawn and Wilshaw (1975) to the conclusion that a median crack is only likely to occur in brittle solids when a sharp indenter is used. However, there can be a wide range of crack patterns even for sharp indenters due to small imperfections of the test configuration. A hemispherical indenter will predominantly lead to hertzian cone cracks (tensile ring cracks) around the indenter. The dominant role of cone cracks is obviously even more pronounced for flat indenters. Regarding the stress field beneath an indenter, a typical constant-cross section cutter is in between a flat and a hemispherical indenter. Thus, the development of cone cracks in an elastic half-space, i.e. a semi-infinite surface, is expected in a brittle solid for a typical disc cutter.

Swain and Lawn (1976) noted that rocks might have a stronger tendency to develop median cracks than ideally elastic-brittle media. The granite rock slabs that they used for the indentation tests, however, had a thickness of only 5 cm which might have led to a stronger tendency towards median cracking due to insufficient confinement at the bottom. Many researchers such as Lindqvist et al. (1984), Larsen et al. (1987), Chen and

Labuz (2006) and Zhang et al. (2012) observed crack propagation during indentation testing in real-time. This requires a visible rock surface that inevitably leads to plane stress conditions causing a strong tendency for median cracking. In contrast to such experimental setups, researchers who used flat indenters combined with sufficient or additional confinement (e.g. Wagner and Schuemann 1970, Cook et al. 1984) observed a predominant role of cone cracks.

The results of the present paper suggest that the role of median cracks caused by rock cutting with constant cross section disc cutters was overemphasized due to the results of the papers mentioned in this section. For example, the widely known sketches of Rostami and Ozdemir (1993) illustrate the dominant role of median cracks. However, even in a state of self-confinement, i.e. a semi-infinite surface without active confinement, most rock types will not develop significant median cracks when typical constant cross-section cutters are used. This is in accordance with fracture mechanics theory as well as the results presented. It is also in accordance with the observations of Gertsch (2000) who showed that crack patterns change significantly when indentation tests are carried out on cemented rock cores on the one hand (large median cracks) or on large rock blocks on the other hand (no median cracking).

Most of the discussed results are focusing on a single indenter / cutter. Efficient Rock cutting however is based on the interaction between adjacent cutting kerfs. In contrast to single pass cutting, the cracks of a subsequent adjacent cutter are more likely to propagate in the direction of the first kerf because of the free surface that is created. Hence, the tendency for lateral cracking is expected to increase even more when cutter interaction is considered.

TBMs have often been used for excavations with high overburden, i.e. high primary stresses. A number of indentation tests with active confinement were carried out to simulate such situations. The studies of Gnirk and Cheatham (1965) and Kaitkay and Lei (2004), already mentioned in section C.1.2, are not representative of a TBM tunnel face because pressure is applied on all sides of the specimens (hydrostatic pressure). Cook et al. (1984) and Huang et al. (1998) observed a slight contact pressure increase with increasing confinement. In spite of this, the change in cracking directions caused by active confinement leads to shallower cracking. Consequently, chipping might become more efficient for large and less efficient for small cutter spacing. The complex nature of the question whether active confinement supports or hinders efficient rock cutting is supported by contradicting in situ experiences which were summarized by Innaurato et al. (2007 and 2011). Besides the isolated process of rock chipping, high primary stresses can obviously lead to severe operational problems due to sudden stress redistributions or blocky rock mass (Delisio et al. 2013). Thus, they are more often challenging than helpful.

### C.4.2. Correlation of cutting forces and rock chips

Typical force displacement curves of scaled cutting tests are shown in Fig. C.7. One of the main characteristics is the sawtooth shape, a continuous increase of force with a subsequent drop. Such drops were often associated with chipping by previous authors. Gnirk and Cheatham (1965) wrote that the force-penetration relationship of brittle rocks is piecewise linear and accompanied by the formation of distinct chips. They associate chip formation with a change in slope, i.e. force drops and recovery of force. Larsen et al. (1987) carried out wedge indentation tests and reported that the formation of chips is accompanied by unloading of the indenter. Their interpretation is based on the simultaneous observation of rock surface and force graph. Jimeno et al. (1995) displayed a force path diagram of a cutting test in sandstone and associated the peaks with the formation of major chips. According to their theory, elastic energy is accumulated and then released in the primary-chipping process. Gertsch (2000) tried to relate sawtooth shapes to specific chipping events. Many sawtooth waveforms occurred without chipping and often chips occurred without a simultaneous force peak. This observation resembles the experience of the authors. Subsequently, arguments are presented to support the hypothesis that sudden stress release is related to transgranular breakage in direct proximity of the cutter tip whereas force drops and slope changes with a smaller rate probably indicate other failure events such as chipping.

In 1867, Rittinger already showed that energy consumption in comminution is proportional to the created rock surface. The crushed zone which develops beneath a cutter consists of fine powder with a large specific surface. It is generally accepted that the majority of cutting energy is consumed in the creation of this zone and that only a few percent (about 3 to 15%), are consumed for crack propagation and thus for efficient chipping (Lawn and Wilshaw 1975, Lindqvist 1982, Mishnaevsky 1995, Gehring 1995, Bruland 1998). Thus, it seems unlikely that peak forces that represent high energy input are associated with a mechanism that consumes little energy (cracking / chipping).

Cook et al. (1984) monitored indentation tests with acoustic emission (AE) sensors. They observed the formation of tensile ring cracks at a loading of about 45% of the peak force. The force curve continued to increase almost linearly in a stable manner without a drop while the cracks propagated. At a load level of about 75% the graph became very irregular accompanied by a strong increase in AE events. This was described as microcracking with simultaneous occurrence of small rock chips very close to the indenter. Lindqvist et al. (1984) investigated indentation tests under a scanning electron microscope. They observed that crack initiation happened during the first ascent of the force graphs accompanied by slight changes in slope but without force drops. The subsequent typical irregular shapes of the graphs are associated with the commencement of chipping. Both studies state that crack initiation and crack growth are not accompanied by significant changes in the force curves.

The development of cracks and chipping is closely related. Fig. C.15 shows a specimen from a small scale cutting test with a large chip on the left side and an intact surface,

but large internal cracks on the right side. In fact, it can be assumed that a subsequent leads to chipping on the right side without significant energy input because the cracks already almost reach the surface. This potential chipping event would then not be associated with a significant force peak and subsequent sudden stress release. However, in accordance with the observations of Cook et al. (1984) and Lindqvist et al. (1984) the change in the resistance against indentation would result in a changed slope of the force graph. Depending on the kinematics of the cutting or indentation process, this could be both, a decrease of force or a less steep further increase.

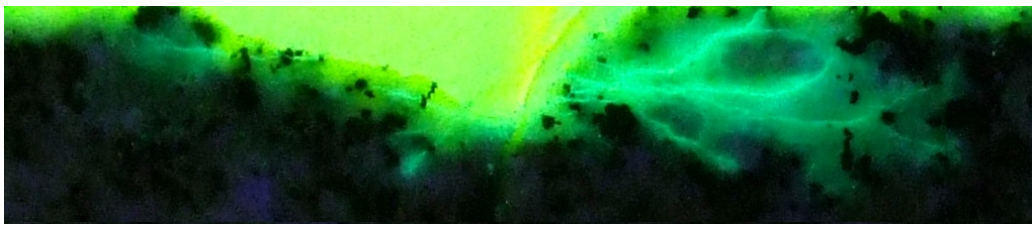

**Fig. C.15.:** BG specimen with chipping (left) and cracks just missing the surface (right)

In order to gain further insights, selected specimens were cut only once (single pass cutting) so that macro- and microscopic damage can be directly compared to the forces that acted on specific spots of the sample and the corresponding sound signature which was recorded during all tests (see section C.2.2). Fig. C.16a shows a force path diagram from an IS specimen that was cut with a penetration of 1.5 mm (single pass). The plot consists of about 16,000 points, i.e. one point every 0.005 mm or 0.005 s. This is about 200 times more dense than the data recorded during a typical full scale cutting test. The audio signal was recorded with 44,100 Hz and is plotted as a linear waveform scaled to 1.

Compared to cutting pre-damaged surfaces, the force graph shows a high number of force peaks followed by sudden stress release. Peaks in the black graph (sound) mark a clearly audible bang. They correspond with force drops with a rate higher than about 100 kN/s. Force drops with a lower rate, such as the ones at 66 and 72 mm are not accompanied by a loud audible bang. Such a threshold existed for all investigated rock types.

Fig. C.16b shows the corresponding rock surface. Besides few visible chips, sectioning of this specimen revealed that there are few short horizontal cracks that did not reach the surface. Altogether, the total number of cracks and chips is much smaller than the number of force peaks / force drops that is seen in Fig. C.16a. But similarly to Fig. C.13, the specimen had a well developed primary and secondary crushed zone. The only difference is observed in the boundary areas where large chips developed (left and right end of Fig. C.13b). The force level is much lower in these areas and while the graphs are irregular, the rate of force drops is low.

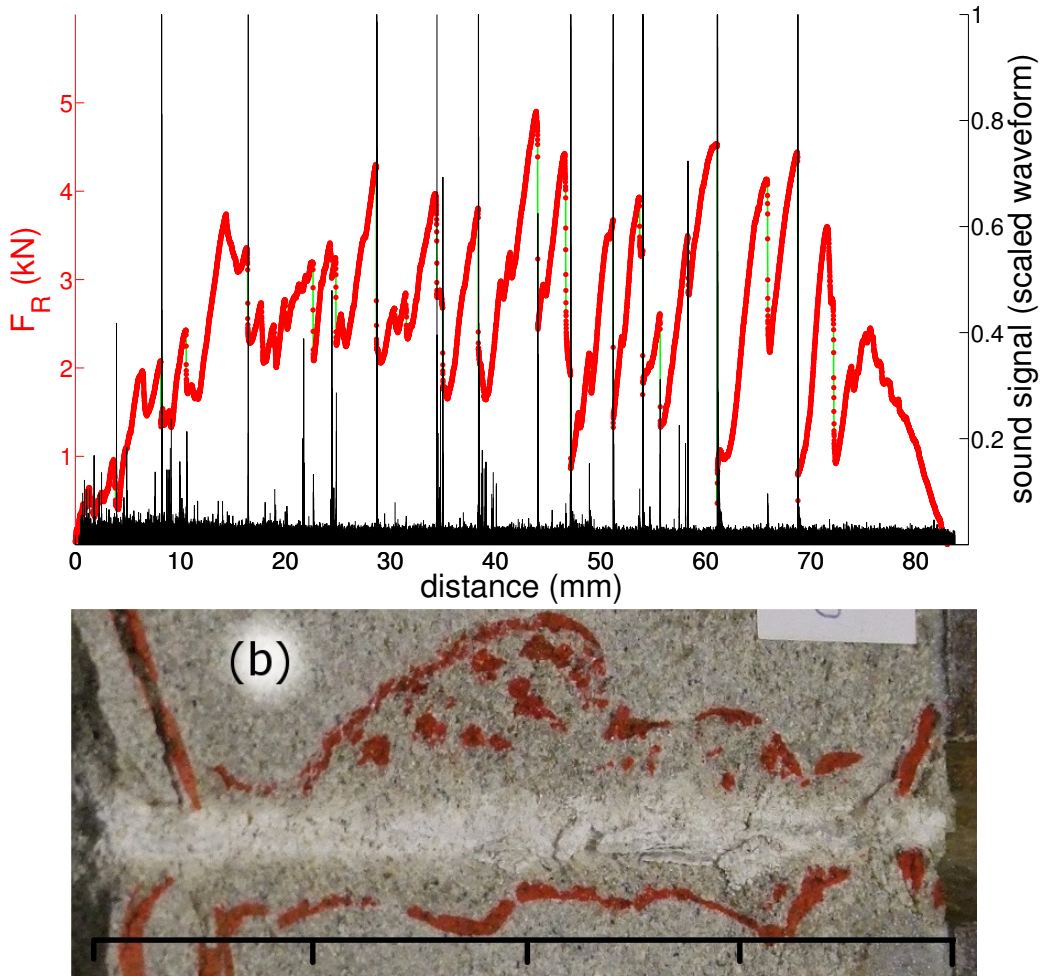


**Fig. C.16.:** Cut of an undamaged IS specimen with (a) corresponding sound signal and (b) rock surface (the edges of the breakouts is marked in red)

In a frequency spectrum, high rate force drops are represented by high frequencies whereas low rate force drops are represented by low frequencies. It was argued in this paper that the first is associated with transgranular breakage in the crushed whereas the latter indicates other failure events such as chipping. This is in accordance with the observations of Rojek and Labra (2013) who correlated cutting frequencies with chip size. They showed that large chips are associated with low cutting frequencies whereas fine powder is associated with high cutting frequencies.

All mentioned observations are in line with the following hypothesis: Force peaks and subsequent sudden energy release with a rate above a certain threshold indicate transgranular mineral breakage in the direct proximity of the cutter tip, i.e. within the primary and secondary crushed zone. Initiation of cracks or chipping consumes only small parts of the total cutting energy. These events cause irregularities in the force graph such as changes in slope, e.g. less steep further force increase or steep force drops but at much smaller rates. This hypothesis is supported by the following observations:

- Lawn and Wilshaw 1975, Lindqvist 1982, Mishnaevsky 1995, Gehring 1995 and Bruland 1998 have shown that the vast majority of cutting energy is consumed in the creation of the crushed zone (about 85 âĂŞ 97%). Hence, a correlation between the highest forces and chipping seems unlikely.
- The observations of Cook et al. (1984) and Lindqvist et al. (1984) revealed that crack initiation and propagation are indicated by changes in slope but not sudden stress release. This is in accordance with the left and right end of Fig. C.16.
- Specimens that were cut only once (single pass cutting) had few cracks / chips and no apparent correlation with the force graph. However, the samples had well developed crushed zones and the force graph had disproportionately many force peaks with subsequent sudden stress release at extremely high rates.
- The high rate of force decrease indicates that failure happens directly underneath the cutter and not at a distant crack tip. The sudden energy releases are also accompanied by loud bangs.

### C.4.3. Size effects due to cutter size

Many of the presented results were obtained from small scale cutting tests. The cutter used in these tests is a 1:8 model of a typical 17" cutter. Thus, size effects have to be investigated. Wagner and Schuemann (1970) carried out indentation tests and observed a size effect that was particularly pronounced for brittle rock types, but less pronounced for ductile rock types. This effect was confirmed by Cook et al. (1984) and Chiaia (2001). It was shown that contact pressure decreases significantly with increasing indenter size. In 1921, Griffith set the foundation for the development of fracture mechanics. His experiments showed that the tensile strength of brittle materials is greatly reduced by imperfections such as microscopic cracks. Consequently, the ultimate strength of geometrically similar specimens is size dependent because larger specimens incorporate more imperfections and the probability of having weak spots increases. The size effect is still an important research topic, recent review papers were published by Danzer et al. (2008) or Bazant (1999).

To examine the size effect, average cutting forces and contact pressures of full and small scale cutting tests are compared. The theoretical contact area is calculated by multiplying the cutter tip width with the cutters indentation length which is a function of cutter radius and indentation depth. Rostami (2013) published results that show what typical pressure distributions beneath a disc cutter look like. It shows that there is no constant pressure distribution along the whole indentation length. To account for this effect, the theoretical contact area was divided by 2 to obtain an assumed contact area that gives reasonable contact pressure values. As explained in section C.2.2, normal force FN is not measured directly in the small scale cutting test. However, $F_N$ can be calculated from $F_R$ with the equations of the CSM model (Rostami and Ozdemir

scale cutting test

| | | | | | | | |
|---|---|---|---|---|---|---|---|
| **R** | 28 mm | | | | | | |
| **p** | 1.5 mm | | **Kontaktlänge** | **Tip width** | **Kontaktfläche** | **Kontaktfläche** | |
| **phi** | 0.3288 | 18.839197 ° | 9.2066 | 2.50 | 23.0 mm² | 11.5 mm² | |

| | | | |
|---|---|---|---|
| | **Kraft RC (last 3 av** | **Pressure (MPa)** | |
| | 12.5 kN | 543.0905157 | |

1993). In fact, $F_N$ and $F_R$ are closely interrelated. Table 2 shows the results of these calculations.

| Cutter radius (mm) | Indentation depth (mm) | Indentation length (mm) | Cutter tip width (mm) | Theoretical contact area (mm²) | Assumed contact area (mm²) | Normal force $F_N$ (kN) | Contact pressure (MPa) |
|---|---|---|---|---|---|---|---|
| 216 | 7.6 | 57.5 | 15.9 | 914 | 457 | 167 | 365 |
| 28 | 1.5 | 9.2 | 2.5 | 23 | 11.5 | 12.5 | 543 |

**Table C.2.:** Contact pressure calculation for full and small scale cutting tests

The estimated average contact pressure is about 50% higher in small scale cutting tests (543 MPa) than in full scale cutting tests (365 MPa). The order of magnitude of these values indicates that the stress state beneath a cutter is clearly triaxial. The results are similar to the observations of Wagner and Schuemann (1970) and Cook et al. (1984). As far as rock cutting efficiency is concerned, the results suggest that the use of large cutter is more efficient than the use of small cutters. This will be especially true for very brittle rock types where size effects are more pronounced.

## C.5. Conclusions

Full scale and small scale cutting tests were analysed with respect to cutting forces and corresponding rock failure mechanisms. A particular focus was put on visualizing and interpreting crack networks and directions. The conclusions of the paper are:

- It was shown that crack directions differ significantly depending on the confinement situation. Lateral crack systems typically develop in rock cutting with constant cross section cutters. In all presented observations, median cracking only occurrs in boundary areas or at free edges, i.e. in insufficiently confined areas. At an actual tunnel face, confinement depends not only on primary stress, but also on the position of the cutter (center, face or gauge area), rock mass properties and pre-damage of the tunnel face.
- The characteristic shape of cutting force graphs is strongly dependent on rock type and condition of the rock surface. Cutting undamaged brittle rock results in a large number of rather regular sawtooth shapes with sudden stress release at very high rates accompanied by loud bangs. On pre-damaged rock, the graph typically becomes more irregular including non-linear areas or plateaus, but also sudden stress releases accompanied by loud bangs. In contrast to that, force graphs from ductile rock types are more regular, have a more gentle noise signature and contain clearly non-linear areas even when undamaged rock is cut. Sudden stress release at very high rates occurs less frequently than in brittle rock.

- The presented results as well as previous studies are in line with the followimg hypothesis: Force peaks and subsequent sudden energy release with a rate above a certain threshold indicate transgranular mineral breakage in the direct proximity of the cutter tip, i.e. within the primary and secondary crushed zone. Initiation of cracks or chipping consumes only small parts of the total cutting energy. These events cause irregularities in the force graph such as changes in slope, e.g. less steep further force increase or steep force drops but at much smaller rates.
- A comparison between full and small scale cutting tests revealed the presence of a size effect. According to previous studies and the results presented in this paper, large cutting tools need less contact stress in excavation than small ones in brittle rock types.

## Acknowledgements

We are indebted to Dr. Christian Frenzel for the supervision of cutting tests and in-depth discussions about disc cutting and to Brian Asbury for the guidance and assistance provided. Stefan Lorenz contributed significantly during small scale cutting testing for which we are very thankful. We would like to thank Thomas Schifko for the preparation of thin sections. The help of Dr. Nina Gegenhuber, Dr. Beate Oswald-Tranta and Mario Sorger is much appreciated. We would also like to thank the reviewers of this paper for their helpful comments. We gratefully acknowledge the financial support of this work by the Austrian Research Promotion Agency (FFG) within the Eurostars project E!5514.

# D. TBM performance prediction with scaled rock cutting tests

This paper is authored by Martin Entacher, Stefan Lorenz and Robert Galler and was submitted to *International Journal of Rock Mechanics and Mining Sciences*.

A scaled rock cutting test developed at the Chair of Subsurface Engineering, Montanuniversität Leoben, is presented. It is designed as an attachment for hydraulic presses commonly available in rock mechanics laboratories. Rotating disc cutters are used to cut rock samples several times with the possibility of adjusting indentation depth and spacing. Standard sample sizes which are available in early phases of a tunnelling project are used in order to enable this test to be used for TBM performance prediction. The results are compared to full scale linear cutting tests and to geotechnical standard values such as uniaxial compressive and Brazilian tensile strength. It is shown that the quality of the results is superior to geotechnical standard tests while at the same time tests are cheaper and easier to conduct compared to full scale rock cutting tests.

## D.1. Introduction

Accurate performance prediction is one of the main concerns in determining the construction time of excavations utilizing mechanical excavators such as tunnel boring machines (TBM). Typically, performance prediction models are based on geotechnical parameters like uniaxial compressive and indirect tensile strength as their main input parameters. The most established model of this kind is the semi-empirical / semi-theoretical performance prediction model of the Colorado School of Mines (Rostami 1997). It was developed by combining basic theoretical relationships with laboratory data obtained from full scale rock cutting tests.

Another well established model is the NTNU hard rock TBM prognosis model (Bruland 1998). It was developed empirically by evaluating TBM field performance in various hard rock tunnelling projects. In contrast to a large number of models based on standard strength parameters, the NTNU model uses separately developed tests to predict the net penetration rate, i.e. brittleness value S20 which is determined with an

impact hammer crushing a rock sample and Sievers' J-Value which is determined by a miniature drilling test and gives a value for surface hardness. Both values are then combined to a drilling rate index (DRI).

Besides the presented models, the best net penetration rate prediction can be obtained by conducting full scale linear cutting tests. The first well-known linear cutting machine was built in the 1970's at the Earth Mechanics Institute of the Colorado School of Mines (Ozdemir et al. 1976). Today, there are several linear cutting rigs which are used for the evaluation of rock cuttability (e.g. Balci and Bilgin 2007, Jeon et al. 2006, Abu Bakar and Gertsch 2012).

Although they provide reliable results, full scale cutting tests are costly and time-consuming. In addition, large rock blocks are needed which are typically not available during an exploration phase of a tunnel project. Hence, full scale cutting tests are rarely carried out for performance prediction purposes before TBM excavation starts. In order to overcome these downsides, cutting tests on a smaller scale might prove useful because rock failure mechanisms are identical to the real excavation process, except for scale effects.

Roxborough and Philipps (1974) developed a rock cutting rig for testing the performance of drag picks. The rig was built as a modification of an industrial shaping machine. It was not meant to be a small scale test as it was capable of testing large rock blocks and focused on the use of full scale drag picks. It is however mentioned in the introduction of the paper that discs and other types of cutters were also used. This was obviously done at a model scale because the testing rig is much smaller than a full scale linear cutting machine. McFeat-Smith and Fowell (1979) used the same test rig and focused on the selection and application of roadheaders. They used rigid picks to cut unconfined rock cores and measured parameters such as specific energy ($MJ/m^3$ yield).

Öztürk et al. (2004) used the same cutting rig for extensive test series with picks at Istanbul Technical University. Bilgin et al. (2010) subsequently developed an improved cutting rig (portable linear cutting machine, PLCM) that was presented at EUROCK 2010. The PLCM is capable of testing small scale disc cutters and rock blocks of about 20x20x10 cm. It is equipped with a triaxial load cell with an accuracy of about 1 kN. The conducted test series is compared with full scale linear cutting tests and proves that small scale cutting tests are very promising.

This paper presents an evaluation of a scaled rock cutting laboratory test developed at the Chair of Subsurface Engineering, Montanuniversität Leoben, that is designed as an attachment fixture for hydraulic presses typically available in rock mechanics laboratories. As it uses existing infrastructure, the test rig is easy to use and causes very little cost. The preciseness of the used load cell allows for fundamental investigations of rock breakage mechanisms. It is shown that high-quality results applicable for TBM performance prediction are obtained with standard specimen geometries that are available during exploration. The results are validated by a comparison will full scale rock cutting tests.

## D.2. Development of a scaled rock cutting test

### D.2.1. Design and assembly

The design of the scaled cutting test was governed by the following boundary conditions:

- Specimen geometry should be such that it can be obtained at early phases of a tunnelling project,
- confinement of samples should ensure similar conditions as a semi-infinite rock surface,
- a rotating scaled disc cutter with realistic geometry should be used,
- indentation depth (penetration) should be very precisely adjustable,
- no measurement equipment should be needed in addition to the load cell of a hydraulic press.

According to these constraints, it was chosen to use rock cores with a diameter of 10 cm that are cut in half and a height of approximately 9 cm because the maximum stroke of a typical hydraulic press is 10 cm. The size of the disc cutter was estimated in order to suit such sample sizes without inducing cracks that reach to the edge of the specimen. It was chosen to use a steel cutter with a carbonitrided surface that approximately represents approximately a 1:8 model of a typical 17" constant cross-section cutter. Geometry details can be seen in Fig. D.1.

During assembly, the disc cutter is heated up and shrunk onto a shaft which is attached to a housing with combined needle / ball bearings to ensure sufficient maximum load capacity and smooth rotation. The cutter housing is attached to a linear bearing that ensures a straight cutting path when the cutter is thrust into the sample. The specimen holder is a stiff steel block into which the rock sample is cemented with a two-component epoxy resin that ensures optimal confinement. It can be attached to its counterpart with bolts either in a central position or with an offset to simulate interacting cuts with spacing in between. Steel spacers are put between the specimen holder and the disc cutter in order to be able to adjust the necessary indentation depth of the cutter. Load is applied via a load application element that can move freely in the horizontal direction. Hence, forces act only in cutting direction. An assembly drawing and a photograph of the complete test setup is shown in Fig. D.2a and Fig. D.2b, respectively.

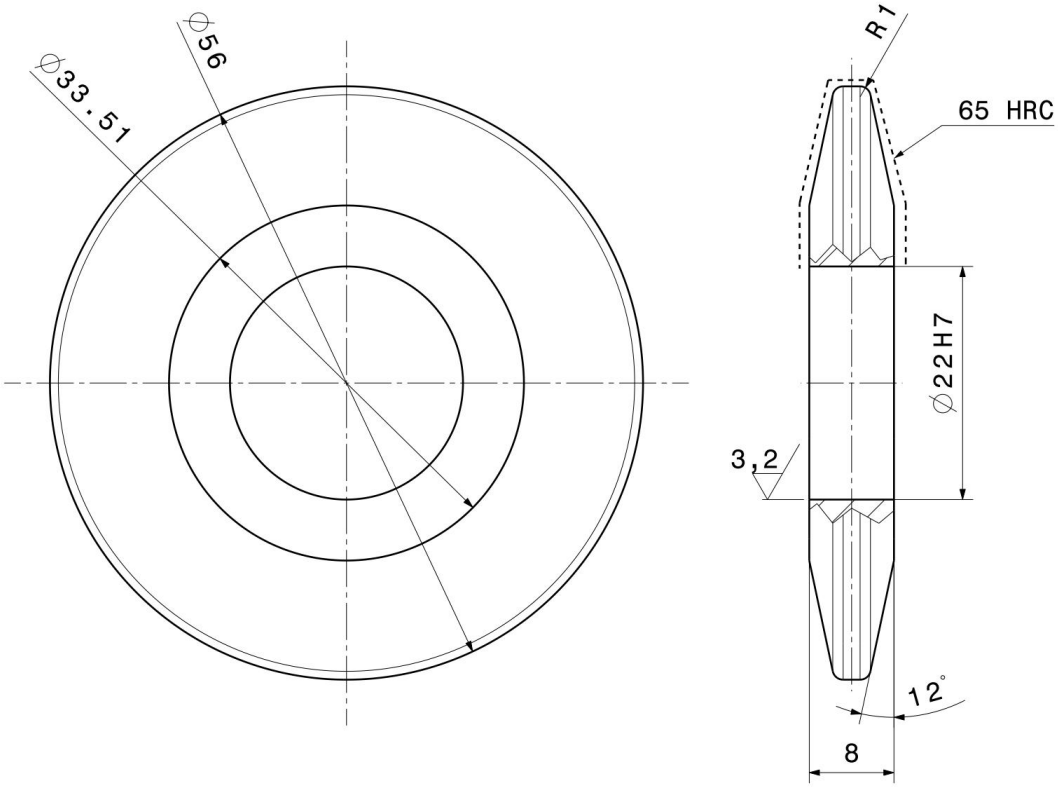


**Fig. D.1.:** Geometry of the disc cutter (dimensions in mm)

Suitable indentation depths for this apparatus are in the range of 1 to 3 mm. Consequently, a very small clearance of all moving parts, especially bearings, is needed to obtain good results. A clearance of $\pm$ 0.2 mm for example would cause scatter in the range of $\pm$ 20% for an indentation depth of 1 mm, which is clearly unacceptable. Hence, all bearings were selected carefully, manufacturing tolerances were chosen to be very small and the process of cementing the specimen into its holder was carried out very precisely. It turned out during the tests that all tolerances are negligibly small as they did not affect the quality of results.

### D.2.2. Sample preparation

The two-component epoxy resin Sikdaur-31 AUT R was used to cement 9 cm high half rock cores with a diameter of 10 cm into the specimen holders. In order to be able to conduct tests every second day, the resin was allowed to harden for about 36 hours before testing. According to its data sheet, the resin will then have a compressive strength of about 60 MPa which is about 75% of its final strength. The cementation process of the sample is illustrated in Fig. D.3.

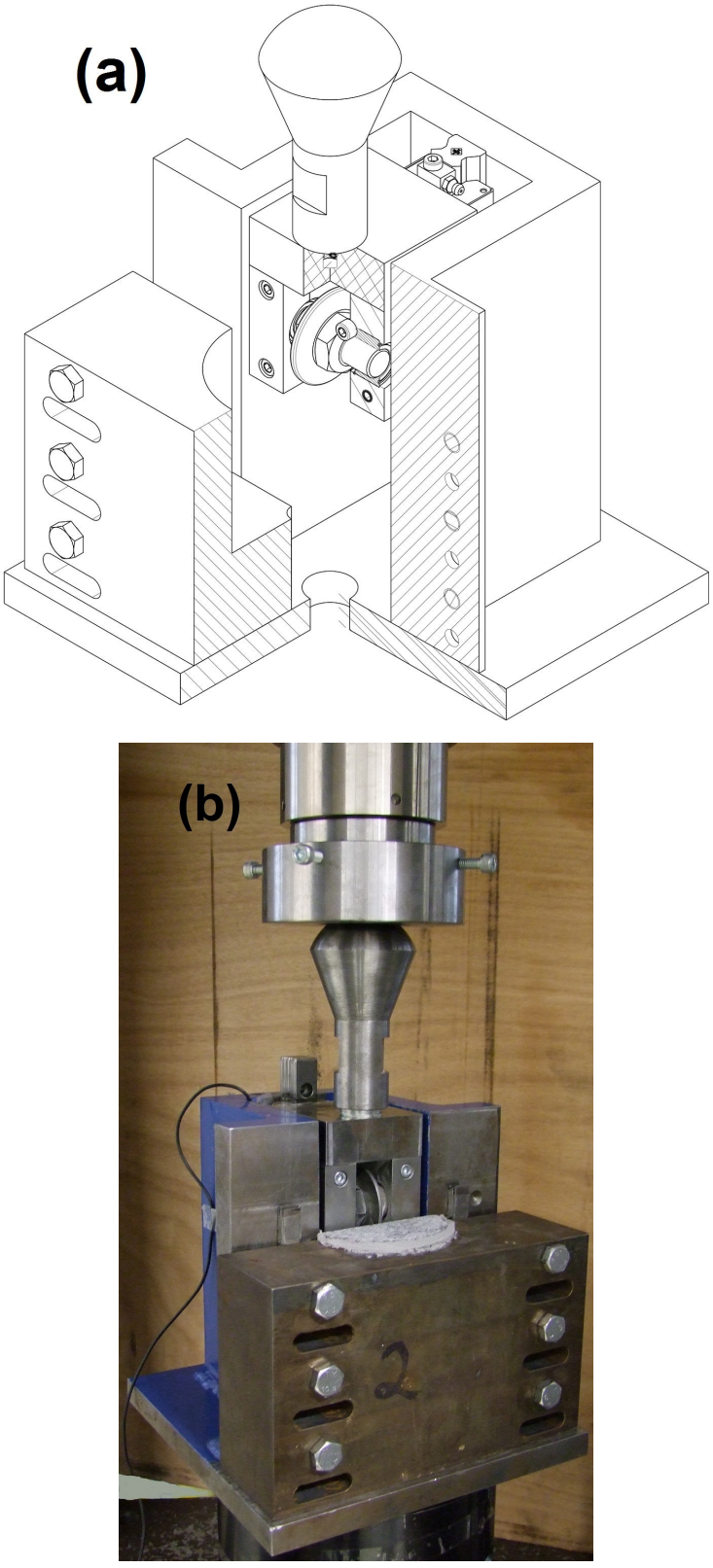


**Fig. D.2.:** Cut-view of the scaled rock cutting test (a), experiment setup (b)

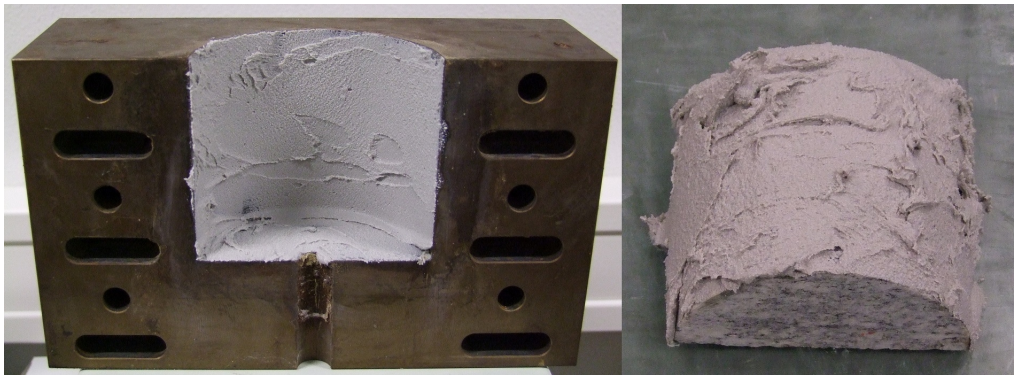

**Fig. D.3.:** Cementation of the sample with epoxy resin

In order to assess the influence of the stiffness of the resin layer a sensitivity analysis was performed by means of the finite element method. An overview of the simulation model is shown in Fig. D.3.

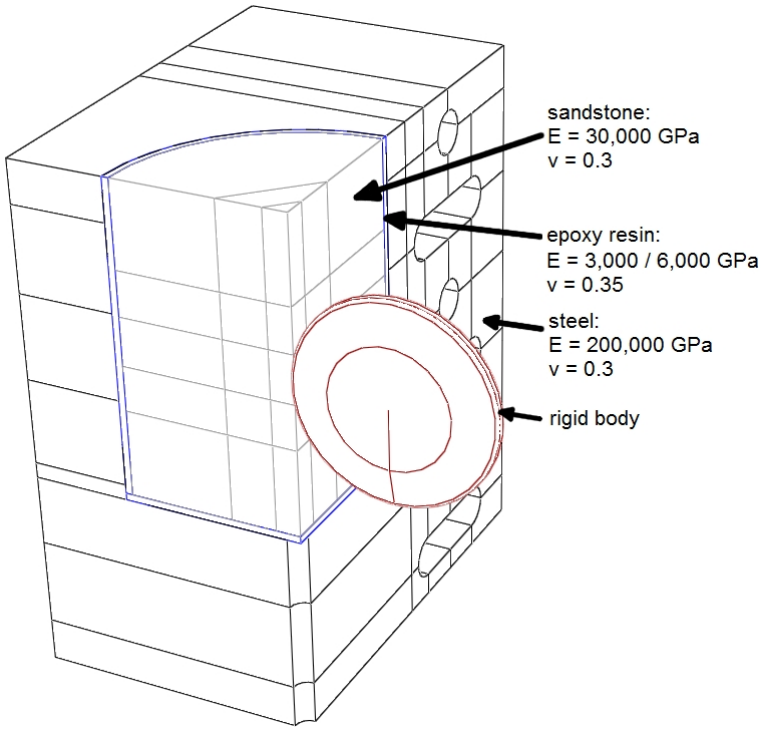


**Fig. D.4.:** Finite element simulation model with material parameters

Two extreme parameter sets are simulated to investigate the influence of epoxy resin thickness and Young's modulus which govern the stiffness of the cementation. For parameter set one, a very thin resin layer and a high Young's modulus of 6,000 MPa are assumed, resulting in the stiffest possible configuration. Parameter set 2 assumes a thick layer of resin with a Young's modulus of 3,000 MPa, i.e. the weakest possible

configuration. The material law is linear elastic, failure criteria are not considered. Hence, the sole purpose of this simulation is to understand the influence of different epoxy resin layers. The interaction between disc cutter and rock surface is defined as “hard contact”, so no indentation into the rock is possible. The cutter is loaded with a normal force $F_N$ of 30 kN, all end nodes of the bolt hole are held in x-, y- and z-direction, a symmetry plane is established at the center line of the specimen. The model was partitioned multiple times to enable a structured meshing routine with 8-node hexahedral elements with reduced integration. The simulation was carried out with Abaqus 6.10. Fig. D.5 shows a cut-view of the deformation in loading direction directly at the indentation point of the cutter for a thick resin layer with low Young’s modulus (Fig. D.5a) and for a thin resin layer with high Young’s modulus (Fig. D.5b). According to the simulation, the differences in deformation at the boundary of the resin layer are about 10% in relative numbers and about 3/1000 mm in absolute numbers which is clearly negligible even for the extreme cases assumed.

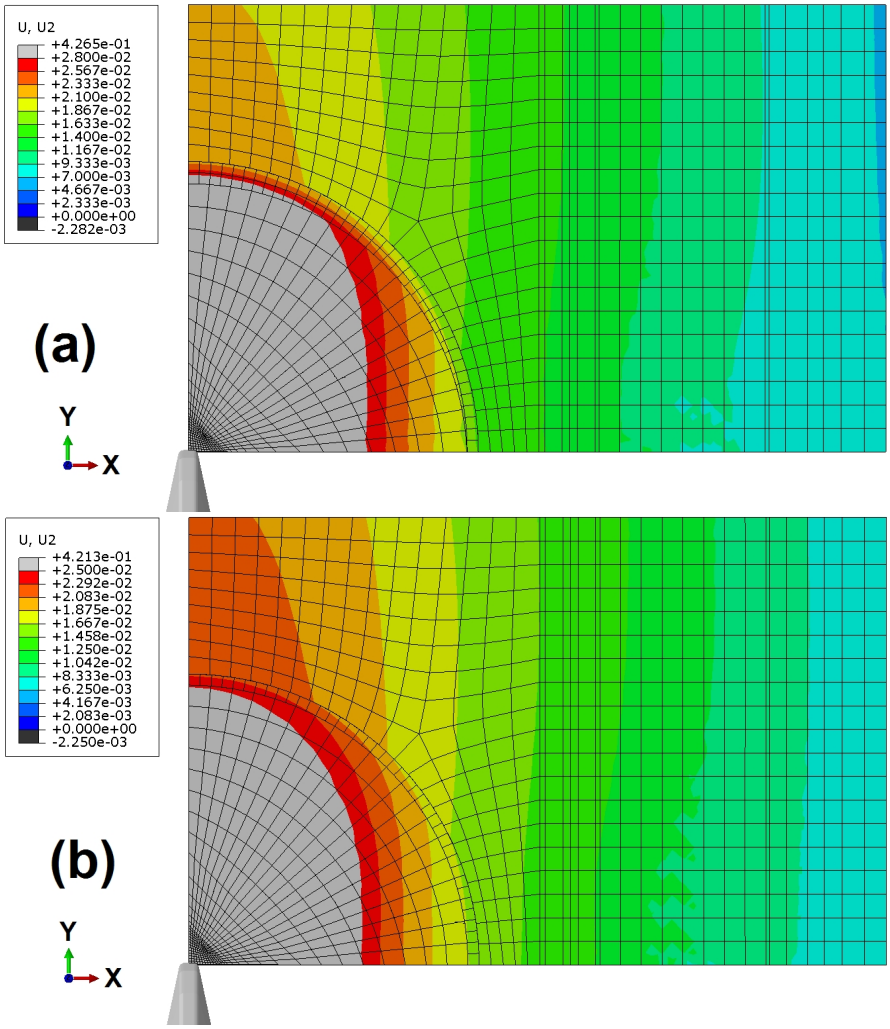


**Fig. D.5.:** Deformations for a thick and weak resin layer (a) and for a thin and stiff layer (b)

### D.2.3. Measurement instrumentation

The scaled cutting test rig is not equipped with sensors. Instead, cutting force is measured with a load cell installed in the frame of the hydraulic press. Normal and side forces are not measured for two reasons. The first one is simplicity, which ensures that the apparatus can easily be installed without additional measurement equipment and calibration procedures. Second, uniaxial load cells are much more accurate than triaxial transducers.

One of the assumptions of the performance prediction model of the Colorado School of Mines is that rolling ($F_R$) and normal force ($F_N$) are not independent of each other. One can be converted into the other with a conversion factor that is a function of penetration depth and cutter radius. The calculation is based on the assumption that there is a constant pressure distribution between cutter and rock over the whole contact length which is described by angle $\Phi$. For a constant pressure distribution, $\beta$ (angle of load application) becomes $\Phi/2$ which is a reasonable assumption. $\Phi$ and $\beta$ are illustrated in Fig. D.6.

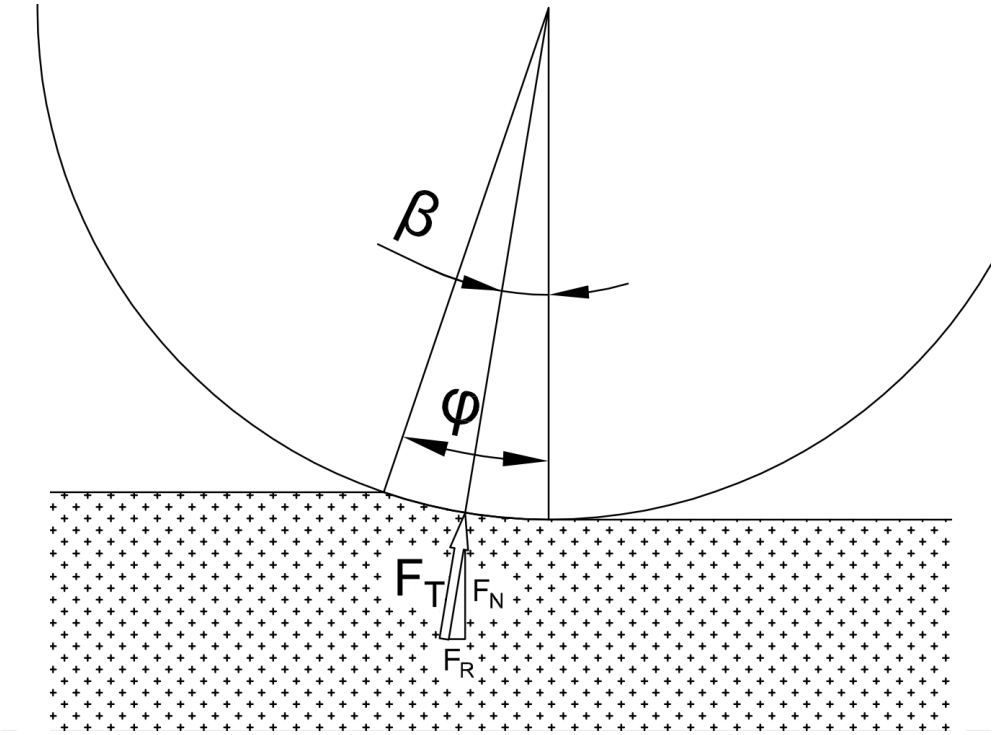


**Fig. D.6.:** Relationship between rolling ($F_R$) and normal force ($F_N$)

In reality, $\beta$ would probably be a little less because it can be assumed that the pressure directly underneath the cutter is higher than in the vicinity of the crushed zone. This pressure distribution was thoroughly investigated by Rostami (2013) with a strain gauge equipped disc cutter. After the calculation of $\beta$, normal and rolling force can be found

using trigonometric functions (R: cutter radius, p: penetration, in-depth explanations can be found in Rostami (1997)):

$$\phi = \arccos\left(\frac{R-p}{R}\right),\ \beta = \frac{\phi}{2} \tag{D.1}$$

$$F_N = F_T\ \cos\beta,\ F_R = F_T\ \sin\beta \tag{D.2}$$

$$\frac{F_N}{\cos\ \beta} = \frac{F_R}{\sin\ \beta} \tag{D.3}$$

$$F_N = \frac{F_R}{\tan\ \beta} \tag{D.4}$$

For the scaled cutting test (r = 28 mm, p = 1.5 mm), β comes out as 9.42°. Hence, $F_N \approx 6\ F_R$. Gertsch et al. (2007) conducted a large series of full scale linear cutting tests with Colorado Red Granite. They experimentally proved that the ratio $F_R$ / $F_R$ increases almost linearly as penetration goes up. 1.5 mm penetration for the scaled disc is equivalent to 12 mm on a 17" disc cutter. For such penetrations, a cutting coefficient (FR / FN) of 1/6 seems to be very realistic according to the results of Gertsch et al.

## D.3. Laboratory testing

### D.3.1. Description of lithologies and geotechnical parameters

Eight different sedimentary, metamorphic and igneous lithologies were investigated. Their uniaxial compressive (Fig. D.7b) and Brazilian tensile strength (Fig. D.7b), Young's modulus (secant modulus), specific weight and mineralogical composition (Rauch 2012) can be seen in Table D.1.

| Rock type (abbreviation) | Loading direction relative to foliation | density (g/cm³) | $\sigma_C$ (sd) (MPa) | $\sigma_{BTS}$ (sd) (MPa) | E (sd) (GPa) | Mineral composition (Rauch,2012) |
|---|---|---|---|---|---|---|
| Augengneiss (AG) | perpendicular | 2.6 | 206 (21) | 19 (0.5) | 35 (4) | feldspar, quartz, biotite |
| Granite gneiss (GG) | perpendicular | 2.6 | 138 (29) | 11.7 (0.3) | 41 (3) | feldspar, quartz, biotite |
| Calcareous mica schist (CMS) | perpendicular | 2.7 | 83 (5) | 9.9 (0.5) | 38 (14) | carbonate, quartz, muscovite |
| Brixen granite (BG) | isotropic | 2.7 | 160 (16) | 13.2 (1.1) | 43 (8) | feldspar, quartz, biotite, chlorite |
| Neuhauser granite (NG) | isotropic | 2.7 | 152 (4) | 11.8 (0.5) | 63 (4) | feldspar, quartz, biotite, muscovite |
| Imberg sandstone (IS) | isotropic | 2.6 | 141 (11) | 11.9 (0.6) | 33 (3) | quartz, carbonate, feldspar, muscov. |
| Herdecke sandstone (HS) | isotropic | 2.5 | 120 (3) | 9.3 (0.7) | 35 (4) | quartz, clay minerals, feldspar |
| Red sandstone (RS) | isotropic | 2.1 | 51 (3) | 3.2 (0.6) | 23 (1) | quartz, clay minerals, feldspar |

**Table D.1.:** Geotechnical parameters and mineral composition of the investigated lithologies including standard deviations (sd)

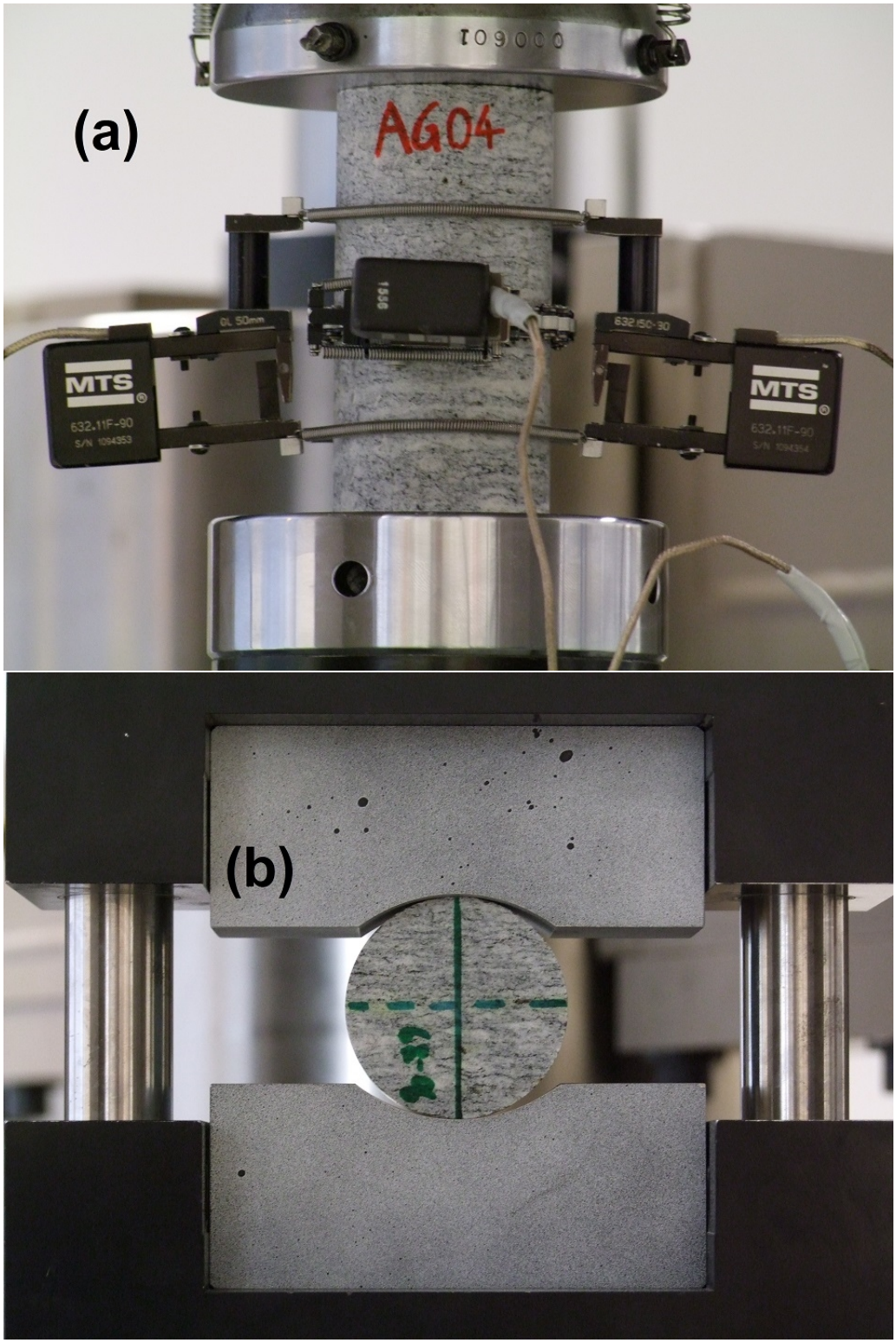


**Fig. D.7.:** Experiment setup for uniaxial compressive strength tests with axial and circumferential extensometers (a) and experiment setup for Brazilian tensile strength tests (b)

Uniaxial compressive strength tests were carried out load-controlled until elasticity parameters were obtained. Afterwards, circumferential strain was used as the control parameter in order to be able to investigate post-failure behaviour.

Kahraman (2002) suggested that besides rock strength parameters, rock brittleness strongly influences cuttability. It is commonly accepted that rocks with characteristics such as little elongation at failure, high Young's modulus or high compressive to tensile strength ratio are regarded as brittle. However, there is no standard definition of brittleness that was proven to be useful for the prediction of rock cuttability. Consequently, uniaxial compressive strength tests were used to qualitatively investigate the post-failure behaviour of the tested lithologies in order to be able to assess their brittleness. Calculation of the destruction work, i.e. a quantification of the post-failure area, is not presented because it very much depends on localized features after failure which can be different for each specimen and also on control and tuning parameters of the hydraulic press.

Fig. D.8 examplarily shows one typical stress-strain curve for each rock type obtained from uniaxial compressive strength tests and photographs of the corresponding rock textures from a sawn surface.

From each lithology between three and five specimen (36 total) were tested with the new scaled rock cutting apparatus. All anisotropic samples were prepared so that the foliation was approximately perpendicular to the cutting kerf. Each sample was cut five times in the same cutting kerf at the center of the specimen. Spacers were reduced after each cut so that indentation depth remained constant at 1.5 mm. Hence, a total of 180 cuts were carried out with one single indentation depth, the only difference being the pre-damage of the sample which increased from cut to cut. Fig. D.9a to Fig. D.9e shows the measured rolling forces of all five cuts from a Brixen Granite specimen. It can be seen that the characteristics of cutting forces are different when cutting undamaged (Fig. D.9a) or pre-damaged rock (Fig. D.9b to e). The corresponding photograph of the sample after all cuts is shown in Fig. D.10.

### D.3.2. Results of scaled rock cutting tests

For Fig. D.9f all cuts were added up. The stacked values were divided by five and then used to calculate mean cutting forces. As indicated, only 55 mm of the samples were used for the mean calculation in order to exclude boundary effects. The same procedure was used for the mean force calculation of each individual cut. A summary of all mean values is presented in Fig. D.11. It can be seen that cutting forces are much higher for the first cut (undamaged sample). For most lithologies, the last three cuts might possibly be regarded as steady-state which means that the degree of pre-damage remains constant.

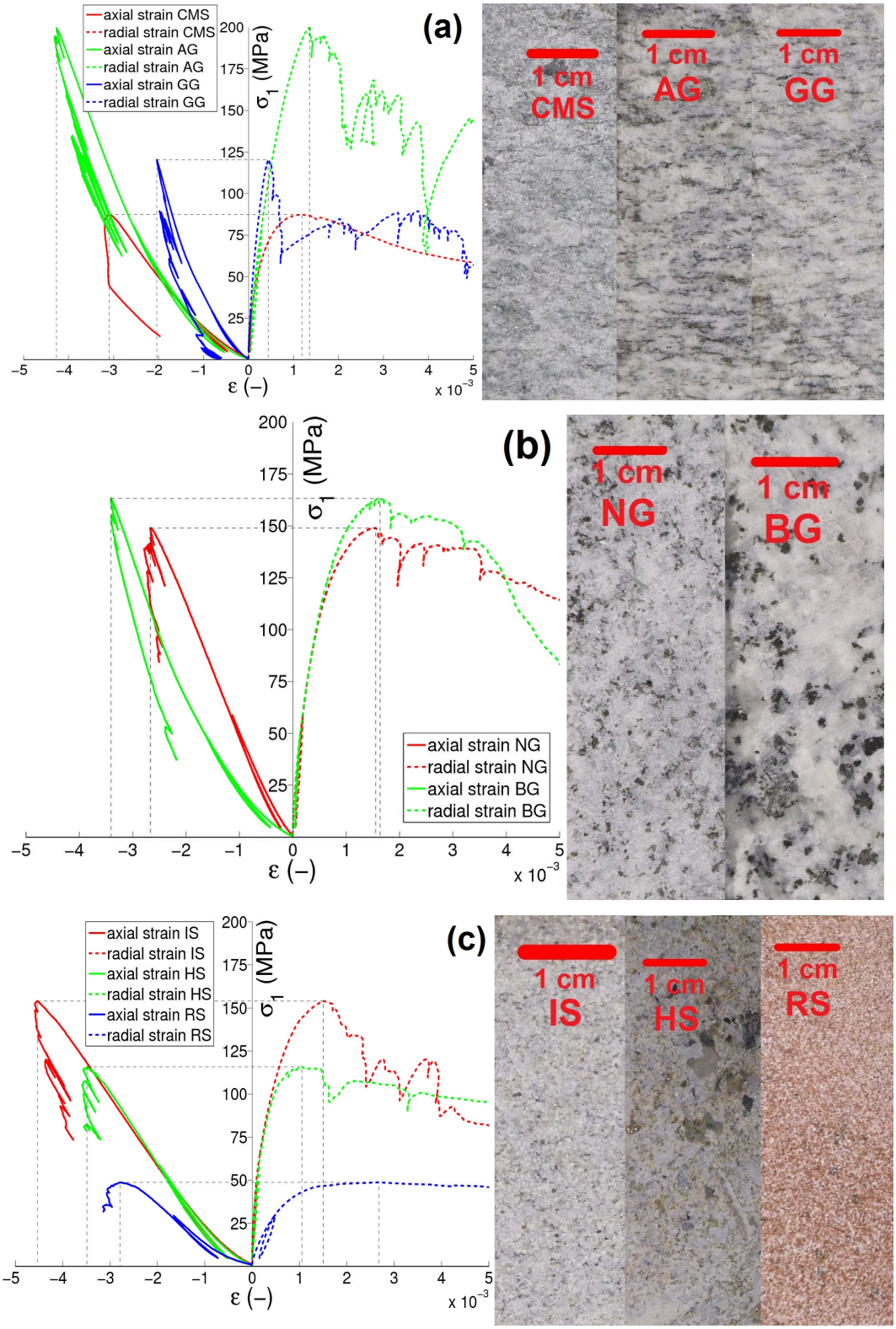


**Fig. D.8.:** Stress-strain curves and rock texture of the investigated metamorphic (a), igneous (b) and sedimentary (c) lithologies

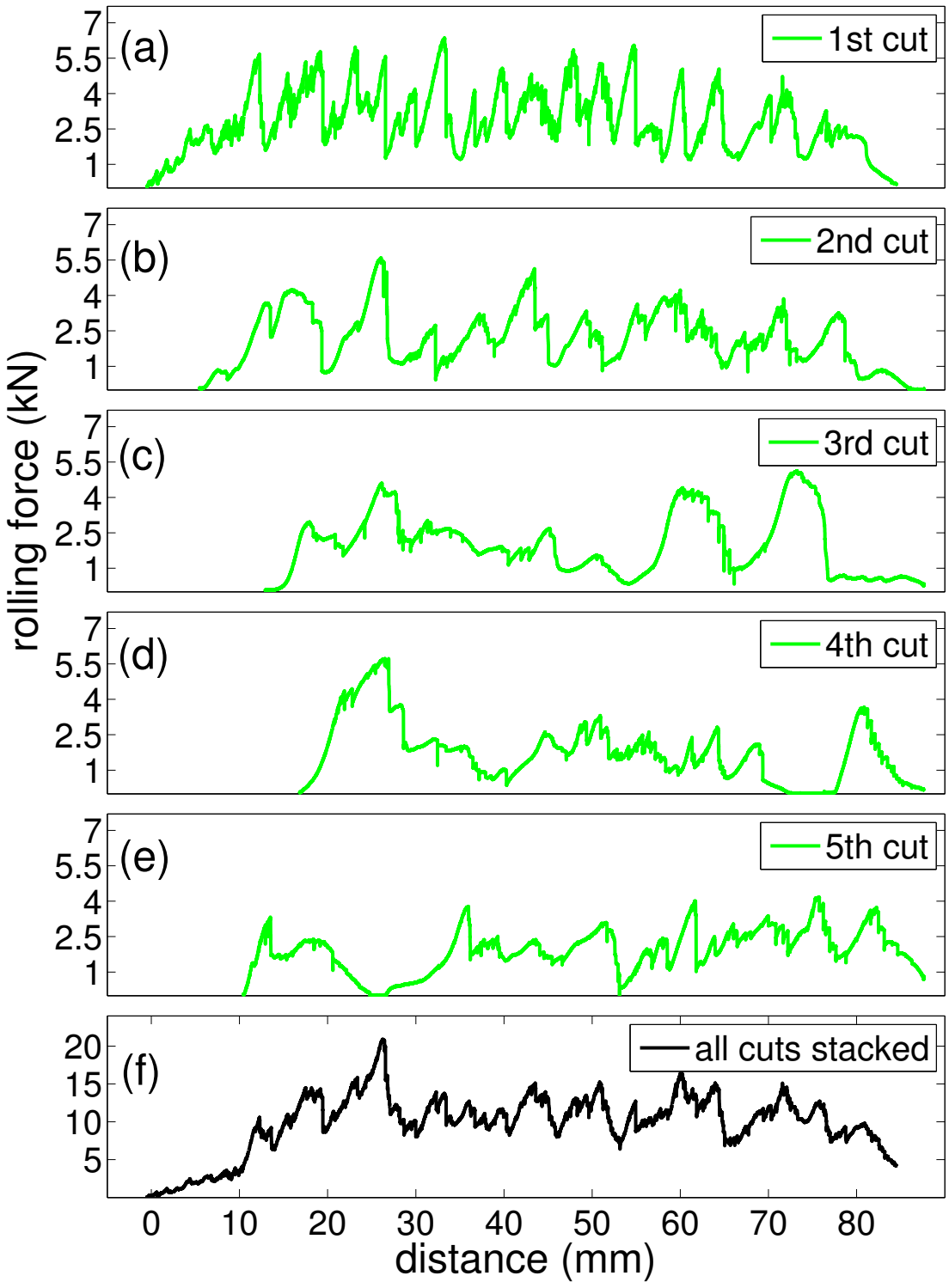


**Fig. D.9.:** Results from scaled rock cutting tests on a BG sample, $1^{st}$ (a) to $5^{th}$ (e) cut and summation of all cuts (f)

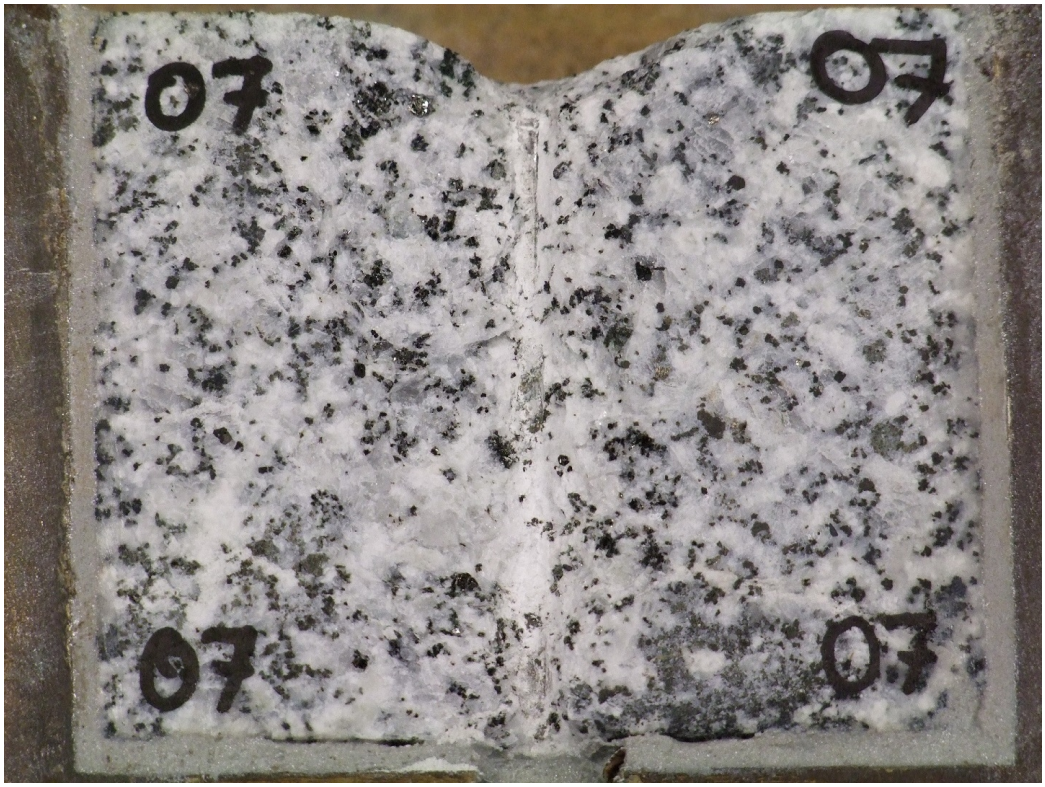


**Fig. D.10.:** BG sample after testing

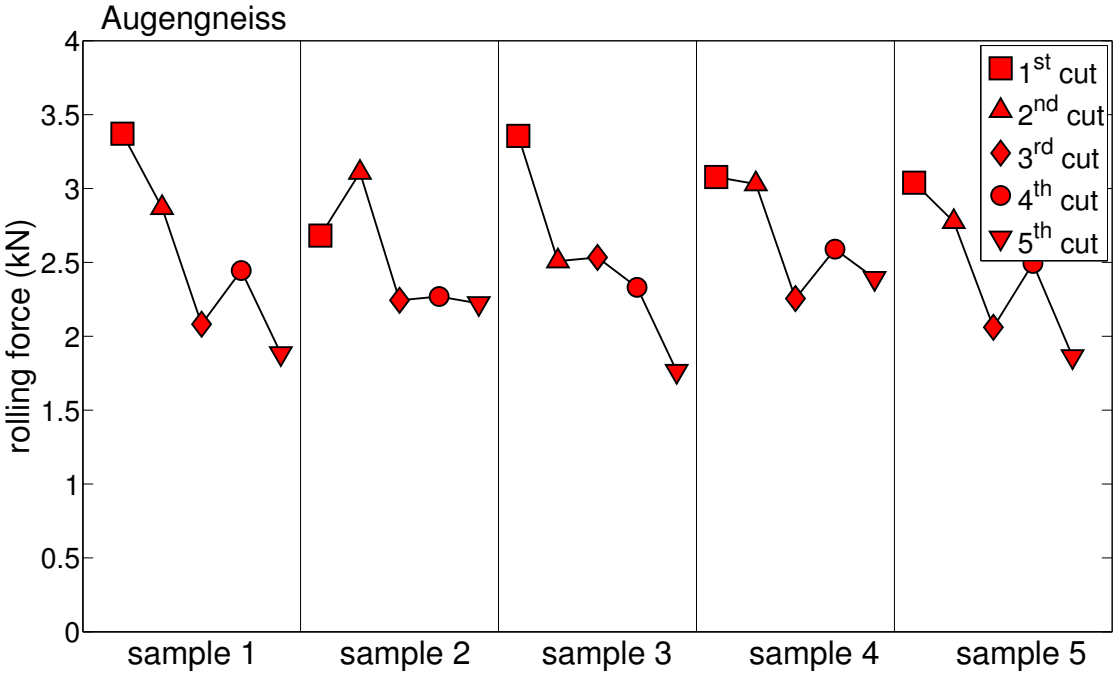

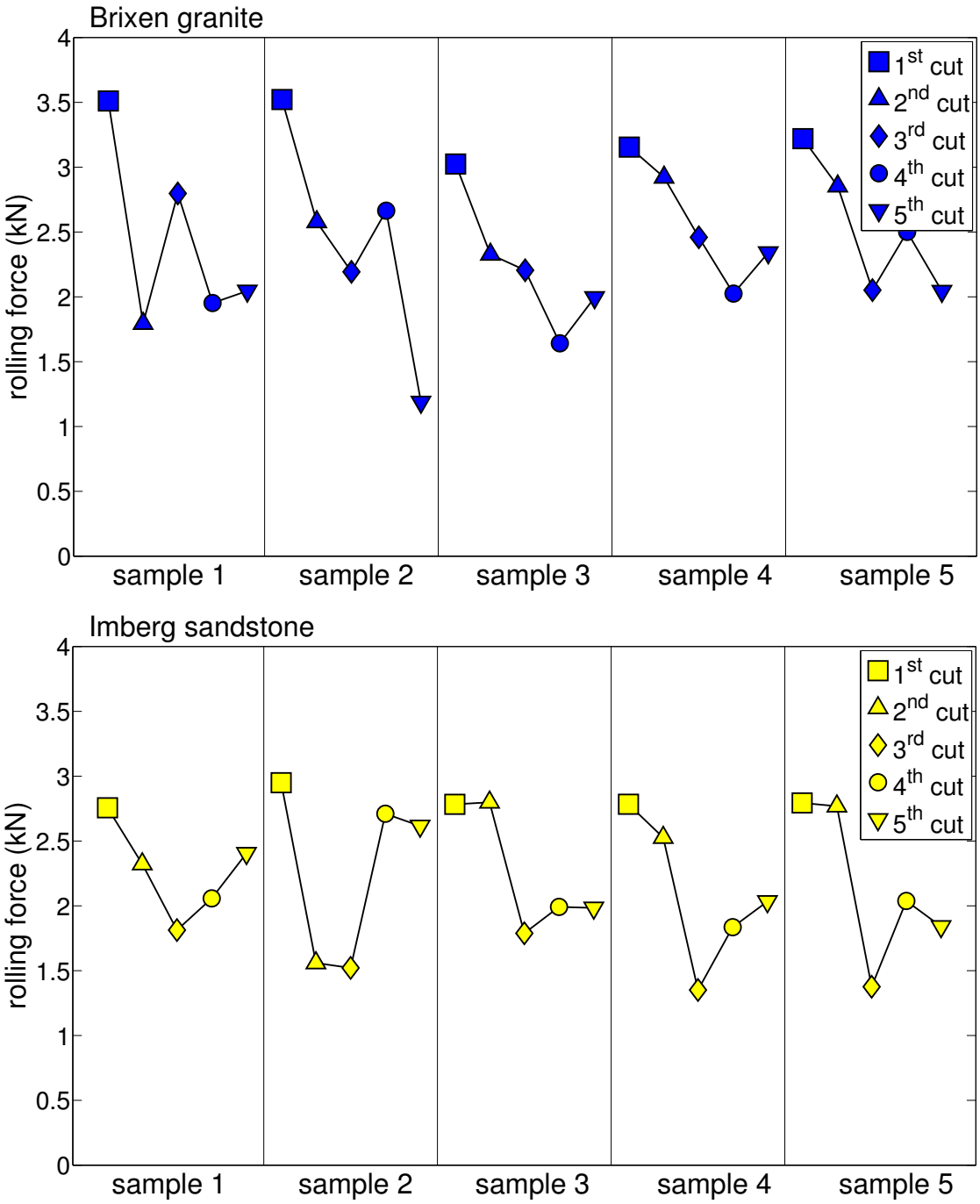
Brixen granite
rolling force (kN)
0
0.5
1
1.5
2
2.5
3
3.5
4
sample 1
sample 2
sample 3
sample 4
sample 5
1st cut
2nd cut
3rd cut
4th cut
5th cut
Imberg sandstone
rolling force (kN)
0
0.5
1
1.5
2
2.5
3
3.5
4
sample 1
sample 2
sample 3
sample 4
sample 5
1st cut
2nd cut
3rd cut
4th cut
5th cut

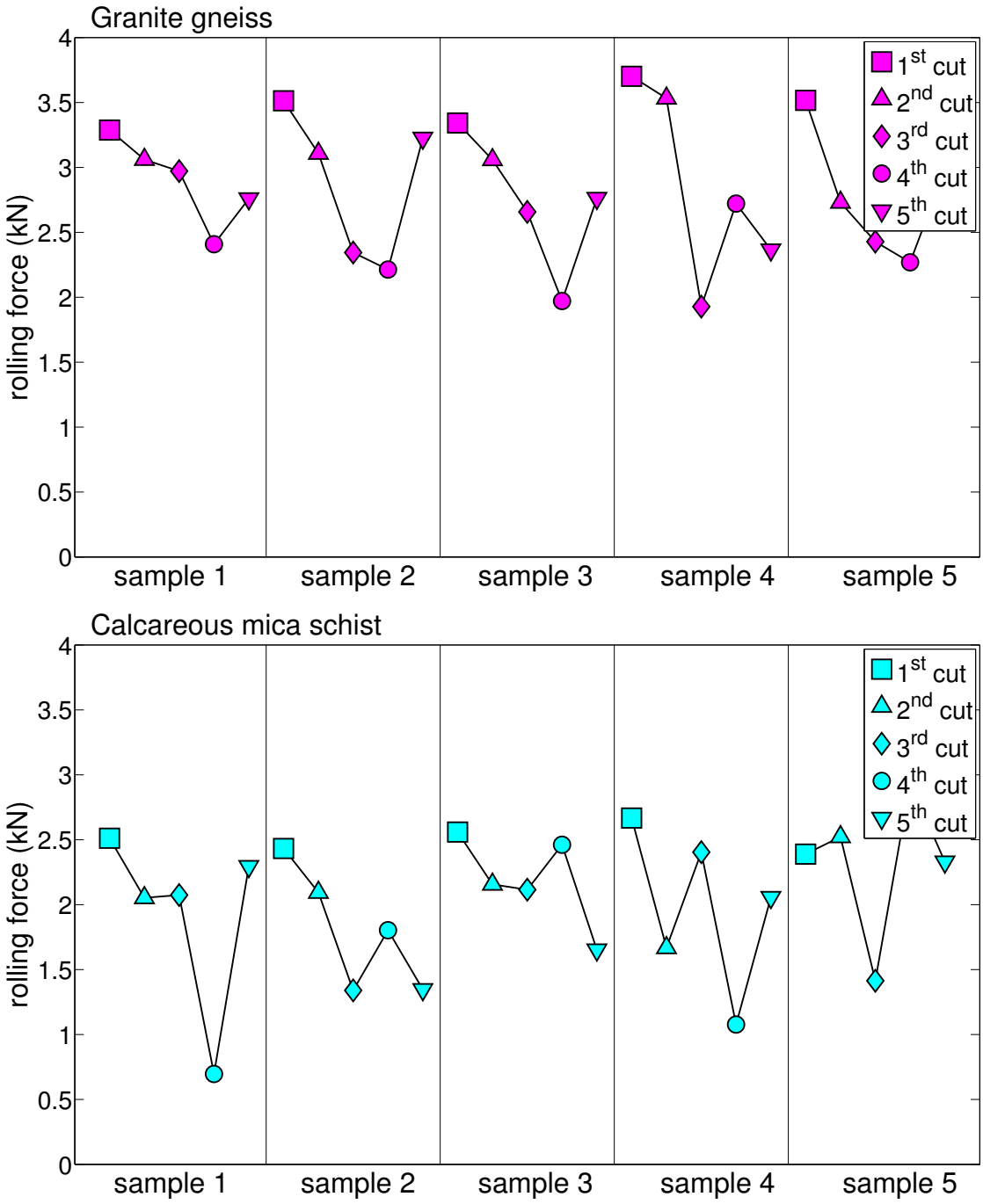
Granite gneiss
rolling force (kN)
0
0.5
1
1.5
2
2.5
3
3.5
4
sample 1
sample 2
sample 3
sample 4
sample 5
1st cut
2nd cut
3rd cut
4th cut
5th cut
Calcareous mica schist
rolling force (kN)
0
0.5
1
1.5
2
2.5
3
3.5
4
sample 1
sample 2
sample 3
sample 4
sample 5
1st cut
2nd cut
3rd cut
4th cut
5th cut

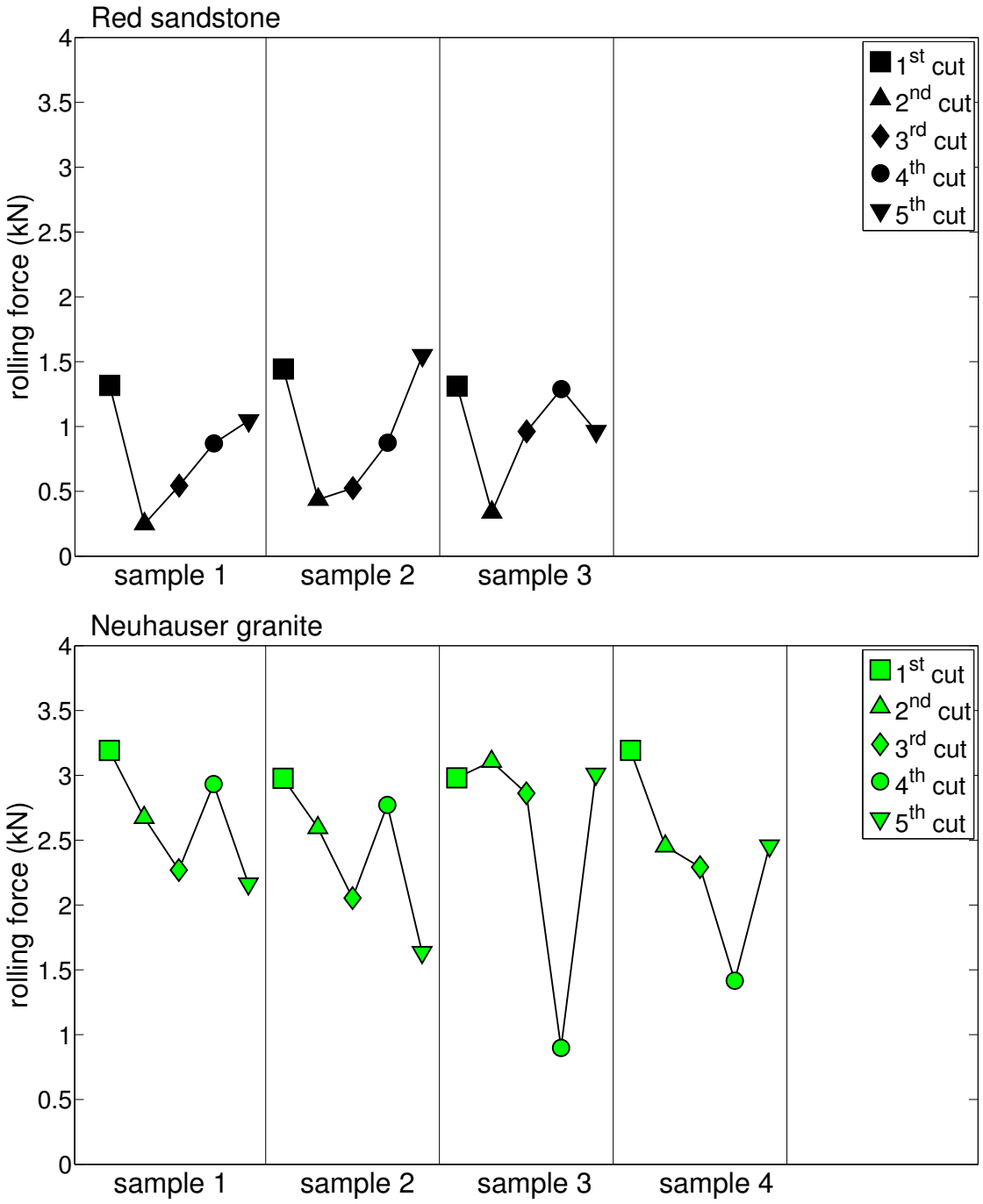
Red sandstone
rolling force (kN)
0
0.5
1
1.5
2
2.5
3
3.5
4
sample 1
sample 2
sample 3
1st cut
2nd cut
3rd cut
4th cut
5th cut
Neuhauser granite
rolling force (kN)
0
0.5
1
1.5
2
2.5
3
3.5
4
sample 1
sample 2
sample 3
sample 4
1st cut
2nd cut
3rd cut
4th cut
5th cut

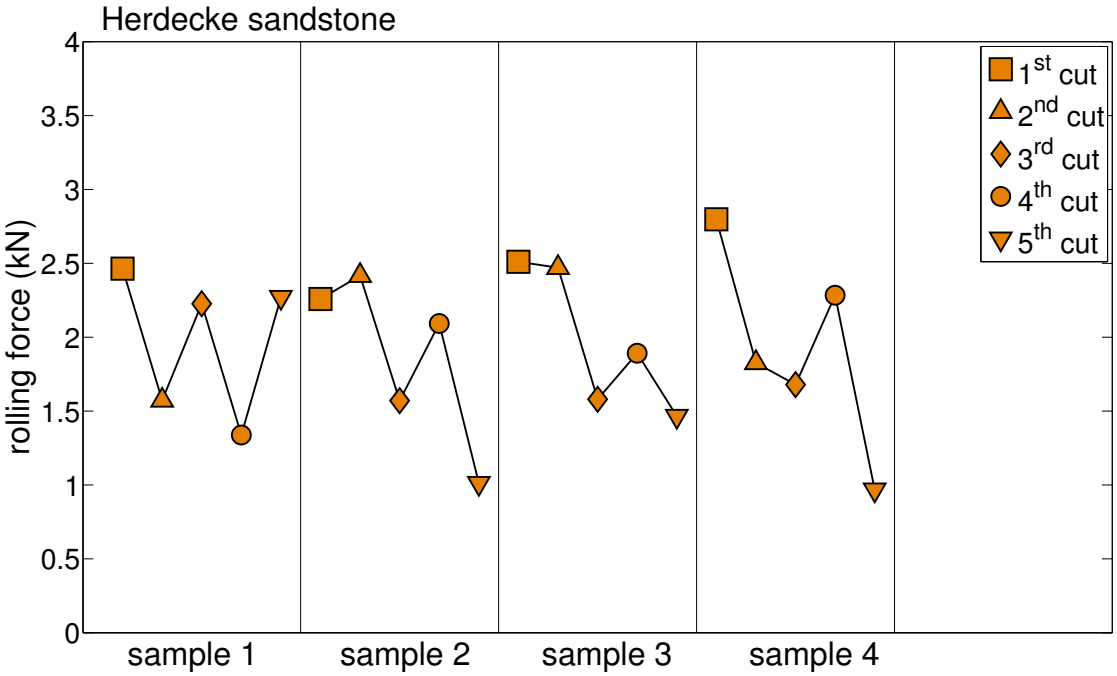


**Fig. D.11.:** Mean cutting force values of all tested samples

### D.3.3. Comparison with full scale cutting tests

A series of full scale linear cutting tests was conducted at the Earth Mechanics Institute of the Colorado School of Mines under the supervision of Christian Frenzel and Brian Asbury with three of the eight presented lithologies. All tests were carried out with a commercial 17" single disc cutter with a tip width of 5/8" (15.9 mm). Fig. D.12 shows a photograph of the experiment setup.

Augengneis (AG) and calcareous mica schist (CMS) were tested by Lisa Mori (2012) with a special focus on size and shape of the excavated material. An analysis of cutting forces of these tests was done by Entacher and Lassnig (2012b), the results are used in this paper to evaluate the newly developed scaled rock cutting test. The results are only taken from samples that were cut in similar directions relative to the foliation as the scaled cutting tests, i.e. the foliation was approximately perpendicular to the cutting kerf. The third lithology, Brixen Granite (BG), was tested by the first author with the purpose of comparing the results with TBM operational data. Fig. D.13 shows the results of the mentioned test series in the form of a penetration - mean normal force graph. In addition, it shows the results of the TBM performance prediction model of the Colorado School of Mines (CSM) with input parameters as shown in Table D.1.

**Fig. D.12.:** Linear cutting machine at Colorado School of Mines

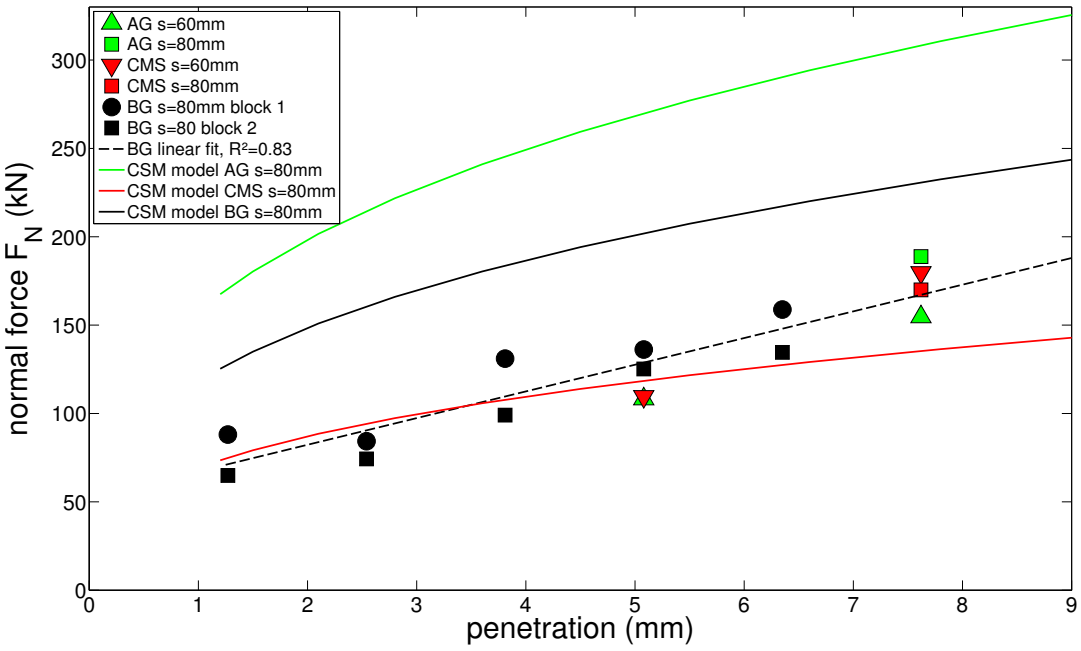


**Fig. D.13.:** Results of full scale cutting tests and corresponding prediction of the CSM model

As indicated in the figure, different penetration depths and spacings were used. In order to be able to use consistent data from all lithologies, it was decided to use a spacing (s) of 80 mm and a penetration depth of 0.3" (7.6 mm) for comparison purposes. In order to be able to do so, BG results were extrapolated to this penetration value as indicated by the linear fit line. Consequently, one value was found for each of the three lithologies.

Fig. D.14 shows a comparison between scaled rock cutting tests, full scale rock cutting tests, uniaxial compressive and brazilian tensile strength with standard deviations (black bar) for all values. The results for the scaled cutting tests are divided in mean values for the first cut on each sample with an undamaged surface (Fig. D.14a), a mean value for all cuts on each sample (Fig. D.14b) and a mean value of the last three cuts (Fig. D.14c) on each sample which is naturally a little lower because of the pre-damage that the sample was exposed to. As explained in section D.3.2, the last three values might be considered "steady-state" cutting which would be closest to the physical conditions of the tunnel face. The measured rolling force is converted into an equivalent normal force by multiplying it by six as explained in section D.2.3.

It is notable that uniaxial compressive strength and Brazilian tensile strength are the most widespread input values for performance prediction models while it is clear from Fig. D.14 that these parameters are very different for lithologies that have approximately the same cuttability. To illustrate this fact more clearly, all values of AG, CMS and BG are investigated more closely in Fig. D.15. All values are normalized so that they are 1 for AG. The green bars are the reference values representing full scale cutting forces. It is obvious that results from the scaled rock cutting test are much closer to the reference results than uniaxial compressive and Brazilian tensile strength.

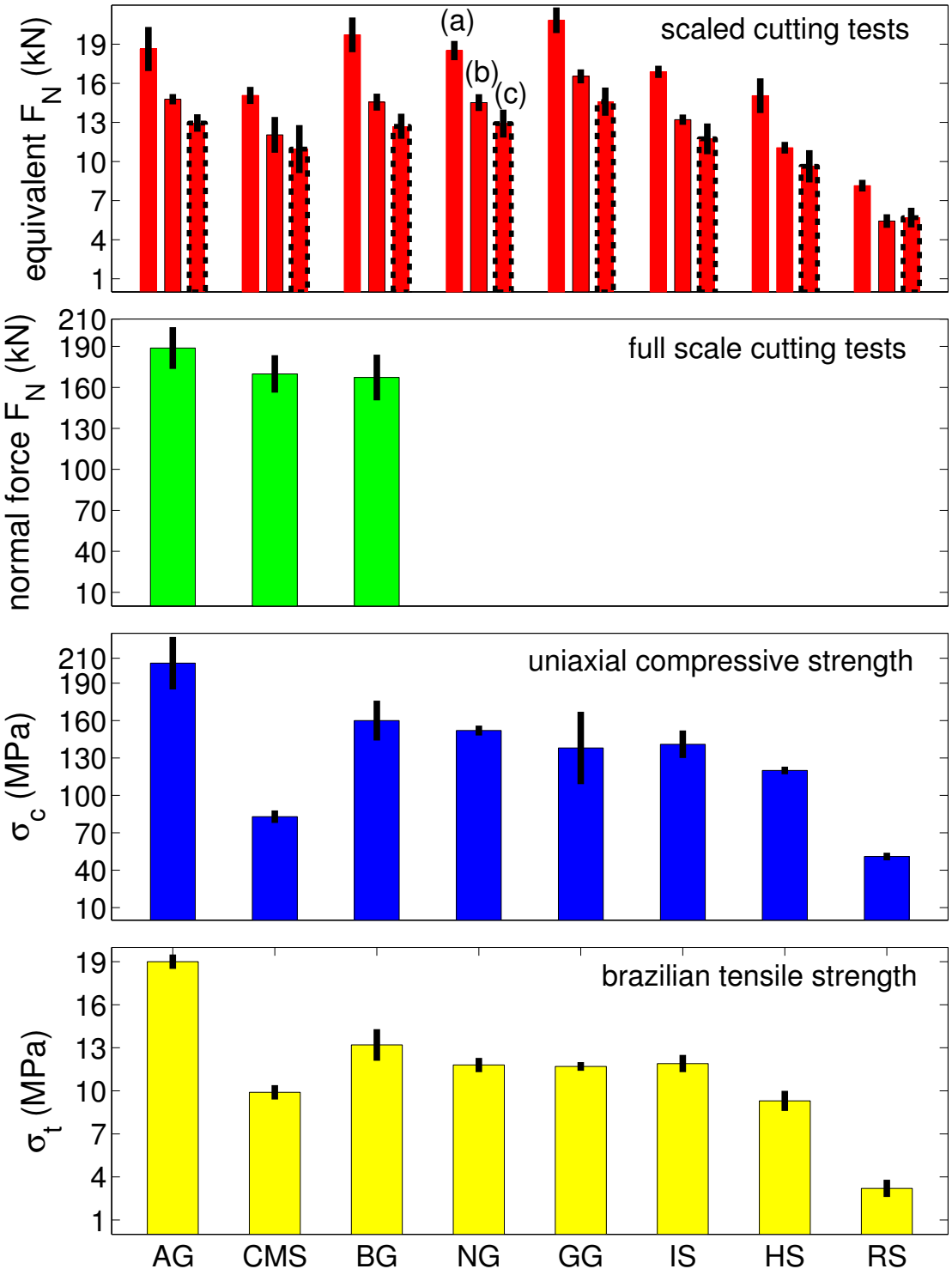


**Fig. D.14.:** A Comparison between scaled cutting tests, full scale cutting tests, uniaxial compressive and Brazilian tensile strength including standard deviations

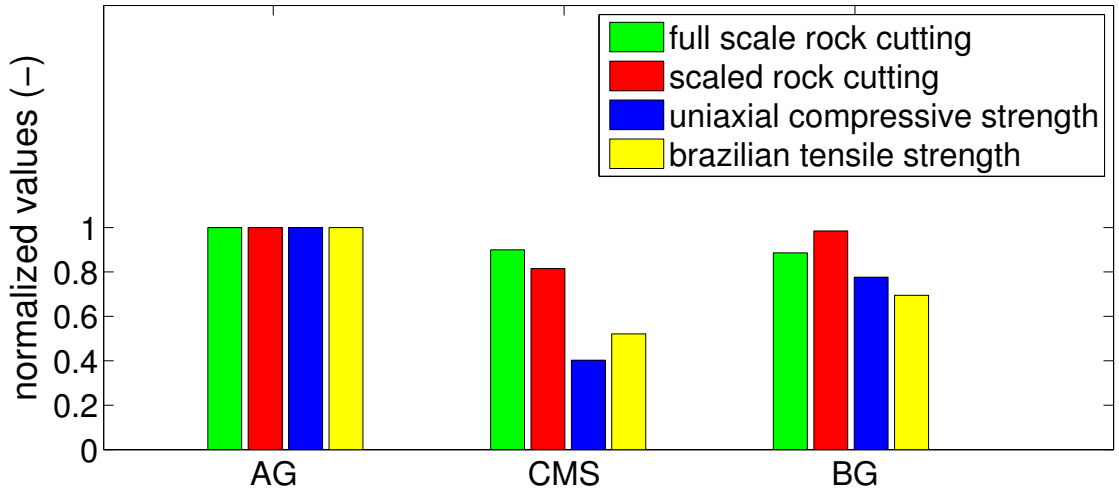


**Fig. D.15.:** A comparison between normalized values of full scale and scaled cutting tests, uniaxial compressive and Brazilian tensile strength

## D.4. Discussion

### D.4.1. Outline of a new TBM performance prediction model

Major TBM performance prediction models focus on the prediction of thrust / normal forces. This is concise as normal forces are by far the biggest forces needed for the disintegration of rock. However, thrust is not always the limiting factor for the excavation process, TBMs can also be torque limited, especially in medium hard rock conditions. In summary, the prediction of thrust and rolling forces seem to be equally important. Hence, there is no reason to change the common practice to focus on thrust prediction in the first place.

The two most widespread TBM performance prediction models that were presented in section D.1 (CSM and NTNU model) use non-linear base functions to describe the relationship between penetration and normal force. Based on data from Villeneuve (2008) and Käsling (2009), Frenzel et al. (2012) showed for a variation of rock types that this relationship can be described with a linear function when neglecting penetrations below 2 mm which are practically irrelevant for TBM tunnelling. The results from full scale cutting tests presented in Fig. D.13 strengthen this assumption. When neglecting the so-called subcritical penetration (penetrations below approximately 2 mm), there is no need for the function to cross the origin which is obviously a physically constrained point. In order to include the origin in mathematical functions, previous models came up with strongly non-linear functions that seem to be inappropriate for higher penetrations. The basic penetration function in a new model should therefore be linear without zero-crossing analogous to the proposal by Frenzel et al. (2012) with normal force

$F_N$, penetration p, a term for friction and subcritical forces $F_F$ and a factor that should represent basic rock properties:

$$F_N\,(kN) = Factor\,(\frac{kN}{mm})\;p\,(mm)\;+\;F_F\,(kN) \tag{D.5}$$

In order to use the results of scaled rock cutting tests as input parameters for this equation, they have to be calibrated with TBM operational data and / or full scale cutting tests. Currently, a complete model cannot be set up due to an insufficient data basis. However, the basic approach is very easy. The slope of the function (Factor) can be determined from the mean cutting force of the scaled rock cutting test, $F_F$ can be estimated based on engineering judgement when no other data are available. A feasible value for subcritical cutting forces might be in the range of 50 kN per cutter for standard 17" disc cutters. Friction forces can be measured with a friction stroke or estimated using engineering judgement. A friction stroke is obviously a simplification because it does not account for vibrations and other effects that occur during TBM operation but it is a very practical approach.

Mainly massive rock samples are investigated during cutting tests. Subsequently, the basic penetration function is only valid for massive rock. Joint intensity, joint orientation and schistosity should be incorporated by using a factor as proposed by Gehring (1997).

Fig. D.13 presents results from full scale linear cutting tests for three different lithologies and the corresponding prediction by means of the CSM model with input parameters from Table D.1. It is striking that the results for Augengneis (AG) are extremely far off the experimental results, whereas they are in better agreement for Calcareous mica schist (CMS) and Brixen granite (BG). Looking at the geotechnical strength parameters of these lithologies, it is obvious that every model which is based on uniaxial compressive and/or Brazilian tensile strength as its main input parameters will always be far off from realistic results for either CMS or AG. The first one has a compressive strength of about 83 MPa whereas the latter has 206 MPa, yet still forces of about the same magnitude are needed to cut them. BG has a uniaxial compressive strength of about 160 MPa and still reaches approximately the same force level during cutting. In spite of these clear findings, these parameters are by far the most established in TBM performance prediction because of their conciseness in terms of sample availability, convenience of experiment setup and quality of results. Besides that, they are available for every project because they are needed for the design of underground structures and dimensioning of support anyway. No matter how practical the use of uniaxial compressive and Brazilian tensile strength tests might be, the presented figures are a clear indication that their use has to be questioned rigorously for future TBM performance prediction.

The first results from scaled rock cutting tests presented in Fig. D.11, Fig. D.14 and Fig. D.15 show very good agreement with full scale cutting tests which are considered the most profound benchmark for the prediction of rock excavability with disc cutters. Hence, the use of this test in TBM performance prediction seems to be feasible. To obtain equivalent thrust forces, rolling forces from the scaled rock cutting tests are

multiplied by six according to the explanations in section 2.3. Three different results are presented. Fig. D.14a shows the mean values of one cut on each sample with an undamaged surface. It is the value with very reasonably controlled conditions. All further cuts depend on the pre-damage caused by previous cuts. Fig. D.14b shows the mean total forces needed for one cut when looking at every cut on each sample. It is the statistically most significant value because it incorporates every cut, giving it the largest database. Fig. D.14c is the mean value of the last three cuts on each sample representing cutting of pre-damaged material. Hence, it is a value with a close physical analogy to the conditions at the tunnel face. The ratio between first cuts and last three cuts is smaller for CMS than it is for AG and BG. Looking at the post-failure behaviour during uniaxial compressive tests (Fig. D.8), it can be observed that the behaviour of CMS is much more ductile compared with AG and BG which can be classified as brittle. It therefore appears that brittleness / ductility plays a significant role for disc cutting. Kahraman (2002), Altindag (2003) and Goktan and Yilmaz (2005) correlated different definitions of brittleness with energy needed to cut rock. All three found that brittleness is in general at least weakly correlated with required cutting energy. Gong and Zhao (2007) analysed the influence of brittleness in a UDEC simulation in a much discussed paper. It shows that rock cuttability needs to be assessed with a combination of rock strength and suitable brittleness indices. There is however no well-established brittleness index that has been generally accepted to be most relevant for cutting efficiency. In order to qualitatively understand the behaviour of a certain rock type, uniaxial compressive strength tests with an investigation of the post-failure zone are presented in this paper. However, a quantification of this behaviour is not recommended by the authors because it is very much dependent on localized damage effects and varies strongly from sample to sample.

### D.4.2. Advantages and limitations of the scaled rock cutting test

The newly developed scaled rock cutting test proved to have superior applicability for TBM performance prediction than geotechnical standard tests such as uniaxial compressive strength and brazilian tensile strength tests. The advantages of these tests are that not only index values can be derived, but also basic physical properties, such as elasticity parameters Young's modulus E and poisson's ratio ν. Hence, they can be used for a large variety of tasks such as design of underground structures. Consequently, full scale or scaled rock cutting cannot substitute geotechnical standard tests, they have to be conducted additionally in order to be able to assess rock cuttability.

Compared to full scale cutting tests, the presented test rig has limitations due to scale effects, i.e. the ratio between grain size and cutter size is different than in a full scale test. Generally, the coalescence of cracks becomes easier as grain size increases (Eberhardt et al. 1999). Hence, a similar effect could be expected as the size of the cutter decreases when grain size remains constant. Looking at the presented results, scale effects do not downgrade the comparability between scaled and full scale tests for AG, CMS and BG.

Bilgin et al. (2010) presented scaled rock cutting tests with single disc cutters at EUROCK 2010. Their results are just as promising as the results of the present study. The applicability of their test rig is different, however, because it is a specially built rig and uses rock blocks as specimen. In contrast to this, the present scaled rock cutting apparatus is designed as an easy and low-cost, yet very precise attachment device to hydraulic presses commonly available in rock mechanics laboratories. The samples used are 10 cm diameter cores cut in half which are available even in very early stages of a tunnelling project.

It was shown that scaled rock cutting tests deliver very feasible input parameters for TBM performance prediction. In addition, the developed scaled rock cutting rig allows for investigating fundamental mechanisms of rock breakage in controlled laboratory conditions. The possibility of comparing cutting in undamaged rock with cutting in damaged rock is an example of this accuracy. In larger test rigs, it is usually impossible to embed a rock sample in such a way that penetration depth can be adjusted very precisely even for the first cut. Hence, in full scale cutting tests conditioning passes are made to even out the surface before measurement can start. The presented cutting rig allows for an exact adjustment of penetration from the beginning on and can help to understand how the propagation of damage evolves.

In summary, scaled rock cutting tests are closing a gap between geotechnical standard tests, which have serious limitations for TBM performance prediction, and full scale rock cutting tests, which are expensive and time-consuming and sometimes impossible to conduct, due to the lack of appropriate samples.

Many publications deal with TBM performance prediction in hard rock. For the sake of completeness, it has to be said that there are conditions where none of them (including the present paper) are applicable. Delisio et al. (2013) described blocky rock conditions at certain sections of the Lötschberg base tunnel. In these sections face instabilities occurred on a regular basis due to high primary stresses and joint intensity and orientation. As soon as large wedges or blocks break out of the tunnel face, a regular TBM operation is not possible anymore. Similar conditions are known from certain sections of the Gotthard base tunnel and might also become imminent in other upcoming base tunnels.

## D.5. Conclusions

A scaled rock cutting test rig has been developed. It is designed as an attachment for hydraulic presses commonly available in rock mechanics laboratories. The main innovation lies in its simplicity, accurate test results and the standard specimen size which can be obtained easily during all phases of a tunnelling project. Thus, it proved to be a promising tool for TBM performance prediction which is superior to geotechnical standards tests and much cheaper than full scale rock cutting tests. Furthermore, controlled

laboratory conditions will enable the investigation of fundamental mechanisms of rock breakage. The conclusions of this study are the following:

- A new scaled rock cutting test rig was developed as an attachment for hydraulic presses with which cutting tests can be conducted at very low cost with high accuracy.
- It was shown that scaled rock cutting tests are superior for TBM performance prediction than geotechnical standard tests such as uniaxial compressive strength and Brazilian tensile strength tests for at least three lithologies.
- TBM performance prediction is one of the main concerns in mechanized tunnelling. An outline of a new model based on the work of Frenzel et al. (2012) was proposed. The data obtained from the new test are however not yet sufficient to calibrate the model with adequate reliability.
- The new test is capable of giving insight into fundamental questions such as the difference between cutting undamaged or pre-damaged rock. It can also be extended to investigate the interactions of multiple cutting kerfs as it is done in full scale cutting tests.

## Acknowledgements

We are very grateful for the support of Dr. Gerhard Winter and Rene Pfingstl during conceptual and final design of the scaled rock cutting test rig. We are indebted to Martin Gimpel who helped us greatly with geotechnical testing, provided material and for fruitful discussions about the new test rig. The supervision of Dr. Christian Frenzel and Brian Asbury during the conduction of rock cutting tests at the Colorado School of Mines is greatly appreciated. We would like to thank Lisa Mori and Klaus Lassnig for the possibility of including some of their rock cutting data into our study. Furthermore, we are indebted to the ABROCK research group for enriching our work by exchanging ideas with peers in the same field of research. We gratefully acknowledge the financial support of this work by the Austrian Research Promotion Agency (FFG) within the Eurostars project E!5514.

# 2. Concluding Remarks

## 2.1. The future of cutter force measurement

The final installation works of the sensors and cables in the cutterhead of the first KAT 2 TBM took place in December 2012. Excavation started in January 2013 and it soon turned out that the installation could withstand the harsh environmental conditions and deliver data. Fig. 2.1 shows photographs of the sensor equipped cutter and cutter casings during maintenance shifts.

**Fig. 2.1.:** Inspection of sensor equipped cutters during maintenance shifts

In spite of that, many obstacles - mainly related to software and database problems - had to be overcome in order to produce meaningful results. Out of the many collected data, few give a complete picture including the exact position of the three cutters on the tunnel face. This is because the angular sensor of the TBM was installed a few weeks after excavation started. Hence, a representative amount of data could be collected, but only few could be used to assess the ability of cutter force measurement as a geological monitoring tool. These processed data however surpassed all expectations and promise interesting future results (see Fig. B.24).

The programmable controller which is the centrepiece of data transmission, was placed in a chamber in the cutterhead that was designed to be impervious. However,

after about one month water penetrated into the chamber and set the controller under water. Since then, no more data were collected. Due to the first results, however, there is great interest in cutter force measurement at KAT 2. Hence, further work will be pursued to ensure a more robust installation.

The basic layout of the cutter force measurement method proved to be successful. It is protected by a utility patent (Entacher and Galler 2013a) that includes not only conical saddle / bayonet systems, but also senor layouts for other mounting systems such as the Wedge-Lock system (see Fig. 2.2). Detailed analytical analyses and simulations were carried out to ensure that the basic design is also applicable for this system. With the practical experience gained it can be said with confidence that this method can be adopted to all common mounting systems.

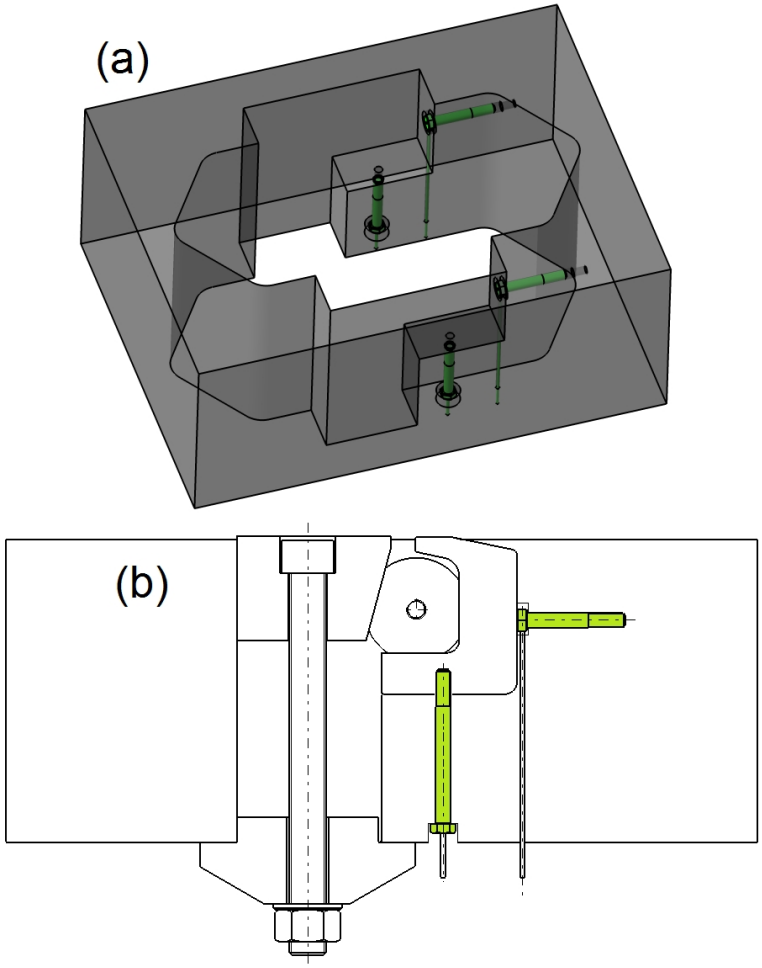


**Fig. 2.2.:** Possible sensor layout for Wedge-Lock systems, (a) isometrical view, (b) cut view (Entacher and Galler 2013a)

The main challenge of future applications will be to ensure a stable and long-lasting installation. Ideally, all cable ducts should be integrally included into the cutterhead at

the design stage. Subsequent attachments that are added afterwards are more likely to fail and are usually very hard to replace. Another approach is to completely avoid cables and place small data transmission units in the vicinity of every cutter. In order to ensure a long battery life in such designs, machine vibrations will have to be used to generate electricity. A lot of automation engineering efforts will be needed.

The main input parameter to determine cutting forces is the change of pre-stress of the measurement bolts. For an external load of 1 MN, this change of pre-stress is in the range of 1.5 kN while the absolute pre-stress is about 60-80 kN. In order to get a sufficient resolution of results, a change of pre-stress in the order of 0.02 % should be possible. It was proven that this is realistic with respect to the sensor itself and the measurement chain. However, due to the small measurement range, the cutter and its adjacent structure is sensitive to temperature-induced deformations. The measurement bolts are equipped with strain gauge full bridges and are thus temperature compensated. However, the overall structure is deformed by a temperature change that subsequently changes the bolts pre-stress.

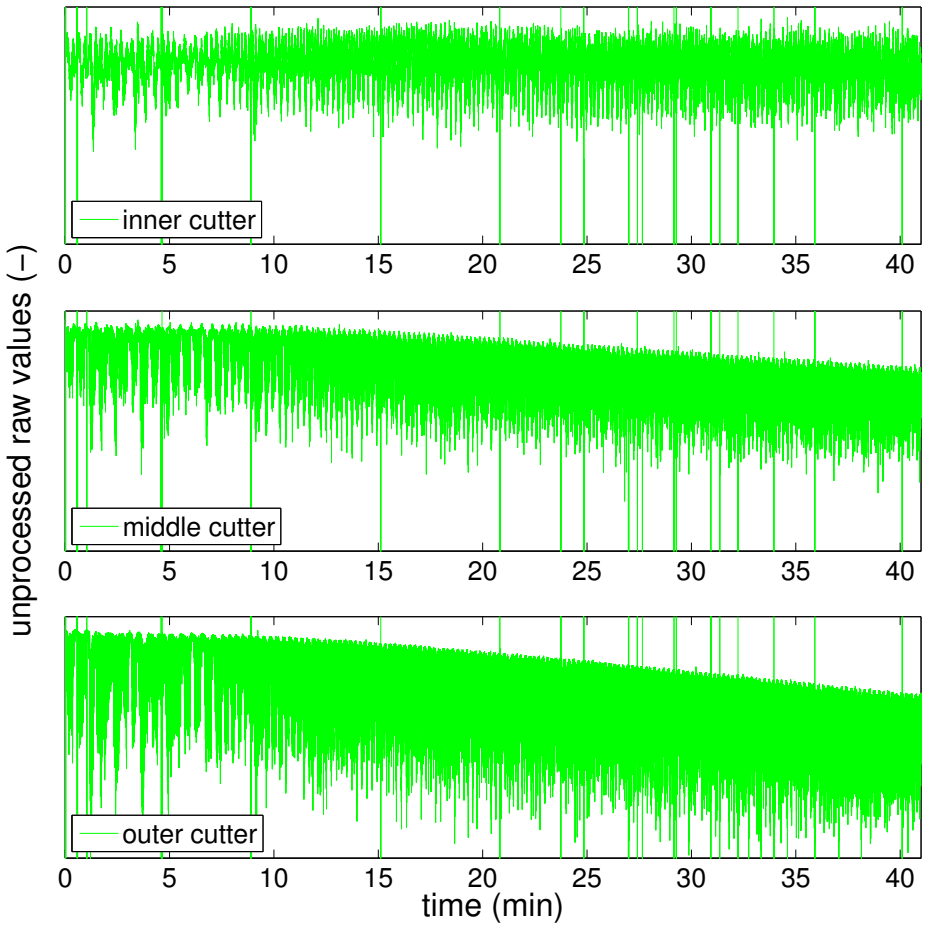


**Fig. 2.3.:** Illustration of temperature drift during a full stroke of the TBM. The effect is more pronounced at the position of the outer cutter due to the higher angular velocity

Fig. 2.3 shows raw measurement data for a complete TBM stroke. It can be seen that the zero-loading point (upper plateau of values) changes as time passes and as the cutterhead structure heats up due to the boring process. The effect is negligible in the center, but very pronounced for the outer cutter that heats up faster due to a higher angular velocity. The knowledge of the actual zero-loading raw value is paramount for the subsequent calculations because the main input parameter is not the absolute, but the relative change of pre-stress. Hence, an initial calibration of this point is not valid anymore after a few minutes. This problem was overcome by automatically finding a new reference point every few minutes because the cutters are not always engaged with the tunnel face. Hence, the maximum raw value in a data set of a few minutes will always be the zero-loading reference value. In spite of this remedy, future applications should include a temperature sensor to be able to automatically eliminate temperature drifts.

Monitoring disc cutter rotation, temperature, wear and forces is among the main research and development topics of TBM manufacturers. Out of all these parameters, force measurement is the only one that is not purely operational. While continuous measurement of parameters such as rotation and wear will prove to be one of the main innovations of TBM operations in the near future, the delivered information does not need to be interpreted in an academic sense. In fact, the information is rather trivial as it will show whether a cutter is rotating or whether it is blocked. In the first case, everything is fine, in the latter case, the cutter will be replaced. The core competence of universities, e.g. the Chair of Subsurface Engineering, comes into play as soon as more complex parameters such as cutting forces are measured. Such data need to be interpreted with respect to rock breakage, geological features such as anisotropy, joints, cobbles, mixed face conditions, etc. Such information could be processed in order to filter important details about TBM operation. In fact, real-time cutter force monitoring opens the path to an automated control and a subsequent complete industrialization of TBM excavation which leads to safer, faster and cheaper tunnelling.

## 2.2. Improving TBM performance prediction

### 2.2.1. General remarks

The knowledge of cutting forces is inherently linked to the prediction of net penetration rates, commonly referred to as TBM performance prediction modelling. The goal of such models is to determine a penetration rate, i.e. TBM advance rate per cutterhead revolution (mm/rev), as a function of cutter load for different ground conditions and other factors such as cutter size, spacing, etc. Penetration rate is the basic parameter that is needed to determine construction time, a key parameter for large infrastructure projects. Two of the most widespread TBM performance prediction models were developed at the Colorado School of Mines (CSM, Rostami and Ozdemir 1993) and at

the Norwegian University of Science and Technology (NTNU, Bruland 1998). They are in worldwide use and have proved to be a valuable aid for many different projects. In spite of their great success, both models have downsides that leave room for major improvements. The goal of this section is to utilize the research findings of this thesis to give an impulse for further development of TBM performance prediction.

Before a model is developed, a comprehensive database is needed. In the past, two approaches were successful to establish such a database. In the first one TBM operational data with a corresponding documentation of geological and geotechnical parameters are gathered, in the second one full scale cutting tests are carried out. The obvious advantage of the first approach is that all data are based on real in situ conditions. However, such data will always contain uncertainties and scatter in contrast to a much more controlled laboratory environment which is the biggest advantage of the second approach. The uncertainties contained in an in situ database are manifold. First of all, penetration and thrust are very global parameters that have a large bandwidth even within the same geological area (see Fig. 2.4).

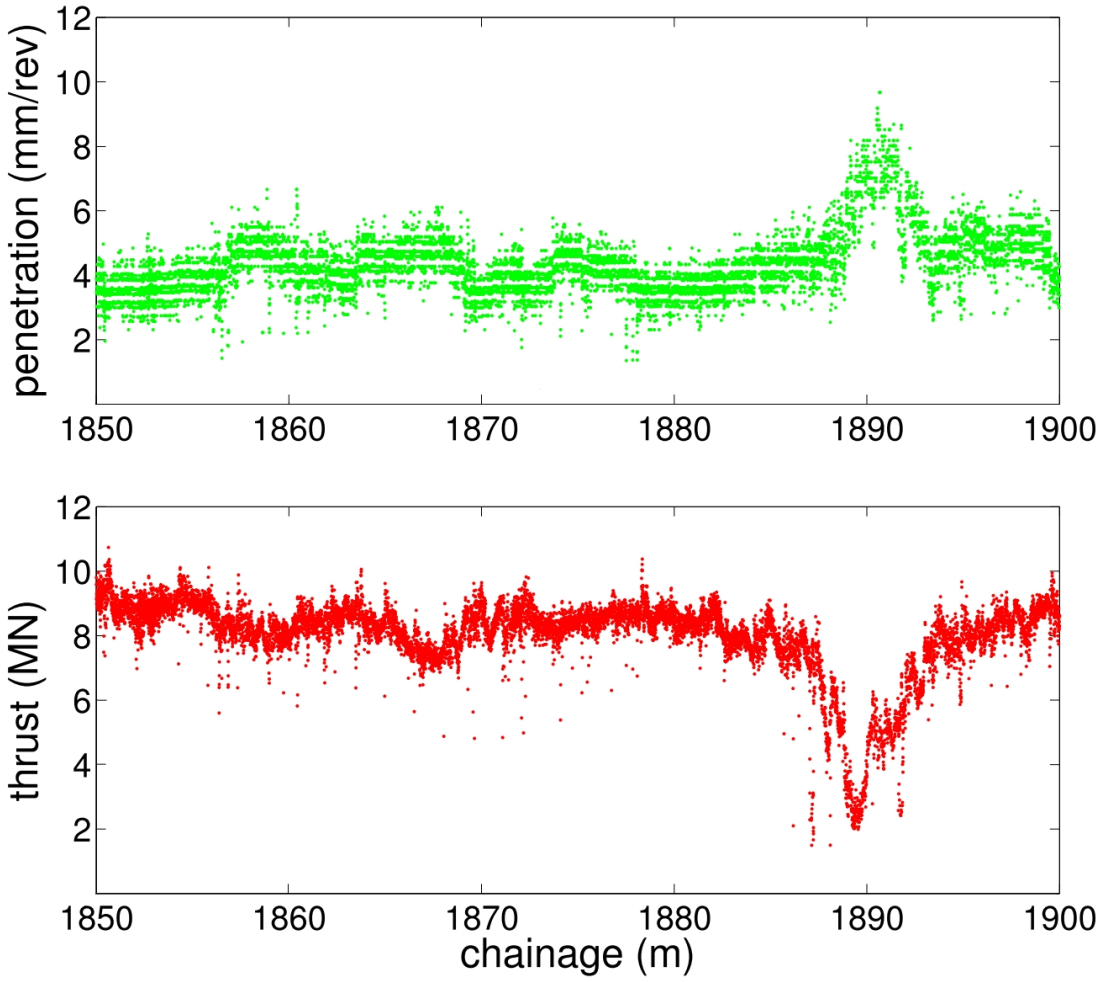


**Fig. 2.4.:** TBM operational data of a double shield TBM in granite

This could be partly overcome by measuring individual cutting forces instead of global thrust. Second, rock cores used to obtain geotechnical parameters in the area of interest are usually bored radially in the vicinity of the tunnel face which might result in a further loss of accuracy. Third, geological documentation is often incomplete due to a tunnel face that is only partly visible. In addition to that, a geological compass should not be used in the heavy steel environment of a cutterhead. Still, joint and foliation angles are documented relative to magnetic north. Regarding TBM performance prediction, it would be more meaningful to document $\alpha$ and $\beta$ which are measured relative to the tunnel axis. $\beta$ is the angle between foliation and the horizontal plane measured perpendicular to the tunnel face. $\alpha$ is the smallest angle between foliation and tunnel axis. The definitions are shown in Fig. 2.5.

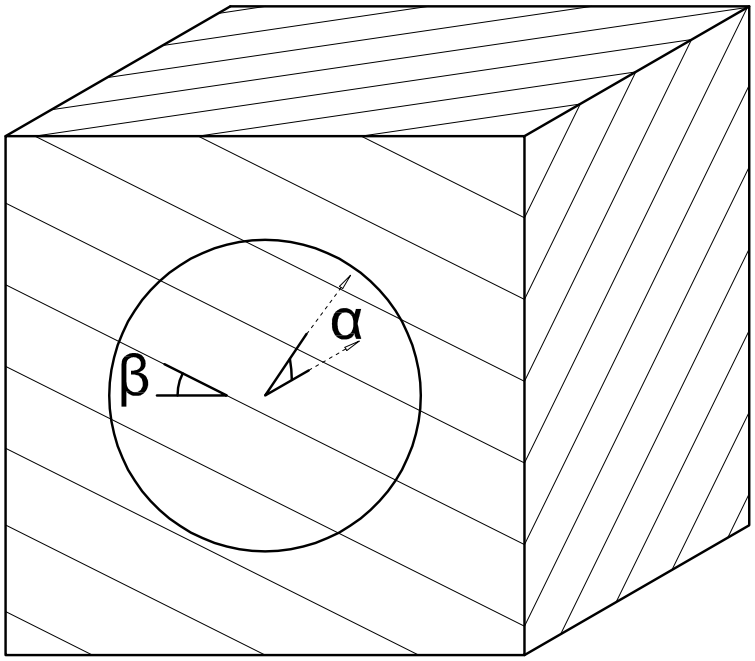


**Fig. 2.5.:** Definition of $\alpha$ and $\beta$

Due to the many uncertainties, data sets from many different projects have to be discarded because no reliable conclusions can be drawn. In some cases, it is possible to come out with a general trend, but the scatter increases even more as soon as the influence of a specific parameter such as cutter size is isolated.

Penetration tests are a good way of overcoming these downsides. In such tests, the TBM is operated at different thrust and torque levels in order to obtain the relationship between different levels of penetration and thrust. To obtain a complete picture, the tunnel face should be documented very carefully including an accurate alpha angle and joint count. In addition, rock cores are needed to determine geotechnical strength parameters. In the case of anisotropic rock types, the direction of foliation has to be considered. Ideally, laboratory tests are carried out parallel and perpendicular to the

foliation as well as in the direction of the tunnel axis. This requires extensive sampling which soon becomes close to impossible. Even in much easier conditions, such efforts are only possible when all project partners are willing to cooperate. In any case, establishing a reliable database takes years of rigorous work. Even then, the question remains whether the standard tests carried out for many years are even suitable basic input parameters. This is an important question raised by this thesis.

In contrast to in situ documentation, full scale cutting tests are bias-free in the sense that the impact of every parameter can be looked at separately. Uncertainties are much smaller and easier to assess. In order to gain a more fundamental understanding of rock breakage, even full scale cutting tests seem to be inadmissible. Many insights presented in this thesis were only possible due to the small scale that was used. For example, a spatial picture of cracks can only be obtained from specimens with limited size. Similarly, the analysis of sudden stress release and corresponding sound events was carried with a density of 200 data points per mm. In full scale cutting rigs, such data rates are not possible and the sound acquisition is disturbed by background noise. Hence, with the experience of analysing TBM operational data and the conduction of full scale as well as small scale cutting tests, it turns out that none of these scales is inferior to the larger one. In fact, scatter and uncertainty decreases significantly as the scale goes down. At the same time, comparability with the complex situation of in situ TBM operation also decreases. Hence, a combination of different methods appears to be most promising.

### 2.2.2. Geotechnical input parameters

The choice of suitable basic geotechnical input parameters that can adequately represent cutting of different rock types is essential for a good model. The most widespread input parameters are UCS and BTS. They are available in all projects because they are also needed to assess the stability of a tunnel. The tests are straightforward and can be conducted with samples already available in very early project phases, e.g. 50 mm rock cores. Consequently, it seems logical that they turned out to be the most widespread basic geotechnical input parameter for TBM performance prediction. However, a closer look is needed to assess whether they are a good choice or not. Fig. 2.6a shows the experiment setup for UCS testing and corresponding failure modes. Fig. 2.6b shows the elastic stress field caused by a point load on a semi-infinite surface in analogy to the situation in rock cutting. The stress state in the vicinity of the cutter is highly triaxial and not comparable to uniaxial testing.

It was proven in section D that cutting forces cannot be predicted in certain rock types with UCS and BTS only. Fig. 2.7 shows that forces for AG and BG are overestimated whereas they are in an acceptable range for CMS. The results clearly indicate that there is an urgent need for improved models.

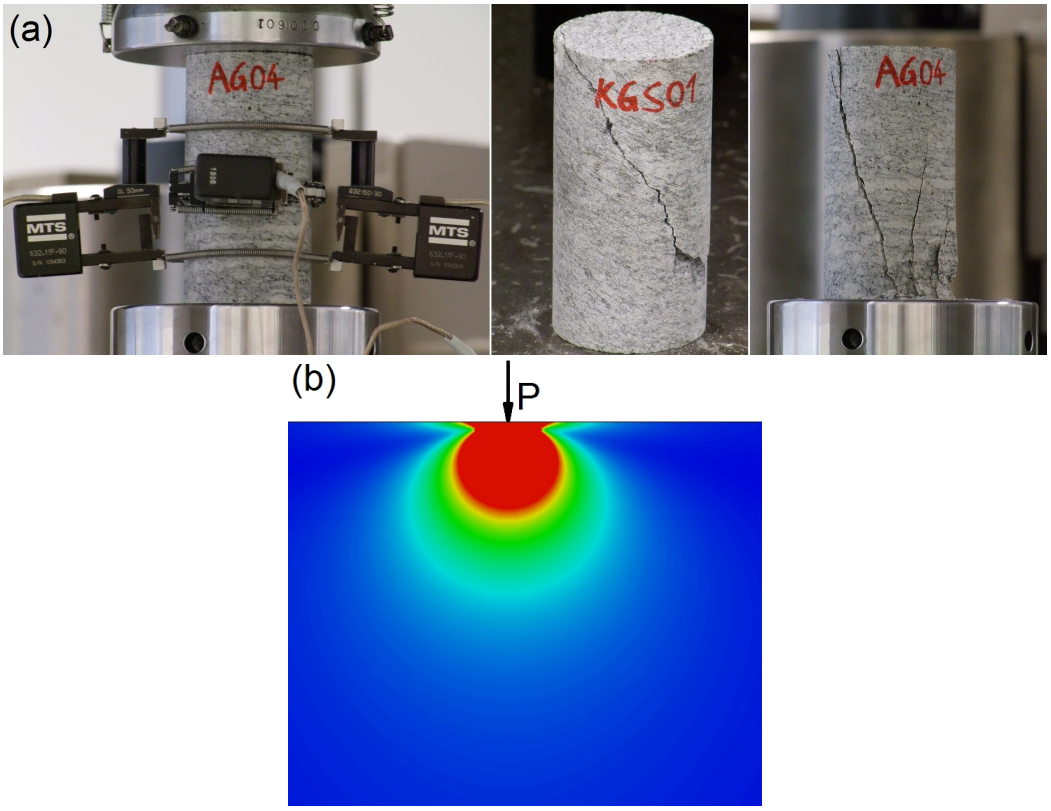


**Fig. 2.6.:** UCS test setup and failure modes (a), elastic stress field (von Mises stress) caused by a point load P (b)

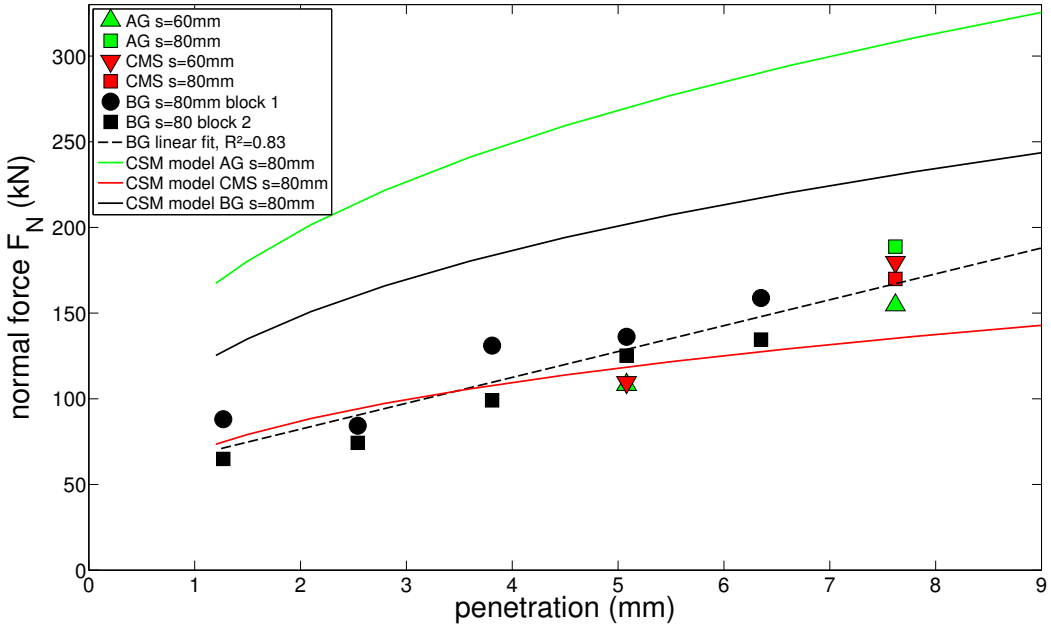


**Fig. 2.7.:** Results of full scale linear cutting tests compared with CSM model predictions (Entacher et al. 2013c)

As AG is a very brittle and CMS a ductile rock type, the results suggest that brittleness has to be accounted for separately. Often this is done by looking at the ratio between UCS and BTS. Both values are taken into account in the CSM model, the results are however not satisfying. A better option would be to quantify brittleness / ductility by a factor. This is not easy because the post-failure behaviour in uniaxial compression varies strongly from sample to sample depending on individual microstructural events and it is also dependent on the stiffness of the hydraulic testing system. Hence, the combination of UCS and / or BTS with an additional brittleness factor seems to be possible, yet rather problematic.

One of the best ways to predict in situ cutting forces is to directly conduct full scale cutting tests which was the basis for the development of the CSM model. However, such tests are time consuming and costly. Furthermore, it is very hard, sometimes even impossible, to obtain samples of adequate size during a tunnel exploration. Many times, such tests were conducted to analyse TBM performance while the tunnel was built or even afterwards, but the true goal of TBM performance prediction is to come up with a good result before the tunnel is built, not afterwards. Hence, a trade-off was accepted, namely direct cutting tests, but on a smaller scale with sample sizes commonly available during exploration phases. The results presented in section D.4 suggest that the small scale cutting test rig delivers a much more appropriate basic geotechnical input parameter than UCS and BTS. It was patented by Montanuniversität Leoben (Entacher and Galler 2013b).

### 2.2.3. Basic penetration function and model architecture

The basic penetration function describes the relationship between penetration (mm/rev) and the normal force of an individual disc cutter or global machine thrust (kN). The CSM and NTNU model utilize non-linear basic penetration functions whereas Gehring derived a linear function from his regression analysis. As a result of the observation of in situ penetration tests, Frenzel et al. (2012) however proposed to use a bi-linear function or - for the sake of conciseness - a linear function that does not cross zero and is valid above the critical penetration value. The basic CSM, NTNU and Gehring functions as well as a proposal for a new curve are shown in Fig. 2.8.

Intuitively, a curve that does not cross zero seems rather inadmissible because zero force will obviously result in zero penetration. Thus, a zero crossing seems to be a natural constraint. However, penetration values below 2 mm are of no practical interest. Hence, it is reasonable to focus on values above this threshold which appear to be linear in many practical examples. Fig. 2.9a shows results from rock cutting tests on BG carried out by the author. Fig. 2.9b shows results from the same cutting rig obtained by Gertsch et al. (2007). Fig. 2.9c and d are results from in situ penetration tests carried out by Gong et al. (2007) and Villeneuve (2008) respectively. While Gong et al. used a non-linear curve for their regression, it is clear that for all four pictures a

linear approximation is perfectly reasonable. The basic penetration function that fits to all graphs of Fig. 2.9 could thus look like this:

$$F_N\,(kN) = Factor\,(\frac{kN}{mm})\;p\,(mm)\;+\;F_F\,(kN) \tag{2.1}$$

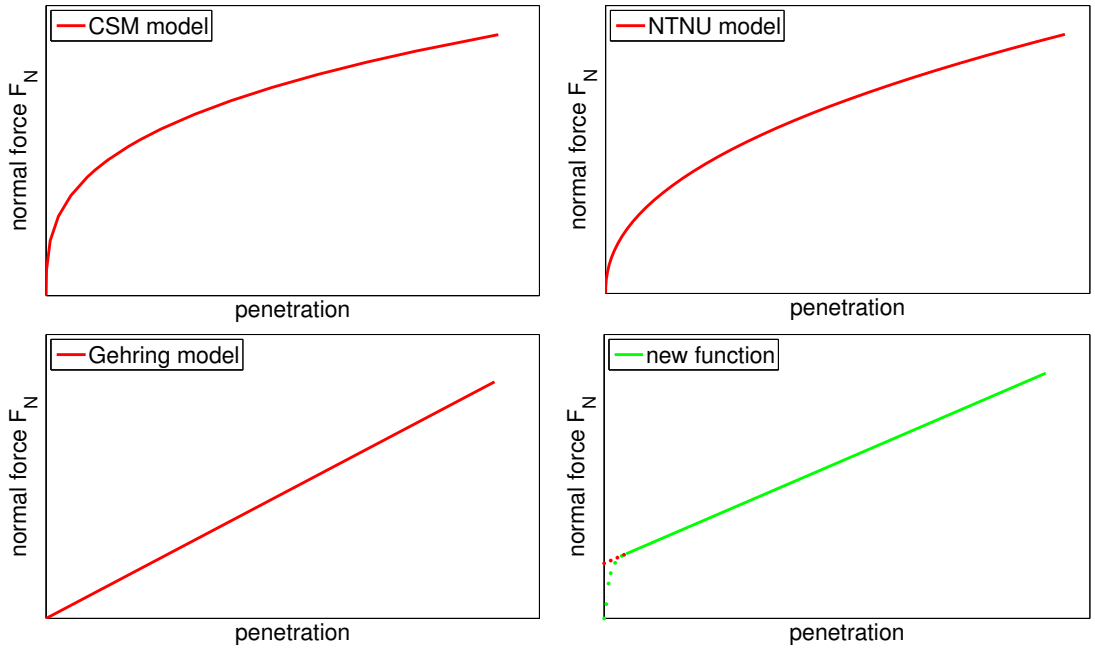


**Fig. 2.8.:** Basic penetration function of the CSM, NTNU and Gehring model as well as the proposal for a new function

The factor, i.e. the steepness of the graph, is a property of the intact material that can be derived from tests such as the scaled rock cutting test or UCS. $F_F$ is the sum of subcritical force and friction. The subcritical force is needed to initiate an efficient rock cutting process in contrast to inefficient grinding. It is the force where the graph starts to become linear and is typically reached at a penetration of about 2 mm. Consequently, this value also depends on material properties. The friction force which will in many cases be the major part of $F_F$, can be estimated from machine parameters such as weight and an adequate friction coefficient in the range of 0.3 to 0.5. Hence, for a typical TBM with a diameter of about 9 m, a few MN, e.g. 4 MN need to be added. The industry has a lot of experience with friction values obtained from no-load TBM strokes. During cutting operation, however, stick-slip effects and other dynamic aspects will come into play resulting in different values. In the future, cutter load measurement will be used to evaluate such effects and determine exact friction values.

The basic penetration function should always be written in terms of $F_N$ because it gives a physical meaning to the constant $F_F$. Often, basic penetration functions are written in terms of p which is not recommended for this model as it will result in generic

constants without physical meaning. The model architecture proposed by the ABROCK group should be in accordance with Gehring's model. In this model, a basic value can be obtained easily with little known parameters and the result becomes more accurate as more parameters are known by the use of correction factors. In most publications, these factors are given with respect to penetration p. For example, rock mass with many planes of weaknesses will lead to a penetration of 10 mm instead of 5 mm compared to competent rock, an increase of 100%. In the chosen model architecture, this factor concept could be implemented in two ways. The first would be to plug 10 mm into the basic penetration function instead of 5 mm. The resulting force would then be multiplied by 0.5 to account for the planes of weaknesses. The second - probably more concise - way would be to plug 5 mm into the equation, obtain a resultant force and then plot the obtained force against 10 mm instead of 5 mm. This would be in accordance with many published results on how to consider fractured rock mass and other factors.

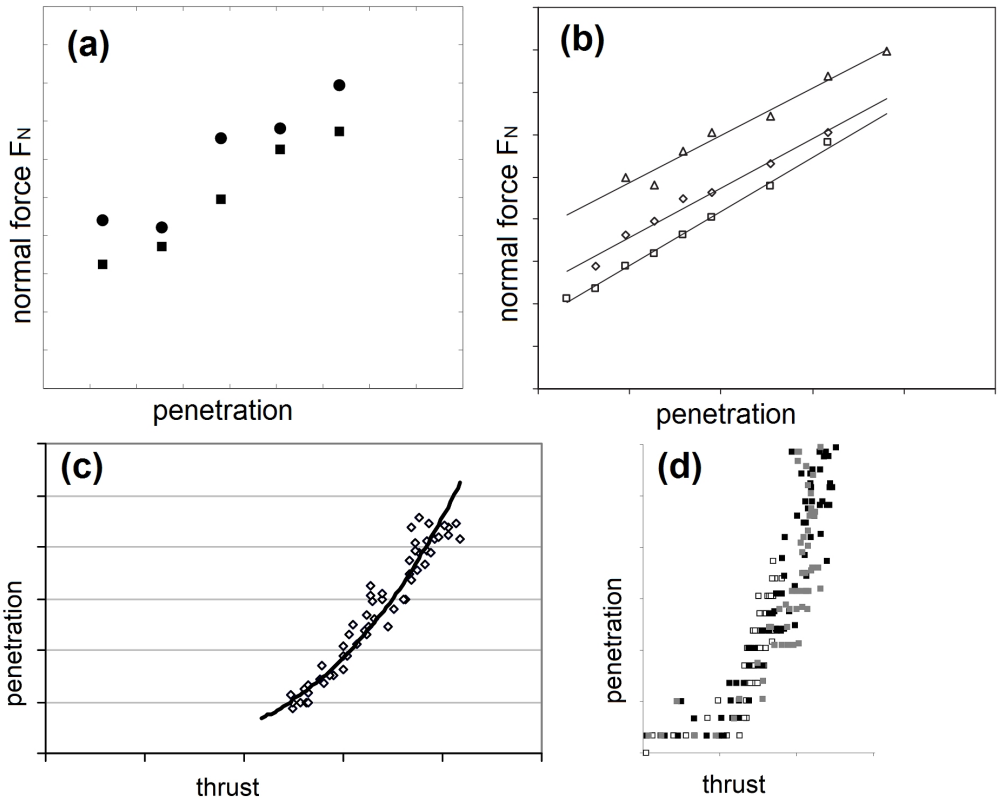


**Fig. 2.9.:** Force penetration curves from linear cutting tests as well as from in situ penetration tests suggest that a linear curve is not only mathematically convenient, but also very accurate. (a) LCM tests carried out by the author, (b) LCM tests carried out by Gertsch et al. (2007), (c) penetration tests modified from Gong et al. (2007), (d) penetration tests modified from Villeneuve (2008). Note that axes are swapped in (c), (d) compared to (a), (b)

### 2.2.4. Rock mass parameters

Penetration is significantly influenced by rock mass parameters such as frequency and orientation of joints, orientation of foliation and primary stress state. The first two influences have been the topic of a large number of papers whose results allow for an approximate consideration of these factors. However, there are effects which are not yet quantified such as the influence of rock strength. Joint sets are a strong aid when excavating in hard rock whereas they are not as beneficial in soft rock. Thus, strength parameters have to be incorporated into a correction factor for joints.

Similarly, correction factors for the spatial orientation of foliation in metamorphic rocks are typically functions of the alpha angle. This consideration is absolutely necessary, but not sufficient because the degree of anisotropy is also a paramount factor that needs to be evaluated. Fig. 2.10 shows the penetration rate increase modified from Thuro and Schormair (2008) and Büchi (1984) in Mica gneiss and two different phyllites.

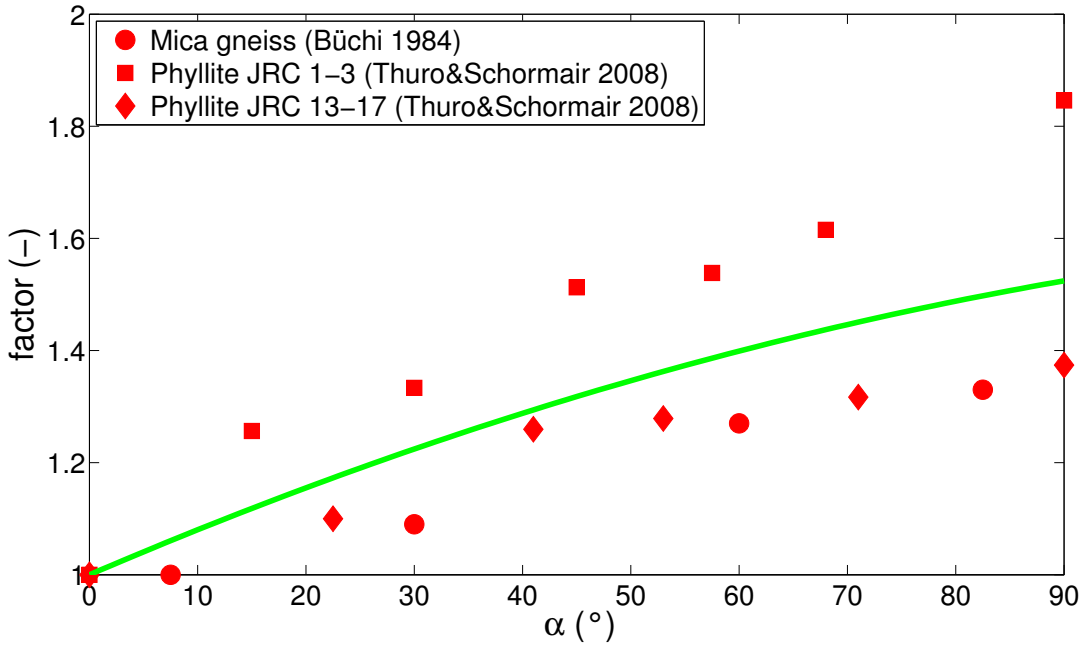


**Fig. 2.10.:** Angular dependence of cuttability in foliated rock types approximated by a quadratic polynomial function. The underlying data were taken from Büchi (1984) and Thuro and Schormair (2008)

All results show a continuous increase of cuttability towards 90° where the foliation is perpendicular to the tunnel axis. The magnitude of the factor ranges from 1.35 to 1.85 in these examples, which demonstrates that without consideration of the degree of anisotropy results can deviate strongly. However, all curves can well be approximated

with a quadratic polynomial function of the form:

$$f(\alpha) = p_1\,\alpha^2 + p_2\,\alpha + 1 \quad with \quad p_1 = -0.0000275 \; and \; p_2 = 0.0083 \tag{2.2}$$

To account for the magnitude, a strength parameter has to be added to the equation. As UCS and BTS are most commonly available, they should be looked at closer. The shape of the curve representing angular dependence of UCS is different from the presented curves. It has its low mark at about 45° and rises towards 0° and 90° (e.g. Nasseri et al. 2003, Thuro 2002). In contrast to that, the angular dependence of BTS can also be approximated by a quadratic polynomial function and it is thus very similar to the results shown in Fig. 2.10. Fig. 2.11 shows BTS values of AG as a function of alpha to illustrate the similarity. The loading direction is perpendicular to the foliation at 90° and parallel to the foliation at 0°.

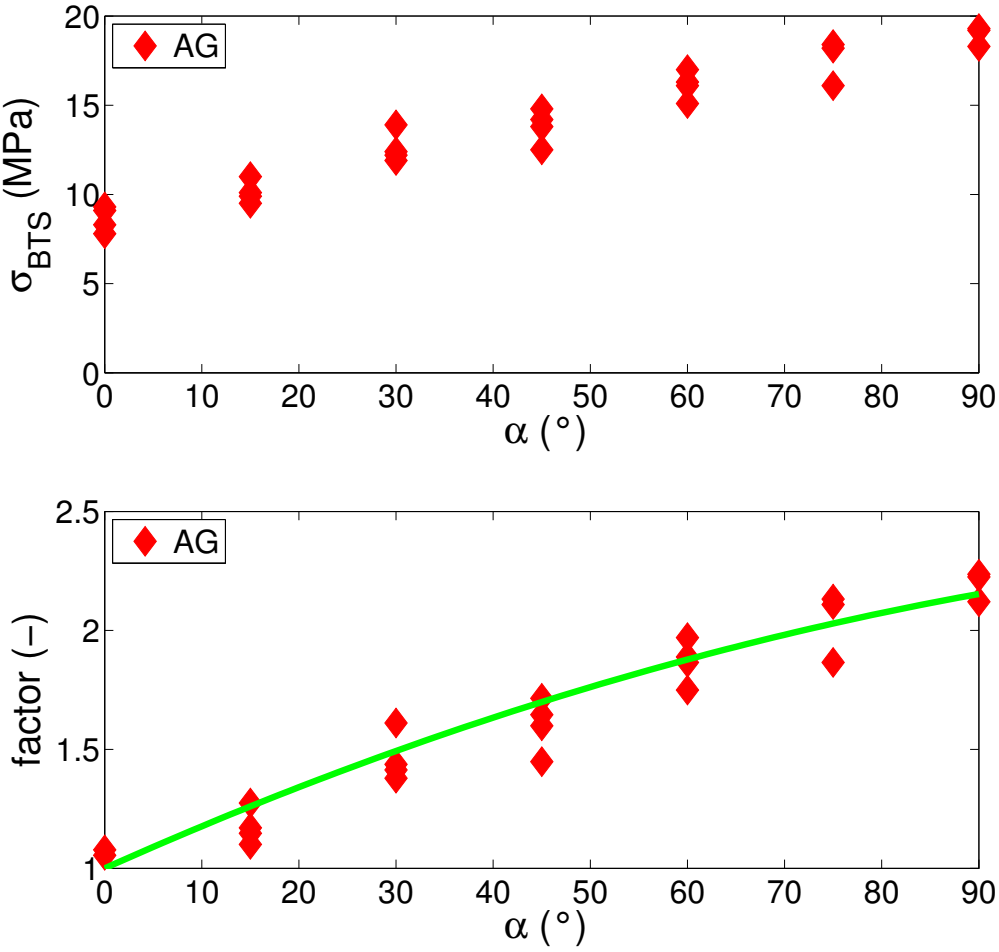


**Fig. 2.11.:** Angular dependence of BTS in absolute (top) and relative values (bottom)

Thus, an equation for the correction factor to consider the spatial orientation of foliation ($k_\alpha$) is proposed ($a_1$ is a generic constant that allows for calibration of real data according to the equation):

$$k_\alpha = a_1 \frac{BTS_{90^\circ}}{BTS_{0^\circ}} (p_1\ \alpha^2 + p_2\ \alpha) + 1 \tag{2.3}$$

Due to the lack of data, this equation is not yet calibrated and is thus only for preliminary use. However, this example shows a way of how factor based TBM performance prediction models can be developed. Similarly to this approach, a future correction factor for rock joints should not be seen independently of strength parameters (e.g. UCS). Otherwise, results will be not accurate enough.

The effect of confinement was extensively discussed in section C, especially in section C.4. It is closely related to tunnels with high overburden which results in high primary stresses. The interaction between cutting process and confinement is on the one hand significant and on the other hand one of the most complex rock mass factors and has lead to many contradicting experiences in TBM operation. Some of them were summarized by Innaurato et al. (2007). Fig. 2.12 illustrates four fundamental situations that can be observed in laboratory indentation or rock cutting tests. In a non-confined or insufficiently confined situation, a large median crack will be pre-dominant (Fig. 2.12a). Fig. 2.12b depicts a state of passive confinement or self-confinement which is - if the specimen is large enough - similar to a semi-infinite surface. This is a good model for the confinement state of the first cut in scaled rock cutting tests or of an undamaged tunnel face in areas with low overburden. Cracks develop mostly in the lateral direction. In contrast to this, active confinement is added in Fig. 2.12c which is representative of a tunnel with high overburden. Due to the added pressure, cracks develop almost horizontally. Fig. 2.12d represents the same confinement situation in foliated rock which completely changes the crack pattern due to pronounced planes of weakness.

The situation at a tunnel face is typically a combination of all four cases. Insufficiently confined situations occur because the tunnel face is pre-damaged and because of joints. In a pre-damaged environment with a variety of cracks, loosening of the ground can take place resulting in reduced confinement. In contrast to this, cracks will not propagate deeply into the tunnel face at high primary stresses, preventing ground loosening. Besides this qualitative illustration of crack length and directions, the contact pressure needed to penetrate into the rock also depends on the confinement situation. As stated in section C, contact pressure increases as confinement goes up, which is unbeneficial. A countervailing favourable effect is that cracks develop right in the direction of adjacent cutters at high confinement which would allow for larger cutter spacing and thus more efficient chipping. Due to this complex situation which also very much depends on the rock type it is not easy to determine the consequences of high primary stress. For an accurate prediction, it is paramount to investigate whether face instabilities are expected or not. If this is the case, the cutting process will be affected greatly and common TBM performance prediction models are no longer valid. If this is not the case, beneficial effects might be exploited due to favourable cracking directions and stress reliefs.

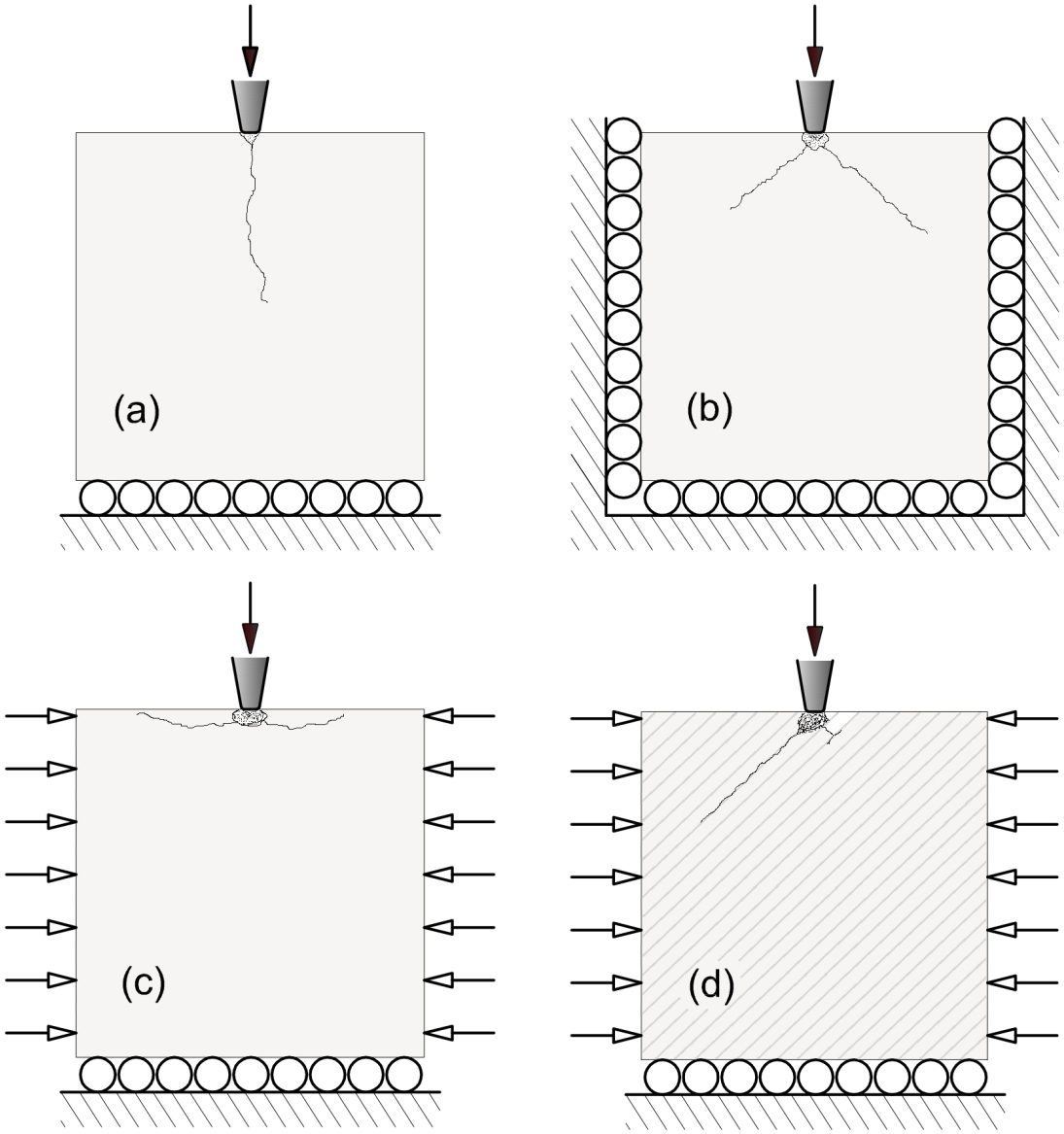


**Fig. 2.12.:** Crack propagation as a function of confinement, (a) no confinement, (b) passive confinement, (c) active confinement, (d) a combination of active confinement and anisotropic rock

### 2.2.5. Machine parameters

The main machine parameters that have to be considered are cutter type, size, shape, spacing and cutterhead diameter. Operational parameters such as thrust are usually included in the basic penetration function. These factors are usually derived by means of regression analysis or rather simple geometrical assumptions. Developing them based on fundamental mechanisms is very difficult and has not yet been done.

A fundamental approach to develop a correction factor for cutter type, size and shape would be based on stress distribution and the area between cutter ring and rock surface. Knowledge of the change of stress distributions with respect to cutter size, shape and rock type would then lead to a correction factor. Such a development is not in sight, although Rostami (2013) recently published a paper that gives first insights into the stress distribution beneath a cutter (see Fig. 2.13).

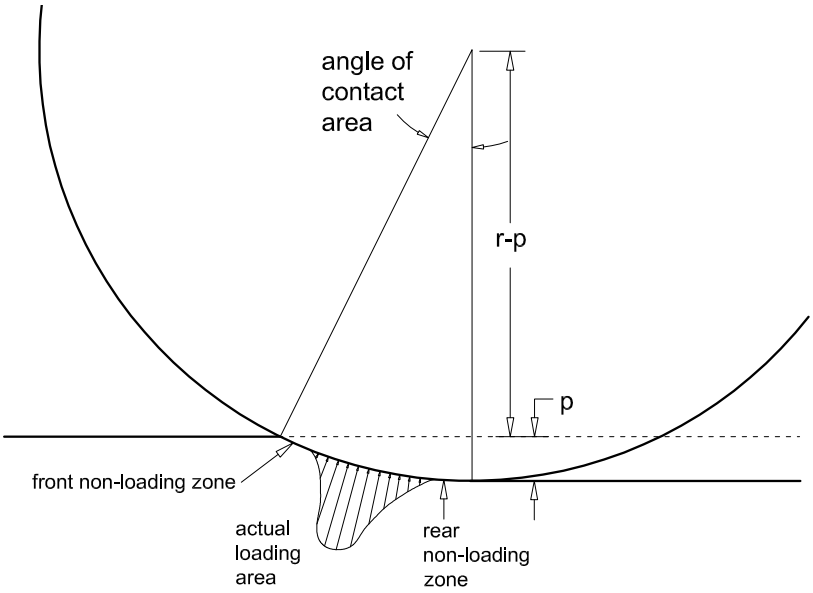


**Fig. 2.13.:** Stress distribution between disc cutter and rock surface (modified from Rostami 2013)

As long as there is no deeper understanding, correction factors for size and shape are, however, limited to relatively simple geometrical assumptions, e.g. cutter engagement length multiplied by tip width of the new cutter over the standard cutter with which the model was developed. Such approaches (see e.g. Türtscher 2011) work very well for the majority of practical applications. Thus, TBM performance prediction models work well in this regard. However, it is a common mistake to think that such simple approaches can aid in the choice of cutter size. This choice is controlled only by factors that are not incorporated into such correction factors, i.e. cutting efficiency due to size effects (see section C.4.3), cutter weight with respect to cutter change, spacing and associated grain size distribution, overall number of cutters and many more. From a rock mechanical point of view, large cutters and spacing should be preferred in brittle hard rock because contact stress needed to break rock decreases with increasing size. Also, a large spacing is very favourable regarding the overall energy input which can be observed by the creation of less fines and large rock chips. In future operations where individual cutting tools are going to be monitored, it is also advantageous to have fewer cutters allowing for fewer sensors and cables.

Similar to tool size, the effect of cutterhead size is complex in nature. First, a larger cutterhead will be less stiff than a small one. Second, face stability decreases as the cavity becomes larger. Third, torque demand increases which makes it harder to rotate at the same speed as in smaller diameters and finally, the tunnel face in the gauge areas might exhibit a dynamical strength increase due to fast angular velocity of gauge cutters and subsequent high loading rates. Due to the complexity of these phenomena, there is a clear trend that excavation becomes slower with increasing cutterhead diameter.

## 2.3. Summary

Remote cutter monitoring is one of the main research and development focuses of many TBM manufacturers. The knowledge of real-time operational parameters of a cutting tool will allow for safer, faster and cheaper tunnel construction. This includes monitoring of rotation and temperature to detect blocked cutters as well as wear to optimize cutter change timing. In this thesis a cutter force measurement method for TBM disc cutters was developed and tested at the Austrian Koralm tunnel. In contrast to previous development that were carried out between 1979 and 2009, its main innovation is the placement of sensors within at the cutter casing. Thus, it provides an opportunity for continuous use on a TBM without disturbing the construction process which is an unique feature.

The development consisted of a number of steps. First, simulations of cutters and different cutter casings were carried out to understand the structural behaviour and find suitable spots for sensor placement. The focus was put on investigation of two common cutter mounting systems, namely conical saddle / bayonet systems and Wedge-Lock systems. Subsequently, a variety of sensor layouts was derived from the simulation results. The two most promising with respect to practical applications were tested in a laboratory setup that allowed for the application of different loading cases, i.e. different combinations of normal, rolling and side force. Hereby, the feasibility of the developed measurement method was proven. The sensors used are measurement bolts with strain implemented strain gauges that are related to the bolt's pre-stress. The change of pre-stress due to an external loading is then mathematically linked to the external load to determine cutting forces.

The promising results opened the door for a practical implementation at the first Koralm tunnel TBM. Three cutter positions on different radii were equipped with sensors to obtain a good representation of the tunnel face. An in situ calibration test with a specially designed clamping device was carried out to account for the changed structural stiffness compared to laboratory boundary conditions and to allow for a large number of different loading cases. Subsequently, the measurement results were mathematically linked to the applied forces and an algorithm for an automated back-calculation was developed. While the mathematics used in this process are concise, the calibration is still more complex than in previous systems that measured the deformation of the cutter axis.

This setup is essentially a beam in bending with lesser sources of non-linearities than a measurement at the cutter saddle. From the beginning of the implementation process on, a strong collaboration with the TBM manufacturer Aker Wirth as well as automation engineers and software developers from Net-Automation and Geodata was necessary. The harsh environment in a TBM cutterhead called for a robust installation of sensors and cables that ensures a lasting operation. Also, the measurement chain changed from laboratory equipment to a programmable controller, wireless radio communication and a database to administrate and process the large amounts of data. Further support was ensured by the construction consortium Arge KAT 2 that guaranteed decent boundary conditions for installation and maintenance works at the tunnelling site. The system was in full operation until the originally impervious chamber of the programmable controller was penetrated by water which stopped the measurements. Generally speaking, of the problems yet to be solved, ensuring a lasting installation of cables and electric parts will be the most challenging.

The obtained results are very promising and allow for a detailed comparison with geological documentations of the tunnel face. The measured peak forces are in the range of 900 kN and in the same order of magnitude at all three positions. However, this was measured in schistose gneiss with a uniaxial compressive strength of about 50 to 100 MPa. Hence, higher peak forces are expected in harder lithologies. The mean forces decrease as radius increases, which could be due to constraints of the circular movement at very small radii, reduced stiffness in the outer areas and due to geological inhomogeneity.

TBM performance prediction aims to find a relationship between thrust force and net penetration rate as a function of geotechnical parameters. In a subsequent step, construction time is derived from net penetration rate. During in situ TBM operations, it is state of the art to measure global thrust and compare it with achieved penetration. This relationship however is smeared by friction forces in the range of several thousand kN. Hence, cutter force measurement is needed to eliminate this influence and deliver a clearer picture of this relationship. Until now, one of the best ways of determining this relationship more accurately is to carry out full scale rock cutting tests. Within the scope of this thesis, such rock cutting tests were carried out at the Colorado School of Mines for a duration of three months. The results were used to gain a deeper understanding of the characteristics of cutting forces in order to optimize the implementation of cutter force measurement regarding sampling rates and subsequent data interpretation. They were also used to gain an understanding of fundamental rock failure mechanisms with respect to corresponding cutting forces. Regarding performance prediction, however, it was concluded that the range of applications of full scale cutting tests is very limited due to the required large sample size. Consequently, the development of a new small scale cutting test rig was started. This test rig allows for high accuracy measurements in controlled laboratory conditions and utilizes rock cores as samples with a diameter of 10 cm. Such specimens are available at early project phases in large tunnelling projects. The cutter can roll freely just like a full sized one and is a 1:8 sized model compared

to a 17" disc cutter. The cutting kerf is in the center of the specimen in the standard setup, but the rig also allows for subsequent cuts with spacing in between to investigate their interaction. Test series on eight different lithologies were carried out to assess the practical usability of the test rig. Results were compared with full scale cutting tests as a reference and with UCS and BTS values. In spite of the small scale, it showed that small scale cutting tests are capable of replicating the results of full scale cutting tests accurately whereas UCS and BTS values turned out to be inferior cutting force predictors, especially if the investigated lithologies are either very brittle or ductile. Subsequently, the outline of a new TBM performance prediction model that utilizes the small scale cutting test to derive a basic geotechnical input parameter was presented.

The controlled laboratory environment and the smaller sample sizes allowed for a variety of scientific investigations that are impossible on larger scales. First, the sound emissions were recorded during all tests and compared with cutting forces and the condition of the specimen. It was concluded that sound emissions are related to the gradient of stress release events that indicate the formation of a crushed zone with intragranular breakage as the dominant failure mechanism. As a result, it was concluded that chipping events are obviously a key parameter to assess whether excavation is efficient or not, yet they are not directly linked to force peaks and subsequent sudden force drops. This was a common misperception of previous studies. Some of the specimens were embedded in fluorescent epoxy resin and ground down layer by layer to obtain a spatial picture of the crack network. It turned out that the samples contained few dominant cracks but much fewer than the number of significant force drops, which is another indicator that these events are independent of each other. Median cracking was found only in boundary areas without sufficient confinement. In the central, well embedded areas crack directions ranged from diagonal to horizontal, depending mostly on the lithology. It was concluded that the role of median cracking is less significant than thought. The dominant role of such cracks originates from previous studies where samples were exposed to plane stress conditions which significantly influenced crack patterns.

In the future reliable cutter force measurement systems combined with fundamental investigations by means of laboratory testing and simulation will enable a deeper understanding of the rock cutting processes in mechanical excavation. This will not only improve the efficiency of mechanical rock cutting, it will also open the path to use cutting forces as the main input parameter for an automated TBM control. This thesis should help to lay a foundation for fully industrialized and automated tunnelling operations that make construction safer, faster and cheaper.

# References


Abu Bakar M., Gertsch L., 2012. Disc cutting tests on dry and saturated sandstone: muck as a performance estimator, In: Proceedings of the SME Annual Meeting, Seattle, USA.

Altindag R., 2003. Correlation of specific energy with rock brittleness concepts on rock cutting. The Journal of the South African Institute of Mining and Metallurgy 4, 163-172.

Balci C., Bilgin N., 2007. Correlative study of linear small and full-scale rock cutting tests to select mechanized excavation machines. International Journal of Rock Mechanics and Mining Sciences 44, 468-476.

Bazant Z., 1999. Size effect on structural strength: a review. Archive of Applied Mechanics 69, 703-725.

Beer G., 2009. Technology Innovation in Underground Construction. Institute for Structural Analysis, Graz University of Technology, 225-237.

Bilgin N., Balci C., Tumac D., Feridunoglu C., Copur H., 2010. Development of a portable rock cutting rig for rock cuttability determination, In: Proceedings of the European Rock Mechanics Symposium, Lausanne, Switzerland.

Büchi E., 1984. Einfluss geologischer Parameter auf die Vortriebsleistung einer Tunnelbohrmaschine. Ph.D. thesis, Universität Bern. in German.

Burger W., Ihle B., Messing M., Köbele T., 2006. Apparatus for detecting the state of rotation of cutting rollers of a shield tunnelling machine. Patent number US 7,014,271 B2.

Bruland A., 1998. Hard rock tunnel boring: vol 1-10. Ph.D. thesis, Norwegian University of Science and Technology.

Bumberger T., Entacher M., Winter G., Godor I., Galler R., 2011. Numerische Modellierung des Verformungszustandes hochbelasteter Abbauwerkzeuge von Tunnelbohrmaschinen. Berg- und Hüttenmännische Monatshefte 156, 492-497. in German.

Carpinteri A., Invernizzi S., 2005. Numerical analysis of the cutting interaction between indenters acting on disordered materials. International Journal of Fracture 131, 143-154.

Chen L.H., Labuz J.F., 2006. Indentation of rock by wedge-shaped tools. International Journal of Rock Mechanics and Mining Sciences 43, 1023-1033.

Chen X., Hutchinson J.W., Evans A.G., 2005. The Mechanics of Indentation Induced Lateral Cracking. Journal of the American Ceramic Society 88, 1233-1238.

Chiaia B., 2001. Fracture mechanisms induced in a brittle material by a hard cutting indenter. International Journal of Solids and Structures 38, 7747-7768.

Cho J., Jeon S., Jeong H., Chang S., 2013. Evaluation of cutting efficiency during TBM disc cutter excavation within a Korean granitic rock using linear-cutting-machine testing and photogrammetric measurement. Tunnelling and Underground Space Technology 35, 37-54.

Cook N., Hood M., Tsai F., 1984. Observations of Crack Growth in Hard Rock Loaded by an Indenter. International Journal of Rock Mechanics and Mining Sciences 21, 97-107.

Danzer R., Lube T., Supancic P., Damani R., 2008. Fracture of Ceramics. Advanced Engineering Materials 10, 275-298.

Delisio A., Zhao J., Einstein H.H., 2013. Analysis and prediction of TBM performance in blocky rock conditions at the Lötschberg Base Tunnel. Tunnelling and Underground Space Technology 33, 131-142.

Edelmann T., Himmelsbach C., 2013. Device for monitoring the state of rotation of a disk cutter arrangement of a shield tunnel boring machine and disk cutter arrangement for a shield tunnel boring machine. Patent number WO 2013/050010 A2.

Entacher M., Galler R., 2013a. Bedienerfreundliche Sensorik zum Ermitteln einer mechanischen Belastung eines Abbauwerkzeugs einer Tunnelbohrmaschine. Utility patent number E21D 9/10. in German.

Entacher M., Galler R., 2013b. Vorrichtung und Verfahren für Modellschneidversuch. Patent submitted 04/24/2013. in German.

Entacher M., Lassnig K., Galler R., 2012a. Analysis of Force Path Diagrams of Linear Cutting Machine Tests regarding Geotechnical Parameters. In: Proceedings of the Geocongress 2012, Oakland, USA.

Entacher M., Lassnig K., 2012b. Findings from disc cutting tests on alpine lithologies. Geomechanics and Tunnelling 5, 547-556.

Entacher M., Lorenz S., Galler R., 2013c. TBM performance prediction with scaled rock cutting tests. Submitted to International Journal of Rock Mechanics and Mining Sciences.

Entacher M., Schuller E., Galler R., 2013d. Rock failure and crack propagation beneath disc cutters. Submitted to Rock Mechanics and Rock Engineering.

Entacher M., Winter G., Bumberger T., Decker K., Godor I., Galler R., 2012c. Cutter force measurement on tunnel boring machines - System design. Tunnelling and Underground Space Technology 31, 97-106.

Entacher, M., Winter, G., Galler, R., 2013e. Cutter force measurement on tunnel boring machines - Implementation at Koralmtunnel. Submitted to Tunnelling and Underground Space Technology.

Farrokh E., Rostami J., Laughton C., 2012. Study of various models for estimation of penetration rate of hard rock TBMs. Tunnelling and Underground Space Technology 30, 110-123.

Fenn D., Bowles B.A., David J.F., Prutheroe B.E., 1981. The in-situ measurement of dynamic cutter forces on a Robbins raiseborer reaming head. Chamber of Mines of South Africa, Research Rept No. 18/81, Project No. GT 2N01.

Frenzel C., Galler R., Käsling H., Villeneuve M., 2012. Penetration tests for TBMs and their practical application. Geomechanics and Tunnelling 5, 557-566.

Fukui K., Okubo S., 2005. Some Attempts for Estimating Rock Strength and Rock Mass Classification from Cutting Force and Investigation of Optimum Operation of Tunnel Boring Machines. Rock Mechanics and Rock Engineering 39, 25-44.

Gajewski J., Jonak J., 2011. Towards the identification of worn picks on cutterdrums based on torque and power signals using Artificial Neural Networks. Tunnelling and Underground Space Technology 26, 22-28.

Gehring K., 1995. Leistungs- und Verschleißprognose im maschinellen Tunnelbau. Felsbau 13, 439-448. in German.

Gehring K., 1997. Classification of Drillability, Cuttability, Borability and Abrasivity in Tunneling. Felsbau 15, 183-191.

Gertsch R., 2000. Rock Toughness and Disc Cutting. Ph.D. thesis, University of Missouri-Rolla.

Gertsch R., Gertsch L., Rostami J., 2007. Disc cutting tests in Colorado Red Granite: Implications for TBM performance prediction. International Journal of Rock Mechanics and Mining Sciences 44, 238-246.

Gnirk P., Cheatham J., 1965. An experimental study of indexed single bit-tooth penetration into dry rock at confining pressures of 0 to 7500 psi. In: Proceedings of the Conference on Drilling and Rock Mechanics, Austin, USA.

Gobetz F.W., 1973. Development of a Boring Machine Cutter Instrumentation Program. Final Report, United Aircraft Research Laboratories to Departmentt of the Interioir. USBM Contract H0122072, UARL Rept M-971373-10.

Goktan R.M., Yilmaz N.G., 2005. A new methodology for the analysis of the relationship between rock brittleness index and drag pick cutting efficiency. The Journal of the South African Institute of Mining and Metallurgy 11, 727-734.

Gong Q.M., Zhao J., 2007. Influence of rock brittleness on TBM penetration rate in Singapore granite. Tunnelling and Underground Space Technology 22, 317-324.

Griffith, A.A. (1921) The phenomena of rupture and flow in solids. Philosophical Transactions 221A:179-180

Hassanpour J., Rostami J., Zhao J., 2011. A new hard rock TBM performance prediction model for project planning. Tunnelling and Underground Space Technology 26, 595-603.

Harer G., Koinig J., 2010. Current state of design, investigation and construction works at the Koralm Tunnel. Geomechanics and Tunnelling 3, 155-162.

Hopkins M., Foden R., 1979. The In-Situ Measurement of Dynamic Cutter Forces on Raiseborer Reaming Heads, In: International Conference on Mining and Machinery, Brisbane, Australia.

Horii H., Nemat-Nasser S., 1986. Brittle Failure in Compression: Splitting, Faulting and Brittle-Ductile Transition. Philosophical Transactions of the Royal Society of London. Series A, Mathematical and Physical Sciences 319, 337-374.

Howarth DF, Bridge E., 1988a. Observation of Cracks at the Bottom of Percussion and Diamond Drill Holes. International Journal of Rock Mechanics and Mining Sciences 25, 39-43.

Howarth DF, Bridge E., 1988b. Microfracture Beneath Blunt Disc Cutters in Rock. International Journal of Rock Mechanics and Mining Sciences 25, 35-38.

Huang H., Damjanac B., Detournay E., 1998. Normal Wedge Indentation in Rocks with Lateral Confinement. Rock Mechanics and Rock Engineering 31, 81-94.

Huang H., Detournay E., 2012. Discrete element modeling of tool-rock interaction II: rock indentation. International Journal for numerical and analytical methods in geomechanics. doi:10.1002/nag.2114.

Hucka V., Das B., 1974. Brittleness Determination of Rocks by Different Methods. International Journal of Rock Mechanics and Mining Sciences 11, 389-392.

Innaurato N., Oggeri C., Oreste P.P., Vinai R., 2006. Experimental and Numerical Studies on Rock Breaking with TBM Tools under High Stress Confinement. Rock Mechanics and Rock Engineering 40, 429-451.

Innaurato N, Oggeri C, Oreste PP, Vinai R (2011) Laboratory tests to study the influence of rock stress confinement on the performances of TBM discs in tunnels. International Journal of Minerals, Metallurgy and Materials 18:253-259

Jeon S., Chang, S., Choi, S., Bae, G., Park K., 2006. Performance estimation of TBM disc cutter by linear cutting machine, In: Proceedings of the 41$^{st}$ US Rock Mechanics Symposium, Golden, USA.

Kahraman S., 2002. Correlation of TBM and drilling machine performances with rock brittleness. Engineering Geology 65, 269-283.

Kahraman S., Altindag R., 2004. A brittleness index to estimate fracture toughness. International Journal of Rock Mechanics and Mining Sciences 41, 343-348.

Kaitkay P., Lei S., 2005. Experimental study of rock cutting under external hydrostatic pressure. Journal of Materials Processing Technology 159, 206-213.

Käsling H., 2009. Bestimmung der Gesteinsabrasivität - Grundlagen, Anwendung und Einsatzgrenzen bei maschinellen Tunnelvortrieben. Ph.D. thesis, Technische Universität München. in German.

Larson D., Morrell R., Mades J., 1987. An investigation of Crack Propagation With a Wedge Indenter To Improve Rock Fragmentation Efficiency. Bureau of Mines report of investigations 9106.

Lawn B., Wilshaw R., 1975. Indentation fracture: principles and applications. Journal of Materials Science 10, 1049-1081.

Lindbergh L., Shanahan A., Cahoon I., Robbins R., Moore J., Brown B., Reilly, T., 2012. Apparatus and method for monitoring tunnel boring efficiency. Patent number US 8,172,334 B2

Lindqvist P.-A., 1982. Rock fragmentation by indentation and disc cutting: Some theoretical and experimental studies. Ph.D. thesis, Lulea University of Technology.

Lindqvist P.-A., Lai H., Alm O., 1984. Indentation Fracture Development in Rock Continuously Observed with a Scanning Electron Microscope. International Journal of Rock Mechanics and Mining Sciences 21, 165-182.

Liu H.Y, Kou S.Q, Lindqvist P.-A., Tang C., 2002. Numerical simulation of the rock fragmentation process induced by indenters. International Journal of Rock Mechanics and Mining Sciences 39, 491-505.

Lopez Jimeno E., Ayala Carcedo FJ., 1995. Drilling and Blasting of rocks. A.A. Balkema, Rotterdam.

Maidl B., Herrenknecht M., Maidl U., Wehrmeyer G., 2012. Mechanised Shield Tunnelling. Ernst & Sohn, Berlin.

Maidl B., Schmid L., Ritz W., Herrenknecht M., 2008. Hardrock Tunnel Boring Machines. Ernst & Sohn, Berlin.

Marshall D., Lawn BR, Evans A., 1982. Elastic/Plastic Indentation Damage in Ceramics: The Lateral Crack System. Journal of the American Ceramic Society 65, 561-566.

McFeat-Smith I., Fowell R.J., 1979. The selection and application of roadheaders for rock tunnelling, In: Proceedings of the Rapid Excavation and Tunneling Conference, Atlanta, USA.

Mishnaevsky L., 1995. Physical Mechanisms of Hard Rock Fragmentation under Mechanical Loading: A Review. International Journal of Rock Mechanics and Mining Sciences & Geomechanics Abstracts 32, 763-766.

Moon T., Oh J., 2011. A Study of Optimal Rock-Cutting Conditions for Hard Rock TBM Using the Discrete Element Method. Rock Mechanics and Rock Engineering 45, 837-849

Mori L., 2012. Results of linear cutting tests on different alpine lithologies. M.Sc. thesis, Montanuniversität Leoben. in German.

Nasseri M.H.B., Rao K.S., Ramamurthy T., 2003. Anisotropic strength and deformational behaviour of Himalayan schists. International Journal of Rock Mechanics and Mining Sciences 40, 3-23

Nishimatsu Y., 1971. The mechanics of rock cutting. International Journal of Rock Mechanics and Mining Sciences 9, 261-270.

Ouchterlony F., 1988. Suggested methods for determining the fracture toughness of rock. International Journal of Rock Mechanics and Mining Sciences 25, 71-96.

Ozdemir L., Miller R., Wang FD., 1976. Mechanical tunnel boring prediction and machine design. National Science Foundation, USA.

Öztürk C., Nasuf E., Bilgin N., 2004. The assessment of rock cutability , and physical and mechanical rock properties from a texture coefficient. The Journal of the South African Institute of Mining and Metallurgy 8, 397-402.

Pang S., Goldsmith, W., 1990. Investigation of Crack Formation During Loading of Brittle Rock. Rock Mechanics and Rock Engineering 23, 53-63.

Ramazanzadeh A., Rostami J., Kastner R., 2005. Influence of Rock Mass Properties on Performance of Hard Rock TBMs. In: Proceedings of the Rapid Excavation and Tunnelling Conference, Seattle, USA.

Rauch R., 2012. Untersuchungen zum Bruchverhalten von ausgewählten Festgesteinen. B.Sc. thesis, Montanuniversität Leoben. in German.

Ritter U., 2013. Koralmtunnel - Baulos KAT 2, Baugeologische Tunneldokumentation Station 1886,29. Unpublished. in German.

Rittinger P., 1867. Taschenbuch der Aufbereitungskunde. Ernst & Korn, Berlin. in German.

Rojek J, Labra C (2013) Discrete element simulation of rock cutting processes. International Workshop: Cutting Tool - Soil Interaction, July 2013, Bochum, Germany

Roby J., Sandell T., Kocab J., Lindbergh L., 2008. The Current State of Disc Cutter Design and Development Directions. In: Proceedings of the North American Tunnel Congress, San Francisco, USA.

Rojek J., Oñate E., Labra C., Kargl H., 2011. Discrete element simulation of rock cutting. International Journal of Rock Mechanics and Mining Sciences 48, 996-1010.

Rostami J., 1997. Development of a force estimation model for rock fragmentation with disc cutters through theoretical modelling and physical measurement of crushed zone pressure. Ph.D. thesis, Colorado School of Mines.

Rostami J (2013) Study of pressure distribution within the crushed zone in the contact area between rock and disc cutters. International Journal of Rock Mechanics and Mining Sciences 57:172-186

Rostami J., Ozdemir L., 1993. A new model for performance prediction of hard rock tbms. In: Proceedings of the Rapid Excavation and Tunneling Conference, Boston, USA.

Rostami J., 2008. Hard Rock TBM Cutterhead Modeling for Design and Performance Prediction. Geomechanics and Tunnelling 1, 18-28.

Rostami J., 2013. Study of pressure distribution within the crushed zone in the contact area between rock and disc cutters. International Journal of Rock Mechanics and Mining Sciences 57, 172-186.

Roxborough F., Philipps H., 1974. Experimental studies on the excavation of rock using picks. In: Proceedings of the $3^{rd}$ ISRM Congress, Denver, USA.

Saksala T., 2013. 3D numerical modelling of bit-rock fracture mechanisms in percussive drilling with a multiple-button bit. International Journal for numerical and analytical methods in geomechanics 37, 309-324.

Samuel A., Seow L., 1984. Disc Force Measurements on a Full-Face Tunnelling Machine. International Journal of Rock Mechanics and Mining Sciences 21, 83-96.

Sänger B., 2006. Disc Cutters for Hardrock TBM 1956-2006 - History and Tendencies of Development. Felsbau 24, 46-51.

Shanahan A., Box Z., 2011. TBM Cutter Instrumentation at Malaysia's Pahang Selangor Water Tunnel and Canada's Niagara Tunnel Project, in: Proceedings of the World Tunnel Congress 2011.

Starloy Corporation, 2003. Disk roller cutter and disk roller cutter monitoring system. Patent number WO 03/087537.

Su O., Ali Akcin N., 2011. Numerical simulation of rock cutting using the discrete element method. International Journal of Rock Mechanics and Mining Sciences 48, 434-442.

Swain M., Atkinson B., 1978. Fracture Surface Energy of Olivine. Pure and Applied Geophysics 116, 866-872.

Swain M., Lawn BR, 1976. Indentation Fracture in Brittle Rocks and Glass. International Journal of Rock Mechanics and Mining Sciences 13, 311-319.

Thuro K., 2002. Geologisch-felsmechanische Grundlagen der Gebirgslösung im Tunnelbau. Habilitationsschrift in Münchner Geologische Hefte B18, München. in German.

Thuro K., Plinninger R.J., 2003. Hard rock tunnel boring, cutting, drilling and blasting: rock parameters for excavability. In: Proceedings of the 10th ISRM Congress, Sandton, South Africa.

Thuro K., Schormair N., 2008. Fracture Propagation in Anisotropic Rock During Drilling and Cutting. Geomechanics and Tunnelling 1, 8-17.

Türtscher M., 2011. Analyse und Penetration von Vortriebsgeschwindigkeit bei maschinellen Vortrieben im Festgestein. Ph.D. thesis, University of Innsbruck. in German.

Villeneuve M., 2008. Examination of geological influence on machine excavation of highly stressed tunnels in massive hard rock. Ph.D. thesis, Queen's University at Kingston, Canada.

Wagner H., Schümann E., 1971. The Stamp-Load Bearing Strength of Rock - An Experimental and Theoretical Investigation. Rock Mechanics 3, 185-207.

Wang S.Y., Sloan S.W., Liu H. Y., Tang C.A., 2010. Numerical simulation of the rock fragmentation process induced by two drill bits subjected to static and dynamic (impact) loading. Rock Mechanics and Rock Engineering 44, 317-332.

Yagiz S., Karahan H., 2011. Prediction of hard rock TBM penetration rate using particle swarm optimization. International Journal of Rock Mechanics and Mining Sciences 48, 427-433.

Zare S., Bruland A., 2013. Applications of NTNU/SINTEF Drillability Indices in Hard Rock Tunneling. Rock Mechanics and Rock Engineering 46, 179-187.

Zhang H., Huang G., Song H., Kang Y., 2012. Experimental investigation of deformation and failure mechanisms in rock under indentation by digital image correlation. Engineering Fracture Mechanics 96, 667-675.

Zhang Z X, Kou S Q, Lindqvist P.-A., 2001. In-situ measurements of TBM cutter temperature in Äspö Hard Rock Laboratory, Sweden. International Journal of Rock Mechanics and Mining Sciences 38, 585-590.

Zhang Z. X., Kou S. Q., Tan X.C., Lindqvist P.-A., 2003a. In-situ Measurements of Cutter Forces on Boring Machine at Äspö Hard Rock Laboratory Part I. Laboratory Calibration and In-situ Measurements. Rock Mechanics and Rock Engineering 36, 39-61.

Zhang Z. X., Kou S. Q., Lindqvist P.-A. 2003b. In-situ Measurements of Cutter Forces on Boring Machine at Äspö Hard Rock Laboratory Part II. Characteristics of Cutter Forces and Examination of Cracks Generated. Rock Mechanics and Rock Engineering 36, 63-83.

Zhao Z., Gong Q., Zhang Y., Zhao J., 2007. Prediction model of tunnel boring machine performance by ensemble neural networks. Geomechanics and Geoengineering 2, 123-128.

# Danksagung

Die vorliegende Arbeit entstand während meiner Tätigkeit als wissenschaftlicher Mitarbeiter am Lehrstuhl für Subsurface Engineering der Montanuniversität Leoben. Für diese lehrreiche Zeit sowie die intensive Betreuung meiner wissenschaftlichen Tätigkeit bin ich Prof. Robert Galler zu allergrößtem Dank verpflichtet.

Für die Übernahme der Zweitbegutachtung sowie die gute Zusammenarbeit in der Abrock Forschungsgruppe gilt mein Dank Prof. Kurosch Thuro.

Ein ganz besonderer Dank gilt Dr. Christian Frenzel, der mich während meines Auslandsaufenthaltes an der Colorado School of Mines hervorragend betreut und durch spannende Diskussionen viele inhaltliche Denkanstöße geliefert hat.

Dr. Gerhard Winter ist mir in maschinenbaulichen Fragen in jeder Phase meiner Dissertation geduldig mit Rat und Tat zur Seite gestanden, wofür ich mich sehr herzlich bedanken möchte. Für ihre Beiträge und Hilfe bedanke ich mich neben ihm auch bei allen weiteren Co-Autoren.

Stellvertretend für die vielen ambitionierten und fähigen Studierenden, mit denen ich zusammenarbeiten durfte, möchte ich mich bei meinen Diplomanden Thomas Bumberger, Stefan Lorenz und Hartmut Erben für die tatkräftige Unterstützung bedanken.

Für die gute und enge Zusammenarbeit im Forschungsprojekt “Enhanced Monitoring and Simulation Assisted Tunnelling” gilt mein Dank der Fa. Geodata GmbH sowie dem Lehrstuhl für Statik und Dynamik der Ruhr-Universität Bochum. Für die Zusammenarbeit bei der Implementierung der Diskenkraftmessung am Koralmtunnel gilt mein besonderer Dank darüber hinaus den Mitarbeitern der Aker Wirth GmbH, der Arge KAT 2 (Strabag AG und Jäger Bau GmbH) sowie der Fa. Net-Automation.

Im Zuge der regelmäßigen Abrock Treffen ergab sich eine fruchtbare Zusammenarbeit mit der BBT SE, für die ich mich bei Dr. Stefan Skuk herzlich bedanken möchte.

Bei den Mitarbeitern des Lehrstuhls für Subsurface Engineering und dem Department Mineral Resources and Petroleum Engineering bedanke ich mich von Herzen für die gute Kollegialität und Zusammenarbeit.

Zu guter Letzt bedanke ich mich bei meiner Familie und meinen Freunden für die langjährige Unterstützung.

# Affidavit

I declare in lieu of oath, that I wrote this thesis and performed the associated research myself, using only literature cited in this volume.

_____

Martin Entacher